

**BI-DIRECTIONAL VULNERABILITY OF BRAIN TUMORS TO WNT SIGNALING**

THE BI-DIRECTIONAL VULNERABILITY OF MALIGNANT BRAIN TUMORS TO  
WNT SIGNALING

BRANAVAN MANORANJAN, B.H.Sc. (Honours)

A Thesis Submitted to the School of Graduate Studies in Partial Fulfillment of the  
Requirements for the Degree Doctor of Philosophy

**Descriptive Note**

DOCTOR OF PHILOSOPHY (2019)  
(Biochemistry & Biomedical Sciences)

McMaster University  
Hamilton, Ontario

TITLE: The Bi-directional Vulnerability of Malignant Brain Tumors to Wnt Signaling

AUTHOR: Branavan Manoranjan, B.H.Sc. (Honours) (McMaster University)

SUPERVISOR: Dr. Sheila K. Singh

NUMBER OF PAGES: xviii, 242

## Abstract

Brain tumors represent a leading cause of cancer mortality, of which medulloblastoma (MB) and glioblastoma (GBM) represent the most frequent malignant pediatric and adult brain tumors, respectively. The identification of a rare clonal population of cells, termed cancer stem cells (CSCs) or brain tumor-initiating cells (BTICs), as having the ability to initiate, proliferate, and maintain tumor growth has offered a developmental framework for studying MB and GBM. Evidence in support of cell signaling programs carried forward from brain development into oncogenesis have provided opportunities for BTIC-directed therapies targeting the key BTIC property of self-renewal. Given that neural stem cells (NSCs) must maintain a relative balance between self-renewal and differentiation, brain tumorigenesis may be conceptualized as a disease of unregulated BTIC self-renewal. In this work, I aim to demonstrate the re-emergence of self-renewal genes that regulate NSCs in BTICs, use the Wnt pathway as a model by which these genes may be regulated in a context-specific manner, and identify clinically tractable therapies directed at the overall BTIC self-renewal signaling machinery. Specifically, in Chapter 2, I describe the presence of a shared signaling program between NSCs and MB BTICs consisting of *Bmi1* and *FoxG1*. In Chapter 3, I provide evidence in support of a context-specific tumor suppressive function for activated Wnt/ $\beta$ -catenin signaling in MB. Lastly, in Chapter 4, I demonstrate a CD133-AKT-Wnt signaling axis in which CD133 functions as a putative cell surface receptor for AKT-dependent Wnt activation in GBM. Overall, the body of this thesis offers a mechanistic model by which BTICs may be regulated and

targeted to impair tumor growth and improve overall survivorship in childhood MB and adult GBM.

## Acknowledgements

“There is no substitute for hard work.” A principle engrained in my head by a man who has been working 2 jobs, night and day, since setting foot on this country 30 years ago. “Trust in God.” A belief shared with me by a woman who has overcome every obstacle in her life with a loving heart. Together, they have motivated me to maintain the discipline and perseverance needed to make a dream a reality. I dedicate this work to you – Ammah and Appah.

The seed to pursue a combined MD/PhD was initially planted in my head by my cousin, Dr. Abi Sriharan, who has been a source of inspiration throughout my academic training. There aren't enough words to describe her strength and resilience. I hope our grandparents can be proud of their legacy.

I am forever grateful for the personal interest that Paul Edwards and Linda Guglietti-Moutinho took in my education. They played an instrumental role in facilitating my high school co-operative education placement in medical research and neurosurgery and their passion for teaching fueled my desire to identify my own passion in life.

My high school co-op placement under the supervision of Dr. Michael Cusimano significantly influenced the trajectory of my life. Dr. Cusimano's compassion towards patients, dedication for research, and humility as an instructor provided the perfect model for a neurosurgeon-scientist who embodied the triple-threat of academic neurosurgery – clinician, researcher, and educator. In him I had my first mentor and a standard by which I will judge my future career as a neurosurgeon-scientist. His interest in sharing his love for

neurosurgery and research with a 17-year-old has resulted in the writing of this thesis. Thank you for looking beyond my age and seeing my potential.

My decision to pursue a combined MD/PhD training program was made a reality thanks to Dr. Sheila Singh who offered a supportive and nurturing environment for me to grow and develop as an independent clinician-scientist. Her passion for improving our understanding of brain tumors served as an infectious source of motivation for her colleagues and patients in our collective fight against brain cancer. I am most grateful for her persistent emphasis on clinically-meaningful and clinically-inspired basic science research. I would consider my career a success if I can contribute half as much as she has to our understanding of brain tumors. Thank you for your commitment to my growth not only as a clinician-scientist, but also as a young man. Thank you to my committee members, Dr. Bradley Doble and Dr. John Hassell, for facilitating my maturation as a scientist and helping me develop this body of work over the past 4 years. I am most appreciative of all the past and present members of the Singh Lab who have contributed their expertise to this thesis. Specifically, Dr. Chitra Venugopal who was not only a colleague but my lab mother. She is the heart beat of the Singh Lab and I owe much of my scientific success to her support and guidance. My sincere gratitude to the several funding agencies who generously supported the work carried out in this thesis, specifically, the Vanier Canada Graduate Scholarship.

While the days in graduate school are long, the years are short. I am most appreciative for my close friends for keeping me grounded and true to my values. Special thanks to Joanne Stephen, Dr. Jagbir Khinda, Sylvia Luu, Sharn Khinda, Brandon Balliram,

Dr. Benny Dua, Monika Birdi, John Atkinson, Laura Bainbridge, Abby Enriquez, Elaine Lau, Dr. Safraz Mohammed, and Dr. Celine Yeung for all the laughs and memories.

Lastly, my most sincere and deepest thanks to all the patients who donated their tumor specimen for this thesis. “You beat cancer by how you live, why you live, and in the manner in which you live.” – Stuart Scott

## Table of Contents

<b>Descriptive Note</b> .....	ii
<b>Abstract</b> .....	iii
<b>Acknowledgements</b> .....	v
<b>List of Figures &amp; Tables</b> .....	xi
<b>List of Abbreviations</b> .....	xiv
<b>Declaration of Academic Achievement</b> .....	xvii
<b>Chapter 1: Introduction</b> .....	19
Preface.....	19
1.1 Pediatric medulloblastoma .....	20
1.1.1 Epidemiology.....	20
1.1.2 <i>Clinical presentation and histopathology</i> .....	20
1.1.3 <i>Risk stratification</i> .....	21
1.1.4 <i>Wnt medulloblastoma</i> .....	23
1.1.5 <i>Shh medulloblastoma</i> .....	24
1.1.6 <i>Group 3 medulloblastoma</i> .....	25
1.1.7 <i>Group 4 medulloblastoma</i> .....	26
1.1.8 <i>Treatment</i> .....	27
1.2 Adult glioblastoma .....	29
1.2.1 <i>Epidemiology</i> .....	29
1.2.2 <i>Clinical presentation and histopathology</i> .....	29
1.2.3 <i>Molecular classification</i> .....	30
1.2.4 <i>Treatment and prognosis</i> .....	32
1.3 Brain tumor-initiating cells .....	33
1.3.1 <i>Brain tumor-initiating cells as a framework for neuro-oncology research</i> .....	33
1.3.2 <i>CD133: A Marker of brain tumor-initiating cells</i> .....	36
1.3.3 <i>Medulloblastoma brain tumor-initiating cells</i> .....	38
1.3.4 <i>Glioblastoma brain tumor-initiating cells</i> .....	42
1.4 Canonical Wnt signaling .....	44
1.4.1 <i>Wnt/<math>\beta</math>-catenin signaling</i> .....	44
1.4.2 <i>Wnt signaling in brain development</i> .....	46

1.4.3	<i>Wnt signaling in non-central nervous system malignancies</i> .....	48
1.4.4	<i>Wnt signaling in pediatric medulloblastoma</i> .....	52
1.4.5	<i>Wnt signaling in adult glioblastoma</i> .....	53
1.5	Summary of Intent.....	55
	<b>Chapter 2: FoxG1 interacts with Bmi1 to regulate self-renewal and tumorigenicity of medulloblastoma stem cells</b> .....	59
	Preamble.....	59
	Abstract .....	64
	Introduction .....	65
	Materials & Methods.....	67
	Results .....	75
	Discussion .....	82
	References .....	85
	<b>Chapter 3: Wnt activation as a therapeutic strategy in medulloblastoma</b> .....	113
	Preamble.....	113
	Introduction .....	117
	Results & Discussion .....	117
	Materials & Methods.....	126
	References .....	139
	<b>Chapter 4: A CD133-AKT-Wnt signaling axis drives glioblastoma brain tumor-initiating cells</b> .....	176
	Preamble.....	176
	Abstract .....	179
	Introduction .....	180
	Results .....	181
	Discussion .....	185
	Materials & Methods.....	187
	References .....	194
	<b>Chapter 5: Discussion</b> .....	210
5.1	Summary of Results .....	210

5.2	Context-specific functions of signaling pathways highlight diverse roles in oncogenesis .....	211
5.3	Future directions.....	214
	<b>Bibliography</b> .....	216
	<b>Appendix I: Copyright Statement</b> .....	234
	<b>Appendix II: Accomplishments</b> .....	236

## List of Figures & Tables

### Chapter 1

**Table 1.** Key clinical and molecular features of MB subgroups.....23

**Figure 1.** Canonical Wnt/ $\beta$ -catenin signaling pathway.....45

### Chapter 2

**Figure 1.** Multiple candidate stem cell genes are preferentially expressed in non-Shh/Wnt subgroup medulloblastomas.....95

**Figure 2.** *FoxG1* and *Bmi1* expression identify non-Shh/Wnt subgroup medulloblastomas.....96

**Figure 3.** *FoxG1* and *Bmi1* are significantly expressed in primary medulloblastoma stem cells and Daoy tumor spheres.....97

**Figure 4.** *FoxG1* and *Bmi1* function to regulate proliferation and self-renewal of medulloblastoma stem cells.....98

**Figure 5.** *Bmi1* and *FoxG1* display differential binding at promoters within distinct CD15+ enriched stem cells.....100

**Figure 6.** *Bmi1* is a novel downstream target of *FoxG1*, through which it exerts an increase in tumorigenicity.....101

**Supplementary Figure 1.** *FoxG1* and *Bmi1* knockdown lead to an efficient reduction in their transcript and protein levels.....102

**Supplementary Figure 2.** Functional characterization of *FoxG1* knockdown/overexpression and *Bmi1* knockdown constructs through *in vitro* limiting dilution assays.....103

**Supplementary Figure 3.** Representative flow cytometric cell sorting plot for CD15 in Daoy and Med8a medulloblastoma stem cells.....104

**Supplementary Figure 4.** *FoxG1* and *Bmi1* are differentially enriched in Med8a medulloblastoma cells.....105

**Supplementary Figure 5.** *FoxG1* regulation of MB BTIC differentiation.....106

**Supplementary Figure 6.** Putative MB BTIC marker, CD15, is preferentially expressed in subgroup 3 and 4 MBs.....107

**Supplementary Table 1.** Candidate gene list.....108

**Supplementary Table 2.** Statistical evaluation of candidate genes.....110

<b>Supplementary Table 3.</b> Medulloblastoma stem cell patient isolates: Clinico-pathological data.....	111
<b>Supplementary Table 4.</b> qRT-PCR & ChIP primers.....	111
<b>Chapter 3</b>	
<b>Figure 1.</b> Wnt-activated MBs are less tumorigenic than non-Wnt MBs.....	145
<b>Figure 2.</b> Ectopic expression of $\beta$ -catenin in treatment-refractory MBs reduces self-renewal gene expression and tumor burden while increasing overall survival.....	147
<b>Figure 3.</b> Characterization of Wnt activity in Wnt and non-Wnt MBs.....	149
<b>Figure 4.</b> Wnt signature is present in a minority of non-Wnt MBs cells.....	150
<b>Figure 5.</b> Rare endogenous Wnt-active MB cells from treatment-refractory MBs have reduced tumorigenic properties.....	151
<b>Figure 6.</b> Wnt activation through novel substrate-competitive peptide Wnt agonist (L807mts) alters the transcriptional profile of non-Wnt MBs and reduces their tumorigenic potential.....	153
<b>Figure 7.</b> Pharmacological activation of Wnt signaling in MB impairs stem cell properties and improves overall survival.....	155
<b>Supplementary Figure 1.</b> MB BTIC lines maintain their subgroup affiliation.....	158
<b>Supplementary Figure 2.</b> Wnt MB patient-derived lines maintain distinct transcriptional profile from Group 3 and Group 4 MB lines.....	160
<b>Supplementary Figure 3.</b> Non-Wnt MB lines display enriched expression in oncogenic pathways compared to Wnt MB.....	162
<b>Supplementary Figure 4.</b> Wnt3A-conditioned medium reduces <i>in vitro</i> stemness in treatment-refractory MB lines.....	163
<b>Supplementary Figure 5</b> Non-Wnt MBs express higher levels of Sox2 and Bmi1 when compared to Wnt MB.....	165
<b>Supplementary Figure 6.</b> Quality control of scRNA-seq data to eliminate potential doublets, damaged and low-quality cells.....	167
<b>Supplementary Figure 7.</b> Visually comparing gene signature scoring methods for scRNA-seq data.....	169
<b>Supplementary Figure 8.</b> Small molecule (CHIR99021) Wnt activation impairs key stem cell properties in treatment-refractory MB lines.....	170

<b>Supplementary Table 1.</b> Maximal fold changes for RNA-seq differential gene expression profile.....	171
<b>Supplementary Table 2.</b> Differential pathway networks enrichment.....	172
<b>Supplementary Table 3.</b> Univariate and multivariate analyses of combined Groups 3 and 4 patients based on the <i>Bmi1</i> signature.....	172
<b>Supplementary Table 4.</b> Univariate and multivariate analyses of combined Groups 3 and 4 patients based on the <i>Sox2</i> signature.....	173
<b>Supplementary Table 5.</b> Univariate and multivariate analyses of Groups 3 patients based on the <i>Wnt</i> signature.....	174
<b>Chapter 4</b>	
<b>Figure 1.</b> CD133 expression correlates with Wnt activity in GBM.....	200
<b>Figure 2.</b> CD133 regulates Wnt in an AKT-dependent manner.....	201
<b>Figure 3.</b> Upstream inhibition of CD133 or AKT impairs downstream Wnt activity...	202
<b>Figure 4.</b> Endogenous Wnt active BT241 GBM cells display enhanced tumorigenicity in an AKT-dependent manner.....	203
<b>Supplementary Figure 1.</b> CD133 cell staining gating strategies in GBM lines.....	204
<b>Supplementary Figure 2.</b> Self-renewal potentials in GBM lines.....	205
<b>Supplementary Figure 3.</b> Gating strategy for GFP+ cell-sorting and limiting dilution assays of OE Control and OE CD133 GBM samples.....	205
<b>Supplementary Figure 4.</b> Small molecule targeting of CD133 or AKT impairs downstream Wnt signaling in GBM BTICs.....	206
<b>Supplementary Figure 5.</b> Flow cytometry analysis of surface CD133 expression following CD133 inhibition.....	207
<b>Supplementary Figure 6.</b> Wnt activation through endogenous mechanisms increase overall tumor burden.....	208
<b>Supplementary Table 1.</b> Clinical demographics.....	209

### List of Abbreviations

$\beta$ -TrCP –  $\beta$ -Transducin repeats-containing proteins  
AKT – protein kinase B  
APC – adenomatous polyposis coli  
ATP – adenosine triphosphate  
Axin2 – axis inhibition protein 2  
bFGF – basic fibroblast growth factor  
Bmi1 – B cell-specific Moloney murine leukemia virus integration site 1  
BT – brain tumor  
BTIC – brain tumor-initiating cell  
CD15 – cluster of differentiation 15  
CD133 – cluster of differentiation 133  
cDNA – complementary DNA  
ChIP – chromatin immunoprecipitation  
CK1 – casein kinase 1  
CNS – central nervous system  
COG – Children’s Oncology Group  
CSC – cancer stem cell  
CSF – cerebrospinal fluid  
CT – computed tomography  
CTNNB1 –  $\beta$ -catenin  
DAPI – 4’,6-diamidino-2-phenylindole  
DMSO – dimethyl sulfoxide  
DNA – deoxyribonucleic acid  
Dvl – dishevelled  
EDTA – ethylenediaminetetraacetic acid  
EGF – epidermal growth factor  
EGFR – epidermal growth factor receptor  
FBS – fetal bovine serum  
FDR – false discovery rate  
FFPE – formalin-fixed paraffin-embedded  
FISH – fluorescent in situ hybridization  
FoxG1 – forkhead box G1  
FSTL5 – follistatin like 5  
Fz – frizzled  
GALNT14 – polypeptide N-Acetylgalactosaminyltransferase 14  
GAPDH – glyceraldehyde 3-phosphate dehydrogenase  
GBM – glioblastoma  
GEO – Gene Expression Omnibus  
GFAP – glial fibrillary acidic protein  
GFI1 – growth factor independent 1  
GFP – green fluorescent protein  
GSEA – gene set enrichment analysis  
GSK-3 – glycogen synthase kinase-3

GSVA – gene set variation analysis  
H&E – hematoxylin and eosin  
HDAC – histone deacetylase  
IF – immunofluorescence  
IgG – immunoglobulin G  
hNSC – human neural stem cell  
KCNA1 – potassium voltage-gated channel subfamily A member 1  
LEF – lymphoid enhancer factor  
LGR5 – leucine-rich repeat-containing G-protein coupled receptor 5  
LRP5/6 – low-density lipoprotein receptor-related protein 5 or 6  
MAD – median absolute deviation  
MAP2 – microtubule-associated protein 2  
MB – medulloblastoma  
MBEN – medulloblastoma with extensive nodularity  
MRI – magnetic resonance imaging  
mRNA – messenger ribonucleic acid  
Myc – v-myc avian myelocytomatosis viral oncogene homolog  
NOD-SCID – nonobese diabetic-severe combined immunodeficiency  
NFATC4 – nuclear factor of activated T cells, cytoplasmic 4  
NPR3 – natriuretic peptide receptor 3  
NSC – neural stem cell  
Oct4 – octamer-binding transcription factor 4  
OE – overexpression  
Olig2 – oligodendrocyte transcription factor 2  
ORF – open reading frame  
p16 – cyclin-dependent kinase inhibitor 2A  
p21 – cyclin-dependent kinase inhibitor 1  
pAKT – phosphorylated protein kinase B  
PBS – phosphate buffered saline  
PCA – principal component analysis  
pGSK – phosphorylated glycogen synthase kinase  
PI3K – phosphatidylinositol 3-kinase  
PTEN – phosphatase and tensin homolog  
qPCR – quantitative polymerase chain reaction  
RNA – ribonucleic acid  
RNA-seq – ribonucleic acid sequencing  
RT – reverse transcriptase  
scRNA – single cell ribonucleic acid  
SFRP1 – secreted frizzled related protein 1  
Shh – sonic hedgehog  
shRNA – short hairpin ribonucleic acid  
Smo – smoothened  
Sox2 – SRY (sex determining region Y)-box 2  
SSEA1 – stage-specific embryonic antigen-1

ssGSEA – single-sample gene set enrichment analysis  
TCF – T-cell factor  
Tert – telomerase reverse transcriptase  
TGF- $\beta$  – transforming growth factor-beta  
TIC – tumor-initiating cell  
TLE – transducin-like enhancer of split  
TMA – tissue microarray  
tSNE – t-distributed stochastic neighbor embedding  
Twist1 – twist family basic helix-loop-helix transcription factor 1  
UMI – unique molecular identifier  
Zic1 – zinc finger of the cerebellum 1

### **Declaration of Academic Achievement**

This thesis represents original work, which I conceptualized and performed with respect to experiments, data analysis and interpretation, and writing of all sections. Dr. Sheila Singh supervised this work. Contributions of co-authors to each publication have been noted in Chapters 2-4. This thesis is presented in the format of a sandwich thesis as outlined in the Guide for Preparation of Master's and Doctoral Theses (v2016).

Chapter 1 provides an overview of the field of medulloblastoma and glioblastoma research.

Chapter 2 is an original published article describing the role of neural stem cell self-renewal pathways in medulloblastoma stem cells. The citation is as follows:

- Manoranjan B, Wang X, Hallet RM, Venugopal C, Mack SC, McFarlane N, Nolte SM, Scheinemann K, Gunnarsson T, Hassell JA, Taylor MD, Lee C, Triscott J, Dunham C, Hawkins C, Dunn SE, Singh SK. FoxG1 interacts with Bmi1 to regulate self-renewal and tumorigenicity of medulloblastoma stem cells. *Stem Cells*. 2013;31:1266-1277.

Chapter 3 describes inhibition of medulloblastoma stem cell self-renewal as a potential mechanism by which activated Wnt signaling promotes a survival advantage in children diagnosed with medulloblastoma. This manuscript was submitted to *Nature Medicine* on December 18, 2018 and is currently under review. The citation is as follows:

- Manoranjan B, Venugopal C, Bakhshinyan D, Richards L, Kameda Smith MM, Adile A, Whitley O, Dvorkin-Gheva A, Subapanditha M, Savage N, Tatari N, Winegarden N, Hallet R, Provias JP, Yarascavitch B, Ajani O, Fleming A, Bader

GD, Pugh T, Doble BW, Singh SK. Wnt activation as a therapeutic strategy in medulloblastoma.

Chapter 4 describes a signaling mechanism by which CD133 activates Wnt signaling in an AKT-dependent pathway. This manuscript was submitted to *Oncogene* on September 25, 2018 and is currently under review. The citation is as follows:

- Manoranjan B, Chokshi C, Venugopal C, Mahendram S, Subapanditha M, Savage N, Tatari N, Provias JP, Murty NK, Moffat J, Doble BW, Singh SK. A CD133-AKT-Wnt signaling axis drives glioblastoma brain tumor-initiating cells.

Chapter 5 discusses the major implications of the research presented in this thesis and explores future research directions to improve our understanding of medulloblastoma and glioblastoma.

## Chapter 1: Introduction

### Preface

This thesis presents research on the role of Wnt/ $\beta$ -catenin signaling in regulating the self-renewal of brain tumor-initiating cells (BTICs) in pediatric medulloblastoma (MB) and adult glioblastoma (GBM). Seminal work for this thesis originates from the identification of BTICs (Hemmati et al., 2003; Singh et al., 2003; Singh et al., 2004), which provided a paradigm shift in the study and treatment of brain tumors. Specifically, for the first time, distinct cell populations were recognized to harbour unique differences in genetic and functional determinants of oncogenesis. Additional foundational work that inspired this thesis stems from the characterization of Wnt/ $\beta$ -catenin signaling in forebrain and hindbrain development where the pathway promotes the expansion (Chenn & Walsh, 2002, 2003; W. Y. Kim et al., 2009; Zechner et al., 2003) and differentiation (Lorenz et al., 2011; Pei, Brun, et al., 2012) of neural stem cells (NSCs), respectively. These observations have been reproduced in human forebrain and hindbrain malignancies where Wnt/ $\beta$ -catenin enhances the self-renewal of GBM BTICs (Rajakulendran, et al., 2018), while a protective role that promotes survivorship has been implied in MB (Northcott, et al., 2011). In this thesis the term MB and GBM will be used in reference to the pediatric and adult forms of these malignancies, respectively. Wnt signaling will be used synonymously with Wnt/ $\beta$ -catenin signaling. This introduction will provide an overview of the current clinico-pathological features of MB and GBM, along with an overview of Wnt/ $\beta$ -catenin signaling in neural development. The chapter closes with a description of

Wnt in MB, GBM, and non-central nervous system (CNS) malignancies that have served as models for the hypotheses generated in this thesis.

## **1.1 Pediatric medulloblastoma**

### *1.1.1 Epidemiology*

MB accounts for up to 20% of all pediatric brain tumors and represents the most common malignant childhood brain tumor. Given the biphasic incidence in age of onset with peaks at 3-4 and 8-9 years of age, most MB cases are diagnosed before 15 years of age, making adult MB a rare occurrence (0.4-1% of adult brain tumors. The annual incidence is estimated at 1:200,000 for children under the age of 15 (McKean-Cowdin et al., 2013; Ostrom et al., 2018).

### *1.1.2 Clinical presentation and histopathology*

Since MB almost exclusively occurs in the posterior fossa, patients often present with signs and symptoms in keeping with raised intracranial pressure secondary to hydrocephalus from obstruction of the fourth ventricle. Symptoms include nausea, vomiting, and headache. Signs include dysmetria, diplopia due to cranial nerve six palsy, and truncal ataxia (Packer, Cogen, Vezina, & Rorke, 1999). Neuroimaging consisting of non-contrast computer tomography (CT) and magnetic resonance imaging (MRI) are used to determine the presence of intracranial mass lesions. On CT, MB often appears as a hyperdense, midline mass that enhances with the use of a contrast dye. MRI with

gadolinium, the ideal imaging study, demonstrates heterogeneous enhancement (Tortori-Donati et al., 1996).

Historically, MB was diagnosed by histology alone. The classic microscopic description based on hematoxylin and eosin (H&E) staining of MB is a small, round, blue cell tumor due to the presence of densely packed cells with prominent nuclei surrounded by scant cytoplasm. Among this general description exist 5 histologic variants (Louis et al., 2007): classic, desmoplastic/nodular, MB with extensive nodularity (MBEN), large cell, and anaplastic. Clinical data indicates a favourable prognosis for the desmoplastic/nodular variant and a worse outcome for children diagnosed with large cell/anaplastic MBs (Louis et al., 2007). However, with the advent of molecular diagnostics, the clinical utility of histology has become limited as molecular subgroups are more closely linked to patient demographics and overall prognosis.

### *1.1.3 Risk stratification*

Clinical trials involving patients with MB have historically risk stratified patients according to clinical rather than biological factors. These trials have collectively yielded 80% and 60% 5-year survival rates for average-risk and high-risk patients, respectively (Ramaswamy et al., 2016). Clinical parameters for risk stratification include age at diagnosis, extent of resection, and presence of metastasis at time of diagnosis. High-risk patients are defined as children <3 years of age, greater than 1.5 cm<sup>2</sup> of residual tumor post-operatively, or with metastatic disease at presentation (Zeltzer et al., 1999). Those patients

without any high-risk features are classified as average-risk leading to a different treatment algorithm.

Recent integrated genomics studies have reconceptualized the biologic heterogeneity in MB. MB is now recognized to contain at least 4 distinct molecular variants: Wnt, sonic hedgehog (Shh), Group 3, and Group 4 (Table 1) (Cho et al., 2011; Kool et al., 2012; Kool et al., 2008; Northcott et al., 2011; Pomeroy et al., 2002; Thompson et al., 2006). These subgroups are characterized by distinct cytogenetic aberrations, transcriptomics, demographics, and survivorship. Diagnostically, the most robust method for clustering patients into discrete subgroups involves the use of a 22-gene nanoString expression signature, which can assign up to 88% of formalin-fixed paraffin-embedded (FFPE) specimens with up to 98% accuracy (Northcott, Shih, et al., 2012).

Further refinement of risk stratification using molecular parameters has defined four risk groups based on survival: low-risk (>90% survival), standard-risk (75-90% survival), high-risk (50-75% survival), and very high-risk (<50% survival) (Ramaswamy et al., 2016). Low-risk patients consist of non-metastatic Wnt MB under the age of 16 and non-metastatic Group 4 MB with loss of chromosome 11. Standard-risk patients comprise the following: non-metastatic Shh MB with wild-type *TP53* (somatic or germline) and no *MYCN* amplification; non-metastatic Group 3 MB without *MYC* amplification; and non-metastatic Group 4 MB without chromosome 11 loss. High-risk patients include metastatic or *MYCN* amplified Shh MB and metastatic Group 4 MB. Lastly, very high-risk patients include *TP53* mutated Shh MB irrespective of metastatic status and metastatic Group 3 MB.

	<b>Wnt</b>	<b>Shh</b>	<b>Group 3</b>	<b>Group 4</b>
<b>Frequency</b>	10%	30%	25%	35%
<b>Gender (M:F)</b>	1:1	3:2	2:1	3:1
<b>Age distribution</b>	children	infant, adult	infant, children	children, adult
<b>Frequency of metastasis</b>	rare	uncommon	very common	common
<b>5-year survival</b>	>95%	75%	50%	75%
<b>Genomic signature</b>	Wnt signaling	Shh signaling	Retinal signature, MYC signature	Neuronal signature
<b>Key recurrent somatic mutations / focal SCNAs</b>	<i>CTNNB1</i> (90.6%), <i>MYC</i> (16.7%), <i>DDX3X</i> (50), <i>SMARCA4</i> (26.3%), <i>TP53</i> (12.5%)	<i>PTCH1</i> (28%), <i>TP53</i> (13.6%), <i>MYCN</i> (8.2%), <i>GLI2</i> (5.2%)	<i>MYC</i> (16.7%), <i>PVT1</i> (11.9%), <i>SMARCA4</i> (10.5%), <i>OTX2</i> (7.7%),	<i>KDM6A</i> (13%), <i>SNCAIP</i> (10.4%), <i>MYCN</i> (6.3%)

Table 1: Key clinical and molecular features of MB subgroups

#### 1.1.4 Wnt medulloblastoma

Wnt MB accounts for approximately 10% of cases and occurs most frequently in older children with a peak incidence in the age group of 10-12 years. Patients less than 16 years with Wnt tumors have an excellent prognosis with 5-year survival rates >95% (Kool et al., 2012; Ramaswamy et al., 2016). Anatomically, Wnt MBs are almost exclusively located near the brainstem and fourth ventricle as they are thought to originate from progenitor cells from the lower rhombic lip (Gibson et al., 2010). Although Wnt MB is primarily a genomically bland tumor, recurrent, activating somatic mutations in exon 3 of *CTNNB1* (which encodes  $\beta$ -catenin) are found in 85-90% of cases and monosomy 6 is seen in 70-80% of patients (Northcott, Jones, et al., 2012). Less frequent somatic mutations have

been detected in *TP53*, the DEAD-box RNA helicase *DDX3X*, involved in cellular growth and division, and the chromatin-modifier *SMARCA4* (Jones et al., 2012; Pugh et al., 2012; Robinson et al., 2012). Rare germline inactivating mutations in adenomatous polyposis coli (*APC*) that are consistent with Turcot syndrome have also been shown to result in Wnt MB (Hamilton et al., 1995). Diagnostically, Wnt MB may be identified with sequencing of exon 3 in *CTNBI*, DNA methylation profiling, immunohistochemistry for nuclear  $\beta$ -catenin, and/or fluorescent *in situ* hybridization (FISH) or DNA copy number array profiling for monosomy 6. Given the remarkable outcome for patients with Wnt MB, current molecular clinical trials are focused on the de-escalation of therapy for these patients: NCT02066220, NCT01878617, NCT02724579.

#### 1.1.5 *Shh medulloblastoma*

Shh MB represents 30% of MBs and occurs in a bimodal age distribution, most frequently in infants (<3 years) and adults (>16 years) (Taylor et al., 2012). Histology is typically of the nodular/desmoplastic type with MBEN being exclusively classified as Shh MB (Taylor et al., 2012). Genetic alterations in Shh tumors are highly age dependent. *Ptch1* mutations are the most prevalent mutation, reported in 36-54% of cases (Kool et al., 2012). These mutations were originally identified as germline mutations present in patients with Gorlin syndrome (nevoid basal-cell carcinoma syndrome) presenting with MB (Smith et al., 2014). Since then *Ptch1* mutations have been found to occur at similar frequencies in infants (36%), children (42%), and adults (54%) (Kool et al., 2012). *SUFU* mutations are found almost exclusively in infants and *Smo* mutations are enriched in adult Shh MB

(Northcott et al., 2017). Children between 3-16 years have mutually exclusive somatic mutations in *Ptch1* or germline and/or somatic *TP53* mutations (Zhukova et al., 2013). As with most other features in Shh MB, patient outcomes are also age-specific (Ramaswamy et al., 2016). Infants with Shh MB maintain an excellent outcome, whereas children with *TP53*-mutant Shh MB have a dismal prognosis compared with *TP53*-wildtype tumors. Shh MBs have benefitted the most from small molecule inhibitors. Specifically, Smo inhibitors are currently being investigated, however, their clinical utility remains to be determined as Shh pathway activation downstream of Smo is frequently seen in high-risk Shh MBs (Kool et al., 2014). Novel therapeutic strategies are currently investigating the role of bromodomain (Tang et al., 2014) and PI3K inhibitors (Buonamici et al., 2010).

#### 1.1.6 Group 3 medulloblastoma

Group 3 MB constitutes 25% of MBs and is associated with a poor prognosis consisting of a 50% 5-year survival as nearly half of all patients present with metastatic disease at diagnosis (Ramaswamy et al., 2016). While GABAergic and photoreceptor pathways are activated in these tumors (Cho et al., 2011; Kool et al., 2008; Northcott et al., 2011), targeted therapies at these signaling programs have yet to show clinical significance. The most common cytogenetic aberration is *MYC* amplification (Kool et al., 2012), which is seen in 10-20% of tumors and may occur as *PVT1-MYC* fusions, representing the first recurrent gene fusion identified in MB (NorthcottShih, et al., 2012). Additional structural variants that place enhancers upstream of the growth factor independent 1 (GF1) family of proto-oncogene locus, termed enhancer hijacking, are observed in 20% of Group 3 MBs

(Northcott et al., 2014). The most frequent chromosomal arm-level copy number alteration is isochromosome 17q (i17q), which is present in 40% of tumors (Taylor et al., 2012). While current treatment regimens consist of high-risk protocols for MB, the presence of aberrant transforming growth factor-beta (TGF- $\beta$ ) signaling in over 20% of tumors (Pei, Moore, et al., 2012; Swartling et al., 2012) and the efficacy of histone deacetylase (HDAC) (Pei et al., 2016) and bromodomain inhibitors (Bandopadhyay et al., 2014) in preclinical studies have provided potential therapeutic agents for Group 3 MB.

#### *1.1.7 Group 4 medulloblastoma*

Group 4 MB is the most frequent subgroup accounting for 35% of all MBs, however, it is the least well characterized biologically. Prior transcriptional data identified the overexpression of neuronal and glutaminergic pathways (Cho et al., 2011; Northcott et al., 2011) with more recent data suggesting these tumors to be driven by copy number alterations. Tandem duplications of *SNCAIP* are seen in 10% of tumors and represent the most common somatic copy number aberration (NorthcottShih, et al., 2012). Although this gene is mutated in a subset of Parkinson's disease patients and is involved in the formation of cytoplasmic inclusions and neurodegeneration, its biological relevance in MB remains to be determined. The duplications in *SNCAIP* are mutually exclusive from *MYCN* amplifications, which are seen in 5-10% of tumors (Northcott, Jones, et al., 2012; NorthcottShih, et al., 2012). Unlike Shh MB, *MYCN* amplification does not correlate with a poor outcome in Group 4 MB (Korshunov et al., 2012; Shih et al., 2014). i17q, which is present in 80% of tumors represents the most common cytogenetic aberration (Northcott

et al., 2011; Taylor et al., 2012). Mutations in chromatin-remodelling genes *KDM6A*, *CHD7*, and overexpression of *EZH2* are thought to maintain Group 4 MB cells in an undifferentiated state, paralleling the role of these genes in normal stem cell function (Jones et al., 2012; Pugh et al., 2012; Robinson et al., 2012). Clinically, Group 4 MBs have an intermediate prognosis with some series reporting an excellent prognosis with >90% survival for patients with non-metastatic tumors (Ramaswamy et al., 2016). Both, loss of chromosome 11 and the presence of *i17q* confer an excellent prognosis irrespective of metastatic status (Shih et al., 2014).

#### *1.1.8 Treatment*

As previously described, patients with MB typically present with signs and symptoms in keeping with hydrocephalus due to obstruction of the fourth ventricle by the tumor. Patients are often initially managed with corticosteroids to reduce peritumoral edema and cerebrospinal fluid (CSF) diversion to manage hydrocephalus. The complete multimodal treatment algorithm consists of maximal safe surgical resection, radiation therapy to the tumor bed and craniospinal axis, and systemic adjuvant chemotherapy (Gilbertson, 2004). In children older than 3 years of age with non-metastatic MB, gross total or near-total surgical resection has consistently been shown to correlate with improved survivorship. Patients are risk stratified into average- or high-risk based on extent of resection.

Radiation therapy allows for the control of residual tumor in the surgical bed and for the treatment of leptomeningeal metastases along the craniospinal axis, which are not

amenable to surgery. Although adjuvant cisplatin-based chemotherapy is used as a radiosensitizer when delivering radiation therapy, toxicity to the developing nervous system has precluded radiotherapy in children less than 3 years of age. Average-risk patients are treated with 2430 cGy to the craniospinal axis and a posterior fossa boost for a total dose of 5400-5580 cGy (Gilbertson, 2004). High-risk patients are treated with a higher craniospinal dosage of 3600 cGy and a posterior fossa boost of 4500 cGy. These regimens have resulted in 5-year survival rates as high as 85% and 65% for average- and high-risk patients, respectively (Gilbertson, 2004)

As a necessary treatment modality in all protocols, chemotherapy is of particular value to those children less than 3 years of age who are not given radiation therapy. As per the Children's Oncology Group (COG) protocol (Packer et al., 2006), average-risk patients receive 4-9 cycles of cisplatin-based adjuvant chemotherapy consisting of vincristine during radiation therapy followed by 8 cycles of one of two protocols (vincristine, cisplatin, and CCNU or vincristine, cisplatin, and cyclophosphamide). High-risk patients generally receive high-dose chemotherapy with autologous hematopoietic stem cell transplantation, and radiotherapy. Management of these children according to COG (Jakacki et al., 2012) involves up to 30 doses of carboplatin with vincristine while receiving radiation followed by 6 months of maintenance chemotherapy.

As current multimodal therapy regimens have resulted in significant improvements in 5-year survivorship for MB patients irrespective of risk status, long-term treatment sequelae have also begun to emerge in surviving patients. These include neuroendocrine dysfunction, neurocognitive deficits, and secondary malignancies (Brodin et al., 2012;

Chemaitilly & Sklar, 2010; Pietila et al., 2012; Schreiber et al., 2014; Tsui et al., 2015). The utility of novel small molecules is largely dependent on their ability to serve as radiosensitizers and thereby reduce the radiation-induced sequelae seen in survivors of MB.

## **1.2 Adult glioblastoma**

### *1.2.1 Epidemiology*

GBM is the most common primary adult brain tumor accounting for 15% of all intracranial neoplasms and approximately 54% of all gliomas (Ostrom et al., 2018). The peak incidence of GBM is estimated to be 3.2 per 100,000 population (Ostrom et al., 2018). A significant increase in incidence is noted after the age of 54, reaching a peak incidence of 14.24 per 100,000 population between 75-84 years (Ostrom et al., 2018).

### *1.2.2 Clinical presentation and histopathology*

Clinically, patients with GBM present with symptoms in keeping with functional deficits of the involved brain region. Headaches, while frequently seen in half the patients at diagnosis, may have a nonspecific pattern or be new in onset with unilateral localization with increasing intensity throughout the day (Alexander & Cloughesy, 2017; Forsyth & Posner, 1993). Additional signs and symptoms in keeping with increased intracranial pressure such as nausea, vomiting, and papilledema may also be present. Additional findings that may be reflective of tumor location include motor or sensory deficits with cognitive impairments and personality changes often being mistaken for psychiatric

disorders or dementia in elderly patients (Alexander & Cloughesy, 2017). 20-40% of patients may present with seizures as the initial sign with no other findings (Glantz et al., 2000), and therefore, neuroimaging plays a critical diagnostic role in these patients. Brain MRI with and without contrast is the gold-standard imaging modality. The typical findings seen on MRI include infiltrative, heterogeneous, ring-enhancing lesions with central necrosis and vasogenic edema (Alexander & Cloughesy, 2017). The increased mitotic activity of GBM cells is appreciated in the rare circumstances where a small, non-enhancing lesion is initially seen and then rapidly changes to a ring-enhancing, necrotic lesion within weeks (Alexander & Cloughesy, 2017).

As with any solid tumor, the diagnosis of GBM is based on the histopathology of FFPE tissue obtained from surgical specimens. Microscopically, tumor cells show diffuse immunoreactivity for the glial cell marker, glial fibrillary acidic protein (GFAP) (Alexander & Cloughesy, 2017). While this feature is shared among all gliomas, the presence of other histopathological features is dependent on the WHO glioma grade. The WHO classification system groups gliomas into 4 histological grades defined by increasing degrees of nuclear pleomorphism, mitotic activity, microvascular proliferation, and necrosis (Alexander & Cloughesy, 2017). All these malignant features are present only in GBM, making it a WHO grade IV glioma. With shortcomings in histology-based diagnostics such as variable clinical behaviour not accurately predicted by WHO grade alone and inter-observer subjectivity, molecular diagnostics have been used to characterize clinical outcomes with greater accuracy.

### *1.2.3 Molecular classification*

GBMs may be classified as primary or secondary based on their evolution (Ohgaki & Kleihues, 2013). Primary GBMs arise *de novo* and account for 90% of all cases. They tend to occur in older individuals (mean age 55 years) and are characterized by *EGFR* overexpression, *PTEN* mutation, and wild-type isocitrate dehydrogenase 1 or 2 (*IDH*) (Brennan et al., 2013; Parsons et al., 2008; Verhaak et al., 2010). By contrast, secondary GBMs arise from the transformation of low-grade diffuse astrocytoma (WHO grade II) or anaplastic astrocytoma (WHO grade III) into a GBM and account for 10% of all GBMs. Clinically, secondary GBMs are seen in younger patients (mean age 40 years) and are characterized by *PDGFRA* amplifications and mutations in *TP53* and *IDH* (Brennan et al., 2013; Parsons et al., 2008; Verhaak et al., 2010). The presence of *IDH* mutations is associated with better outcome and increased overall survival.

Similar to MB, integrated genomics have provided a framework to interrogate the extensive molecular heterogeneity present in GBM by identifying four subgroups: neural, proneural, classical, and mesenchymal; with the latter three subgroups having been validated by several datasets (Brennan et al., 2013; Parsons et al., 2008; Phillips et al., 2006; Verhaak et al., 2010). Proneural tumors are characterized by *IDH* and *TP53* mutations, *PDGFRA* amplification and mutations, and the expression of a stem cell gene signature. By contrast, the classical subgroup primarily contains *EGFR* amplifications and mutations. The mesenchymal subgroup contains mutations in *PTEN*, *TP53*, and *NF1* deletions and mutations. The neural subgroup was initially characterized by the expression of neuronal markers (*NEFL*, *GABRA1*) but subsequent reports suggested the subgroup to represent normal cell infiltrates as opposed to true tumor cells (Patel et al., 2014). While

the classification of GBM into molecular subgroups attempted to address the presence of molecular heterogeneity with the hope of targeted therapies, recent work has demonstrated subgroup affiliation to vary within different regions of a given tumor (Sottoriva et al., 2013). Single cell RNA-sequencing has provided further evidence to question the clinical utility of GBM subgroups as individual cells of a given tumor have been shown to consist of a heterogeneous mixture of cells representative of all subgroups (Patel et al., 2014), highlighting the need for personalized polytherapy in which multiple pathways are targeted to account for the high degree of genomic heterogeneity.

#### *1.2.4 Treatment and prognosis*

Standard of care for the multimodal management of GBM involves maximal safe surgical resection followed by the Stupp protocol (Stupp et al., 2005) consisting of radiotherapy and chemotherapy with the DNA alkylating agent temozolomide (TMZ). The initial temporary management of symptoms related to the compression of nearby brain structures from peritumoral edema consists of corticosteroids with antiepileptics reserved only for those patients who present with seizures (Glantz et al., 2000). Surgical resection aims to relieve mass effect and provide adequate tissue for histology and molecular diagnostics. Subsequent adjuvant radiotherapy and chemotherapy consists of 60 Gy divided into 30 fractions and daily low-dose TMZ (75 mg/m<sup>2</sup>), respectively. This is followed by six courses of adjuvant TMZ (150-200 mg/m<sup>2</sup>) per day on days 1-5 of a 4-week course. The use of combined radiation and chemotherapy with TMZ has increased median survival from 12 to 14.6 months and 2-year survivorship from 10 to 27% (Stupp et

al., 2005). The biological mechanism for this survival benefit has been attributed to promoter methylation of the DNA repair enzyme O6-methylguanine-DNA methyltransferase (MGMT), which prevents the repair of TMZ-induced methylation of guanine residues allowing for tumor cell apoptosis (Hegi et al., 2005). Recently, patients with MGMT methylated GBMs have been shown to benefit from the addition of lomustine to the Stupp protocol with an improvement in median overall survival from 31.4 months with TMZ to 48.1 months with lomustine-TMZ (Herrlinger et al., 2019). However, given the small sample size of this study, additional large-scale studies are required to validate the benefit of adding lomustine to current standard of practice in MGMT methylated GBM.

Unfortunately, all patients with GBM invariably relapse after first-line treatment with a median progression-free survival (PFS) of 7-10 months (Omuro & DeAngelis, 2013). Surgical resection may be considered to relieve mass effect or to determine the molecular characteristics of the recurrent tumor, but survival benefits have been equivocal (van Linde et al., 2017). Furthermore, surgery is not indicated in most relapsed patients due to tumor location, widespread disease, or poor physical performance status. Given uniform first-line treatment failure in GBM, novel therapeutic strategies are warranted.

### **1.3 Brain tumor-initiating cells**

#### *1.3.1 Brain tumor-initiating cells as a framework for neuro-oncology research*

James Homer Wright identified MB as a distinct CNS tumor in 1910 (Wright, 1910). At the time Wright believed MB to arise from restricted neuronal precursors termed *neuroblasts*. Shortly thereafter in 1925, Percival Bailey and Harvey Cushing described the

presence of glial and neuronal cells in MB suggesting the cell of origin to be of a more primitive embryonic neuroepithelial cell, which they termed *medulloblast*, resulting in the conceptual link between NSCs and brain tumorigenesis (BAILEY & CUSHING, 1925). Since then this observation has evolved into what is now termed the cancer stem cell (CSC) hypothesis (Kreso & Dick, 2014; Magee, Piskounova, & Morrison, 2012; Shackleton, Quintana, Fearon, & Morrison, 2009). This hypothesis suggests that a relatively small fraction of tumor cells, termed *CSCs*, have the ability to self-renew, proliferate, and maintain tumor growth. This is in sharp contrast to all other cells of the bulk tumor, which are characterized by limited self-renewal and proliferative capacity and a more specified lineage potential. It is important to note that *CSCs* are based on a functional definition, having no implication on the cellular origin of a tumor, and therefore, a *CSC* may represent a transformed tissue-specific stem, progenitor, or differentiated cell.

*CSCs* have classically been defined with cell surface markers, isolated using flow cytometric cell sorting, and functionally validated based on their ability to initiate and serially propagate orthotopic xenografts in immunodeficient mice. The first demonstration of a *CSC* hierarchy in human disease was in acute myeloid leukemia where *CD34<sup>+</sup>/CD38<sup>-</sup>* cells were shown to contain the leukemic cell fraction capable of generating xenografts, which resembled human leukemia (Lapidot et al., 1994). Similarly, *CD133* was originally used to enrich for BTICs in human MB and GBM (Singh et al., 2003; Singh et al., 2004). The use of single-cell RNA-seq technology to assess clonal populations inherently present in GBM has provided further insight into the clonal architecture of GBM (Patel et al., 2014). Interestingly, a developmental hierarchy has been shown to exist in GBM where

rare undifferentiated cells are driven by NSC signaling programs in contrast to the bulk tumor, which is enriched in the expression of differentiation pathways (Patel et al., 2014). These data support the propagation of developmental signaling programs from ontogeny into oncology to establish a functional cellular hierarchy reminiscent of tissue-specific stem cells.

The clinical importance of BTICs is demonstrated by increasing BTIC frequency and BTIC self-renewal capacity to be associated with poor patient outcome (Laks et al., 2009; Pallini et al., 2011; Panosyan et al., 2010). Furthermore, by evading chemotherapy (Chen et al., 2012; G. Liu et al., 2006) and radiation (Bao et al., 2006), BTICs function to promote tumor recurrence and patient relapse. Fewer than 12% of diagnostic genetic events have been shown to be present in recurrent MB when compared to matched-primary samples (Morrissy et al., 2016). While clonal divergence may account for this difference in temporal changes of dominant clones seen at diagnosis and recurrence, subclonal analysis revealed the presence of a slow-cycling clone that was present at both disease onset and recurrence (Morrissy et al., 2016). Similar observations have been made in GBM where recurrent tumors are derived from subclonal cell populations present at diagnosis (Johnson et al., 2014). The presence of clonal cell populations shared between primary and recurrent tumors further supports the role of BTICs in initiating tumor growth, escaping therapy, and promoting disease recurrence.

### 1.3.2 *CD133: A Marker of brain tumor-initiating cells*

*CD133 (Prominin1)* is located on chromosome 4 in humans and chromosome 5 in mice with approximately 60% homology between primates and rodents (Corbeil et al., 2013). Transcription of human *CD133* is driven by five alternative promoters, three of which are located on CpG islands and are partially regulated by methylation. These promoter regions often result in alternative splicing of *CD133* mRNA, resulting in tissue-specific *CD133* structural variants (Shmelkov et al., 2004). The protein product of *CD133* is a 97 kDa cell surface glycoprotein that contains five transmembrane regions with extracellular domains, which may be glycosylated at nine different sites to produce a 120 kDa protein (Corbeil et al., 2013). While the biologic function of *CD133* is poorly understood, *CD133* is known to be preferentially localized in plasma membrane protrusions and microvilli, indicating a possible role in membrane organization (Corbeil et al., 2001; Roper et al., 2000). Specifically, *CD133* has been shown to bind directly to cholesterol-containing lipid rafts (Corbeil et al., 2001; Roper et al., 2000). *CD133* knockout mice support the presumed role of *CD133* as a scaffolding protein as these mice display defects of the outer segment of photoreceptor cells (Zacchigna et al., 2009).

With respect to a developmental role for *CD133*, it was initially discovered as a hematopoietic stem cell marker (Yin et al., 1997). In an attempt to characterize markers of NSCs, Uchida, *et al.* (Uchida et al., 2000) selected hybridomas that produced monoclonal antibodies against clonogenic NSCs from human fetal brain. Using these antibodies, they were able to isolate *CD133*<sup>+</sup>/*CD34*<sup>-</sup>/*CD45*<sup>-</sup> cells that adequately separated human fetal brain cells with an enhanced neurosphere-forming capacity that were able to function as

clonogenic NSCs. Specifically, the CD133 enriched fraction of cells functioned as clonogenic human NSCs *in vitro* and *in vivo*, identifying 95% of all neurosphere-forming cells, and 1-6% of total fetal brain.

CD133 further identifies TIC populations in multiple human cancers where CD133+ cells exhibit an enriched ability to self-renew and regenerate histologically similar tumors in immunocomprised mouse xenografts (Grosse-Gehling et al., 2013). Clinically, CD133 expression correlates with disease progression, metastasis, recurrence, and poor overall survival in several human malignancies, but insight into its function remains limited (Shibahara et al., 2013; Zeppernick et al., 2008). The few mechanistic studies that have aimed elucidate regulators of CD133 in normal and malignant stem cell populations have identified a unique cell cycle dependence in which CD133 levels are elevated when cells enter the G2/M phase (Jaksch et al., 2008). Moreover, a hypoxic niche has been shown to maintain stemness and CD133 expression *via* hypoxia-inducible factor-1 $\alpha$  (HIF-1 $\alpha$ ), which implicates CD133 as a downstream component of metabolic signaling (Soeda et al., 2009). In order to identify a developmental signaling role for CD133, Mak, *et al.* (Mak et al., 2012) found HDAC6, CD133, and  $\beta$ -catenin to physically interact with one another and exist in a ternary complex. This association stabilizes  $\beta$ -catenin *via* HDAC6 deacetylase activity, leading to activation of downstream targets of  $\beta$ -catenin signaling. By contrast, inhibition of either CD133 or HDAC6 resulted in increased  $\beta$ -catenin acetylation and subsequent degradation, which correlated with impaired proliferation and tumorigenesis. Further therapeutic evidence to suggest a role for CD133 in regulating the Wnt signaling pathway comes from work in GBM, in which the anti-helminthic compound, pyrinium,

has been shown to target CD133+ cells in a Wnt-dependent manner (Venugopal et al., 2015). These data support a putative mechanistic role for CD133 in regulating developmental pathways in malignant cell populations and serve as a foundation for the work presented in Chapter 4.

### 1.3.3 *Medulloblastoma brain tumor-initiating cells*

Following the original description of MB BTICs (Hemmati et al., 2003; Singh et al., 2003; Singh et al., 2004), attempts were made to correlate subsequent MB BTIC cell surface markers with their lineage potential. The carbohydrate moiety, CD15, was initially shown to mark a progenitor cell population capable of initiating tumors in transgenic mice haploinsufficient for *Ptch1* (*Ptch1*<sup>+/-</sup>); a mouse model of Shh MB that generates MB in 15-20% of mice (Goodrich, Milenkovic, Higgins, & Scott, 1997). In their original description, CD15+ MB BTICs were shown to not form tumorspheres or display multilineage differentiation in culture (Read et al., 2009), and therefore, it was believed that these cells marked progenitor cells as opposed to a more primitive stem-like cell. Follow-up work by Ward, *et al.* (Ward et al., 2009) demonstrated the propagation of multipotent, self-renewing CD15+ MB stem cells from *Ptch1*<sup>+/-</sup> mice. The difference in cellular phenotype was attributed to culture conditions as the culture of CD15+ MB BTICs in serum-free conditions enhanced their stemness and self-renewal capacity, which highlighted growth factors as one of the determinants of stemness in BTICs.

In order to further delineate those cells most capable of functioning as BTICs, several murine models of MB have been derived by overexpressing oncogenes or

inactivating tumor suppressor genes within cell populations of different lineages. Using CRE recombinase-mediated deletion of *Ptch1* within *Math1*- (also known as *Atoh1*) expressing cerebellar granule neuron precursors (GNPs), Yang, *et al.* (Z. J. Yang et al., 2008) demonstrated the ability of GNPs to form Shh MB. Interestingly, only those cells committed to a GNP phenotype were again capable of MB formation when a GFAP promoter was used to control CRE expression and thereby inactivate *Ptch1* in NSCs. Using a constitutively active *Smo* allele (*SmoM2*), Schuller, *et al.* (Schuller et al., 2008) targeted NSCs, GNPs, and differentiated Purkinje neurons in the developing mouse brain. While ectopic Shh signaling in Purkinje cells did not generate tumors, MBs were observed in both NSC- and GNP-targeted mice. Of note, a GNP phenotype was again necessary for NSCs to generate Shh MB. These studies have implicated the acquisition of a GNP phenotype to be a critical stage in oncogenesis for Shh MB. Although the evidence for a GNP BTIC is strong, it remains unclear as to how these cells propagate and transform over the course of tumorigenesis as defined by their regulatory mechanism and marker expression.

Validated transgenic mouse models for Group 3 MB have elucidated the role of *Myc* in MB initiation and the specific cell population that may be vulnerable to transformation (Kawauchi et al., 2012; Pei, Moore, et al., 2012). Using postnatal murine cerebellar stem cells based on the expression of Prominin1 and lacking expression of lineage-specific markers for GNPs, Pei, *et al.* (Pei, Moore, et al., 2012) introduced a mutant, stabilized *Myc* construct with a dominant negative TP53, which induced *in vivo* MBs distinct from Shh and Wnt murine tumors. In contrast, Kawuchi, *et al.* (Kawauchi et al., 2012) generated Group 3 MBs *in vivo* by introducing *Myc ex vivo* into *Trp53* null GNPs

sorted for the neuronal lineage marker *Atoh1*. Both groups demonstrated that MBs generated from their transgenic cells recapitulate many histopathological and genomic features of human Group 3 MB. Most interestingly, protein and genomic expression profiles of tumors generated by both groups overlapped most with those of NSCs, induced-pluripotent stem cells, and embryonic stem cells. Although, Kawauchi, *et al.* (Kawauchi et al., 2012) had initially injected cells sorted for GNP negative for stem cell markers such as *Prominin1*, the resulting tumors had lost *Atoh1* expression and instead displayed increased expression of *Prominin1* and other stem cell markers. Similarly, Pei *et al.* (Pei, Moore, et al., 2012) observed an increase in markers of undifferentiated cells in the resulting tumors, suggesting Group 3 to either arise from cerebellar stem cells or through a process of de-differentiation in which distinct tumor cells took on a stem cell-like phenotype. The indication of a cerebellar stem cell as the target for initiation and propagation of Group 3 MBs is in keeping with the aggressive clinical features of these tumors being resistant to therapeutic interventions and often presenting with metastatic spread.

In order to assess the clonal architecture of Shh MB, Vanner, *et al.* (Vanner et al., 2014) performed lineage tracing experiments in *Ptch1*<sup>+/-</sup> mice. Using a tamoxifen-inducible Cre recombinase driven by the endogenous *Sox2* promoter and Cre-activated tdTomato fluorescent reporter, slow cycling *Sox2*<sup>+</sup> cells were found to be at the top of the tumor cell hierarchy. *Sox2*<sup>+</sup> cells gave rise to rapidly cycling *Dcx*<sup>+</sup> progenitors, which differentiated into *NeuN*<sup>+</sup> cells that eventually underwent apoptosis. *In vivo* treatment with antimetabolic drugs or Shh pathway inhibitors resulted in residual tumors that were enriched

in Sox2+ cells, suggesting these cells escape therapy and are responsible for disease recurrence. The presence of a restricted subclone in the primary tumor that re-emerges as the dominant clone in metastatic lesions is further supported by the identification of shared clonal mutations between primary and matched-metastatic MBs (Wu et al., 2012). Given that tumor cells capable of initiating metastasis or disease recurrence must inherently function as BTICs, developmental pathways such as Notch signaling have recently been identified as critical regulators of MB metastasis-initiating cells (Kahn et al., 2018). Interestingly, both MB metastasis (Kahn et al., 2018) and recurrence (Bakhshinyan et al., 2019) appear to be dependent on the epigenetic regulator of fate determination and proliferation, Bmi1. As a component of the polycomb repressive complex 1 (PRC1), Bmi1 functions to repress the *Ink4a/Arf* and *p21* loci (Bruggeman et al., 2005; Jacobs, Kieboom, Marino, DePinho, & van Lohuizen, 1999; Lessard & Sauvageau, 2003; Molofsky et al., 2003; Sauvageau & Sauvageau, 2010) and has been implicated in the pathogenesis of MB (Badodi et al., 2017; Bakhshinyan et al., 2019; Leung et al., 2004; Manoranjan et al., 2013; Wang et al., 2012) and GBM (Abdouh et al., 2009; Bruggeman et al., 2007; Gargiulo et al., 2013; Jin et al., 2017; Venugopal et al., 2012). With an 11-gene stemness signature (Glinsky, Berezovska, & Glinskii, 2005) representing a conserved Bmi1-regulated transcriptional network that reliably predicts poor treatment response, recurrence, metastatic potential, and death in 11 cancer models, including MB, therapeutic strategies targeting Bmi1 may potentially eradicate those MB BTICs with an enhanced potential for evading current therapies and promoting disease recurrence and/or metastasis (Bakhshinyan et al., 2019).

#### 1.3.4 *Glioblastoma brain tumor-initiating cells*

Although CD133 was initially described as a GBM BTIC marker (Hemmati et al., 2003; Singh et al., 2003; Singh et al., 2004), subsequent studies have demonstrated the BTIC population to co-exist in additional cell fractions, which have been prospectively isolated using a variety of cell surface proteins. For example, CD15 has been shown to enrich for GBM BTICs in patient samples with minimal CD133 expression (Son, Woolard, Nam, Lee, & Fine, 2009). While the mechanistic function of CD133 and CD15 in regulating GBM BTICs remains to be determined, proteins with a known signaling role between NSCs and their surrounding microenvironment such as L1CAM (Bao et al., 2008) and integrin  $\alpha 6$  (Lathia et al., 2010) have also been shown to identify GBM BTICs. These interactions provide novel therapeutic opportunities that may target both the BTIC and its surrounding microenvironment.

A variety of GBM mouse models have been developed using disease-relevant mutations in tumor suppressors (*Pten*, *Trp53*, *Nf1*, *Cdkn2a*, *Rb1*) and oncogenes (*EGFRvIII*, *Pdgfra*). These models have characterized the ability of cells with varying lineage potentials to function as GBM BTICs. Specifically, murine GBMs have been derived with mutations restricted to quiescent NSCs (*GFAP*) (Chow et al., 2011), neural progenitors (*Nestin*) (S. Alcantara Llaguno et al., 2009), adult bipotential progenitors (*Ascl1*) (S. R. Alcantara Llaguno et al., 2015), oligodendrocyte progenitors (*NG2*) (Galvao et al., 2014), mature neurons (*CamK2A*) (S. Alcantara Llaguno et al., 2019), and mature astrocytes (*GFAP*) (Chow et al., 2011). Interestingly, a greater incidence of tumor formation with a shorter latency of 6-10 weeks has been observed when targeting H-Ras

V12 and *TP53* mutations in *GFAP-cre*, *nestin-cre*, and *Sox2-cre* populations compared to the 9-12 months required for tumor formation when terminal neurons (*CamK2A-cre*) are targeted (Friedmann-Morvinski et al., 2012). *In vivo* lineage tracing studies have provided additional evidence in support of a cellular hierarchy driven by cells with a stem cell phenotype in GBM. By using a *Nestin* transgene that labelled quiescent subventricular zone adult NSCs with GFP expression in a murine model of GBM, Chen *et al.* (Chen et al., 2012) demonstrated TMZ treatment to eradicate GFP- progenitors, leaving behind Nestin-expressing GFP+ BTICs. Although the GFP+ cells were initially slow-cycling, pulse-chase experiments revealed the enhanced proliferative capacity of these cells following TMZ treatment as the cellular hierarchy of GFP+ BTICs and GFP- non-BTICs was re-established, leading to tumor recurrence. These findings have been validated by more recent work, which has used DNA barcoding to map the clonal architecture of GBM (Lan et al., 2017). Through serial *in vivo* transplantation studies, primary human GBM was shown to consist of a subpopulation of slow-cycling stem-like cells capable of self-renewal and differentiation into rapidly cycling progenitors, which generated short-lived, non-dividing cells. With emerging experimental evidence in support of human GBM BTICs, the biggest challenge for targeted therapies remains our limited understanding of how multiple signaling programs may interact to regulate these cells. Additional work linking BTIC cell surface markers to their downstream pathways may provide key nodes of signaling integration responsible for tumorigenesis and disease recurrence.

## 1.4 Canonical Wnt signaling

### 1.4.1 *Wnt/β-catenin signaling*

The canonical Wnt pathway exists in 2 states, “off” and “on” (Clevers & Nusse, 2012). Activation of the canonical Wnt pathway by extracellular Wnt ligands leads to β-catenin mediated signal transduction (Clevers & Nusse, 2012; Valenta, Hausmann, & Basler, 2012). In the absence of a Wnt signal, β-catenin is located in adherens junctions where it is bound by E-cadherin, p120-catenin, and α-catenin (Hartsock & Nelson, 2008). The non-junctional pool of cytosolic β-catenin is targeted for degradation by the multiprotein “destruction complex” (Stamos & Weis, 2013). The destruction complex is formed by glycogen synthase kinase-3 (GSK-3), casein kinase 1 (CK1), β-Transducin repeats-containing proteins (β-TrCP), APC, and the scaffolding proteins Axin and dishevelled (Dvl). CK1 initially phosphorylates β-catenin at serine 45 (S45), which primes it for further phosphorylation by GSK-3 at threonine 41 (T41), S37, and S33 (C. Liu et al., 2002). Once phosphorylated, S33 and S37 function as β-TrCP-binding sites, allowing for the β-TrCP-mediated ubiquitination and subsequent proteasomal degradation of β-catenin (Aberle, Bauer, Stappert, Kispert, & Kemler, 1997; Orford, Crockett, Jensen, Weissman, & Byers, 1997). The lack of free cytoplasmic and nuclear β-catenin enables the downstream mediators of the pathway, T-Cell Factor/Lymphoid Enhancer Factors (TCF/LEFs), to function as transcriptional repressors by interacting with corepressors of the Transducin-like enhancer of split (TLE) family of proteins (Daniels & Weis, 2005).

Activation of the pathway requires the binding of Wnt ligands to two receptors, Frizzled (Fzd), and a co-receptor, low-density lipoprotein receptor related protein 5 or 6 (LRP5/6) (Nusse & Varmus, 1992). Fzd is a seven-pass transmembrane receptor, whereas LRP5/6 is a single-pass transmembrane protein. The intact destruction complex is recruited to the phosphorylated LRP, and while the complex is still able to capture and phosphorylate  $\beta$ -catenin, ubiquitination by  $\beta$ -TRCP is blocked (Tamai et al., 2004). Newly synthesized  $\beta$ -catenin is then able to accumulate in the cytoplasm and translocate to the nucleus where it acts as a transcriptional co-activator by interacting with TCF/LEFs and various chromatin-remodeling proteins to collectively transcribe target genes (Angers & Moon, 2009).

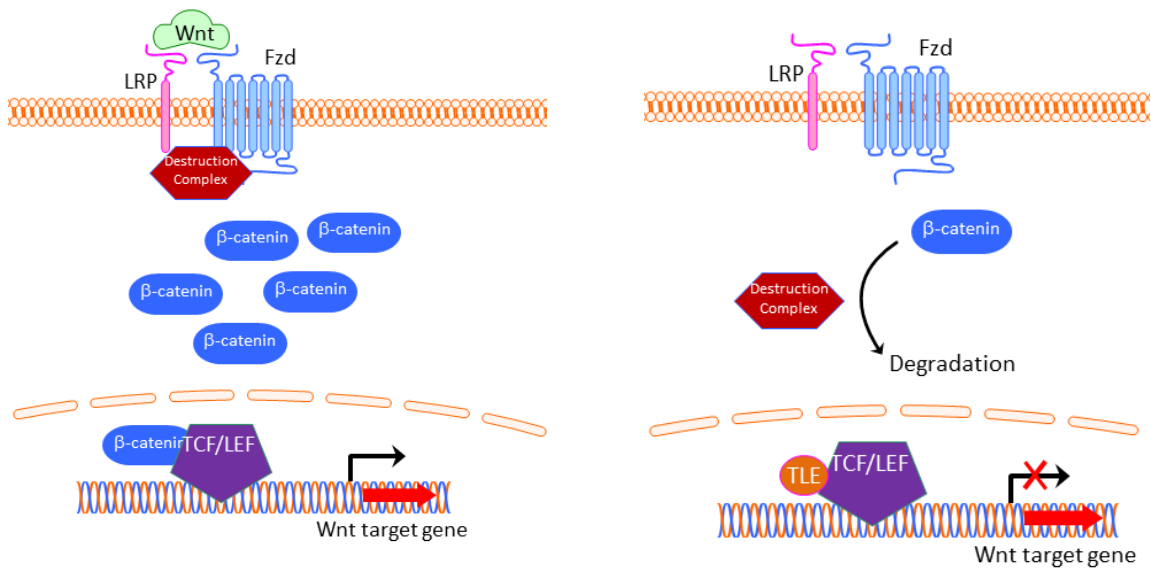


**Figure 1: Canonical Wnt/β-catenin signaling.** (Left) Upon Wnt ligand binding to the Fzd-LRP5/6 complex, the destruction complex is recruited to the membrane and inactivated. β-catenin subsequently accumulates in the cytosol and translocates into the nucleus where it binds to TCF/LEFs to transactivate Wnt target genes. (Right) In the

absence of Wnt ligand,  $\beta$ -catenin is targeted for degradation by the destruction complex leading to the repression of Wnt target gene expression by the binding of nuclear TCF/LEF transcription factors to corepressors such as the TLE protein family.

#### 1.4.2 *Wnt signaling in brain development*

The balance between proliferation and differentiation of NSCs during CNS development is tightly regulated by several signaling pathways of which the Wnt pathway is involved in every step including anterior-posterior axis specification of the neural plate (Kiecker & Niehrs, 2001), fate determination of NSCs (Zechner et al., 2003), neuronal migration (Vivancos et al., 2009), and the development of axons and dendrites (Ciani et al., 2011; Ciani & Salinas, 2005). In normal forebrain development, the Wnt pathway expands the progenitor pool by promoting symmetric division of NSCs (Woodhead, Mutch, Olson, & Chenn, 2006), which is later depleted through asymmetric division and neural differentiation (Hirabayashi et al., 2004). This wave of differentiation migrates from anterolateral to posteromedial regions (Kiecker & Niehrs, 2001; Megason & McMahon, 2002), which coincides with a reduction in Wnt signaling. Transgenic mouse models have provided additional details into the role of Wnt signaling in forebrain development (Chenn & Walsh, 2002, 2003; W. Y. Kim et al., 2009; Zechner et al., 2003). Constitutive Wnt activation in *nestin*-driven NSCs results in significantly enlarged forebrains due to an increase in cell cycle re-entry of the progenitor cell population and the subsequent expansion of these cells (Chenn & Walsh, 2002). These findings were validated in a conditional GSK-3 knockout model ( $GSK-3\alpha^{-/-}GSK-3\beta^{loxP/loxP}$ ) crossed with a *nestin-cre*

line that would maintain activated Wnt signaling in NSCs secondary to the loss of GSK-3 function (W. Y. Kim et al., 2009). GSK-3-deficient progenitors were found to maintain a progenitor phenotype with an inability to generate more differentiated lineages, indicating activated Wnt signaling to promote self-renewal and suppress differentiation of NSCs and progenitor cells in the forebrain. Conversely, conditional deletion of  $\beta$ -catenin in the neocortical ventricular zone of developing mouse embryos leads to premature cell cycle exit and neuronal differentiation of progenitor cells (Woodhead et al., 2006; Zechner et al., 2003). These findings are also associated with multiple structural defects due to alterations in cell migration and dorso-ventral cell identity.

With respect to the hindbrain, the Wnt pathway plays a critical role in establishing the midbrain-hindbrain boundary that gives rise to the cerebellum (Rhinn, Lun, Luz, Werner, & Brand, 2005). Either, loss-of-function mutations in *Wnt1* (K. R. Thomas & Capecchi, 1990) or the conditional deletion of  $\beta$ -catenin (Brault et al., 2001) result in mice completely lacking a midbrain and cerebellum. Loss of  $\beta$ -catenin in *nestin*-expressing progenitors leads to premature neuronal differentiation and hypoplasia of the cerebellar vermis, indicating a role for the Wnt pathway in regulating the growth and differentiation of embryonic and early postnatal cerebellar cells (Schuller & Rowitch, 2007). Interestingly, the ectopic expression of  $\beta$ -catenin promotes the proliferation of cerebellar stem cells and impairs the expansion of GNPs (Pei, Brun, et al., 2012), which are considered the cell of origin for Shh MB. However, since the enhanced proliferative capacity of Wnt-activated cerebellar stem cells is not sustained and rather characterized by a marked reduction in self-renewal, these cells are unable to generate neoplastic lesions. In order to assess postnatal

effects of Wnt activation on cerebellar development,  $\beta$ -catenin was conditionally activated in NSCs through the generation of *hGFAP-cre;CTNNB1(ex3)<sup>FL/+</sup>* mice (Poschl, Grammel, Dorostkar, Kretzschmar, & Schuller, 2013). Cells arising from the cerebella of these mice were hypoplastic and displayed a loss of neuronal differentiation. Moreover, while GNPs were found to proliferate in response to activated Wnt signaling, they did not adequately migrate from the external to inner granule layer resulting in severe lamination defects. While Wnt activation enhances or diminishes the growth of the forebrain or hindbrain, respectively, the effects on individual cell populations remains to be determined as many of the observed effects are dependent on the developmental period and cell population in which Wnt is activated.

#### *1.4.3 Wnt signaling in non-central nervous system malignancies*

As the most well characterized malignancy associated with Wnt pathway activation, colorectal cancer continues to serve as a biological model for studying the oncogenic role of Wnt signaling. Overactivation of the Wnt pathway and the formation of adenomas is often the first step in colorectal cancer as 85% of all sporadic and hereditary colorectal tumors show loss of APC function in early precursor lesions (Fearon & Vogelstein, 1990; Kinzler & Vogelstein, 1996). Recent studies have also highlighted the role of R-spondins in regulating Wnt-mediated colorectal cancer (Han et al., 2017; Hilkens et al., 2017). By binding to their receptors, Lgr4 and Lgr5 (leucine-rich repeat-containing G-protein coupled receptor 4 and 5), R-spondins function to enhance Wnt signaling through Fzd/LRP6 (Carmon, Gong, Lin, Thomas, & Liu, 2011; de Lau et al., 2011; Glinka

et al., 2011; K. A. Kim et al., 2005). Given that the Wnt pathway is also implicated in the maintenance of Lgr5+ intestinal crypt stem cells during normal development and adult life (Clevers, 2013), the aberrant activation of the pathway has been linked to the regulation of Lgr5+ colorectal cancer stem cells (Barker et al., 2009; Schepers et al., 2012). Specifically, *APC* mutations have been shown to generate neoplastic transformation when targeted to intestinal crypt stem cells rather than differentiated cells (Barker et al., 2009). By repopulating the cellular architecture of the crypt with mutant cells, mutant intestinal stem cells invariably prime the crypt for neoplastic transformation (Snippert, Schepers, van Es, Simons, & Clevers, 2014; Vermeulen et al., 2013). Given the shared expression of Lgr5 between normal and malignant intestinal stem cell populations, recent work has taken advantage of neoplastic and normal human organoids to model and identify therapies that uniquely target the clonal architecture and microenvironment of neoplastic intestinal crypts (van de Wetering et al., 2015). To further investigate the stepwise progression of colorectal cancer growth, conditional loss of *APC* was used to generate the *APC*<sup>min/+</sup> mouse (Moser, Dove, Roth, & Gordon, 1992; Moser, Pitot, & Dove, 1990). These transgenic mice model familial adenomatous polyposis (FAP) in which patients have germline *APC* mutations resulting in hundreds to thousands of polyps at a young age (Kinzler & Vogelstein, 1996). Of those colorectal tumors with wild-type *APC*, 15% show point mutations in *CTNNB1* that result in a non-degradable, constitutively active form of  $\beta$ -catenin (Bienz & Clevers, 2000). Interestingly, *APC* and *CTNNB1* mutations are mutually exclusive and contribute to intertumoral heterogeneity (Sparks, Morin, Vogelstein, & Kinzler, 1998) as *CTNNB1*

mutations are more often seen in well-circumscribed and non-invasive lesions (Samowitz et al., 1999).

While Wnt activation maintains the self-renewal capacity of intestinal crypt stem cells, it induces the differentiation of neural crest cells towards the melanocytic lineage (Dunn, Williams, Li, & Pavan, 2000; A. J. Thomas & Erickson, 2008). Of note, TCF3-mediated inhibition of the Wnt pathway is required for the self-renewal of hair follicle bulge stem cells located in the skin (Nguyen, Rendl, & Fuchs, 2006). The variable context and tissue-specific role of Wnt in modulating stemness is carried forward into how the pathway functions to regulate oncogenesis or tumor suppression. Although recurrent activating mutations in the Wnt pathway are rare in melanoma (Omholt, Platz, Ringborg, & Hansson, 2001; Pollock & Hayward, 2002; Reifemberger et al., 2002; Rubinfeld et al., 1997), benign nevi and a substantial number of melanoma tumors demonstrate increased nuclear  $\beta$ -catenin expression (Bachmann, Straume, Puntervoll, Kalvenes, & Akslen, 2005; Kageshita et al., 2001; Maelandsmo, Holm, Nesland, Fodstad, & Florenes, 2003). Clinically, patients with elevated nuclear  $\beta$ -catenin are associated with an improved prognosis (Bachmann et al., 2005; Chien et al., 2009). Experimental work in support of these findings are seen with the overexpression of Wnt3A in murine and human melanoma cells resulting in a reduction in cell proliferation and *in vivo* tumor growth due to enhanced tumor cell differentiation into melanocytes (Chien et al., 2009). With respect to tumor initiation, transgenic mice expressing a constitutively active mutant  $\beta$ -catenin within melanocytes are unable to generate tumors and require additional oncogenic mutations with *NRAS* for neoplastic transformation (Delmas et al., 2007). While Wnt activation appears to

be a poor oncogenic driver in melanoma, the loss of Wnt signaling may be critical for melanoma progression and metastasis (Arozarena et al., 2011; Kageshita et al., 2001; Maelandsmo et al., 2003) as transcriptional changes seen following the ectopic expression of Wnt3A are downregulated in metastatic melanoma (Ryu, Kim, Deluca, & Alani, 2007). Patients with BRAF<sup>V600E</sup> mutant melanomas often relapse after dramatic remissions due to growing resistance to small molecule BRAF inhibitors (Villanueva et al., 2010). Kinome studies have described melanoma cells with elevated  $\beta$ -catenin expression to be more sensitive to small molecule BRAF inhibitors (Biechele et al., 2012), whereas resistance may be achieved through the knockdown of  $\beta$ -catenin (Biechele et al., 2012). Specifically, Wnt3A treatment of BRAF<sup>V600E</sup> mutant melanoma cells was able to synergize with the antimitotic effects of the BRAF inhibitor PLX4720 to induce apoptosis and decrease *in vivo* tumor burden (Biechele et al., 2012). Another small molecule, riluzole, which functions as a putative glutamate receptor antagonist has been shown to impair the proliferative capacity and enhance the differentiation of melanoma cells by synergizing with Wnt3A (Biechele et al., 2010). Moreover, LY2090314, a highly selective GSK-3 inhibitor capable of activating Wnt signaling, has been shown to induce apoptosis of melanoma cells resistant to the BRAF inhibitor vemurafenib with marked *in vivo* tumor growth delay (Atkinson et al., 2015). These data provide reproducible evidence in support of Wnt activation as a therapeutic strategy in melanoma, specifically for those patients with BRAF mutant tumors.

#### 1.4.4 *Wnt signaling in pediatric medulloblastoma*

The first transgenic Wnt MB mouse model was developed by Gibson, *et al.* (Gibson *et al.*, 2010) who used *Blbp-Cre<sup>+/-</sup>;CTNNB1<sup>+lox(ex3)</sup>;TP53<sup>+flx</sup>* mice in which Wnt activation in a *TP53* heterozygous background was used to drive the proliferation of *Blbp* expressing brain stem progenitors. The model identified a distinct germinal zone outside the cerebellum within the dorsal brainstem where progenitor cells of the lower rhombic lip were found to be the putative cell of origin for Wnt MB. Additional validation of this model as an adequate representation of human Wnt MB has come from transcriptional profiling, which has identified a shared genomic landscape among murine Wnt MB cells, human Wnt MB and human embryonic dorsal brainstem cells (Gibson *et al.*, 2010). Although, the murine Wnt MB has provided the MB research community with an opportunity to further characterize the cell of origin for these tumors, the power of this model is derived in our ability to elucidate mechanisms for the improved prognosis seen in children with Wnt MB.

One proposed mechanism for the excellent outcomes seen in children diagnosed with Wnt MB has been a disrupted blood-brain barrier (BBB), which leads to higher chemotherapy exposure in tumors and thus higher response rates compared to other subgroups (Phoenix *et al.*, 2016). Mechanistically, activation of the Wnt pathway within tumor cells promotes the secretion of Wnt antagonists (WIF1, DKK1), which inhibit Wnt signaling in adjacent endothelial cells of the BBB. Consequently, the transformed blood vessels become highly fenestrated with disturbed tight junctions enabling chemotherapeutic agents to more easily penetrate the tumor. Additional work into the biological significance of Wnt activation in MB has investigated Wnt MB in the context

of *TP53* mutations. With a 5-year overall survival (OS;  $\pm$  SE) for patients with *TP53*-mutated Shh and Wnt MB of  $41\% \pm 9\%$  and  $90\% \pm 9\%$ , respectively (Zhukova et al., 2013), Zukhova, *et al.* (Zhukova et al., 2014) hypothesized that Wnt activation could overcome *TP53* related radioresistance and could be used to sensitize *TP53* mutant tumors for radiation. As an activator of the Wnt pathway, lithium was found to selectively sensitize *TP53* mutant MB cells to radiation without sensitizing NSCs, suggesting lithium to be an attractive therapeutic adjuvant in high-risk MB. The most impressive work in suggesting a therapeutic benefit for Wnt activation in MB has come from comparing *Math1-cre;SmoM2<sup>Fl/+</sup>* with *Math1-cre;SmoM2<sup>Fl/+</sup>;CTNNB1(ex3)<sup>Fl/+</sup>* mice (Poschl et al., 2014). Although the former murine model generates spontaneous Shh MB, the introduction of a conditionally active  $\beta$ -catenin results in significantly reduced tumor growth and cerebellar size with a corresponding increase in overall survival. These data were validated using the *hGFAP* promoter where *hGFAP-cre;SmoM2<sup>Fl/+</sup>;CTNNB1(ex3)<sup>Fl/+</sup>* mice generated thinned EGL due to an impaired proliferative capacity of GNPs (Poschl et al., 2013). By contrast, mice lacking Wnt activation developed spontaneous Shh MB. These studies elegantly support the ability of activated Wnt signaling to decrease the proliferation and oncogenic potential of Shh-dependent cerebellar GNPs and NSCs.

#### 1.4.5 *Wnt signaling in adult glioblastoma*

While recurrent mutations in components of the canonical Wnt pathway have yet to be identified in GBM, few studies have attempted to address the observation of increased nuclear  $\beta$ -catenin immunoreactivity corresponding to an increase in glioma grade (Rossi et

al., 2011; L. Y. Zhang et al., 2010). In performing comparative analyses of chromatin maps for GBM BTICs, differentiated GBM cells and normal human astrocytes, ASCL1 was identified as a transcription factor essential for the maintenance of BTIC stemness and *in vivo* tumorigenicity *via* repression of *DKK1* and subsequent activation of the Wnt pathway (Rheinbay et al., 2013). FoxM1, another transcription factor, has been shown to directly interact with  $\beta$ -catenin and promote its nuclear accumulation in GBM cells (N. Zhang et al., 2011). Furthermore, FoxM1 and  $\beta$ -catenin form a functional complex with TCF on Wnt target gene promoters to promote self-renewal and tumor formation. Similarly, PLAGL2 was found to upregulate the Wnt pathway in GBM BTICs and thereby promote the maintenance of an undifferentiated state in GBM (Zheng et al., 2010). Therapeutically, small molecule inhibitors of the acyltransferase Porcupine, which block the palmitoylation of Wnt proteins and their subsequent secretion, have been shown to impair the proliferative capacity and clonogenic potential of GBM BTICs (Kahlert et al., 2015). Recent data have identified activated Wnt signaling to contribute to the functional heterogeneity of GBM BTICs as a small fraction of cells are dependent on Wnt for the maintenance of a BTIC fate (Rajakulendran et al., 2019). Interestingly, these cells display an ability for terminal neuronal differentiation in response to Wnt and Notch inhibition. While a limited number of transcription factors are thought to be essential for activated Wnt signaling in GBM, the manner in which they interact with one another or with additional developmental pathways to regulate unique BTIC populations remain elusive and may be of greater clinical utility for therapeutic targeting.

## 1.5 Summary of Intent

Tumor-initiating cells (TICs) are organized into a hierarchy in which only a rare clonal population of cells can initiate, proliferate, and maintain tumor growth. This is in sharp contrast to all other cells of the bulk tumor, characterized by a limited proliferative capacity and restricted lineage potential (Kreso & Dick, 2014; Magee et al., 2012; Shackleton et al., 2009). A unique property by which TICs may induce oncogenesis is self-renewal, defined as the ability of the parental cell to generate an identical daughter cell and a second daughter cell of the same or different phenotype (Gage, 2000; Reynolds & Weiss, 1996). Given that NSCs must maintain a relative balance between self-renewal and differentiation, brain tumorigenesis may be conceptualized as a disease of unregulated BTIC self-renewal (Kreso & Dick, 2014; Magee et al., 2012; Shackleton et al., 2009). With prior work having demonstrated increasing BTIC frequency to be associated with tumor aggressiveness (Singh et al., 2003; Singh et al., 2004) and poor patient outcome (Laks et al., 2009; Pallini et al., 2011; Panosyan et al., 2010), genes enriched in poor-outcome tumors may represent key self-renewal genes and thereby serve as surrogates when assessing the efficacy of targeted BTIC therapies.

As the most common malignant pediatric brain tumor, MB is defined by four molecular subgroups (Wnt, Shh, Group 3, Group 4) based on transcriptional and epigenetic profiles (Northcott et al., 2017; Ramaswamy et al., 2016). Wnt MBs have the most favorable prognosis with a >95% 5-year survivorship (Ramaswamy et al., 2016). By contrast, non-Wnt MBs are characterized by metastatic disease, increased rates of recurrence, and intermediate-poor overall survivorship (Ramaswamy et al., 2016). Given

that Wnt MBs represent the only subgroup in which metastasis is not indicative of a poor prognosis (von Bueren et al., 2016), it has been suggested that Wnt signaling may contribute to their remarkable response to therapy (Gibson et al., 2010; Pfaff et al., 2010; Phoenix et al., 2016; Poschl et al., 2014; Zhukova et al., 2014). With a paucity of treatment options for non-Wnt MBs, a rational therapeutic option would be to augment the protective effects of Wnt MB through targeted Wnt activation in non-Wnt MBs in order to impair the self-renewal of MB BTICs.

Upstream of TIC self-renewal genes are cell surface markers, which have traditionally been used to characterize the continuum of cellular phenotypes generated in ontogeny and carried forward into oncology as TICs. With few markers of clinical utility in adult GBM, CD133 has reproducibly been shown to correlate with disease progression, recurrence, and poor overall survivorship (Shibahara et al., 2013; Zeppernick et al., 2008) but insight into its function remains limited. Given the activation of AKT signaling in approximately 50% of GBMs secondary to EGFR amplification and/or overexpression, activating mutations in PI3K, or inactivation mutations in PTEN (Verhaak et al., 2010), emerging studies have suggested CD133 to function as a novel receptor for the PI3K/AKT pathway (Wei et al., 2013). With persistent overexpression of  $\beta$ -catenin in GBM (Rossi et al., 2011; L. Y. Zhang et al., 2010) not being accounted for by recurrent mutations in Wnt signaling (Brennan et al., 2013; Hu et al., 2016; Ji et al., 2009; Morris et al., 2013; Pulvirenti et al., 2011; Rheinbay et al., 2013; Verhaak et al., 2010; W. Yang et al., 2011; N. Zhang et al., 2011; Zheng et al., 2010), novel non-canonical mechanisms through

CD133 and AKT may be responsible for driving Wnt-dependent BTIC self-renewal in GBM.

**I hypothesize that the function of the Wnt signaling pathway in regulating self-renewal of forebrain and hindbrain NSCs to be conserved in the modulation of GBM and MB BTIC self-renewal, respectively.** The experimental aims to test this hypothesis are as follows:

- 1) To identify critical human BTIC self-renewal genes and discern mechanisms by which they initiate and maintain tumorigenesis
- 2) To investigate the role of activated Wnt signaling in reducing the function of human BTIC self-renewal genes in pediatric MB, leading to a reduction in tumorigenesis
- 3) To investigate the mechanism by which the putative BTIC marker, CD133, promotes the activation of Wnt signaling in human GBM leading to tumorigenesis.

In order to address the aims of this thesis, I initially worked with our bioinformatics colleagues to profile candidate stem cell self-renewal genes in poor-outcome MBs. This work yielded *Bmi1* and *FoxG1* as being enriched in poor-outcome MBs. Knockdown and overexpression studies validated the functional significance of these genes in regulating MB BTIC self-renewal. Chromatin immunoprecipitation (ChIP) experiments in MB BTICs further demonstrated the preservation of a shared NSC regulatory pathway consisting of *Bmi1* and *FoxG1* (**Chapter 2**).

Having identified key BTIC self-renewal genes, I then assessed the expression of *Bmi1* and *Sox2* in Wnt, Group 3, and Group 4 MB BTIC lines. Subgroup-specific differences in *in vitro* stem cell assays and *in vivo* tumor formation were assessed. Ectopic

expression of  $\beta$ -catenin in non-Wnt MB BTICs was used to evaluate the tumor restrictive role of Wnt/ $\beta$ -catenin signaling in MB. Single cell RNA-seq was performed to determine the presence of Wnt active cells in non-Wnt MB tumors. The presence of such cells led to the use of a Wnt reporter to identify endogenously Wnt-active cells in non-Wnt MBs based on flow cytometric cell sorting for GFP expression. The *in vitro* self-renewal potential and *in vivo* tumor formation capacity of Wnt-active cells (TGP+) was compared to the bulk Wnt-inactive cells (TGP-). Having identified a substrate-competitive peptide Wnt agonist that converts to an inhibitor of GSK-3, I then demonstrated the clinical utility of activating Wnt signaling using *in vivo* orthotopic xenografts of non-Wnt MBs (**Chapter 3**).

In order to assess stemness regulators upstream of BTIC self-renewal genes, I aimed to identify a functional role for CD133 in GBM BTICs. CD133 expression and Wnt TCF reporter expression were serially profiled among several GBM BTIC lines. CD133 was ectopically expressed in CD133<sup>low</sup> lines to assess the downstream effect on pAKT, pGSK-3, and  $\beta$ -catenin expression. *In vitro* functional stem cell assays and Wnt reporter assays were then performed on CD133<sup>high</sup> lines following treatment with a CD133 specific monoclonal antibody and a small molecule pan-AKT inhibitor. The integrity of the CD133-AKT-Wnt pathway was interrogated in GBM BTICs with (TGP+) and without (TGP-) endogenous Wnt activity using a Wnt reporter with a GFP tag. *In vivo* tumor formation and survival studies were completed with TGP+ and TGP- cells to assess tumor burden and overall survival (**Chapter 4**).

## **Chapter 2: FoxG1 interacts with Bmi1 to regulate self-renewal and tumorigenicity of medulloblastoma stem cells**

### **Preamble**

This chapter is an original published article presented in its published format in *Stem Cells*, available online at <https://doi.org/10.1002/stem.1401>.

Manoranjan B, Wang X, Hallett RM, Venugopal C, Mack SC, McFarlane N, Nolte SM, Schienemann K, Gunnarsson T, Hassell JA, Taylor MD, Lee C, Triscott J, Foster CM, Dunham C, Hawkins C, Dunn SE, Singh SK. *FoxG1 interacts with Bmi1 to regulate self-renewal and tumorigenicity of medulloblastoma stem cells*. *Stem Cells*. 2013 Jul 31;(7):1266-1277. doi: 10.1002/stem.1401.

Experimental concept and study design were developed by myself, X. Wang, R.M. Hallett, C. Venugopal, and S.K. Singh. All microarray analysis was performed by R.M. Hallett under the supervision of J.A. Hassell. nCounter System (NanoString) gene expression profiling were performed by C. Lee, J. Triscott, C.M. Foster under the supervision of S.E. Dunn and C. Dunham. MB samples and clinical details were provided by S.K. Singh, T. Gunnarsson, and K. Schinemann or obtained from commercially available sources. I performed all dissociation of primary MB tissue and neurosphere cultures and quantitative real-time-polymerase chain reactions. Viral production and transduction was performed by myself and C. Venugopal. Western blots were generated by C. Venugopal. C. Hawkins developed the tissue microarray and supervised immunohistochemistry staining. Scoring of stains was performed by X. Wang and S.C.

Mack. I performed neurosphere size, cell proliferation, secondary sphere, and differentiation assays. Chromatin immunoprecipitation was performed by myself and C. Venugopal. Flow cytometric cell sorting was performed by N. McFarlane. All *in vivo* experiments were led and performed by myself with assistance from S.M Nolte.

The main objective of this body of work was to identify putative BTIC self-renewal genes in poor-outcome MBs since BTICs typically comprise a minority of tumor cells and may therefore go undetected on bulk tumor analyses used by current gene expression platforms. Having identified *Bmi1* and *FoxG1* as self-renewal genes enriched in poor-outcome MBs, I further characterized their functional significance in regulating CD15+ MB BTICs. This work provided the first evidence of a developmentally conserved NSC signaling program in MB BTICs derived from poor-outcome non-Shh (sonic hedgehog)/Wnt MBs.

**FoxG1 interacts with Bmi1 to regulate self-renewal and tumorigenicity of  
medulloblastoma stem cells**

Branavan Manoranjan<sup>1,2</sup> Hon BHSc, Xin Wang<sup>3</sup> Hon BHSc, Robin M. Hallett<sup>2,4</sup> PhD,  
Chitra Venugopal<sup>1</sup> PhD, Stephen C. Mack<sup>3</sup> PhD, Nicole McFarlane<sup>1</sup>, Sara M. Nolte<sup>1,2</sup> Hon  
BHSc, MSc, Katrin Scheinemann<sup>5</sup> MD, PhD, Thorsteinn Gunnarsson<sup>6</sup> MD, John A.  
Hassell<sup>2,4</sup> PhD, Michael D. Taylor<sup>3,7</sup> MD, PhD, Cathy Lee<sup>8</sup>, Joanna Triscott<sup>8</sup>, Colleen M.  
Foster<sup>8</sup>, Christopher Dunham MD<sup>10</sup>, Cynthia Hawkins<sup>3,9</sup> MD, PhD, Sandra E. Dunn<sup>8</sup> PhD,  
and Sheila K. Singh<sup>1,2,6</sup> MD, PhD

<sup>1</sup>McMaster Stem Cell and Cancer Research Institute, McMaster University, Hamilton,  
Ontario, L8S 4K1, Canada

Departments of <sup>2</sup>Biochemistry and Biomedical Sciences, <sup>5</sup>Pediatrics, and <sup>6</sup>Surgery, Faculty  
of Health Sciences, McMaster University, 1200 Main Street West, Hamilton, Ontario, L8N  
3Z5, Canada

<sup>3</sup>Arthur and Sonia Labatt Brain Tumor Research Centre, The Hospital for Sick Children,  
University of Toronto, Toronto, Ontario, M5G 1X8, Canada

<sup>4</sup>McMaster Centre for Functional Genomics, McMaster University, 1200 Main Street  
West, Hamilton, Ontario, L8N 3Z5, Canada

Departments of <sup>7</sup>Surgery and <sup>9</sup>Pediatric Laboratory Medicine, The Hospital for Sick  
Children, University of Toronto, Toronto, Ontario, M5G 1X8, Canada

<sup>8</sup>Departments of Pediatrics, Experimental Medicine and Medical Genetics, Child and Family Research Institute, University of British Columbia, Vancouver, British Columbia, V5Z 4H4, Canada

<sup>10</sup>Department of Pathology & Laboratory Medicine, Division of Anatomic Pathology, BC Children's Hospital, 4500 Oak Street, Vancouver, BC, Canada V6H 3N1

### **Running Title**

FoxG1/Bmi1 regulate medulloblastoma stem cells

### **Author Contributions**

Branavan Manoranjan: Conception and design, Collection and/or assembly of data, Data analysis and interpretation, Manuscript writing, Final approval of manuscript

Xin Wang, Robin M. Hallett, Chitra Venugopal: Conception and design, Collection and/or assembly of data, Final approval of manuscript

Stephen Mack, Nicole McFarlane, Sara M. Nolte, Cathy Lee, Joanna Triscott, Colleen M. Foster, Christopher Dunham: Collection and/or assembly of data, Data analysis and interpretation

Katrin Scheinemann, John A. Hassell, Michael D. Taylor, Cynthia Hawkins: Data analysis and interpretation

Thorsteinn Gunnarsson: Provision of study material or patients

Sandra E. Dunn: Conception and design, Provision of study material or patients, Collection and/or assembly of data, Data analysis and interpretation, Final approval of manuscript

Sheila K. Singh: Conception and design, Data analysis and interpretation, Manuscript writing, Final approval of manuscript

### **Acknowledgements**

B.M. is supported by a Canadian Institutes of Health Research Vanier Canada Graduate Scholarship. S.K.S. is supported by the Neurosurgical Research and Education Foundation and American Association of Neurological surgeons, Pediatric Section, the Ontario Institute for Cancer Research, and McMaster University Department of Surgery.

**Keywords:** brain tumor-initiating cell, medulloblastoma, stem cells, FoxG1, Bmi1, self-renewal

### **Corresponding Author**

Sheila K. Singh, MD, PhD, FRCS(C)

Associate Professor of Pediatric Neurosurgery,

Department of Surgery, McMaster Children's Hospital,

Scientist, McMaster Stem Cell & Cancer Research Institute

MDCL 5027, 1280 Main Street West, Hamilton, ON, L8S 4K1, Canada

T: 905-521-2100 x75237

F: 905-521-992

Email: [ssingh@mcmaster.ca](mailto:ssingh@mcmaster.ca)

## Abstract

Brain tumors represent the leading cause of childhood cancer mortality, of which medulloblastoma (MB) is the most frequent malignant tumor. Recent studies have demonstrated the presence of several MB molecular subgroups, each distinct in terms of prognosis and predicted therapeutic response. Groups 1 and 2 are characterized by relatively good clinical outcomes and activation of the Wnt and Shh pathways, respectively. In contrast, Groups 3 and 4 (“non-Shh/Wnt MBs”) are distinguished by metastatic disease, poor patient outcome, and lack a molecular pathway phenotype. Current gene expression platforms have not detected brain tumor-initiating cell (BTIC) self-renewal genes in Group 3 and 4 MBs as BTICs typically comprise a minority of tumor cells and may therefore go undetected on bulk tumor analyses. Since increasing BTIC frequency has been associated with increasing tumor aggressiveness and poor patient outcome, we investigated the subgroup-specific gene expression profile of candidate stem cell genes within 251 primary human MBs from four non-overlapping MB transcriptional databases (Amsterdam, Memphis, Toronto, Boston) and 74 NanoString-subgrouped MBs (Vancouver). We assessed the functional relevance of two genes, *FoxG1* and *Bmi1*, which were significantly enriched in non-Shh/Wnt MBs, and showed these genes to mediate MB stem cell self-renewal and tumor initiation in mice. We also identified their transcriptional regulation through reciprocal promoter occupancy in CD15+ MB stem cells. Our work demonstrates the application of stem cell data gathered from genomic platforms to guide functional BTIC assays, which may then be used to develop novel BTIC self-renewal mechanisms amenable to therapeutic targeting.

## Introduction

Medulloblastoma (MB) is the most frequent malignant pediatric brain tumor, representing 20% of newly diagnosed childhood central nervous system malignancies(1). Despite current multimodal therapy consisting of surgical resection, radiation and chemotherapy jointly yielding an 80% 5-year survivorship, significant treatment-induced morbidity and long-term clinical sequelae are common and adversely affect quality-of-life(1-4). Given the limitations of current clinico-pathological parameters to accurately predict treatment response(1, 2, 5), multiple genomic platforms have been used to characterize the aberrant expression of signaling pathways in MB. This has re-conceptualized the heterogeneity that exists within pathological subgroups along with giving context to the role of key stem cell signaling pathways in MB pathogenesis(6-10).

The recent molecular classification of MB consists of four subgroups, each distinct in terms of prognosis and predicted therapeutic response. Groups 1 and 2 are characterized by upregulation of genes in the canonical Wnt or Sonic hedgehog (Shh) pathways, respectively(7, 8, 10-13). These two subgroups are separated from each other and all others by principal component analysis, and both are associated with relatively good clinical outcomes(8). Wnt-driven MBs are primarily characterized by monosomy 6, activating mutations of *CTNNB1*, and an excellent prognosis(7, 10, 11, 14), whereas targeted Shh inhibitors have shown promising results in patients with Shh-driven MBs(15, 16). However, Group 3 and 4 MBs are associated with metastatic disease and poor patient outcome (6-8). These aggressive MBs, which have been collectively labeled as “non-Shh/Wnt” subgroups(4), remain refractory to current treatment modalities, and lack

aberrant activation of known signaling pathways. Furthermore, recent genomic meta-analyses have revealed evidence for the existence of subtypes within Group 3 and 4 MBs, now labeled as 3 $\alpha$ , 3 $\beta$ , 4 $\alpha$  and 4 $\beta$ , each with distinct gene mutations and transcriptome profiles(6, 13, 17). Recently, two mouse models of *c-MYC*-driven MB (18, 19) have been shown to recapitulate a subclass of Group 3 human MBs (Group 3 $\alpha$ ), implicating *c-MYC* amplification as a driver of tumor formation in this subset. Other reports have shown non-Shh/Wnt MBs to express genes associated with increased photoreceptor(6) or neuronal differentiation(7) and more recently the exclusive expression of *NPR3*(8), *KCNA1*(8), or *FSTL5*(20). However, these reports do not address the role of stem cell regulatory genes in driving MB tumorigenesis, which is in keeping with the minimal literature on examining selectively activated developmental signaling pathways in non-Shh/Wnt MBs(21-23), and even fewer reports linking aberrant MB stem cell self-renewal signaling to patient prognosis and outcome(24).

The Cancer Stem Cell (CSC) hypothesis suggests that tumors are organized into a hierarchy in which only a rare clonal population of cells, termed CSCs or tumor-initiating cells (TICs), have the ability to initiate, proliferate, and maintain tumor growth. This is in sharp contrast to all other cells of the bulk tumor, characterized by a limited proliferative capacity and restricted lineage potential(25, 26). By applying culture conditions and assays used to characterize normal neural stem cells (NSCs), we were among the first researchers to identify cells from a variety of human brain tumors (including MB), termed brain tumor-initiating cells (BTICs), which exhibited the stem cell properties of self-renewal and differentiation(27, 28). A unique property by which stem cells may induce oncogenesis is

self-renewal, defined as the ability of the parental cell to generate an identical daughter cell and a second daughter cell of the same or different phenotype(29, 30). Given that normal NSCs must maintain a relative balance between self-renewal and differentiation, brain tumorigenesis may be conceptualized as a disease of unregulated BTIC self-renewal(25, 26). Despite the promise of novel therapies targeting the MB BTIC self-renewal machinery to improve outcomes in those who remain refractory to current treatment, the regulatory mechanisms of these pathways remain unknown.

In this study, we have characterized the role of MB stem cell-specific pathways specifically enriched in non-Shh/Wnt MBs. Since prior work has demonstrated increasing BTIC frequency to be associated with tumor aggressiveness(27, 28) and poor patient outcome(24, 31, 32), we have investigated the likelihood of BTIC self-renewal genes in specifying Group 3 and 4 non-Shh/Wnt MBs. While these MBs and their further fractionated subtypes may display characteristic gene mutations, amplifications or gene expression profiles(13), we hypothesized that all of these MB subtypes may be aberrantly driven by stem cell regulatory genes promoting enhanced BTIC self-renewal. If BTIC self-renewal genes and their signaling pathways are specifically identified in aggressive MB subgroups, mechanistic studies of their regulatory function can then be conducted through application of our *in vitro* and *in vivo* BTIC models.

## **Materials & Methods**

### ***Stem cell gene profiling in non-Shh/Wnt subtype medulloblastoma***

MB microarray data for 103 MBs were downloaded from GEO (GSE21140). These data consisted of processed Affymetrix CEL files (Affymetrix Human Exon 1.0 ST Array [transcript (gene) version]) that had undergone gene-level analysis (CORE content), quantile normalization (sketch), and summarization using PLIER with PM-GCBG background correction for 103 MBs. Clinical annotations for each MB tumor, including subgroup (Wnt, Shh, Group 3, Group 4) were also downloaded from this location. Expression values for Group 3 and 4 tumors were pooled into one group titled, “non-Shh/Wnt”. The expression of each gene was plotted as the normalized fluorescence intensity of the corresponding affymetrix probes. Similarly, raw Affymetrix datasets for 62 primary human MBs, 40 primary human MBs, 15 Daoy MB cell line samples, and 46 primary human MBs were respectively downloaded and processed from GEO (GSE10327, GSE12992, GSE7578) or <http://www.stjudereseearch.org/site/data/medulloblastoma> (Thompson, et al.(10)) and normalized using RMA(33). When available, clinical annotations for each tumor were also downloaded from these locations. When multiple probesets identified the same gene, the probeset with the highest mean expression across all patients in the dataset was used.

### ***nCounter System (NanoString) gene expression profiling***

RNA was extracted from paraffin-embedded (FFPE) tissue using Qiagen RNeasy FFPE kit. Exactly 250ng of RNA was run for each patient sample. Analysis using nCounter Gene Expression system was conducted at the Centre for Translational and Applied Genomics (CTAG) [BC Cancer Agency, Vancouver, BC]. A custom codeset synthesized by nCounter (NanoString Technologies, Seattle, WA, USA) was designed including 22

MB specific subgrouping gene probes(72) in addition to other genes of interest which include: CD15 (RefSeq NM\_002033.2), BMI1 (NM\_005180.5), FOXG1 (NM\_005249.3), SOX2 (NM\_003106.2), and POU5F1 (RefSeq NM\_002701.4). The recommendations outlined by NanoString Technologies were all followed regarding mRNA sample preparation, hybridization, detection and scanning, and data normalization.

### ***Dissociation of primary medulloblastoma tissue and neurosphere culture***

Human brain tumor samples (see Supplementary Table 3) were obtained from consenting patients, as approved by the Hamilton Health Sciences/McMaster Health Sciences Research Ethics Board. Briefly, samples were dissociated in artificial cerebrospinal fluid containing 0.2 Wunisch unit/mL Liberase Blendzyme 3 (Roche filtered through 70 µm cell strainer. Tumor cells were resuspended in tumor sphere medium consisting of a chemically defined serum-free NSC medium, and plated in an ultra-low attachment plate (Corning). The components of our complete NSC media per 500 mL include: Dulbecco's modified Eagle's medium/F12 (450 mL; Invitrogen), N2-supplement (5 mL; Invitrogen), HEPES (5 mL; Wisent), glucose (3 g; Invitrogen), *N*-acetylcysteine (60 µg/mL; Sigma), neural survival factor-1 (10 mL; Lonza), epidermal growth factor (20 ng/mL; Sigma), basic fibroblast growth factor (20 ng/mL; Invitrogen), leukemic inhibitory factor (10 ng/mL; Cehmicon). The BTIC patient isolates shown in Supplementary Table 3 are not renewable cell lines, but rather minimally cultured cell isolates (24 hours to <1 week) within stem cell conditions to select for stem cell populations. Daoy MB (American Type Culture Collection) and H9 human embryonic stem cell-derived NSCs (Invitrogen)

were also cultured in tumor sphere medium conditions and as per manufacturer's instructions, respectively.

### ***Quantitative real-time-polymerase chain reaction***

Total RNA from samples was isolated using the Qiagen RNeasy Micro kit (Qiagen) and reverse transcribed using Invitrogen's Superscript III First Strand Synthesis kit (Invitrogen). Quantitative PCR was performed using the Chroma4 (Bio-Rad) with iQSYBR Green qPCR kit (Quanta VWR). Data were presented as the ratio of the gene of interest to *GAPDH* (glyceraldehyde-3-phosphate dehydrogenase) as control. The program Primer3 (NCBI, Primer-BLAST, <http://www.ncbi.nlm.nih.gov/tools/primer-blast>) was used to design primer sequences provided in Supplementary Table 4.

### ***Viral production and transduction***

Lentiviral vectors (CS-H1-shRNA-EF-1 a-EGFP) expressing shRNA that targets human Bmi1 and luciferase were kind gifts from Dr Atushi Iwama. Lentiviral vectors expressing shRNA that targets FoxG1 and ORF expression clone for FOXG1 were from GeneCopoeia. Replication-incompetent lentivirus was produced by co-transfection of the expression vector and ViraPower packaging mix (Invitrogen). Viral supernatant was harvested 48 hours after transfection, filtered through a 0.45-mm cellulose acetate filter and precipitated by PEGit (System Biosciences). The viral pellet was resuspended in 0.5 ml of phosphate-buffered saline and stored at 80°C. Daoy cells were transduced with lentiviral vectors and treated with the respective antibiotics after 48 hours of transduction to develop stable lines.

### ***Western blotting***

Denatured total protein (20 µg) was separated using 10% sodium dodecyl sulphate–polyacrylamide gel electrophoresis and transferred to polyvinylidene fluoride membrane. Western blots were probed with monoclonal mouse-anti-human Bmi1 antibody (Upstate), polyclonal rabbit-anti-human FoxG1 antibody (Abcam) and anti-GAPDH antibody (Abcam). The secondary antibody was horseradish peroxidase conjugated goat anti-mouse IgG (Bio-Rad) or goat anti-rabbit IgG (Sigma). The bands were visualized using an Immobilon Western kit (Millipore).

### ***Immunohistochemistry***

The original histologic slides were reviewed on all cases to confirm the diagnosis of MB. A tissue microarray (TMA) was subsequently constructed from the original blocks; triplicate 1 mm cores extracted from every tumor resection performed on the patient. A total of 83 patients were included. There was patient outcomes data available for 74 of the 83 cases. Antibodies to NRP3, KCNA1 and SFRP1 were used to subgroup the Group 3, Group 4 and SHH tumor subtypes as previously described (8).  $\beta$ -catenin was used for the identification of the WNT subgroup. For these proposed subgroup specific antibodies, the Ventana Benchmark XT autostainer was employed; vendors, clones, dilutions and protocols are listed as follows:  $\beta$ -catenin - BD (ab610154) antibody, dilution 1:100, protocol cc1; SFRP - Abcam (ab4193) antibody, dilution 1:200, protocol cc1; NPR3 - Sigma (HPA031065) antibody, dilution 1:30, protease protocol; KCNA1 - Abcam (ab32433) antibody, dilution 1:200, protocol cc1. CD15 (Beckman Coulter, IM1954U)

immunohistochemical staining was performed as previously published(34). All immunohistochemical stains (with the exception of  $\beta$ -catenin) were score semi-quantitatively using a 4 point scale (0-3) that took into consideration the intensity and the diffusivity of the staining; subsequently, these scores were binarized into “low” (0,1) or “high” (2,3) categories for survival analysis.  $\beta$ -catenin was scored according to the presence of nuclear staining only; cases were considered to be either nuclear positive or negative.

#### ***Neurosphere size assay to determine BTIC proliferative potential***

Proliferative potential of MB stem cells was determined according to neurosphere size. 200 single cells were plated in a 96-microwell plate in 0.2 mL tumor sphere medium. After 5 days in culture, the size (diameter) of resulting secondary neurospheres was determined using light microscopy and Metamorph 7.1 (Molecular Devices). Similarly, neurosphere size was determined 3 days after siRNA treatment.

#### ***Cell Proliferation Assay***

Single cells were plated at a density of 1,000 cells/well in complete tumor sphere media in triplicate, in a 96-well plate (100 $\mu$ L/well) and incubated for three days. Alamar Blue (Invitrogen), a Resazurin-based fluorescent indicator of cell metabolism, was added (20 $\mu$ L) to each well approximately 18 hours prior to the readout time point. Fluorescence was measured using a FLUOstar Omega Fluorescence 556 Microplate reader (BMG LABTECH) at excitation and emission wavelengths of 535nm and 600nm respectively, according to recommendations given by the manufacturer. Readings were analyzed using

Omega analysis software. Proliferation was calculated as fold increase in viable cells over day 0.

### ***Secondary Sphere Formation Assay***

After primary sphere formation was noted, spheres were dissociated to single cells and replated in tumor sphere medium as previously described(27). To quantify stem cell frequency, the secondary and tertiary sphere formation rate was calculated from the number of spheres forming from 2000 dissociated single cells.

### ***Differentiation Assay***

Cells were differentiated in NSC media supplemented with 20% FBS which was replaced every other day. Differentiation was carried out for 7 days after which, differentiated cells were trypsinized and harvested for subsequent gene expression analyses.

### ***Chromatin Immunoprecipitation***

ChIP assays were performed using Low cell# ChiP kit (Diagenode) according to the manufacturer's instructions. Briefly, cross-linked chromatin was immunoprecipitated using anti-Bmi1 (Upstate) and anti-FoxG1 (Upstate). The input DNA was defined as an aliquot of sheared chromatin before immunoprecipitation, and was used to normalize the sample to the amount of chromatin added to each ChIP. DNA was purified from input and immunoprecipitated samples with corresponding antibodies. qPCR was performed using

the SYBR Green system on the Choma4 RT-PCR system (Bio-Rad). ChIP Primers are displayed in Supplementary Table 4.

### ***Flow Cytometric Cell Sorting***

Primary Daoy tumor spheres were dissociated to single cell suspension. CD15+ cells were enriched using flow cytometric sorting (MoFlo XDP) using PE-labeled anti-CD15 antibodies (Beckman Coulter). The percentage expression of CD15 for each group of unsorted cells and purities for CD15+/CD15- sorted cells from flow cytometric sorting were determined. The appropriate isotype control served as the negative control.

### ***In vivo MB stem cell injections and H&E staining of xenograft tumors***

BTIC xenografts from Daoy MB cell line expressing control vector, OE FoxG1, and shBmi1+OE FoxG1 were generated as previously described(35). Briefly, BTIC samples were injected into the right frontal lobe of NOD-CB17-SCID mouse brains according to Research Ethics Board-approved protocols (n=9). Mice were injected with biological replicates consisting of  $10^6$  single-cell suspensions. The resulting human tumor xenografts were fixed, embedded in paraffin for hematoxylin and eosin (H&E) staining; images were taken using an Aperio Slide Scanner and analyzed using ImageScope v11.1.2.760 software (Aperio).

### ***Statistical Analysis***

For all *in vitro* studies, biological replicates from at least three tumors are compiled for each experiment in order to achieve statistical power; unique samples were not pooled

before analyses. Data represent mean $\pm$ s.e.m., n values are listed in figure legends. Student's *t*-test analyses were performed accordingly, using the Prism 4.03 software package (GraphPad Software). The independent Student's *t*-test was used to compare the continuous variables between two groups. The level of statistical significance was set at 0.05 for all tests.

## **Results**

### ***Identification of stem cell genes preferentially expressed in non-Shh/Wnt subgroup medulloblastoma***

Current unsupervised hierarchical clustering analyses of all published MB functional genomics platforms have produced 4 molecular subgroups: Wnt, Shh, Group 3 and Group 4(13). Groups 3 and 4 share a poor clinical outcome, and as their names denote, have yet to be defined by activation of specific signaling pathways (4). Given prior work has shown increasing BTIC frequency to be associated with features of increasing tumor aggressiveness(27, 28) and reduced patient survival (24, 31, 32), we hypothesized that a candidate gene approach for known stem cell-associated genes would specify non-Shh/Wnt poor-outcome MBs. Therefore, we took the novel approach of probing four existing MB transcriptional databases (Boston(6), Amsterdam(7), Toronto(8), Memphis(10)) along with a recent NanoString-subgrouped cohort of MBs for differential stem cell gene expression patterns in Wnt, Shh, Group 3, Group 4, and non-Shh/Wnt MBs.

Examination of our candidate gene list (described in Supplementary Table 1 with their regulatory functions) (18, 19, 22, 27, 28, 36-61) consisting of genes implicated in the

self-renewal and proliferation of a number of normal and cancer stem cell populations showed enriched expression in the non-Shh/Wnt subgroup (Figure 1). Interestingly, we were able to identify *FoxG1* and *Bmi1* as being preferentially expressed in non-Shh/Wnt MBs (Figure 2, Supplementary Table 2). Although *Bmi1* has been previously studied by our group (35) and others, *FoxG1* warranted further investigation as it was the strongest overall predictor of Groups 3 and 4, and the most independently predictive gene of these tumors (see Supplementary Table 2). In addition, Fasano, et al.(41) have shown *Bmi1* and *FoxG1* to act as co-mediators of normal NSC self-renewal. *FoxG1* is a forkhead-box family transcription factor that is developmentally active in forebrain specification, and it has been shown to be frequently dysregulated in MB(62). The functional relevance of these two genes in MB stem cells was subsequently assessed using *in vitro* stem cell assays.

### ***Bmi1 and FoxG1 function as regulators of medulloblastoma stem cell properties***

Probing of MB transcriptional databases revealed a strong association of *Bmi1* and *FoxG1* with Group 3 and 4 MBs, but their functional role in MB remains unknown. We therefore decided to apply our *in vitro* and *in vivo* BTIC model systems to further interrogate the role of these genes in MB stem cells.

Having previously characterized BTIC populations from primary human MB(27, 28), we applied this experimental model system to 3 primary pediatric MBs (see Supplementary Table 3). We have called these specimens “MB stem cell patient isolates” to emphasize the fact that these cells are not renewable cell lines, but are cell isolates minimally cultured (24 hours to 1 week) under conditions that select for stem cell

populations. Owing to limited primary sample availability, we have supplemented our experimental work on human primary MB stem cells with studies of the Daoy(35), and MED8a(63) cell lines.

Given that all current MB transcriptional databases do not profile cells enriched for tumor sphere populations, we assessed the differential transcript levels of the two stem cell genes most preferentially expressed in non-Shh/Wnt subgroup MBs, *FoxG1* and *Bmi1*, within normal NSCs, Daoy and MED8a tumor spheres, and primary MB stem cells. Primer sequences are listed in Supplementary Table 4. We found *FoxG1* and *Bmi1* transcript levels to be significantly elevated in Daoy spheres, primary MB stem cells (Figure 3 a and 3b), and MED8a spheres (Supplementary Figure 4a and 4b) when compared to NSCs. No significant difference was observed in the expression of *FoxG1* and *Bmi1* between Daoy spheres, MED8a spheres and primary MB stem cells.

To interrogate the functional significance of FoxG1 and Bmi1 in regulating stem cell properties essential for promoting MB tumorigenesis, we generated FoxG1 overexpression constructs (OE FoxG1) and performed shRNA-mediated knockdown of both genes (shBmi1, shFoxG1) using multiple constructs. The efficiency of gene knockdown and overexpression was validated at protein and transcript levels for all constructs (Supplementary Figure 1). *In vitro* limiting dilutions assays for each construct correlated with the levels of FoxG1 and Bmi1 (Supplementary Figure 2). shFoxG1-2 and shBmi1-3, displaying the best gene and functional knockdowns, were chosen for further study. Tumor sphere size in cells treated with shFoxG1 and shBmi1 or OE FoxG1 was markedly reduced or increased, respectively in comparison to spheres generated from cells

treated with control vector (Figures 4a, 4b). To assess whether these genes may drive MB tumor cell proliferation we also measured the proliferative potential of tumor spheres. Cells treated with shRNA and overexpression constructs were less and more proliferative, respectively, than those cells treated with control vector (Figure 4c). Since brain tumorigenesis may be attributed to unregulated BTIC self-renewal, we assessed the self-renewal capacity of Daoy tumor spheres. Secondary tumor sphere formation was significantly diminished following knockdown, which suggested both genes to independently function as putative BTIC self-renewal genes (Figure 4d). Since *Bmi1* has been shown to co-operate with *FoxG1* in maintaining the self-renewal machinery of normal NSCs(41), we co-transduced both sh*Bmi1* and sh*FoxG1* constructs to determine if there may be an additive effect in self-renewal reduction. Interestingly, we observed a significant reduction in self-renewal compared to cells transduced with control vector. Finally we performed differentiation assays on primary MB stem cells, Daoy and Med8a tumor spheres. Although we found Daoy and Med8a tumor spheres to be refractory to standard differentiation conditions, in minimally-cultured primary human MB stem cells, we observed a decrease in neural lineage marker expression with OE *FoxG1* (Supplementary Figure 5a) and an increase with sh*FoxG1* cells (Supplementary Figure 5b). Furthermore, *FoxG1* expression decreased with differentiation of primary human MB stem cells (Supplementary Figure 5c), suggesting a role for *FoxG1* in maintaining a stem cell state.

Therefore, it became apparent that *Bmi1* and *FoxG1* function as mediators of self-renewal, proliferation, and differentiation in MB and may in fact be interacting with one another in a manner akin to normal NSCs(41). As hypothesized, OE *FoxG1*

demonstrated a significant increase in secondary sphere formation compared to control cells (Figure 4d). However, OE FoxG1+shBmi1 cells displayed a significant reduction in self-renewal capacity compared to control cells, suggesting FoxG1 overexpression to not completely rescue the reduced self-renewal capacity observed with Bmi1 knockdown (Figure 4d).

### ***FoxG1 and Bmi1 show reciprocal promoter occupancy only in CD15+ MB stem cells***

Although FoxG1 and Bmi1 have previously been shown to interact with one another through correlative overexpression and knockdown studies of either gene(41) and in our hands have been implicated in co-operating with one another to regulate self-renewal in MB tumor spheres, the mechanism for their interaction has yet to be elucidated. We hypothesized that both proteins may regulate each other's transcriptional activity through binding at one another's promoter. Consequently we performed chromatin immunoprecipitation (ChIP) experiments to assess the enrichment of FoxG1 at the *Bmi1* promoter (Figure 5a) and Bmi1 at the *FoxG1* promoter (Figure 5b). We observed no difference for enrichment at either promoter, and hypothesized that this may in fact resemble the current inability of genomic profiling of bulk tumors to identify stem cell genes preferentially expressed in poor outcome MBs, since our ChIP experiments were performed on unsorted tumor sphere populations that had not been sort-enriched for putative MB stem cells. Having validated CD15 protein expression as a marker of aggressive, poor-outcome subgroup 3 and 4 MBs from 74 MBs (Supplementary Figure 6), we performed flow cytometric cell sorting for CD15(37, 38), a marker which allows for sorting of distinct and reproducible positive and negative populations across multiple MB

model systems and cell lines (Supplementary Figure 3). We then assessed *FoxG1* and *Bmi1* transcript levels in CD15+ and CD15- cells, and found that both genes were significantly expressed in the CD15+ cell fraction when compared to the CD15- cells (Figures 5c, 5d). We then performed our ChIP experiments on CD15-sorted MB tumor cells and found a marked enrichment for FoxG1 at the *Bmi1* promoter (Figure 5e) and Bmi1 at the *FoxG1* promoter (Figure 5f) in the CD15+ cell fraction with no significant enrichment at either promoter in the CD15- population.

The cell cycle inhibitors p16 and p21 are well-defined downstream targets for repression by FoxG1 and Bmi1 to promote self-renewal in a number of tissues and malignancies(41, 64-68). We found both, *p16* (Figure 5g) and *p21* (Figure 5h) levels to be significantly elevated in the CD15- cell fraction when compared to CD15+ MB stem cells, suggesting a novel mechanism for MB stem cell self-renewal by which FoxG1 and Bmi1 may interact with one another to co-operatively inhibit p16 and p21 in CD15+ MB stem cells.

### ***In vitro and in vivo functional characterization of FoxG1/Bmi1 interactions***

In order to further interrogate the mechanistic significance of FoxG1 and Bmi1 sharing promoter occupancy, we investigated the expression of *Bmi1* levels in our stable shFoxG1, OE FoxG1, and OE FoxG1+shBmi1 cell lines. Interestingly, *Bmi1* levels were reduced and increased following FoxG1 knockdown and overexpression, respectively, when compared to stable control cells (Figure 6a). This data suggests Bmi1 to be a novel downstream target for FoxG1 signaling. Following OE FoxG1+shBmi1, we observed a

significant decrease in *Bmi1* levels when compared to control cells, revealing that FoxG1 overexpression may not be sufficient to rescue *Bmi1* knockdown at the transcript level. *Bmi1* regulation of *FoxG1* was assessed following sh*Bmi1* (Figure 6b), and a positive feedback was identified as *FoxG1* expression was significantly reduced in sh*Bmi1* cells compared to control. Moreover, OE FoxG1+sh*Bmi1* cells displayed elevated *FoxG1* levels compared to control. This data alludes to the presence of additional novel downstream targets of FoxG1 signaling aside from *Bmi1*, which may have a stronger affinity for positively regulating FoxG1 expression.

*In vivo* analysis of FoxG1 and *Bmi1* functional relevance on MB stem cell-driven tumorigenesis demonstrated OE FoxG1 MB stem cells to generate much larger and infiltrative tumors compared to smaller, well-circumscribed control tumors (Figure 6c). *In vitro* self-renewal analysis showed a reduction in self-renewal capacity in OE FoxG1+sh*Bmi1* cells compared to OE FoxG1 and control cells (Supplementary Figure 2). This finding mirrored *in vivo* characteristics of tumor size and invasiveness, as OE FoxG1+sh*Bmi1*-generated tumors were smaller than OE FoxG1 tumors and more circumscribed than control tumors. Our previously published *in vivo* findings have implicated *Bmi1* in regulating tumor size in MB(35) glioblastoma (GBM)(69), and it appears that *Bmi1* may also critically regulate tumor size and invasiveness downstream of FoxG1.

## Discussion

The classification of MB has progressively evolved to include a combination of clinico-pathological and molecular factors that reflect the clinically relevant and potentially prognostic aspects of tumor biology(4). Our understanding of the pathogenesis and basic biology of MB has been advanced considerably by the application of integrated genomics platforms to characterize molecular subgroups(6-10). It has since been widely accepted that a combination of clinical and molecular factors will afford a more reliable means of assigning disease risk in patients with MB(70, 71), allowing for a de-escalation of current therapy and a progression toward risk-tailored, individualized and targeted patient therapy.

Herein, we have characterized the functional and clinical significance of two BTIC-specific genes, *FoxG1* and *Bmi1* in regulating self-renewal of MB stem cells. Since increasing BTIC frequency is associated with decreased survival and poor patient outcome(69), we hypothesized that genes governing BTIC self-renewal may segregate aggressive, poor-outcome MBs from other subgroups. We applied this clinical outcomes-driven rationale to 251 primary human MBs through several published non-overlapping MB transcriptional databases(6-8, 10) and 74 recently NanoString-subgrouped primary MBs for candidate genes previously implicated in CSC and BTIC populations. This allowed us to ascertain a differential stem cell gene expression profile within Wnt, Shh, and non-Shh/Wnt MB subgroups. A subsequent series of step-wise knockdown, overexpression, *in vitro*, *in vivo* and ChIP analyses have allowed us to demonstrate for the first time that *FoxG1* and *Bmi1* are preferentially expressed in MB stem cells and cooperatively function to regulate their self-renewal and tumorigenicity (Figure 6d). Our

model illustrates that Bmi1 is a novel downstream target of FoxG1, through which it exerts an increase in stem cell self-renewal and tumorigenicity by inhibition of p16 and p21. This finding is of great clinical significance as BTIC self-renewal genes and their regulatory pathways may serve as novel factors used to characterize poor-outcome non-Shh/Wnt MBs in future studies.

Our ChIP data demonstrates that a differential transcriptional regulatory mechanism exists between unsorted and sort-enriched stem cell populations, in which Bmi1 and FoxG1 show reciprocal promoter binding only in CD15+ MB stem cells. Our data further suggests this difference to repress cell cycle inhibitors, p16 and p21, in CD15+ MB stem cells, permitting extensive self-renewal and proliferation in this cell fraction, while CD15- cells are maintained under the control of these cell cycle inhibitors. Recently, we have identified additional cell-cell differences between MB BTIC and non-BTICs based on the characterization of Shh-receiving and Shh-signalling cells, respectively(35). In GBM BTICs, we have observed time-dependent functional differences in Bmi1 based on the stage of BTIC differentiation and cell type as Bmi1 contributes to self-renewal in BTICs but regulates proliferation and cell fate determination in non-BTICs(69). Given these critical differences in sort-enriched BTIC and non-BTIC cell compartments of a heterogeneous tumor such as brain tumors, future characterization of MB functional genomics platforms would benefit from subgrouping based on sort-enriched MB tumor cells for elucidating novel pathways that may be aberrantly activated in MB BTICs.

The study of BTICs has reconceptualized the heterogeneity of brain tumors in terms of their biological framework and predicted therapeutic response. However, several

limitations remain in our ability to characterize these rare clonal populations of cells and this is particularly true for a rare tumor such as MB. Although our stem cell profiling technique shows promise to further characterize current high-risk MBs, the small primary sample size for our *in vitro* and *in vivo* functional studies limits the true determination of its specificity as a unique and independent identifier of high-risk disease. Although several stem cell self-renewal genes (such as Nanog, Oct4, and Lgr5) did not show enriched expression in high-risk non-Shh/Wnt MBs, our findings illustrate that regulation of self-renewal may be regional and context-dependent, explaining why some self-renewal genes critical to embryonic or epithelial stem cells may not be active in a neural micro-environment. Primary human MB BTIC cultures are technically challenging, provide limited cell numbers for data acquisition, and require specific infrastructure; therefore our platform is unlikely to be widely adapted for routine laboratory use at this point. However, continued study of larger numbers of human MB BTIC specimens will eventually elucidate key stem cell signaling pathways and molecular mechanisms of self-renewal that could provide specific targets for poor-outcome MBs. Specifically, as current transcriptional profiling of MB consists of the cellular bulk tumor population, rare stem cell fractions may be missed and therefore, future transcriptional analyses of stem cell genes may benefit from tissue banks consisting of prospectively sorted BTIC RNA. Current practice for MB molecular profiling from a single tumor biopsy or resection sample may also underestimate the genomic landscape(72), providing the BTIC model system as an ideal approach for addressing intratumor heterogeneity. Our work provides encouraging evidence to suggest that identifying and subsequently modulating stem cell populations in MB may improve

clinical outcome for those patients with metastatic and high-risk disease. Future implications of our model system may take advantage of our *in vitro* BTIC self-renewal assay, which has previously been validated to correlate with clinical outcome in pediatric brain tumors, including MB(24). With the recent application of the NanoString assay to MB molecular subgrouping(73), academic hospitals may discern low-level stem cell gene transcript levels within paraffin-embedded tissues in conjunction with our established *in vitro* self-renewal assays. Such analyses may assist in rapidly determining the stem cell phenotype of a given MB and may in turn promote more targeted and individualized treatment for a patient-specific BTIC profiles.

### **Acknowledgements**

B.M. is supported by a Canadian Institutes of Health Research Vanier Canada Graduate Scholarship. S.K.S. is supported by the Neurosurgical Research and Education Foundation and American Association of Neurological surgeons, Pediatric Section, the Ontario Institute for Cancer Research, and McMaster University Department of Surgery.

### **Conflict of Interest**

The authors declare that they have no conflict of interest.

### **References**

1. Crawford JR, MacDonald TJ, Packer RJ. Medulloblastoma in childhood: new biological advances. *Lancet Neurol* 2007;6:1073-1085.

2. Gilbertson RJ. Medulloblastoma: signalling a change in treatment. *Lancet Oncol* 2004;5:209-218.
3. Huse JT, Holland EC. Targeting brain cancer: advances in the molecular pathology of malignant glioma and medulloblastoma. *Nat Rev Cancer* 2010;10:1-13.
4. Ellison DW. Childhood medulloblastoma: novel approaches to the classification of a heterogeneous disease. *Acta Neuropathol* 2010;120:305-316.
5. Korshunov A, Remke M, Werft W, et al. Adult and pediatric medulloblastomas are genetically distinct and require different algorithms for molecular risk stratification. *J Clin Oncol* 2010;28:3054-3060.
6. Cho YJ, Tsherniak A, Tamayo P, et al. Integrative genomic analysis of medulloblastoma identifies a molecular subgroup that drives poor clinical outcome. *J Clin Oncol* 2011;29:1424-1130.
7. Kool M, Koster J, Bunt J, et al. Integrated genomics identifies five medulloblastoma subtypes with distinct genetic profiles, pathway signatures and clinicopathological features. *PLoS ONE* 2008;3:e3088.
8. Northcott PA, Korshunov A, Witt H, et al. Medulloblastoma comprises four distinct molecular variants. *J Clin Oncol* 2011;29:1408-1414.
9. Pomeroy SL, Tamayo P, Gaasenbeek M, et al. Prediction of central nervous system embryonal tumour outcome based on gene expression. *Nature* 2002;415:436-442.

10. Thompson MC, Fuller C, Hogg TL, et al. Genomics identifies medulloblastoma subgroups that are enriched for specific genetic alterations. *J Clin Oncol* 2006;24:1924-1931.
11. Ellison DW, Onilude OE, Lindsey JC, et al. beta-Catenin status predicts a favorable outcome in childhood medulloblastoma: the United Kingdom Children's Cancer Study Group Brain Tumour Committee. *J Clin Oncol* 2005;23:7951-7957.
12. Fattet S, Haberler C, Legoix P, et al. Beta-catenin status in paediatric medulloblastomas: correlation of immunohistochemical expression with mutational status, genetic profiles, and clinical characteristics. *J Pathol.* 2009;218:86-94.
13. Taylor MD, Northcott PA, Korshunov A, et al. Molecular subgroups of medulloblastoma: the current consensus. *Acta Neuropathol* 2012;123:465-472.
14. Pfister S, Remke M, Benner A, et al. Outcome prediction in pediatric medulloblastoma based on DNA copy-number aberrations of chromosomes 6q and 17q and the MYC and MYCN loci. *J Clin Oncol* 2009;27:1627-1636.
15. Romer JT, Kimura H, Magdaleno S, et al. Suppression of the Shh pathway using a small molecule inhibitor eliminates medulloblastoma in *Ptc1<sup>+/-</sup>p53<sup>-/-</sup>* mice. *Cancer Cell* 2004;6:229-240.
16. Rudin CM, Hann CL, Laterra J, et al. Treatment of medulloblastoma with hedgehog pathway inhibitor GDC-0449. *N Engl J Med* 2009;361:1173-1178.

17. Kool M, Korshunov A, Remke M, et al. Molecular subgroups of medulloblastoma: an international meta-analysis of transcriptome, genetic aberrations, and clinical data of WNT, SHH, Group 3, and Group 4 medulloblastomas. *Acta Neuropathol* 2012;123:473-484.
18. Pei Y, Moore CE, Wang J, et al. An animal model of MYC-driven medulloblastoma. *Cancer Cell* 2012;21:155-167.
19. Kawauchi D, Robinson G, Uziel T, et al. A mouse model of the most aggressive subgroup of human medulloblastoma. *Cancer Cell* 2012;21:168-180.
20. Remke M, Hielscher T, Korshunov A, et al. FSTL5 Is a marker of poor prognosis in non-WNT/non-SHH medulloblastoma. *J Clin Oncol* 2011;29:3852-3861.
21. Fan X, Khaki L, Zhu TS, et al. Notch pathway blockade depletes CD133-positive glioblastoma cells and inhibits growth of tumor neurospheres and xenografts. *Stem Cells* 2010;28:5-16.
22. Leung C, Lingbeek M, Shakhova O, et al. Bmi1 is essential for cerebellar development and is overexpressed in human medulloblastomas. *Nature* 2004;428: 337-341.
23. Schreck KC, Taylor P, Marchionni L, et al. The notch target Hes1 directly modulates Gli1 expression and hedgehog signaling: A potential mechanism of therapeutic resistance. *Clin Cancer Res* 2010;16:6060-6070.

24. Panosyan EH, Laks DR, Masterman-Smith M, et al. Clinical outcome in pediatric glial and embryonal brain tumors correlates with in vitro multi-passageable neurosphere formation. *Pediatr Blood Cancer* 2010;55:644-651.
25. Clarke MF, Dick JE, Dirks PB, et al. Cancer stem cells--Perspectives on current status and future directions: AACR workshop on cancer stem cells. *Cancer Res* 2006;66:9339-9944.
26. Reya T, Morrison S, Clarke M. Stem cells, cancer, and cancer stem cells. *Nature* 2001;414:105-111.
27. Singh S, Clarke I, Terasaki M, et al. Identification of a cancer stem cell in human brain tumors. *Cancer Res* 2003;63:5821-5828.
28. Singh SK, Hawkins C, Clarke ID, et al. Identification of human brain tumour initiating cells. *Nature* 2004;432:396-401.
29. Gage F. Mammalian neural stem cells. *Science* 2000;287:1433-1438.
30. Reynolds BA, Weiss S. Clonal and population analyses demonstrate that an EGF-responsive mammalian embryonic CNS precursor is a stem cell. *Dev Biol* 1996;175:1-13.
31. Laks DR, Masterman-Smith M, Visnyei K, et al. Neurosphere formation is an independent predictor of clinical outcome in malignant glioma. *Stem Cells* 2009;27:980-987.
32. Pallini R, Ricci-Vitiani L, Montano N, et al. Expression of the stem cell marker CD133 in recurrent glioblastoma and its value for prognosis. *Cancer* 2010;117:162-174.

33. Irizarry RA, Hobbs B, Collin F, et al. Exploration, normalization, and summaries of high density oligonucleotide array probe level data. *Biostatistics* 2003;4:249-264
34. Lee C, Fotovati A, Triscott J, et al. Polo-Like Kinase 1 (PLK1) inhibition kills glioblastoma multiforme brain tumour cells in part through loss of Sox2 and delays tumour progression in mice. *Stem Cells*. 2012;30:1064-1075.
35. Wang X, Venugopal C, Manoranjan B, et al. Sonic hedgehog regulates Bmi1 in human medulloblastoma brain tumor-initiating cells. *Oncogene* 2012;31:187-199
36. Lessard J, Sauvageau G. Bmi-1 determines the proliferative capacity of normal and leukaemic stem cells. *Nature* 2003;423:255-260.
37. Read TA, Fogarty MP, Markant SL, et al. Identification of CD15 as a marker for tumor-propagating cells in a mouse model of medulloblastoma. *Cancer Cell* 2009;15:135-47.
38. Ward RJ, Lee L, Graham K, et al. Multipotent CD15+ cancer stem cells in patched-1-deficient mouse medulloblastoma. *Cancer Res* 2009;69:4682-4890.
39. O'Brien CA, Pollett A, Gallinger S, et al. A human colon cancer cell capable of initiating tumour growth in immunodeficient mice. *Nature* 2007;445:106-110.
40. Ricci-Vitiani L, Lombardi DG, Pilozzi E, et al. Identification and expansion of human colon-cancer-initiating cells. *Nature* 2007;445:111-115.
41. Fasano CA, Phoenix TN, Kokovay E, et al. Bmi-1 cooperates with Foxg1 to maintain neural stem cell self-renewal in the forebrain. *Genes Dev* 2009;23:561-574.

42. Regad T, Roth M, Bredenkamp N, et al. The neural progenitor-specifying activity of FoxG1 is antagonistically regulated by CKI and FGF. *Nat Cell Biol* 2007;9:532-540.
43. Barker N, Ridgway RA, van Es JH, et al. Crypt stem cells as the cells-of-origin of intestinal cancer. *Nature* 2009;457:608-611.
44. Kanemura Y, Mori K, Sakakibara S, et al. Musashi1, an evolutionarily conserved neural RNA-binding protein, is a versatile marker of human glioma cells in determining their cellular origin, malignancy, and proliferative activity. *Differentiation* 2001;68:141-152.
45. Po A, Ferretti E, Miele E, et al. Hedgehog controls neural stem cells through p53-independent regulation of Nanog. *EMBO J* 2010;25:1-13.
46. Fareh M, Turchi L, Virolle V, et al. The miR 302-367 cluster drastically affects self-renewal and infiltration properties of glioma-initiating cells through CXCR4 repression and consequent disruption of the SHH-GLI-NANOG network. *Cell Death Differ* 2012;19:232-244.
47. Jeter CR, Liu B, Liu X, et al. NANOG promotes cancer stem cell characteristics and prostate cancer resistance to androgen deprivation. *Oncogene*. 2011;30:3833-3845.
48. Chiou SH, Wang ML, Chou YT, et al. Coexpression of Oct4 and Nanog enhances malignancy in lung adenocarcinoma by inducing cancer stem cell-like properties and epithelial-mesenchymal transdifferentiation. *Cancer Res* 2010;70: 10433-10444.

49. Moon JH, Yoon BS, Kim B, et al. Induction of neural stem cell-like cells (NSCLCs) from mouse astrocytes by Bmi1. *Biochem Biophys Res Commun* 2008;371: 267-272.
50. Rodini CO, Suzuki DE, Saba-Silva N, et al. Expression analysis of stem cell-related genes reveal OCT4 as a predictor of poor clinical outcome in medulloblastoma. *J Neurooncol* 2012;106:71-79.
51. Beltran AS, Rivenbark AG, Richardson BT, et al. Generation of tumor-initiating cells by exogenous delivery of OCT4 transcription factor. *Breast Cancer Res* 2011;13: R94.
52. Hagerstrand D, He X, Bradic Lindh M, et al. Identification of a SOX2-dependent subset of tumor- and sphere-forming glioblastoma cells with a distinct tyrosine kinase inhibitor sensitivity profile. *Neuro Oncol* 2011;13:1178-1191.
53. Sutter R, Shakhova O, Bhagat H, et al. Cerebellar stem cells act as medulloblastoma-initiating cells in a mouse model and a neural stem cell signature characterizes a subset of human medulloblastomas. *Oncogene* 2010;29:1845-1856.
54. Leis O, Eguiara A, Lopez-Arribillaga E, et al. Sox2 expression in breast tumours and activation in breast cancer stem cells. *Oncogene* 2011; 31:1354-1365.
55. Basu-Roy U, Seo E, Ramanathapuram L, et al. Sox2 maintains self renewal of tumor-initiating cells in osteosarcomas. *Oncogene* 2012;31:2270-2282.
56. Beck S, Jin X, Sohn YW, et al. Telomerase activity-independent function of TERT allows glioma cells to attain cancer stem cell characteristics by inducing EGFR expression. *Mol Cells* 2011;31:9-15.

57. Didiano D, Shalaby T, Lang D, et al. Telomere maintenance in childhood primitive neuroectodermal brain tumors. *Neuro Oncol* 2004;6:1-8.
58. Yang MH, Hsu DS, Wang HW, et al. Bmi1 is essential in Twist1-induced epithelial–mesenchymal transition. *Nat Cell Biol* 2010;12:982-992.
59. Mikheeva SA, Mikheev AM, Petit A, et al. TWIST1 promotes invasion through mesenchymal change in human glioblastoma. *Mol Cancer* 2010;9:194.
60. Gibson P, Tong Y, Robinson G, et al. Subtypes of medulloblastoma have distinct developmental origins. *Nature* 2010;468:1095-1099.
61. Kim J, Woo AJ, Chu J, et al. A Myc network accounts for similarities between embryonic stem and cancer cell transcription programs. *Cell* 2010;143:313-324.
62. Adesina AM, Nguyen Y, Mehta V, et al. FOXP1 dysregulation is a frequent event in medulloblastoma. *J Neurooncol* 2007;85:111-122.
63. Northcott PA, Shih DJ, Peacock J, et al. Subgroup-specific structural variation across 1,000 medulloblastoma genomes. *Nature* 2012;488:49-56.
64. Yadirgi G, Leinster V, Acquati S, et al. Conditional activation of Bmi1 expression regulates self-renewal, apoptosis, and differentiation of neural stem/progenitor cells in vitro and in vivo. *Stem Cells* 2011;29:700-712.
65. Chan DW, Liu VW, To RM, et al. Overexpression of FOXP1 contributes to TGF-beta resistance through inhibition of p21WAF1/CIP1 expression in ovarian cancer. *Br J Cancer* 2009;101:1433-1443.

66. Fasano CA, Dimos JT, Ivanova NB, et al. shRNA knockdown of Bmi-1 reveals a critical role for p21-Rb pathway in NSC self-renewal during development. *Cell Stem Cell* 2007;1:87-99.
67. Subkhankulova T, Zhang X, Leung C, et al. Bmi1 directly represses p21Waf1/Cip1 in Shh-induced proliferation of cerebellar granule cell progenitors. *Mol Cell Neurosci* 2010;45:151-162.
68. Molofsky AV, Pardal R, Iwashita T, et al. Bmi-1 dependence distinguishes neural stem cell self-renewal from progenitor proliferation. *Nature* 2003;425:962-967.
69. Venugopal C, Li N, Wang X, et al. Bmi1 marks intermediate precursors during differentiation of human brain tumor initiating cells. *Stem Cell Res* 2012;8:141-153.
70. Gilbertson R, Wickramasinghe C, Hernan R, et al. Clinical and molecular stratification of disease risk in medulloblastoma. *Br J Cancer* 2001;85:705-712.
71. Gilbertson RJ, Ellison DW. The origins of medulloblastoma subtypes. *Annu Rev Pathol* 2008;3:341-365.
72. Gerlinger M, Rowan AJ, Horswell S, et al. Intratumor heterogeneity and branched evolution revealed by multiregion sequencing. *N Engl J Med* 2012;366:883-892.
73. Northcott PA, Shih DJ, Remke M, et al. Rapid, reliable, and reproducible molecular sub-grouping of clinical medulloblastoma samples. *Acta Neuropathol* 2012; 123:615-626.

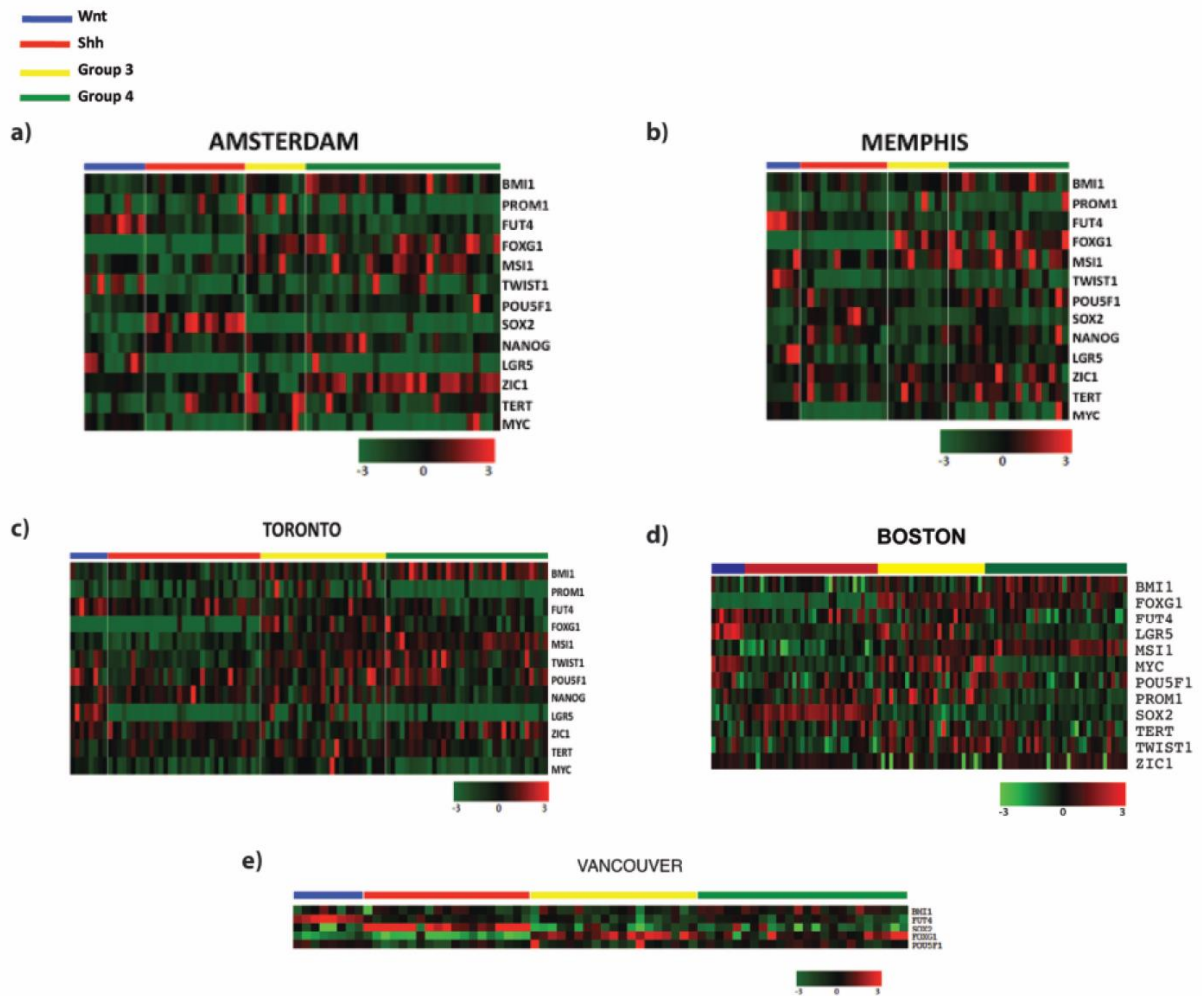


**Figure 1: Multiple candidate stem cell genes are preferentially expressed in non-Shh/Wnt subgroup medulloblastomas.** (a-d) Affymetix exon array data in four independent datasets shows a differential expression pattern in which many candidate cancer stem cell genes are associated with poor outcome Group 3 and 4 MBs. (e) NanoString gene expression data for select genes showing enrichment in Group 3 and 4 MBs.

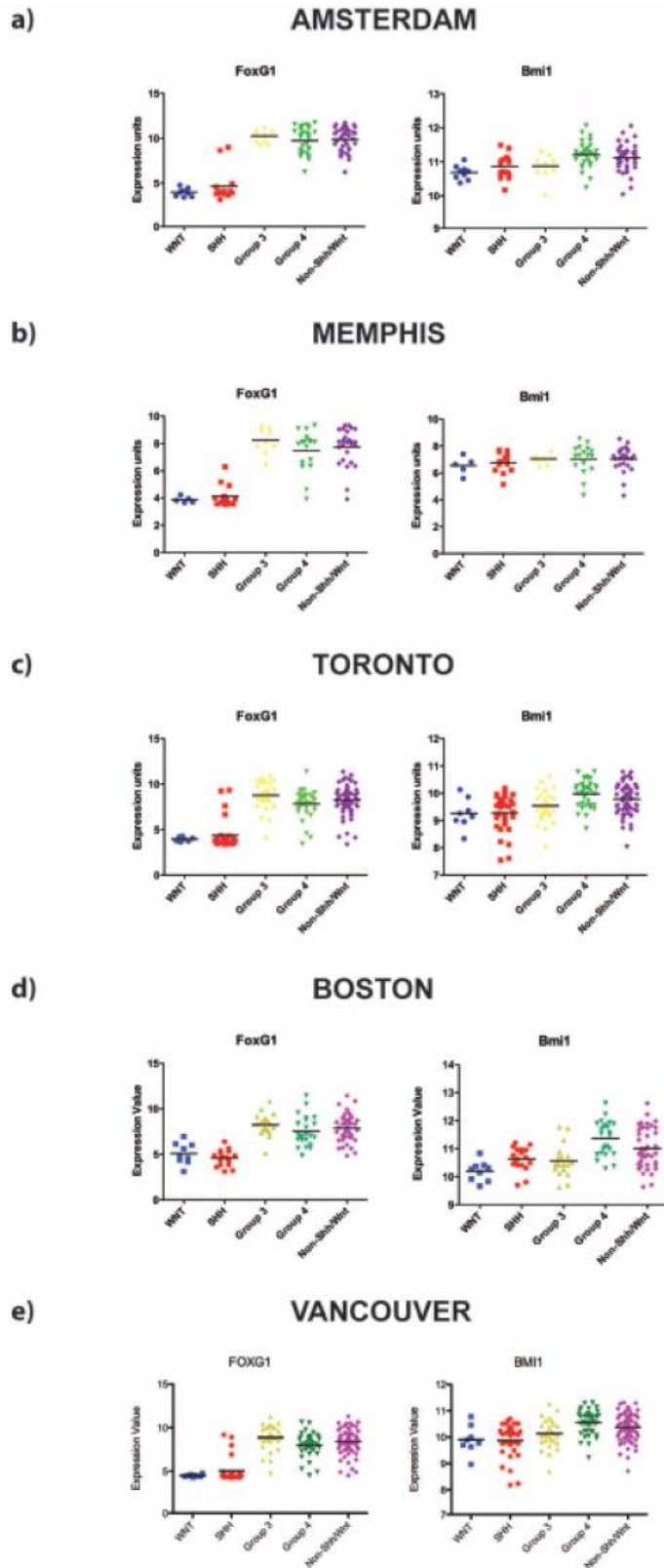


**Figure 2: *FoxG1* and *Bmi1* expression identify non-Shh/Wnt subgroup medulloblastomas.** (a-d) Affymetix exon array and (e) NanoString data show enriched *FoxG1* and *Bmi1* expression in poor-outcome MB subgroups ( $P<0.05$ ). Data are presented as log<sub>2</sub>-transformed signal intensity (that is, expression).

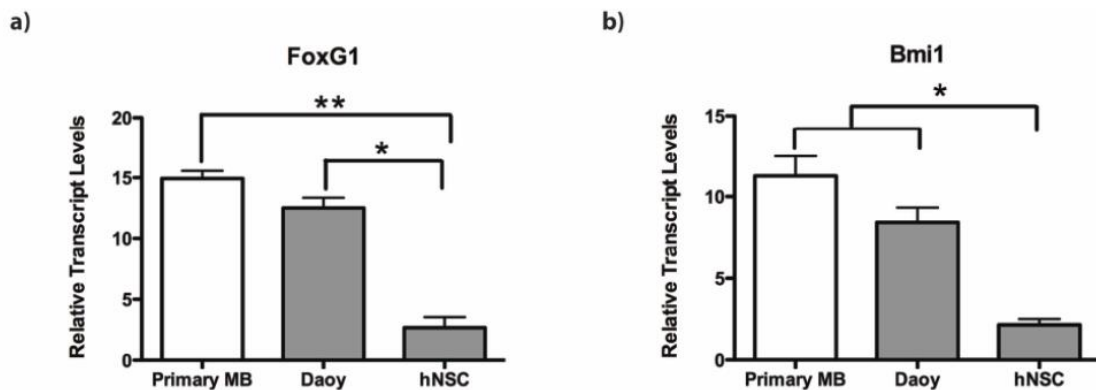


**Figure 3: *FoxG1* and *Bmi1* are significantly expressed in primary medulloblastoma stem cells and Daoy tumor spheres.** (a) *FoxG1* transcript levels are significantly elevated in primary human MB stem cells (n=3, BT1-3,  $P=0.0075$ ) and Daoy MB tumor spheres (n=3,  $P=0.0146$ ) when compared to normal human NSCs (n=3). (b) Similarly, *Bmi1* transcript levels are significantly elevated in primary human MB stem cells (n=3, BT1-3,  $P=0.0191$ ) and Daoy MB tumor spheres (n=3,  $P=0.0238$ ) when compared to normal human NSCs (n=3). \* $P<0.05$ , \*\* $P<0.01$

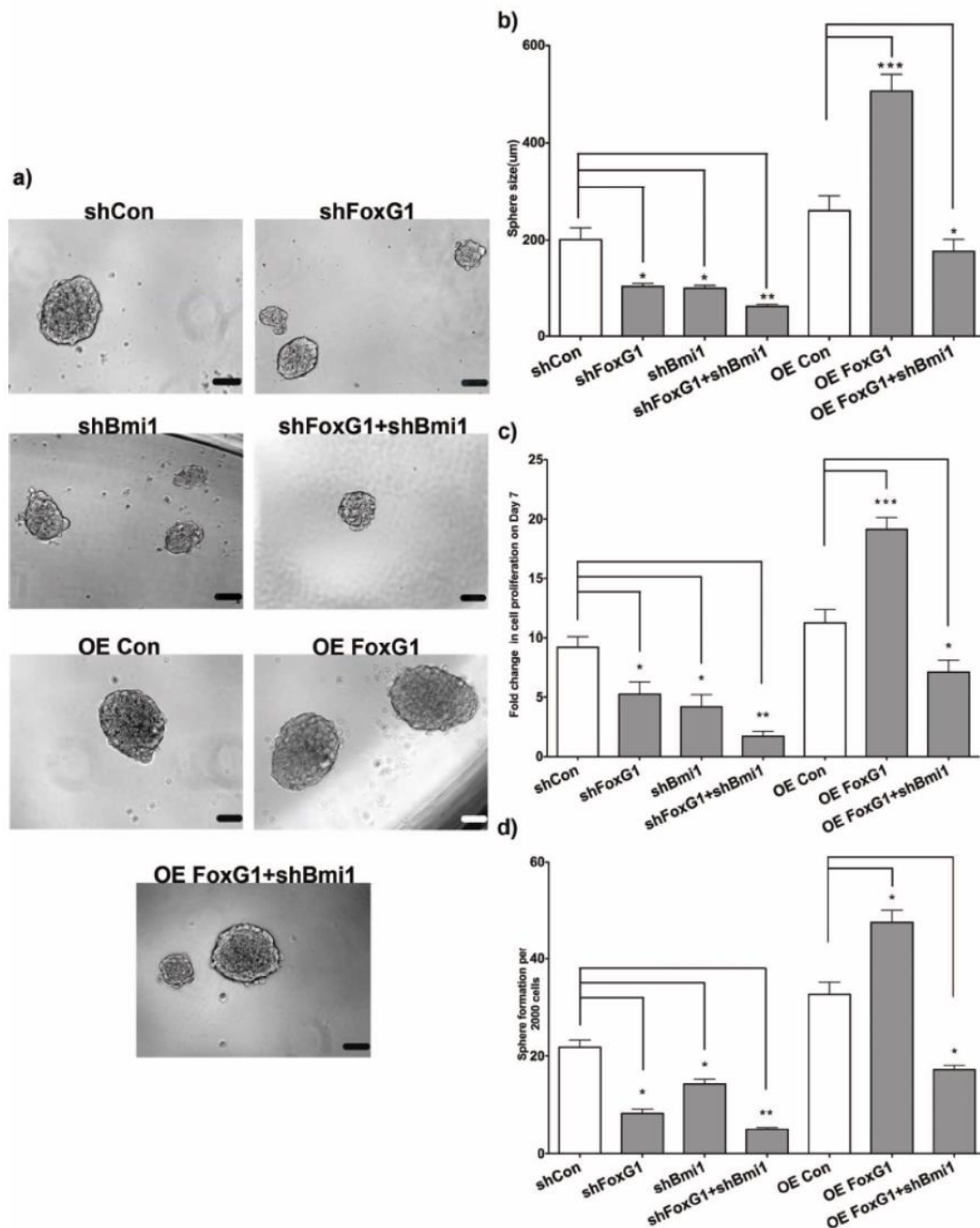


**Figure 4: *FoxG1* and *Bmi1* function to regulate proliferation and self-renewal of medulloblastoma stem cells.** Daoy tumor spheres knocked down for FoxG1 (shFoxG1), Bmi1 (shBmi1), and FoxG1+Bmi1 (shFoxG1+shBmi1) showed a decrease in (a, b) sphere size (n=3,  $P=0.034$ ; n=3,  $P=0.027$ ; n=3,  $P=0.003$ , respectively) when compared to control

cells. Conversely, Daoy tumor spheres overexpressing FoxG1 (OE FoxG1) showed an increase in (a, b) sphere size ( $n=3$ ,  $P=0.0003$ ), but a reduction compared to control cells when cotransduced shBmi1 ( $n=3$ ,  $P=0.042$ ). (c) Daoy tumor sphere proliferative potential was significantly reduced with shFoxG1, shBmi1, shFoxG1+shBmi1 ( $n=3$ ,  $P=0.0103$ ;  $n=3$ ,  $P=0.0481$ ;  $n=3$ ,  $P=0.0017$ , respectively) and significantly elevated in OE FoxG1 cells ( $n=3$ ,  $P=0.0003$ ). Together, OE FoxG1+shBmi1 reduced the proliferative potential of tumor spheres, suggesting Bmi1 as a possible feedback regulator of FoxG1 expression ( $n=3$ ,  $P=0.0113$ ). (d) Self-renewal capacity was further diminished following shFoxG1, shBmi1, and shFoxG1+shBmi1 ( $n=3$ ,  $P=0.0170$ ;  $n=3$ ,  $P=0.0431$ ;  $n=3$ ,  $P=0.00087$ , respectively) when compared to control cells. In contrast, self-renewal capacity is enhanced in OE FoxG1 cells ( $n=3$ ,  $P=0.0412$ ) and reduced in OE FoxG1+shBmi1 cells ( $n=3$ ,  $P=0.0285$ ) compared to control. Scale bar = 100  $\mu\text{m}$ . \* $P<0.05$ , \*\* $P<0.005$ , \*\*\* $P<0.0005$ .

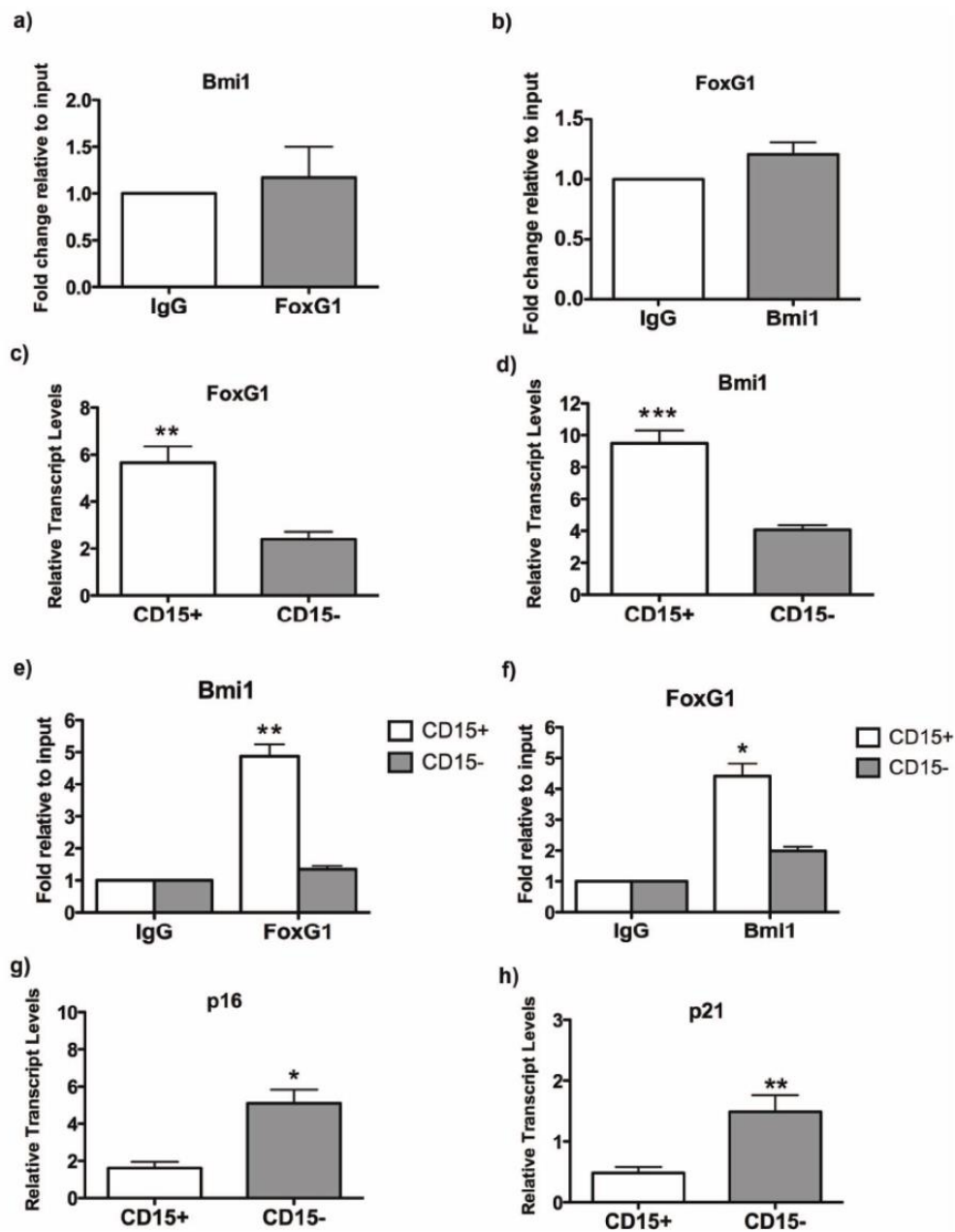


**Figure 5: Bmi1 and FoxG1 display differential binding at promoters within distinct CD15+ enriched stem cells.** Neither (a) FoxG1 nor (b) Bmi1 appear to enrich at the *Bmi1* or *FoxG1* promoters, respectively, in unsorted tumor sphere populations (n=5,  $P=0.3253$ ; n=5,  $P=0.8848$ , respectively). Cell sorting for CD15, shows CD15+ cells to contain

significantly elevated transcript levels of (c) *FoxG1* (n=3,  $P=0.0016$ ) and (d) *Bmi1* (n=3,  $P<0.0001$ ) when compared to CD15<sup>-</sup> cells. ChIP experiments in CD15<sup>-</sup> sorted tumor sphere populations demonstrate significant enrichments for (e) FoxG1 at the *Bmi1* promoter (n=5,  $P=0.0151$ ) and (f) Bmi1 at the *FoxG1* promoter (n=5,  $P=0.0044$ ) in the CD15<sup>+</sup> cell fraction. There were no enrichments observed in the CD15<sup>-</sup> cell fraction for either (e) FoxG1 at the *Bmi1* promoter (n=5,  $P=0.0759$ ) or (f) Bmi1 at the *FoxG1* promoter (n=5,  $P=0.2323$ ). CD15<sup>-</sup> cells display increased expression levels of downstream targets of FoxG1 and Bmi1, (g) *p16* (n=3,  $P=0.0062$ ) and (h) *p21* (n=3,  $P=0.0015$ ) when compared to CD15<sup>+</sup> cells. \* $P<0.05$ , \*\* $P<0.005$ , \*\*\* $P<0.0001$

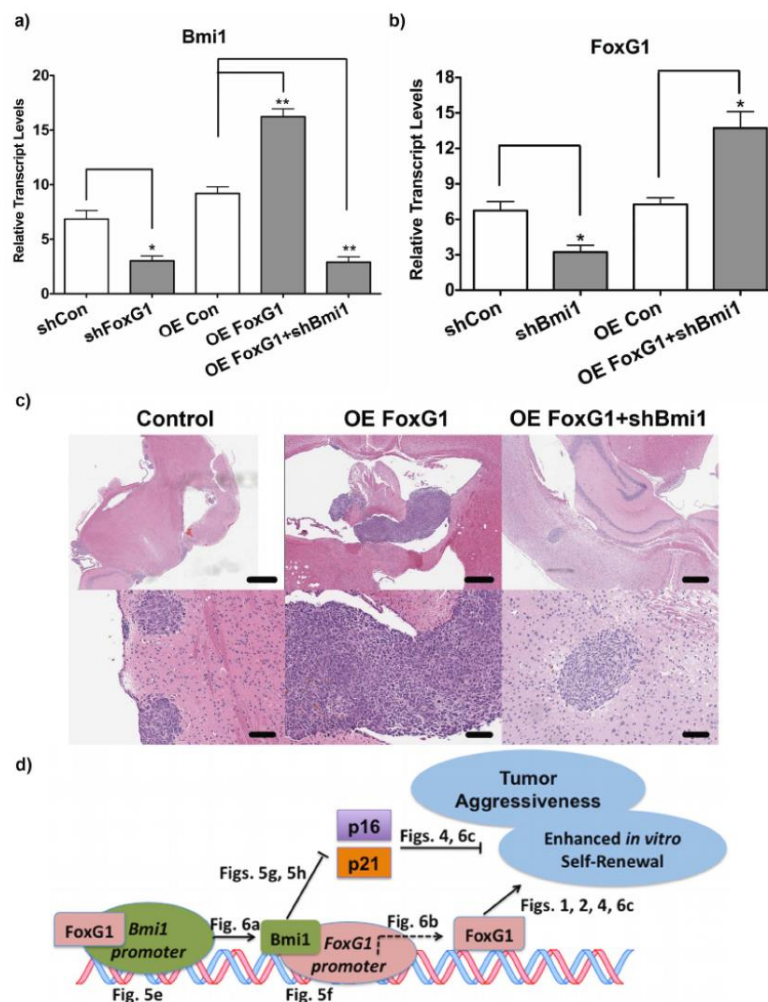
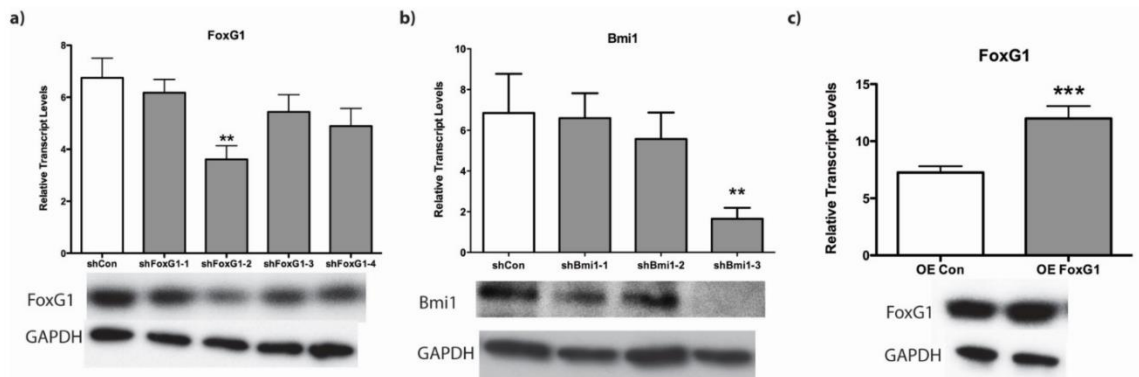
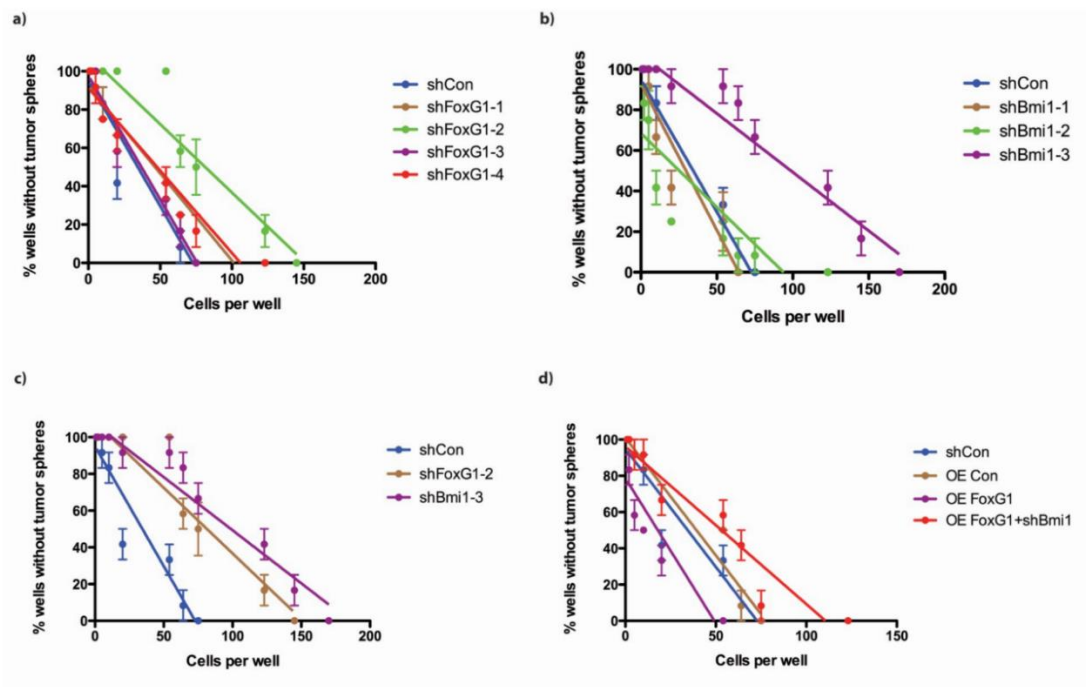


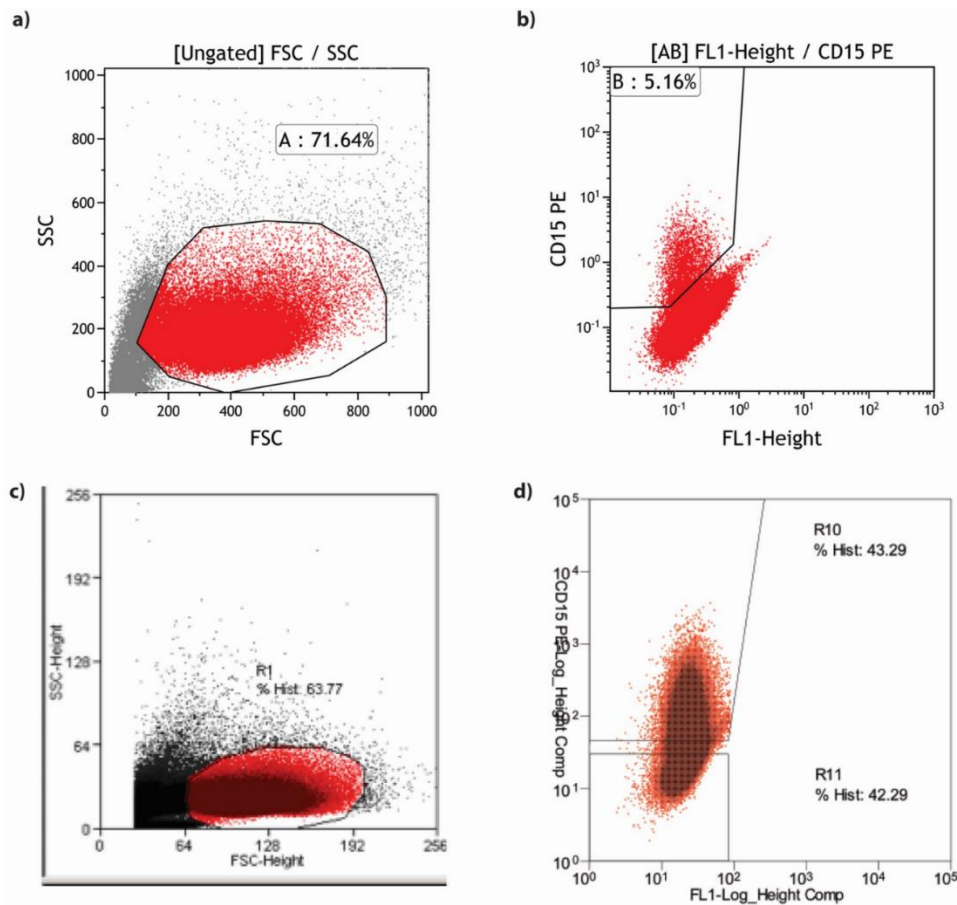
**Figure 6: Bmi1 is a novel downstream target of FoxG1, through which it exerts an increase in tumorigenicity.** (a) *Bmi1* levels are reduced and increased following shFoxG1 and OE FoxG1, respectively, when compared to stable control cells (n=3,  $P=0.0063$ ; n=3,  $P=0.0001$ , respectively). OE FoxG1+shBmi1 resulted in a significant decrease in *Bmi1* levels compared to control cells (n=3,  $P=0.0001$ ), revealing that FoxG1 overexpression may not be sufficient to rescue Bmi1 knockdown at the transcript level. (b) A positive feedback with Bmi1 on *FoxG1* expression was demonstrated with a reduction in *FoxG1* levels compared to control cells with shBmi1 (n=3,  $P=0.0209$ ) and an elevation in *FoxG1* expression within OE FoxG1+shBmi1 cells (n=3,  $P=0.0143$ ). (c) *In vivo* analysis (top panel, x20; bottom panel, x100) demonstrated OE FoxG1 MB stem cells to generate much larger and infiltrative tumors compared to smaller, well-circumscribed control tumors. Interestingly, OE FoxG1+shBmi1 tumors were smaller than OE FoxG1 tumors and more circumscribed than control tumors. (d) Model of FoxG1 regulation of Bmi1 expression and Bmi1 feedback on FoxG1 expression to promote *in vivo* tumor aggressiveness and enhanced *in vitro* stem cell self-renewal. Scale bar = 100  $\mu\text{m}$ . \* $P<0.05$ , \*\* $P<0.0001$



**Supplementary Figure 1: FoxG1 and Bmi1 knockdown lead to an efficient reduction in their transcript and protein levels.** shRNA-mediated knockdown of (a) FoxG1 revealed a significant knockdown in shFoxG1-2 construct when compared to cells transduced with a control shRNA construct (n=3,  $P=0.0047$ ). All other constructs, shFoxG1-1, shFoxG1-3, shFoxG1-4 had varying levels of knockdown but were not significant at transcript level (n=3,  $P=0.5669$ , n=3,  $P=0.2636$  and n=3,  $P=0.1425$ , respectively). (b) shRNA-mediated knockdown of (b) Bmi1 revealed a significant knockdown in shBmi1-3 construct when compared to cells transduced with a control shRNA construct (n=3,  $P=0.001$ ). All other constructs, shBmi1-1 and shBmi1-2, had varying levels of knockdown but were not significant at transcript level (n=3,  $P=0.7923$ , and n=3,  $P=0.2064$ , respectively). (c) Overexpression construct for FoxG1 revealed a significant increase in FoxG1 expression compared to cells transduced with a control construct (n=3,  $P=0.0018$ ). \*\* $P<0.05$ , \*\*\* $P<0.005$

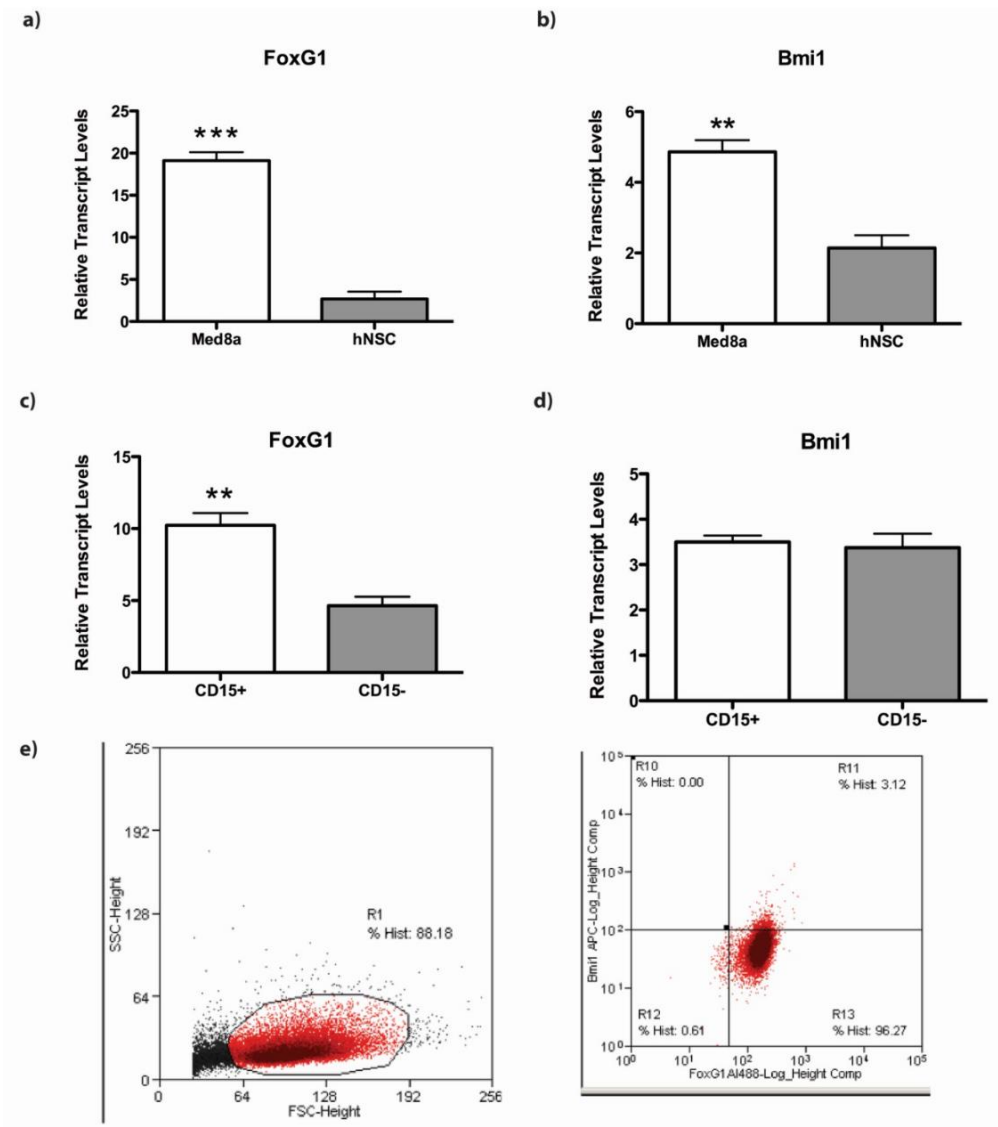


**Supplementary Figure 2: Functional characterization of FoxG1 knockdown/overexpression and Bmi1 knockdown constructs through *in vitro* limiting dilution assays.** Characterization of (a) 4 shFoxG1 and (b) 3 shBmi1 constructs with (c) shFoxG1-2 and shBmi1-3 showing the greatest reduction in sphere-forming capacity. (d) Cells transduced with OE FoxG1 and OE FoxG1+shBmi1 constructs displayed an increase and decrease in sphere-forming capacity, respectively.



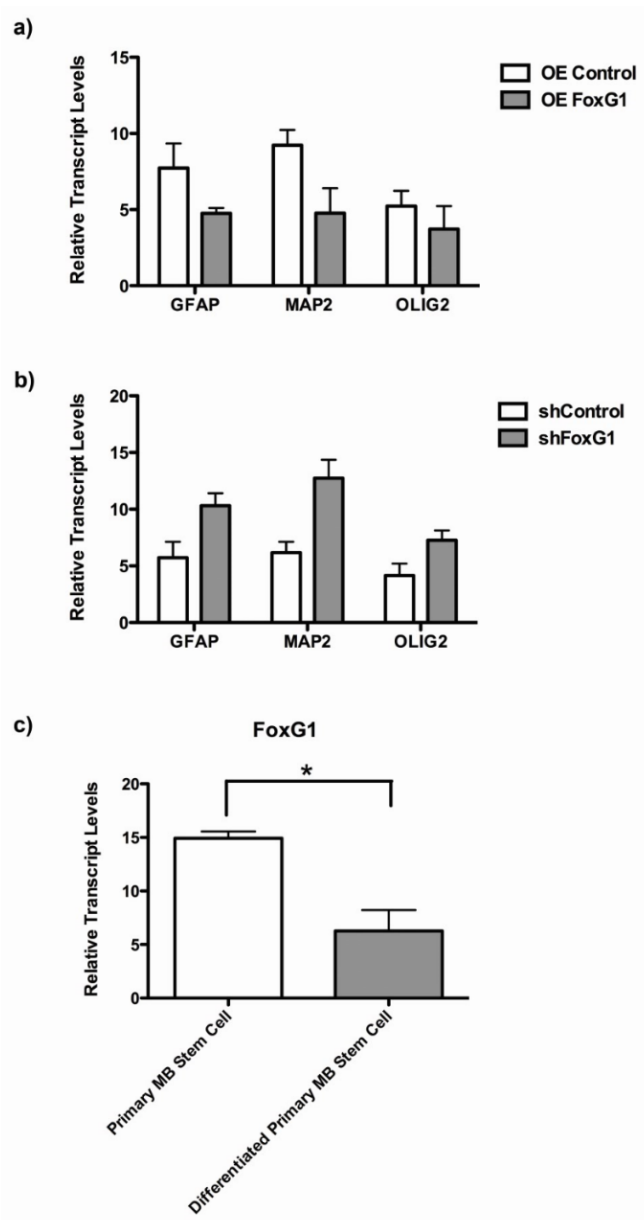
**Supplementary Figure 3: Representative flow cytometric cell sorting plot for CD15 in Daoy and Med8a medulloblastoma stem cells.** (a) Flow plot showing side scatter against forward scatter for Daoy MB stem cells. (b) Flow plot of sort sample showing

5.16% of cells being CD15+. (c) Flow plot showing side scatter against forward scatter for Med8a MB stem cells. (d) Flow plot of sort sample showing 43.29% of cells being CD15+.

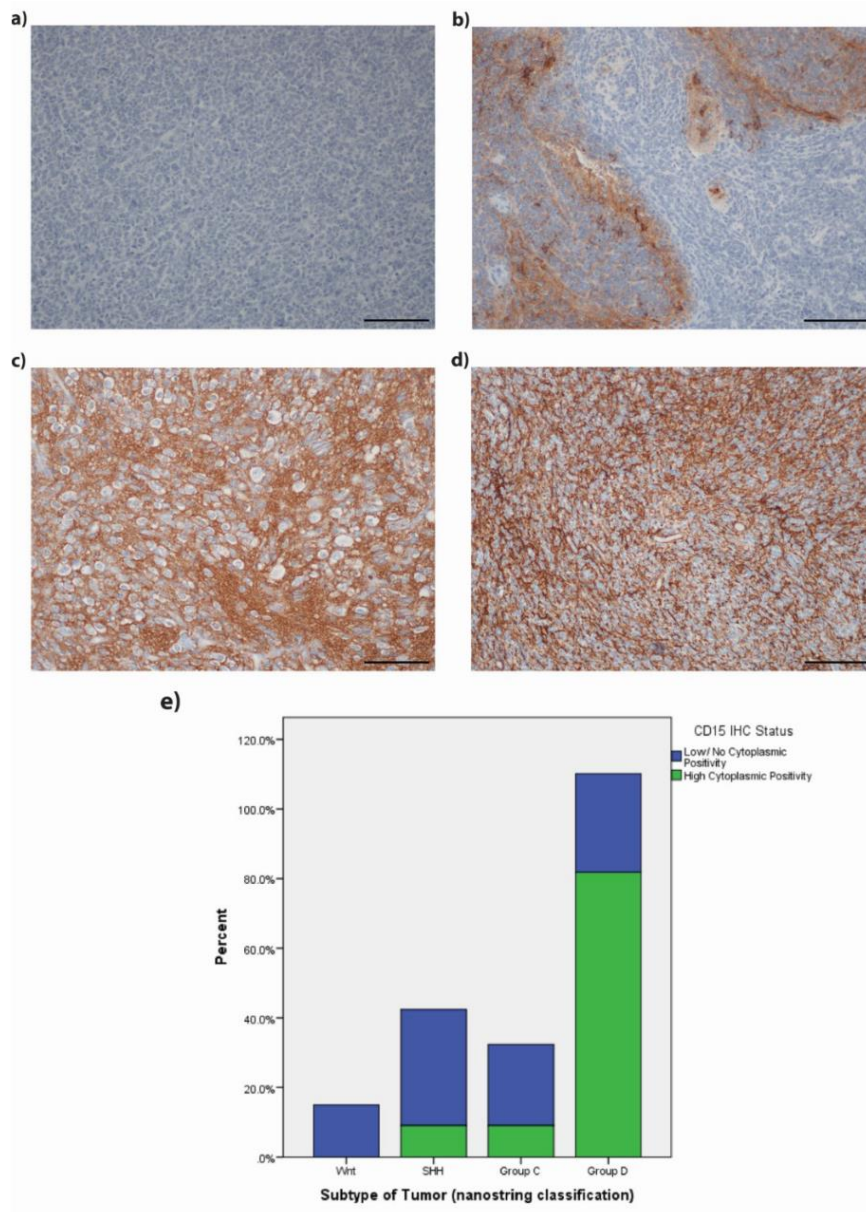


**Supplementary Figure 4: FoxG1 and Bmi1 are differentially enriched in Med8a medulloblastoma cells.** (a) *FoxG1* (n=3,  $P=0.00044$ ) and (b) *Bmi1* (n=3,  $P=0.0031$ ) expression are significantly elevated in Med8a MB cells grown in NSC conditions

compared to normal human NSCs (n=3). (c) *FoxG1* is specifically enriched in CD15+ Med8a MB stem cells compared to CD15- cells (n=5,  $P=0.00041$ ), however, (d) no difference is observed in *Bmi1* expression between CD15+ and CD15- cells (n=5,  $P=0.7332$ ). (e) Flow plot (left) showing side scatter against forward scatter for Med8a MB stem cells along with (right) FoxG1 and Bmi1 levels showing 99.39% positivity for FoxG1 and 3.12% positivity for Bmi1.  $**P<0.005$ ,  $***P<0.0005$



**Supplementary Figure 5: FoxG1 regulation of MB BTIC differentiation.** A general trend demonstrating a (a) decrease in *GFAP*, *MAP2*, and *OLIG2* expression was observed in OE FoxG1 cells compared to control cells (n=3), whereas an (b) increase in neural differentiation marker expression was observed in shFoxG1 cells when compared to control cells (n=3). (c) Additionally, *FoxG1* expression was found to decrease with differentiation in primary human MB BTICs (n=3,  $P=0.0482$ ). \* $P<0.05$



**Supplementary Figure 6: Putative MB BTIC marker, CD15, is preferentially expressed in subgroup 3 and 4 MBs.** Representative images of differential cytoplasmic CD15 expression in (a) Wnt, (b) Shh, (c) Group 3, and (d) Group 4 MBs. (e) Graphical representation of low/no cytoplasmic CD15 staining to high cytoplasmic positivity within MB subgroups. CD15 staining is marked in non-Shh/Wnt subgroups. (Magnification: x200)

<b>Gene</b>	<b>Description</b>	<b>References</b>
<b><i>Bmi1</i></b>	As a member of the Polycomb Group 1, <i>Bmi1</i> is a key regulator of self-renewal in a number of normal and malignant stem cell populations through repression of the <i>ink4a/Arf</i> locus.	22, 35, 36
<b><i>CD15 (Fut4, SSEA1, Lewis-X)</i></b>	CD15 is a carbohydrate moiety that is an established neural stem cell marker and has more recently been identified as a novel marker for brain tumor-initiating cells using a <i>Ptch</i> <sup>+/-</sup> mouse model.	37, 38
<b><i>CD133 (Prominin1)</i></b>	CD133 is a cell surface glycoprotein that has been used to mark hematopoietic and neural stem cells along with the more recent characterization of brain tumor and colon cancer-initiating cells.	27, 28, 39, 40
<b><i>FoxG1</i></b>	<i>FoxG1</i> is a forebrain-specific transcription factor that functions to prevent neuronal progenitor cells from undergoing premature differentiation and thereby maintains stemness.	41, 42
<b><i>Lgr5</i></b>	<i>Lgr5</i> has been used to mark both normal and malignant stem cell populations within the intestinal crypt.	43
<b><i>Musashi1</i></b>	<i>Musashi1</i> is an evolutionarily well-conserved neural RNA-binding protein used to mark neural precursor cells whose loss has been shown to have	44

	a detrimental effect on the maintenance of tumor sphere populations.	
<i>Myc</i>	Myc is a marker of stem cell populations and has been shown to be responsible for an embryonic stem cell signature in cancer along with initiating tumors when ectopically expressed in stem cell populations.	18, 19, 61
<i>Nanog</i>	Nanog is an essential pluripotency factor in embryonic stem cells and may be required for reactivating the stemness properties of several cancer stem cell populations.	45, 46, 47, 48, 49
<i>Oct4</i>	Oct4 is the key factor required for reprogramming cell fates and is essential in maintaining the self-renewal and pluripotency properties of embryonic stem cells.	48, 50, 51
<i>Sox2</i>	Sox2 encodes a family of high-mobility group transcription factors that have critical roles in organogenesis. Recently, Sox2 has been used to characterize tumor-initiating cells in the brain, breast, and osteosarcoma to name a few.	52, 53, 54, 55
<i>Tert</i>	Tert is the catalytic subunit of the enzyme telomerase and functions to enable cells to avoid chromosomal shortening during repeated replication through maintaining telomere length.	56, 57
<i>Twist1</i>	Twist1, an upstream regulator of Bmi1, is a basic helix-loop-helix transcription factor, which promotes epithelial-mesenchymal transition in normal development and metastatic/invasive properties in cancer.	58, 59
<i>Zic1</i>	Zic1 marks neural precursor cells at various stages throughout development and has recently been used to mark subtype-specific cells of origin in MB.	60

**Supplementary Table 1:** Candidate gene list

Upregulated in Groups 3 and 4 Medulloblastomas										
	Amsterdam		Memphis		Toronto		Boston		Vancouver	
	FC	<i>P</i>	FC	<i>P</i>	FC	<i>P</i>	FC	<i>P</i>	FC	<i>P</i>
<b>Bmi1</b>	1.3	0.014	1.3	0.058	1.4	0.002	1.7	9.4 x 10 <sup>-5</sup>	1.4	3.6 x10 <sup>-4</sup>
<b>CD15</b>	-2.3	0.002	-1.4	0.006	-1.1	0.005	-1.4	0.012	-1.7	0.00765
<b>CD133</b>	-1.3	0.64	1.9	0.14	1.8	0.22	-1.1	0.492	N/A	N/A
<b>FoxG1</b>	24	0.002	15	0.002	9.6	0.002	2.0	0	8.6	7.14x 10 <sup>-16</sup>
<b>Lgr5</b>	-2.6	0.13	-1.2	0.28	-1.6	0.35	-1.1	0.736	N/A	N/A
<b>Musashi1</b>	1.2	0.001	1.1	0.06	1.8	0.002	2.5	2.3 x 10 <sup>-12</sup>	N/A	N/A
<b>Myc</b>	1.9	0.32	2.6	0.12	1.5	0.16	1.2	0.205	N/A	N/A
<b>Nanog</b>	1.1	0.19	1	0.77	-1.2	0.08	N/A	N/A	N/A	N/A
<b>Oct4</b>	1.2	0.43	1	0.77	1	0.72	1.1	0.703	1.4	0.08832
<b>Sox2</b>	-11.2	0.002	-1.9	0.004	N/A	N/A	-2.8	1.4 x 10 <sup>-12</sup>	-4.5	0.00073
<b>Tert</b>	1.1	0.26	1.9	0.36	1	0.53	1.0	0.904	N/A	N/A
<b>Twist1</b>	1.4	0.5	-2.1	0.1	1.2	0.004	1.7	3.7 x 10 <sup>-5</sup>	N/A	N/A
<b>Zic1</b>	1.4	0.014	1.2	0.12	-1.2	0.18	-1.3	0.059	N/A	N/A

FC: fold change

**Supplementary Table 2:** Statistical evaluation of candidate genes

<b>SAMPLE ID</b>	<b>GENDER</b>	<b>AGE AT DIAGNOSIS</b>	<b>PATHOLOGICAL SYBTYPE</b>
BT 1	F	3	Classic
BT 2	M	12	Classic
BT 3	M	17	Classic

BT: brain tumor

F: female

M: male

**Supplementary Table 3:** Medulloblastoma stem cell patient isolates: Clinico-pathological data

<b>RT-PCR Primers</b>	
GAPDH F	5'TGCACCACCAACTGCTTAGC3'
GAPDH R	5'GGCATGGACTGTGGTCATGAG3'
Bmi1 F	5'GGAGGAGGTGAATGATAAAAGAT3'
Bmi1 R	5'AGGTTCCCTCCTCATAATGACA3'
FoxG1 F	5'GCCACAATCTGTCCCTCAAC3'
FoxG1 R	5'GACGGGTCCAGCATCCAGTA3'
p16 F	5'CAGGTGGGTAGAGGGTCTGC3'
p16 R	5'GCCAGGAGGAGGTCTGTGATT3'
p21 F	5'TGTCACTGTCTTGTACCCTTG3'
p21 R	5'GGCGTTTGGAGTGGTAGAA3'
GFAP F	5'AGATTCGAGAAACCAGCCTGGACA3'
GFAP R	5'TCCTGCCTCACATCACATCCTTGT3'
Map2 F	5'TTCTGTGAGTGCAGATGCTGAGGT3'
Map2 R	5'AGGTGATGGCAATGGGACTGTGTA3'
Olig2 F	5'TAAGCTGTTTGCTCACGTGACTGC3'
Olig2 R	5'CTACAAAGCCCAGTTTGCAACGCA3'

ChIP Primers	
Bmi1 F	5'CCACTCTGCCTTCAGCGGTGCA3'
Bmi1 R	5'CATACTACGATTATTTTCATAGTTGC3'
FoxG1 F	5'CCCATGTGGGATGAAACAGCCTTT3'
FoxG1 R	5'AGGTTCGGTTGGAGGTTGAAGTGA3'

**Supplementary Table 4:** qRT-PCR & ChIP primers

### **Chapter 3: Wnt activation as a therapeutic strategy in medulloblastoma**

#### **Preamble**

This chapter is an original manuscript submitted on February 22, 2019 to *Cell Stem Cell*.

Extended datasets and Supplementary Tables 1 and 2 will be available upon publication.

Manoranjan B, Venugopal C, Bakhshinyan D, Richards L, Kameda-Smith MM, Adile AA, Whitley O, Dvorkin-Gheva A, Subapanditha M, Savage N, Tatari N, Winegarten N, Hallett R, Provias JP, Yarascavitch B, Ajani O, Fleming A, Bader GD, Pugh TJ, Doble BW, Singh SK

Experimental concept and study design were developed by myself, C. Venugopal, B.W. Doble, and S.K. Singh. MB samples and clinical details were provided by J.P. Provias, B. Yarascavitch, O. Ajani, A. Fleming, and S.K. Singh. I performed RNA extraction for RNA-seq. RNA-seq was outsourced to McMaster core facility. RNA-seq analysis was performed by O. Whitley under the supervision of G.D. Bader and A. Dvorkin-Gheva with input from R. Hallett. I performed all Wnt/TCF reporter, cell proliferation, secondary sphere formation assays with assistance from D. Bakhshinyan and A.A. Adile for revision experiments. *In vivo* experiments were led and performed by myself with assistance from N. Savage. *In vivo* experiments for revision experiments were performed by M.M. Kameda-Smith, D. Bakhshinyan, and A.A. Adile. Immunofluorescence on xenografts was performed by N. Tatari. I performed all Wnt3A conditioned medium experiments and quantitative real-time polymerase chain reactions. I

performed all western immunoblotting with assistance from A.A. Adile and M.M. Kameda-Smith for manuscript revisions. Lentiviral studies were all performed by myself and C. Venugopal. Flow cytometric analysis and cell-sorting were performed by M. Subapanditha. I performed all small molecule Wnt activation experiments and *in vitro* radiotherapy. Single-cell RNA-seq prep was performed by D. Bakhshinyan. Samples were run by N. Winegarden and analysis performed by L. Richards under the supervision of T. Pugh.

The main objective of this body of work was to determine if the observed clinical differences in overall survival for patients with Wnt and non-Wnt MBs may be due to Wnt-driven inhibition of BTIC self-renewal genes. This preclinical findings from this work establishes activated Wnt signaling as an innovative treatment paradigm with high clinical utility in childhood MB and provides evidence for the context-specific tumor suppressive function of the Wnt/ $\beta$ -catenin pathway.

**Wnt activation as a therapeutic strategy in medulloblastoma**

Branavan Manoranjan<sup>1,2,3</sup>, Chitra Venugopal<sup>2</sup>, David Bakhshinyan<sup>2,3</sup>, Laura Richards<sup>4,5</sup>, Michelle M. Kameda-Smith<sup>2,3</sup>, Ashley A. Adile<sup>2,3</sup>, Owen Whitley<sup>6,8</sup>, Anna Dvorkin-Gheva<sup>9</sup>, Minomi Subapanditha<sup>2</sup>, Neil Savage<sup>2</sup>, Nazanin Tatari<sup>2</sup>, Neil Winegarden<sup>4,5</sup>, Robin Hallett<sup>2</sup>, John P. Provias<sup>9</sup>, Blake Yarascavitch<sup>10</sup>, Olufemi Ajani<sup>10</sup>, Adam Fleming<sup>11</sup>, Gary D. Bader<sup>6,7,8</sup>, Trevor J. Pugh<sup>4,5</sup>, Bradley W. Doble<sup>2,3</sup>, Sheila K. Singh<sup>2,3,10</sup>

<sup>1</sup>Michael G. DeGroote School of Medicine, McMaster University, Hamilton, Ontario, L8S 4K1, Canada

<sup>2</sup>McMaster Stem Cell and Cancer Research Institute, McMaster University, Hamilton, Ontario, L8S 4K1, Canada

Departments of <sup>3</sup>Biochemistry and Biomedical Sciences, <sup>9</sup>Pathology, <sup>10</sup>Surgery, <sup>11</sup>Pediatrics, Faculty of Health Sciences, McMaster University, 1200 Main Street West, Hamilton, Ontario, L8N 3Z5, Canada

<sup>4</sup>Princess Margaret Cancer Centre, University Health Network, Toronto, Ontario M5G 2M9, Canada

Departments of <sup>5</sup>Medical Biophysics, <sup>6</sup>Molecular Genetics, <sup>7</sup>Computer Science, University of Toronto, Toronto, Ontario M5S 1A8, Canada

<sup>8</sup>The Donnelly Centre, University of Toronto, Toronto, Ontario, M5S 3E1, Canada

## **Running Title**

Wnt activation to treat pediatric medulloblastoma

**Keywords:** medulloblastoma, Wnt, beta-catenin, Bmi1, Sox2, brain tumor-initiating cell

## **Acknowledgements**

B.M. is supported by a Canadian Institutes of Health Research Vanier Canada Graduate Scholarship, American Brain Tumor Association Medical Student Summer Fellowship, Alex's Lemonade Stand Foundation for Childhood Cancer Pediatric Oncology Student Training Program (POST), Mac-Gaensslen Foundation of Canada Medical Student Research Grant, and Brain Tumour Foundation of Canada Medical Student Research Scholarship. S.K.S. is supported by the Canadian Institutes of Health Research Operating Grant, Neurosurgical Research and Education Foundation and American Association of Neurological Surgeons, Pediatric Section, the Ontario Institute for Cancer Research, Brain Tumour Foundation of Canada and McMaster University Department of Surgery.

## **Corresponding Author**

Sheila K. Singh, MD, PhD, FRCS(C)

Associate Professor of Pediatric Neurosurgery,

Department of Surgery, McMaster Children's Hospital,

Scientist, McMaster Stem Cell & Cancer Research Institute

MDCL 5027, 1280 Main Street West, Hamilton, ON, L8S 4K1, Canada

T: 905-521-2100 x75237

F: 905-521-992

Email: [ssingh@mcmaster.ca](mailto:ssingh@mcmaster.ca)

## Introduction

Medulloblastoma (MB), the most common malignant pediatric brain tumor, is defined by four molecular subgroups (Wnt, Shh, Group 3, Group 4) based on transcriptional and epigenetic profiles<sup>1,2</sup>. Wnt MB accounts for 10% of cases with the majority harboring somatic *CTNNB1* mutations and chromosomal alterations for monosomy 6<sup>1</sup>. Clinically, Wnt MBs have the most favorable prognosis with a >95% 5-year survivorship<sup>2</sup>. By contrast, non-Wnt MBs are characterized by metastatic disease, increased rates of recurrence, and intermediate-poor overall survivorship<sup>2</sup>. Given that Wnt MBs represent the only subgroup in which metastasis is not indicative of a poor prognosis<sup>3</sup>, it has been suggested that Wnt signaling may contribute to their remarkable response to therapy<sup>4-8</sup>. Using primary patient-derived MB brain tumor-initiating cell (BTIC) lines, we have characterized intrinsic differences in the tumor-initiating capacity of Wnt and non-Wnt MBs. In this work, we aimed to discover if Wnt activation in non-Wnt MBs could serve as a rationale for therapy employing a novel substrate-competitive peptide Wnt agonist. Our preclinical work establishes activated Wnt signaling as an innovative treatment paradigm with high clinical utility in childhood MB and provides evidence for the context-specific tumor suppressive function of the Wnt/ $\beta$ -catenin pathway.

## Results & Discussion

To assess the biological validity of our MB BTIC model, we asked if gene expression differences between subgroups in bulk MB manifested themselves in our model. We performed differential expression analysis from bulk MB data<sup>9</sup> to identify upregulated genes specific to each subgroup, and scored both the bulk MB data and our

MB BTIC lines for these upregulated gene expression signatures using single-sample gene set enrichment analysis (ssGSEA)<sup>10</sup>. As expected, the WNT upregulated genes (n = 6326), Group 3 upregulated genes (n = 7491), and Group 4 upregulated genes (n = 6510) showed strongest positive enrichment in bulk MB WNT samples, Group 3 samples, and Group 4 samples, respectively, validating the specificity of the signatures (Supplementary Fig. 1a). Interestingly, the WNT, Group 3, and Group 4 MB signatures showed strongest relative enrichment in our WNT (BT853), Group 3 (SU\_MB002), and Group 4 (ICB1299) MB BTIC lines, respectively (Supplementary Fig. 1b), showing preservation of subgroup affiliation among our MB BTIC lines.

Using principal component analyses (PCA), we examined the inter-subgroup heterogeneity between MB BTIC lines from Wnt, Group 3, and Group 4 MBs (Supplementary Fig. 2a). RNA-seq data from these lines yielded distinct gene expression profiles between Wnt and non-Wnt MBs (Supplementary Fig. 2b-e, Supplementary Table 1). Specifically, several genes implicated in the self-renewal of malignant stem cell populations and previously described by our group to be enriched in poor-outcome MBs<sup>11</sup> were more highly expressed in Group 3 and 4 MBs when compared to Wnt MB (Supplementary Fig. 2f). *Bmi1* and *Sox2* are hallmark master regulatory stem cell genes essential to BTIC self-renewal, and thus enriched in experimental BTIC models<sup>12-14</sup>. Gene set enrichment analysis (GSEA) of non-Wnt MB (Group 3 MB line (Supplementary Fig 3a) and Group 4 MB line (Supplementary Fig 3b)) showed enrichment of genes in the *Bmi1* signature, which function as key epigenetic regulators of fate determination and self-renewal in normal and malignant cerebellar stem cells<sup>13</sup>. By contrast, cell cycle checkpoint

and apoptosis gene signatures were more active in Wnt MB lines (Supplementary Fig. 3b) when compared to Group 4 MBs. Pathway network analysis further identified an increase in DNA replication, transcriptional regulation, ribosomal processing, and translational regulation in non-Wnt MB lines (Supplementary Fig. 3c, Supplementary Table 2), suggestive of a hyperproliferative state.

Additional differences between Wnt and non-Wnt MBs were determined using *in vitro* and *in vivo* tumorigenic assays. TCF reporter assays showed a significant increase in endogenous Wnt activity in Wnt compared to non-Wnt MBs (Fig. 1a). Similar to the Wnt-mediated inhibition of cerebellar stem cell self-renewal<sup>15</sup>, proliferation (Fig. 1b) and self-renewal (Fig. 1c) were impaired in Wnt MBs. Xenografts generated with  $5.0 \times 10^5$  Wnt MB cells led to tumor formation in 4/5 mice, whereas no tumors formed with  $1.0 \times 10^5$  cells (0/5 mice). By contrast, all non-Wnt MB xenografts formed tumors at both numbers (10/10 mice) (Fig. 1d). Overall tumor volume was higher in non-Wnt than Wnt MB xenografts (Fig. 1e). Wnt MBs also contained a marked survival advantage compared to non-Wnt MBs when pooling survival for xenografts generated with  $1.0 \times 10^5$  and  $5.0 \times 10^5$  cells (Fig. 1f). The observed *in vivo* growth differences are most likely reflective of the *in vitro* differences in proliferation and self-renewal between Wnt and non-Wnt MBs. These findings support the clinical observations of prognostic variations among MB subgroups.

Previous work hypothesized the improved outcome in Wnt MB to be due to the secretion of soluble Wnt antagonists by tumor cells that may impair the blood-brain-barrier, rendering it more susceptible to chemotherapy<sup>7</sup>. Our data suggests the inhibition of self-renewal pathways to explain the improved outcome seen in Wnt MB. The integrity of the

Wnt/ $\beta$ -catenin pathway in non-Wnt MBs was assessed using Wnt3A-conditioned medium. A significant increase in *Axin2* expression, a conserved downstream Wnt target gene<sup>16</sup>, was noted in cells cultured in Wnt3A-conditioned medium (Supplementary Fig. 4a). Wnt3A-mediated pathway activation also reduced secondary tumor sphere size (Supplementary Fig. 4b-c), frequency (Supplementary Fig. 4d), and cell proliferation in non-Wnt MBs (Supplementary Fig. 4e). These findings support a transient alteration in the oncogenic phenotype of aggressive MBs following Wnt activation.

Since developmental processes may be carried forward from ontogeny into oncology and both *Bmi1* and *Sox2* have been implicated in cerebellar and MB development<sup>13,17</sup>, we investigated their clinical utility in a cohort of 377 Group 3 and 4 MBs<sup>9</sup>. Using a *Bmi1* gene signature that predicts metastasis, tumor progression, and death from cancer<sup>18</sup>, we found a reduced overall survivorship for patients with elevated expression of the signature (Fig. 2a). Using a similar approach, a *Sox2* gene signature<sup>19</sup> identified *Sox2*<sup>high</sup> patients to have a significant reduction in overall survival (Fig. 2b). To further understand factors associated with patient outcome, we performed univariate and multivariate survival analyses, which included the index, age, metastatic status and subgroup. *Bmi1* signature genes (Supplementary Table 3) showed a significant association with patient outcome in a univariate analysis ( $p=0.0113$ ), which remained significant ( $p=0.0287$ ) when adjusted for age, metastatic status, and subgroup. Metastatic status alone was not significantly associated with patient outcome in both univariate and multivariate analyses, but it was significantly associated with the index ( $p=0.03339$ ). The *Sox2* signature index (Supplementary Table 4) showed a significant association with patient

survival in univariate analysis ( $p = 0.00441$ ) but became a trend when it was adjusted for age, metastatic status, and subgroup for the multivariate analysis ( $p = 0.0924$ ). In addition, it showed association with metastatic status and subgroup ( $p=0.03888,0.02943$  respectively). The expression of both self-renewal genes *Bmi1* and *Sox2* were reduced in Wnt MB BTICs when compared to non-Wnt MB BTICs (Fig. 2c and Supplementary Fig. 5a-c), indicating differences in self-renewal activity across MB subgroups.

Considering that *CTNGB1*, which encodes  $\beta$ -catenin, is mutated in 86% of Wnt MBs, we ectopically expressed a stabilized  $\beta$ -catenin mutant in non-Wnt MBs. *Axin2* expression was used to determine sufficient overexpression (Fig. 2c-d). *Bmi1* and *Sox2* were reduced following  $\beta$ -catenin overexpression (Fig. 2c-d). The self-renewal capacity of  $\beta$ -catenin-overexpressing lines was markedly reduced when compared to controls (Fig. 2e). Orthotopic injections of non-Wnt MB cells revealed a significant reduction in overall tumor burden (Fig. 2f-g) and increase in survival (Fig. 2h) following the ectopic expression of  $\beta$ -catenin.

While genetic heterogeneity exists within individual MB subgroups<sup>9</sup>, general subgroup affiliation does not change at recurrence<sup>20</sup>, metastasis<sup>21</sup>, or within different regions of a tumor<sup>22</sup>. However, much of this work has been done on bulk tumor samples without considering subclonal variations observed at a single cell level. Given that emerging data in other malignancies have implicated subclonal genetic drivers in disease progression and relapse<sup>23,24</sup>, we performed single cell RNA-seq on Wnt and non-Wnt MB lines (Fig. 3a, Fig. 4, Supplementary Fig. 6-7) to understand the functional relevance of subclonal Wnt activity in MB cells. As expected, cells from the Wnt MB line had the

highest enrichment for the Wnt subgroup gene signature (Fig. 3c-d). Intriguingly, we identified that a small population of cells in Group 3 and 4 MB lines exhibited high Wnt subgroup signature scores, similar to cells of Wnt subgroup origin (Fig. 3b). These results support the presence of a rare population of cells in Group 3 and 4 MBs that resemble Wnt subgroup cells. We then wondered if these Wnt-active cells maintained the reduced tumorigenic potential observed in Wnt MB. Using a lentiviral Wnt reporter (7XTCF-GFP)<sup>25</sup>, we identified rare Wnt-active cells (TGP+) from non-Wnt MBs. Both Wnt-active (TGP+) and Wnt-inactive (TGP-) cells were isolated using flow cytometric cell sorting. Wnt activity in TGP+ cells were validated with the TCF Wnt reporter assay (Fig. 5a) and *Axin2* transcript levels (Fig. 5b). TGP+ cells contained reduced levels of *Bmi1* and *Sox2* transcript (Fig. 5b) and protein expression (Fig. 5c). Decreased proliferative (Fig. 5d) and self-renewal (Fig. 5e) indices were also noted in TGP+ compared to TGP- cells. Separate xenografts generated from orthotopic injections of TGP+ or TGP- cells revealed a reduced tumor burden (Fig. 5f) and enhanced survival (Fig. 5g) in TGP+ xenografts compared to TGP-. These data highlight the intrinsic tumor suppressive role of activated Wnt signaling in MB. To examine the clinical utility of our model systems, we used the Wnt hallmark gene signature to probe a clinically annotated dataset of 113 Group 3 human MBs<sup>9</sup> for differences in overall survival. Group 3 patients with high expression of the Wnt hallmark signature maintained a longer overall survival compared to those with low expression (Fig. 5h). As a result, endogenous Wnt activity in non-Wnt MBs appears to be a powerful predictor of improved survivorship in MBs that are otherwise metastatic and refractory to current treatments. To further understand factors associated with patient outcome, we

performed univariate and multivariate survival analyses, which included the index, age and metastatic status. The index based on the *Wnt* signature (see Supplementary Table 5) was the only factor that showed a significant association with patient survival in univariate analysis ( $p = 0.0158$ ) and when it was adjusted for the other factors, such as age and metastatic status ( $p = 0.0103$ ).

To develop a therapeutic strategy employing Wnt activation, we initially used the small molecule GSK-3 inhibitor, CHIR99021, which acts as a competitive inhibitor of ATP binding<sup>26</sup>. GSK-3 functions to inhibit Wnt/ $\beta$ -catenin signaling by phosphorylating the downstream Wnt effector,  $\beta$ -catenin, rendering it nonfunctional. TCF reporter measured Wnt activation following exposure to CHIR99021 in non-Wnt MB lines (Supplementary Fig. 8a-b). *Axin2* transcript levels (Supplementary Fig. 8c-d) and increase in nuclear and cytoplasmic  $\beta$ -catenin levels (Supplementary Fig. 8e) provided further validation of Wnt activation. *Bmi1* and *Sox2* expression were decreased following CHIR99021 treatment (Supplementary Fig. 8c-d). Although CHIR99021 also reduced the proliferative and self-renewal abilities (Supplementary Fig. 8f-g) of non-Wnt MBs, we were unable to proceed to preclinical studies due to limited blood-brain-barrier permeability.

In an attempt to find a suitable preclinical molecule, we identified L807mts, a novel GSK-3 inhibitor that functions through a substrate-to-inhibitor conversion mechanism within the GSK-3 catalytic site<sup>27</sup>. TCF reporter activity confirmed Wnt activation in L807mts-treated cells (Fig. 6a-b), which was further corroborated with *Axin2* expression (Fig. 7e-f) and  $\beta$ -catenin expression (Supplementary Fig. 8e). PCA was used to examine changes in the transcriptional machinery following L807mts treatment (Fig. 7a). RNA-seq

data from L807mts-treated cells showed diverging gene expression profiles (Fig. 7b, Fig. 6c-e, Supplementary Table 2). We obtained a gene signature for non-Wnt MBs by comparing them separately to Group 3 and 4 MBs. In order to assess the activation of Wnt by L807mts treatment, we examined enrichment of the top 50 and top 100 signatures in the samples treated with L807mts relative to the matching samples treated with PBS. Enrichment analysis was performed with GSEA<sup>28,29</sup>. Top genes up-regulated in Wnt MBs were found to be enriched in corresponding non-Wnt MB samples treated with L807mts. This provides supportive evidence for the observed activation of Wnt signaling in non-Wnt MBs treated with L807mts (Fig. 6f-g). The *Bmi1* gene signature was also reduced in L807mts-treated samples as per GSEA (Fig. 7c). Additional GSEA identified an increase in the expression of apoptotic and G2M checkpoint-related gene signatures in L807mts-treated samples (Fig. 7c). Our single cell RNA-seq data also revealed that several Wnt activation genes that were highly enriched in endogenous single cells from non-Wnt MBs, including *NFATC4* and *GALNT14*, were also upregulated in L807mts-treated non-Wnt MBs (*NFATC4*  $fc=4.33$ , *GALNT14*  $fc=2.43$ , Supplementary Table 2). These findings support the activation of Wnt-driven tumor suppressive pathways following L807mts treatment. Given the enhanced expression of apoptotic and cell cycle inhibition pathways in L807mts-treated cells and prior reports that have indicated *TP53*-mutated Wnt MBs to be more radiosensitive than *TP53*-mutated non-Wnt MBs<sup>4,5</sup>, we investigated the potential to radiosensitize treatment-refractory MBs with L807mts. A significant increase in radiosensitization was observed with L807mts treatment (Fig. 7d). L807mts treatment also decreased *Bmi1* and *Sox2* (Fig. 7e-f) levels and impaired the proliferation and self-renewal

(Fig. 7g-h) of non-Wnt MBs. Preclinical studies were performed on three separate patient-derived MB lines. A reduction in overall tumor burden (Fig. 7i,) and increase in overall survival (Fig. 7j-l) were observed in xenografts treated with L807mts. These preclinical studies provide evidence in support of a highly specific small molecule Wnt agonist with potential clinical utility for treating MB.

Current MB clinical trials have based risk-adapted therapy on molecular subgroups. Trials focused on Wnt-driven MB are deescalating chemo/radiotherapy (NCT01878617, NCT02724579, NCT02212574). By contrast, trials for aggressive non-Wnt MBs are escalating therapy with the hope of improving survivorship with recurrent MB patients treated with palliation alone<sup>2</sup>. Given the few targeted treatment options for non-Wnt MBs, our work highlights a rational therapeutic option in which the protective effects of Wnt-driven MBs may be augmented in non-Wnt MBs through targeted Wnt activation. We further illustrate an emerging paradigm in Wnt biology in which functions of the pathway may be conserved in a context-dependent manner<sup>30-35</sup>, such as a hindbrain-specific function in which self-renewal is impaired from ontogeny to oncology. As molecular oncology trials continue to develop, novel approaches to overcome the dependence of tumors on malignant pathways are warranted and as such we provide a therapeutic rationale with clinical appeal that may alter our approach to cancer by reactivating anti-oncogenic programs that have been developmentally silenced in a tissue-specific manner.

### **Conflict of Interest**

The authors declare that they have no conflict of interest.

## **Author Contributions**

BM, CV, BWD, and SKS conceptualized and designed the experiments. BM, CV, DB, LR, MMK, AAA, MS, NS, NT, NW performed experiments and acquired data. BM, CV, AD, RH, LR, TP, OW, GDB, BWD, SKS analyzed and interpreted data. BM wrote the manuscript with revisions contributed by CV, BWD, and SKS. RH provided technical support for bioinformatics analysis. JPP, BY, OA provided pediatric MB study samples. AF provided guidance pertaining to design of pediatric neuro-oncology preclinical studies. BWD and SKS supervised the study. All authors reviewed results and commented on the manuscript.

## **Materials & Methods**

### ***Culture of primary MB samples***

Primary human pediatric MBs, BT853 and BT992 were obtained from consenting patients and families as approved by the Hamilton Health Sciences/McMaster Health Sciences Research Ethics Board. BT853 is a primary Wnt subgroup MB, whereas BT992 is a primary Shh subgroup from a patient who later relapsed. Both samples were dissociated in PBS containing 0.2 Wünsch unit/mL of Liberase Blendzyme 3 (Roche), and incubated at 37°C in a shaker for 15 minutes. The dissociated tissue was filtered through a 70 µm cell strainer and collected by centrifugation (450g, 3 minutes). Tumor cells were resuspended in a serum-free BTIC enrichment medium, and replated on ultra-low attachment plates (Corning). Additional primary human pediatric MB cultures were obtained from collaborators as kind gifts. SU\_MB002, a treatment-refractory group 3 MB acquired at

autopsy was received from Dr. Yoon-Jae Cho. Dr. Robert Wechsler-Reya provided RCMB40. Dr. Till Milde provided HD-MB03, a treatment-naïve group 3 MBs. ICB1299, a treatment-naïve group 4 MB was obtained from Dr. Silvia Marino. D425, D458 (Group 3) and Daoy (Shh subgroup) were commercially available cell lines. All samples were cultured in BTIC enrichment medium for at least 48 hours prior to experimentation. BTIC enrichment medium was composed of NeuroCult complete medium (STEMCell Technologies, 10 ng/mL bFGF, 20 ng/mL EGF, 2 µg/mL heparin). Expansion medium was used prior to experimentation and BTIC enrichment. SU\_MB002 was expanded using the same BTIC enrichment medium BT853, BT992, and RCMB40 were expanded with the BTIC enrichment medium supplemented with 10% fetal bovine serum (FBS). ICB1299 was expanded with Dulbecco's Modified Eagle's Medium high glucose (Life Technologies #11965-118) supplemented with 10% FBS.

### ***RNA-seq***

Total RNA was extracted using the Norgen Total RNA isolation kit and quantified using a NanoDrop Spectrophotometer ND-1000. The RNA was sequenced using single-end 50 bp reads on the Illumina HiSeq platform (Illumina, San Diego CA, USA). Raw sequence data were exported to FASTQ format and were filtered based on quality scores (Quality cutoff of 20 for at least 90% of the bases in the sequence). Next the reads were mapped to the UCSC mRNA transcript human database based on the GRCh38/hg38 version using HISAT<sup>36</sup>. The counts were obtained by using ht-seq count with the “intersection-strict” option<sup>36</sup>. Counts were transformed with TMM transformation and then normalized with VOOM (package “limma” in R)<sup>37</sup>. Distributions of samples were

examined by performing Principal Component Analyses with “rgl” package in R (<https://cran.r-project.org/web/packages/rgl/index.html>) and by examining a dendrogram built with “hclust” function from “stats” package in R with Euclidean distance and average linkage.

Differential expression was obtained by using “limma” package, p-values were adjusted for multiple testing with BH method<sup>38</sup> and resulting values <0.05 were considered to be significant. Pathway analysis was performed by using the Reactome tool (<https://reactome.org/PathwayBrowser/#TOOL=AT>), and only terms yielding FDR < 0.05 were considered to be significant and were used for further examination.

Gene Set Enrichment Analysis (GSEA)<sup>28,29</sup> was performed by using Oncogenic (C6) and Hallmark MSigDB collections of gene sets. Further GSEA analysis was performed using top 50 and top 100 genes belonging to the signatures obtained from the differential expression analysis.

Survival analysis was performed by using the following signatures: (1) Sox2 signature (BENPORATH\_SOX2\_TARGETS signature deposited in C2 MSigDB collection), (2) WNT Hallmark signature (HALLMARK\_WNT\_BETA\_CATENIN\_SIGNALING signature deposited in the Hallmark MSigDB collection), and (3) BMI1 Glinsky signature<sup>18</sup>. For each signature a signature score was calculated for each patient:  $\frac{\sum_{i \in R} x_i}{n_R}$ , where x is the log2-transformed expression, R is the set of genes comprising the signature of interest, and n is the number of genes in that signature, similar to as described previously<sup>39,40</sup> but using only the genes regulated in the same direction. For each signature, patients were divided into “High” and

“Low” signature index groups using tertiles (1/3 of the patients were assigned to the “High” category and 2/3 were assigned to the “Low” category). Additional factors, such as age, metastatic status, and subgroup were used. Univariate and multivariate *survival analyses were performed using the “survival” package in R* (<https://cran.r-project.org/web/packages/survival/index.html>).

### ***Comparative analysis of transcriptomic data of bulk MB and MB BTIC lines***

All analyses were performed in R 3.4.4. The RNA microarray data was downloaded from GEO (GSE85217)<sup>9</sup>. Before performing analyses with this data, the data was subsetted for 540 WNT, Group 3 and Group 4 samples (i.e. no SHH). Additionally, ENSG identifiers were mapped to HGNC symbols using Ensembl version 77, with mappings downloaded using the BioMART package<sup>41,42</sup>.

Differential expression was conducted using voom and limma for RNA-seq data (this study) and using limma for microarray data (Cavalli 2017 data). Differentially expressed genes were filtered at False Discovery Rate (FDR) 0.05 (Benjamini-Hochberg procedure). Differential expression was performed for the Cavalli data in three ‘one vs. all others’ comparisons (one for each MB subtype), and differential expression was calculated in a similar manner for untreated MB stem cell lines from this study.

The Cavalli, *et al.* 2017 dataset<sup>9</sup> and our MB BTIC samples were scored for gene expression signatures separately using ssgsea<sup>10</sup> as implemented in the GSVA package<sup>43</sup>, using default settings for GSVA::gsva(expr = expression.matrix, gset.idx.list = genesets, method = ‘ssgsea’), where expression.matrix is an expression matrix, genesets is a list of gene sets, and method ‘ssgsea’ specifies to use ssgsea method for scoring.

***Wnt/TCF reporter assay***

MB cells were cotransfected with the constructs 8XTOPFlash (1.8 mg), driving firefly luciferase, and pRL-CMV (0.2 mg), driving the expression of Renilla luciferase for normalization (Promega). After 24 hours, MB cells were supplemented with BTIC enrichment medium. Cells were washed twice with PBS 24 hours following medium change and were lysed with passive lysis buffer (Promega). The luciferase reporter activities were measured using a luminometer as per the manufacturer's instructions (Promega Dual-Light System).

***Cell proliferation assay***

Single cells were plated in 96-well plates, at a density of 1,000 cells/200  $\mu$ L per well in quadruplicate for each sample and incubated for four days. 20  $\mu$ L of Presto Blue (Life Technologies), a fluorescent cell metabolism indicator, was added to each well approximately 4 hours prior to the readout time point. Fluorescence was measured with a FLUOstar Omega Fluorescence 556 Microplate reader (BMG LABTECH) at an excitation and emission wavelength of 540 and 570 nm, respectively. Readings were analyzed using the Omega software.

***Secondary sphere formation analysis***

SU\_MB002 MB tumorspheres were mechanically dissociated with a 1000  $\mu$ L pipette tip. Cells were plated at 200 cells per well in 200  $\mu$ L of BTIC enrichment medium in a 96-well plate. Cultures were left undisturbed at 37°C with 5% CO<sub>2</sub>. After 3 days, the number of secondary spheres per well was counted and used to estimate the mean number of spheres/2000 cells.

### ***In vivo experiments***

All *in vivo* studies were performed according to McMaster University Animal Research Ethics Board approved protocols. Intracranial injections were performed as previously described<sup>44</sup> using the following human MB samples: BT853, BT992, SU\_MB002, RCMB40. Briefly, the appropriate number of live cells, determined by Trypan Blue exclusion, was resuspended in 10  $\mu$ L of PBS. NOD-SCID mice were anaesthetized using isoflurane gas (5% induction, 2.5% maintenance) and cells were injected into the frontal lobe using a 10  $\mu$ L Hamilton syringe.

With regards to specific treatment groups and injected cell numbers, comparative tumor-initiating capacities of BT853 and SU\_MB002 were performed at limiting dilutions consisting of  $1.0 \times 10^5$  and  $5.0 \times 10^5$  with 5 mice in each group ( $n=10$  BT853,  $n=10$  SU\_MB002). Mice were assessed for both histological differences in tumor formation along with length of survival. Comparative histological and survival analyses of mice containing intracranial tumors generated from stable lines of SU\_MB002 with  $\beta$ -catenin overexpression ( $n=5$ ) or negative-control construct expression ( $n=5$ ) were performed by using  $1.0 \times 10^4$  cells from each line. Tumor-initiating capacity, histological differences in tumor size, and survival analysis of SU\_MB002 TGP+ (endogenous Wnt-active cells,  $n=10$ ) compared with SU\_MB002 TGP- (endogenous Wnt-inactive cells,  $n=10$ ) were performed using 5 mice per dilution at dilutions of  $1.0 \times 10^4$ ,  $5.0 \times 10^4$ . Tumor-initiating capacity and histological differences of HD-MB03 TGP+ compared with HD-MB03 TGP- cells were performed using two dilutions of  $5 \times 10^2$  and  $1 \times 10^3$  cells with 4 and 12 mice, respectively. L807mts treatment and PBS controls were delivered *via* intranasal injection

to mice following brief anesthetization with isofluorane gas (2.5% induction). Treatment was given at 50 µg/kg every other day, following a 2-week engraftment incubation. Treatment and control mice were injected with  $1.0 \times 10^4$  cells for SU\_MB002 ( $n=12$ ),  $1.0 \times 10^4$  cells for BT992 ( $n=12$ ), and  $1.0 \times 10^5$  cells for RCMB40 ( $n=12$ ). All mice were sacrificed at endpoint, brains were harvested, formalin-fixed, and paraffin-embedded for hematoxylin and eosin staining. Images were taken using the Aperio Slide Scanner and analyzed using ImageScope v11.1.2.760 software (Aperio).

### ***Immunofluorescence (IF) on xenografts***

5-µm patient derived xenograft paraffin embedded tissues were deparaffinized in xylene and processed through a graded series of alcohol concentrations. Antigen retrieval was performed at 95-100°C for 10 minutes in citrate buffer pH 6.0. Samples were then incubated with blocking solution (1% BSA, 0.2% Triton 100X and 5% goat animal serum in 1x TRIS-buffered saline) for 45 min at room temperature followed by overnight incubation in primary antibody, rabbit anti-human polyclonal Sox2 antibody (1:100, Abcam) at 4°C. The next day samples were washed in 1XTBS and treated with secondary antibody, Alexa Flour 488 goat anti-rabbit IgG (1:200, Life Technologies), for 2 hours at room temperature. Slides were then washed extensively with 1XTBS and counterstained with prolong gold anti-fade mountant with DAPI (Life technologies). Images were acquired using Olympus microscope and Volocity software. Nuclei from 20 high power fields were counted and positivity for Sox2 marker expression was quantified and expressed as % positive cells.

### ***Wnt3A-conditioned medium***

L Wnt-3A cells (ATCC #CRL-2647) transgenic mouse fibroblasts transfected with a Wnt3A expression vector, and control L cells (ATCC #CRL-2648) were cultured according to ATCC's recommendations. Briefly, L Wnt-3A cells were maintained in DMEM and 10% FBS with 0.4 mg/mL G418. Control L cells were maintained in DMEM and 10% FBS. Both, L Wnt-3A and control L cells were subcultured 1:10 in culture medium without G418 and grown until confluency. Culture media were then removed and filtered (0.2 µm). Wnt3A and control conditioned media were separately mixed with BTIC enrichment medium at 1:1 for all subsequent experiments on primary human MB cells.

#### ***Quantitative real-time polymerase chain reaction***

Total RNA was extracted using the Norgen Total RNA isolation kit and quantified using a NanoDrop Spectrophotometer ND-1000. Complementary DNA was synthesized from 0.5-1 µg RNA using the qScript cDNA Super Mix (Quanta Biosciences) and a C1000 Thermo Cycler (Bio-Rad) with the following cycle parameters: 4 minutes at 25°C, 30 minutes at 42°C, 5 minutes at 85°C, hold at 4°C. qRT-PCR was performed using the Perfecta SybrGreen (Quanta Biosciences) and CFX96 instrument (Bio-Rad). CFX Manager 3.0 software was used for quantification of gene expression and levels were normalized to GAPDH expression with secondary validation normalized to Actin expression. Primers include: *Actin* (F: 5'-TATCCCTGTACGCCTCT-3'; R: 5'-AGGTCTTTGCGGATGT-3'), *Axin2* (F: 5'-TGGAGCCGGCTGCGCTTTGAT-3'; R: 5'-CTGGGGTCCGGGAGGCAAGTC-3'), *Bmi1* (F: 5'-GGAGGAGGTGAATGATAAAAGAT-3'; R: 5'-AGGTTCCCTCCTCATAACATGACA-3'), *GAPDH* (F: 5'-TGCACCACCAACTGCTTAGC-3'; R: 5'-

GGCATGGACTGTGGTCATGAG-3'), *Sox2* (F: 5'-  
TCAGGAGTTGTCAAGGCAGAGAAG-3'; R: 5'-  
GCCGCCGCCGATGATTGTTATTAT-3').

### ***Western immunoblotting***

10ug of denatured total protein or 7.5ug of nuclear and cytoplasmic extracts (NEPER reagents, Thermo Scientific) was separated using 10% Bis-Tris gel electrophoresis and transferred to polyvinylidene fluoride membrane. Western blots were probed with the following primary antibodies: Bmi1 (mouse; 1:1000; Millipore #051321), Sox2 (mouse; 1:2,000; BD Biosciences #561469),  $\beta$ -catenin (rabbit; 1:500; Cell Signaling #9581), HDAC1 (rabbit; 1:200 Millipore #06-720) and  $\beta$ -tubulin (rabbit; 1:50,000; Abcam #ab6046). The secondary antibody was horseradish peroxidase conjugated goat anti-mouse IgG (Bio-Rad) or goat anti-rabbit IgG (Sigma). The bands were visualized using an Immobilon Western kit (Millipore) and Chemidoc (Bio-Rad).

### ***Lentiviral studies***

$\beta$ -catenin (#24313) overexpression and control (#12252) vectors and the TGP endogenous canonical Wnt reporter (8X TOPFlash TCF reporter) (#24305) were purchased from Addgene. Replication-incompetent lentiviruses were produced by cotransfection of the expression vector and packaging vectors pMD2G and psPAX2 in HEK293FT cells. Viral supernatants were harvested 72 hours after transfection, filtered through a 0.45  $\mu$ m cellulose acetate filter, and precipitated with PEGit (System Biosciences). The viral pellet was resuspended in 1.0 mL of DMEM media and stored at -80°C. Stable cell lines were

generated by transduction followed by maintenance of cultures with puromycin or flow cytometric cell sorting for GFP<sup>+</sup> and GFP<sup>-</sup> cells.

### ***Flow cytometric analysis and cell-sorting***

Tumorspheres were dissociated and single cells resuspended in PBS. Samples were sorted using a MoFlo XDP Cell Sorter (Beckman Coulter). Dead cells were excluded using the viability dye 7AAD (1:10, Beckman Coulter) or using a near IR Live/Dead fixable staining kit (Life Technologies). Compensation was performed using mouse IgG CompBeads (BD). GFP expression was defined as positive or negative based on the analysis of regions established by the isotype control. Cells were sorted into tubes containing 1 mL BTIC enrichment medium and small aliquots from each sort tube were analyzed to determine the purity of the sorted populations. Cells were allowed to equilibrate at 37°C for a few hours prior to experimentation. Intracellular levels of Bmi1 and Sox2 were determined following preparation using Fixation/Permeabilization Solution Kit (Cat # 554714, BD Biosciences) along with antibodies anti-Bmi1 (1:11; Cat # 130-106-736, Miltenyi) and anti-Sox2 (1:20; Cat # 561610, BD Horizons), for which viable cells were stained using LIVE/DEAD™ Fixable Near-IR Dead Cell Stain Kit (Cat # L10119, Thermo Scientific).

### ***Small molecule Wnt activation***

The competitive ATP inhibitor that functions as a selective GSK-3 inhibitor, CHIR99021, was used to activate the canonical Wnt pathway in SU\_MB002 and ICB1299 cells. Similarly, the novel substrate-competitive peptide inhibitor of GSK-3, L807mts, was also used to activate the canonical Wnt pathway in SU\_MB002 and ICB1299 cells.  $2 \times 10^5$

cells were plated in a 24-well plate in triplicate at a volume of 500  $\mu\text{L}$ /well at CHIR99021 concentrations of 1, 3, 5, 7, 10  $\mu\text{M}$ . DMSO was used as a control. CHIR99021 and DMSO were replenished after 24 and 48 hours and cultures were used for qRT-PCR, self-renewal, proliferation, or radiation assays after 3 days.  $2 \times 10^5$  cells were plated in a 24-well plate in triplicate at a volume of 500  $\mu\text{L}$ /well at L807mts concentrations of 1, 5, 10,  $\mu\text{M}$ . PBS was used as a control. L807mts and PBS were replenished after 24 and 48 hours and cultures were used for qRT-PCR, self-renewal, and proliferation.

### ***In vitro radiotherapy***

Cells were plated at density of  $1 \times 10^6$  cells/mL and treated with one dose of 2 Gy radiation (Faxitron RX-650) and incubated for a week. Functional self-renewal and proliferation assays were performed following incubation.

### ***Single-cell RNA-seq and library preparation.***

Single-cell suspensions of 1000 cells with a final viability of  $>80\%$  was used. Single-cell library preparation was carried out as per the 10X Genomics Chromium single-cell protocol using the v2 chemistry reagent kit (10X Genomics, Pleasanton, CA, USA). Cell suspensions were loaded onto individual channels of a Chromium Single-Cell Chip along reverse transcription (RT) master mix and single cell 3' gel beads, aiming for 1000 captured cells per sample. Following generation of gel bead-in-emulsions (GEMs), cDNA was underwent a two-stage purification process with Dynal MyONE Silane beads (Thermo Fisher Scientific), followed by SPRIselect beads (Beckman Coulter). RT and cDNA amplification were performed using a 96-well Veriti Thermocycler (Life Technologies). Amplified cDNA purified using SPRIselect beads and sequencing libraries were generated

with unique sample indexes (SI). Dual sided SPRIselect cleanup was used to clean up samples and size select. Libraries were sequenced on an Illumina 2500 in Highoutput mode at the Princess Margaret Genomics Centre (Toronto, ON) using the 10X Genomics recommended sequencing parameters. Samples were quantified by Kapa Library Quantification kit (Roche) and normalized to achieve the desired median read depth per cell.

### **Single-cell RNA-seq data preprocessing**

The Cell Ranger software pipeline (version 2.1.0) developed by 10X Genomics was used to demultiplex cell barcodes, map reads to the transcriptome (GRCh38) using STAR aligner and down-sample reads as required to generate normalized aggregate data across samples. The number of reads per cell barcode was calculated using the BamTagHistogram function in the [Drop-seq Alignment Cookbook](#)<sup>45</sup>. Subsequently, the number of cells per sample was determined by calculating the cumulative fraction of reads corresponding to each individual cell barcode in a library. Cell barcodes were sorted in decreasing order and the inflection point was identified using the R package [Dropbead](#)<sup>46</sup> (version 0.3.1) to distinguish between empty droplets with only ambient RNA and true droplets containing a cell. The raw matrix of gene counts versus cells from Cell Ranger output was filtered by cell barcodes identified from Dropbead. We processed the resultant unique molecular identifier (UMI) count matrix using the R package Seurat<sup>47</sup> (version 2.3.4).

### **Single-cell RNA-seq quality control, normalization and dimensionality reduction.**

For each cell, we quantified three quality control metrics: the number of genes with at least one UMI, the total number of UMIs detected and the percentage UMI counts

belonging to expressed mitochondrial genes. We excluded all cells with >30% mitochondrial UMIs, potentially indicative of damaged cells with compromised cellular membranes.

Similar to the workflow in Lun et al.<sup>48</sup>, likely multiplet captures were removed if log-library size exceeded 2 median absolute deviations (MAD) above the median. We further discarded low-quality cells where below 500 genes were detected. We filtered out lowly expressed genes detected in less than 5 cells across the aggregated dataset, corresponding to 1% of cells in the smallest library. After applying these QC criteria, 3725 single cells and 18721 genes remained and were included in downstream analysis. Expression normalization was performed in Seurat on the filtered matrix to obtain log-normalized counts scaled to library size. Relative gene expression was calculated by centering expression across all cells in the cohort using the `ScaleData()` function in Seurat. Identification of highly variable genes (4140 genes), principal component analysis (11 significant PCs determined by a scree plot) and SNN-Cliq-inspired clustering were performed in Seurat to generate t-distributed stochastic neighbor embedding (t-SNE) visualizations (Rtsne: Use the Rtsne package Barnes-Hut implementation of tSNE; default in Seurat).

### **Single-cell RNA-seq gene signature scoring and classification**

Gene signature scores in individual cells were calculated with two methods. The first being the `AddModuleScore()` function in the R package Seurat (version 2.3.4). In brief, the average relative expression level for each gene signature was calculated on a single cell level and subtracted by the aggregated relative expression of control gene sets. Control

gene sets were defined by binning all 18,721 expressed genes into 25 bins of aggregate expression levels and then for each gene in the gene signature of interest, randomly selecting 100 genes from the comparable expression bin. As a result, control gene sets have comparable expression level distributions to the gene signature of interest. A second set of gene signature enrichment scores were calculated using [Gene Set Variation Analysis](#) (GSVA) with default parameters.

To estimate the significance of gene signature scores, a hundred sets of randomly selected genes sets with the same size as the gene signatures were generated and scored using both methods described above. Random sets were then used to define a 5% cutoff for the expected gene signature scores. Cells were classified as “enriched” for a given signature if they surpassed the 5% threshold.

### ***Statistical analysis***

At least three biological replicates were performed for each experiment. Data represent mean  $\pm$  standard error (mean) with  $n$  values listed in figure legends. Student  $t$ -test analyses were performed using GraphPad Prism™ with significance set to  $P < 0.05$ . Kaplan-Meier survival curves were visualized using GraphPad Prism™. All statistical analysis and data visualization for scRNA-seq was performed in R (version 3.5.0).

### **References**

1. Northcott, P.A., *et al.* The whole-genome landscape of medulloblastoma subtypes. *Nature* **547**, 311-317 (2017).
2. Ramaswamy, V., *et al.* Risk stratification of childhood medulloblastoma in the molecular era: the current consensus. *Acta Neuropathol* **131**, 821-831 (2016).

3. von Bueren, A.O., *et al.* Treatment of Children and Adolescents With Metastatic Medulloblastoma and Prognostic Relevance of Clinical and Biologic Parameters. *J Clin Oncol* **34**, 4151-4160 (2016).
4. Zhukova, N., *et al.* WNT activation by lithium abrogates TP53 mutation associated radiation resistance in medulloblastoma. *Acta Neuropathol Commun* **2**, 174 (2014).
5. Pfaff, E., *et al.* TP53 mutation is frequently associated with CTNNB1 mutation or MYCN amplification and is compatible with long-term survival in medulloblastoma. *J Clin Oncol* **28**, 5188-5196 (2010).
6. Gibson, P., *et al.* Subtypes of medulloblastoma have distinct developmental origins. *Nature* **468**, 1095-1099 (2010).
7. Phoenix, T.N., *et al.* Medulloblastoma Genotype Dictates Blood Brain Barrier Phenotype. *Cancer Cell* **29**, 508-522 (2016).
8. Poschl, J., *et al.* Wnt/beta-catenin signaling inhibits the Shh pathway and impairs tumor growth in Shh-dependent medulloblastoma. *Acta Neuropathol* **127**, 605-607 (2014).
9. Cavalli, F.M.G., *et al.* Intertumoral Heterogeneity within Medulloblastoma Subgroups. *Cancer Cell* **31**, 737-754 e736 (2017).
10. Barbie, D.A., *et al.* Systematic RNA interference reveals that oncogenic KRAS-driven cancers require TBK1. *Nature* **462**, 108-112 (2009).
11. Manoranjan, B., *et al.* FoxG1 interacts with Bmi1 to regulate self-renewal and tumorigenicity of medulloblastoma stem cells. *Stem Cells* **31**, 1266-1277 (2013).

12. Bruggeman, S.W., *et al.* Bmi1 controls tumor development in an Ink4a/Arf-independent manner in a mouse model for glioma. *Cancer Cell* **12**, 328-341 (2007).
13. Leung, C., *et al.* Bmi1 is essential for cerebellar development and is overexpressed in human medulloblastomas. *Nature* **428**, 337-341 (2004).
14. Wang, X., *et al.* Sonic hedgehog regulates Bmi1 in human medulloblastoma brain tumor-initiating cells. *Oncogene* **31**, 187-199 (2012).
15. Pei, Y., *et al.* WNT signaling increases proliferation and impairs differentiation of stem cells in the developing cerebellum. *Development* **139**, 1724-1733 (2012).
16. Nusse, R. & Clevers, H. Wnt/beta-Catenin Signaling, Disease, and Emerging Therapeutic Modalities. *Cell* **169**, 985-999 (2017).
17. Vanner, R.J., *et al.* Quiescent sox2(+) cells drive hierarchical growth and relapse in sonic hedgehog subgroup medulloblastoma. *Cancer Cell* **26**, 33-47 (2014).
18. Glinsky, G.V., Berezovska, O. & Glinskii, A.B. Microarray analysis identifies a death-from-cancer signature predicting therapy failure in patients with multiple types of cancer. *J Clin Invest* **115**, 1503-1521 (2005).
19. Ben-Porath, I., *et al.* An embryonic stem cell-like gene expression signature in poorly differentiated aggressive human tumors. *Nat Genet* **40**, 499-507 (2008).
20. Ramaswamy, V., *et al.* Recurrence patterns across medulloblastoma subgroups: an integrated clinical and molecular analysis. *Lancet Oncol* **14**, 1200-1207 (2013).
21. Wang, X., *et al.* Medulloblastoma subgroups remain stable across primary and metastatic compartments. *Acta Neuropathol* **129**, 449-457 (2015).

22. Morrissy, A.S., *et al.* Spatial heterogeneity in medulloblastoma. *Nat Genet* **49**, 780-788 (2017).
23. Karaayvaz, M., *et al.* Unravelling subclonal heterogeneity and aggressive disease states in TNBC through single-cell RNA-seq. *Nat Commun* **9**, 3588 (2018).
24. Rambow, F., *et al.* Toward Minimal Residual Disease-Directed Therapy in Melanoma. *Cell* **174**, 843-855 e819 (2018).
25. Fuerer, C. & Nusse, R. Lentiviral vectors to probe and manipulate the Wnt signaling pathway. *PLoS One* **5**, e9370 (2010).
26. Ring, D.B., *et al.* Selective glycogen synthase kinase 3 inhibitors potentiate insulin activation of glucose transport and utilization in vitro and in vivo. *Diabetes* **52**, 588-595 (2003).
27. Licht-Murava, A., *et al.* A unique type of GSK-3 inhibitor brings new opportunities to the clinic. *Sci Signal* **9**, ra110 (2016).
28. Subramanian, A., *et al.* Gene set enrichment analysis: a knowledge-based approach for interpreting genome-wide expression profiles. *Proc Natl Acad Sci U S A* **102**, 15545-15550 (2005).
29. Mootha, V.K., *et al.* PGC-1alpha-responsive genes involved in oxidative phosphorylation are coordinately downregulated in human diabetes. *Nat Genet* **34**, 267-273 (2003).
30. Biechele, T.L., *et al.* Chemical-genetic screen identifies riluzole as an enhancer of Wnt/beta-catenin signaling in melanoma. *Chem Biol* **17**, 1177-1182 (2010).

31. Biechele, T.L., *et al.* Wnt/beta-catenin signaling and AXIN1 regulate apoptosis triggered by inhibition of the mutant kinase BRAFV600E in human melanoma. *Sci Signal* **5**, ra3 (2012).
32. Chien, A.J., *et al.* Activated Wnt/beta-catenin signaling in melanoma is associated with decreased proliferation in patient tumors and a murine melanoma model. *Proc Natl Acad Sci U S A* **106**, 1193-1198 (2009).
33. Green, J.L., *et al.* Paracrine Wnt signaling both promotes and inhibits human breast tumor growth. *Proc Natl Acad Sci U S A* **110**, 6991-6996 (2013).
34. Dickey, A., *et al.* GSK-3beta inhibition promotes cell death, apoptosis, and in vivo tumor growth delay in neuroblastoma Neuro-2A cell line. *J Neurooncol* **104**, 145-153 (2011).
35. Matushansky, I., *et al.* Derivation of sarcomas from mesenchymal stem cells via inactivation of the Wnt pathway. *J Clin Invest* **117**, 3248-3257 (2007).
36. Kim, D., Langmead, B. & Salzberg, S.L. HISAT: a fast spliced aligner with low memory requirements. *Nat Methods* **12**, 357-360 (2015).
37. Law, C.W., Chen, Y., Shi, W. & Smyth, G.K. voom: Precision weights unlock linear model analysis tools for RNA-seq read counts. *Genome Biol* **15**, R29 (2014).
38. Benjamini, Y. & Hochberg, Y. Controlling the False Discovery Rate: A Practical and Powerful Approach to Multiple Testing. *Journal of the Royal Statistical Society. Series B (Methodological)* **57**, 289-300 (1995).

39. Hallett, R.M., Pond, G. & Hassell, J.A. A target based approach identifies genomic predictors of breast cancer patient response to chemotherapy. *BMC Med Genomics* **5**, 16 (2012).
40. Chorlton, S.D., Hallett, R.M. & Hassell, J.A. A program to identify prognostic and predictive gene signatures. *BMC Res Notes* **7**, 546 (2014).
41. Durinck, S., Spellman, P.T., Birney, E. & Huber, W. Mapping identifiers for the integration of genomic datasets with the R/Bioconductor package biomaRt. *Nat Protoc* **4**, 1184-1191 (2009).
42. Durinck, S., *et al.* BioMart and Bioconductor: a powerful link between biological databases and microarray data analysis. *Bioinformatics* **21**, 3439-3440 (2005).
43. Hanzelmann, S., Castelo, R. & Guinney, J. GSEA: gene set variation analysis for microarray and RNA-seq data. *BMC Bioinformatics* **14**, 7 (2013).
44. Singh, S.K., *et al.* Identification of human brain tumour initiating cells. *Nature* **432**, 396-401 (2004).
45. Macosko, E.Z., *et al.* Highly Parallel Genome-wide Expression Profiling of Individual Cells Using Nanoliter Droplets. *Cell* **161**, 1202-1214 (2015).
46. Alles, J., *et al.* Cell fixation and preservation for droplet-based single-cell transcriptomics. *BMC Biol* **15**, 44 (2017).
47. Butler, A., Hoffman, P., Smibert, P., Papalexi, E. & Satija, R. Integrating single-cell transcriptomic data across different conditions, technologies, and species. *Nat Biotechnol* **36**, 411-420 (2018).

48. Lun, A.T., McCarthy, D.J. & Marioni, J.C. A step-by-step workflow for low-level analysis of single-cell RNA-seq data with Bioconductor. *F1000Res* **5**, 2122 (2016).

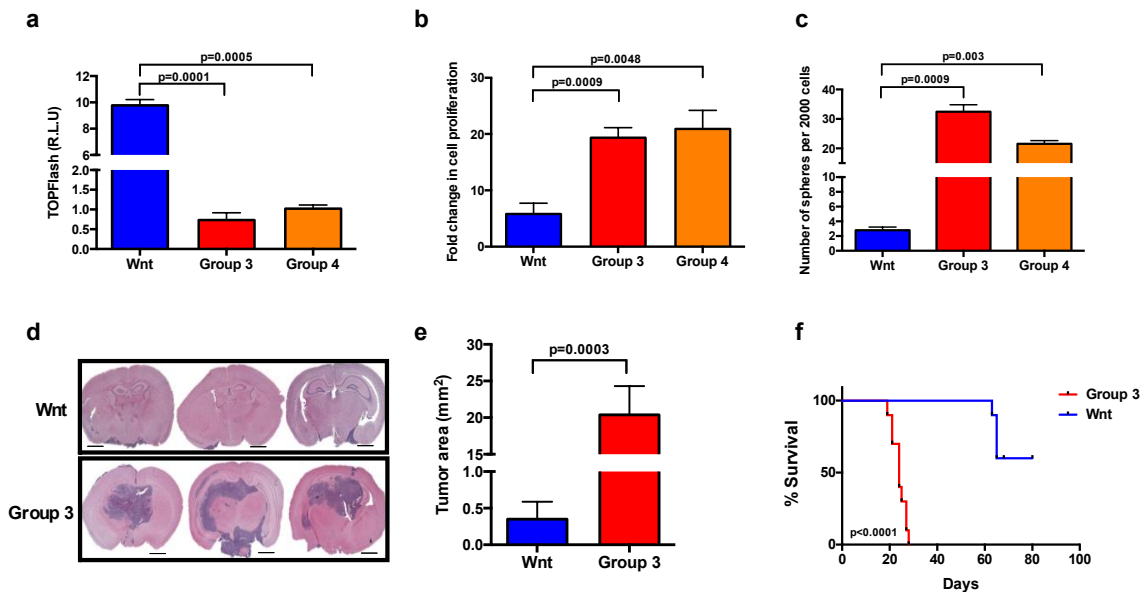


**Figure 1: Wnt-activated MBs are less tumorigenic than non-Wnt MBs.** (a) Differential Wnt reporter activity between Wnt and Group 3 (p=0.0001) or Group 4 MB (p=0.0005) (n=3, independent experiments per MB line; 1 line per subgroup). (b) Wnt MBs display a reduced proliferative capacity when compared to Group 3 (p=0.0009), Group 4 MB (p=0.0048) (n=3, independent experiments per MB line). (c) Wnt MBs maintain a reduced self-renewal capacity when compared to Group 3 (p=0.0009) and Group 4 MB (p=0.003) (n=3, independent experiments per MB line). (d) Representative histology images of Wnt and Group 3 MB xenografts demonstrate significant tumor reduction in Wnt (n=10) compared to Group 3 MB xenografts (n=10). (e) Tumor volume in Wnt xenografts (n=10) is significantly reduced compared to Group 3 xenografts (n=10) (p=0.0003). (f) Wnt MB

xenografts (n=10) display a significant increase in overall survival (median survival undefined) when compared to Group 3 xenografts (median survival 24 days) (n=10) ( $p < 0.0001$ ). Histology image scale bar = 5000  $\mu\text{m}$ .

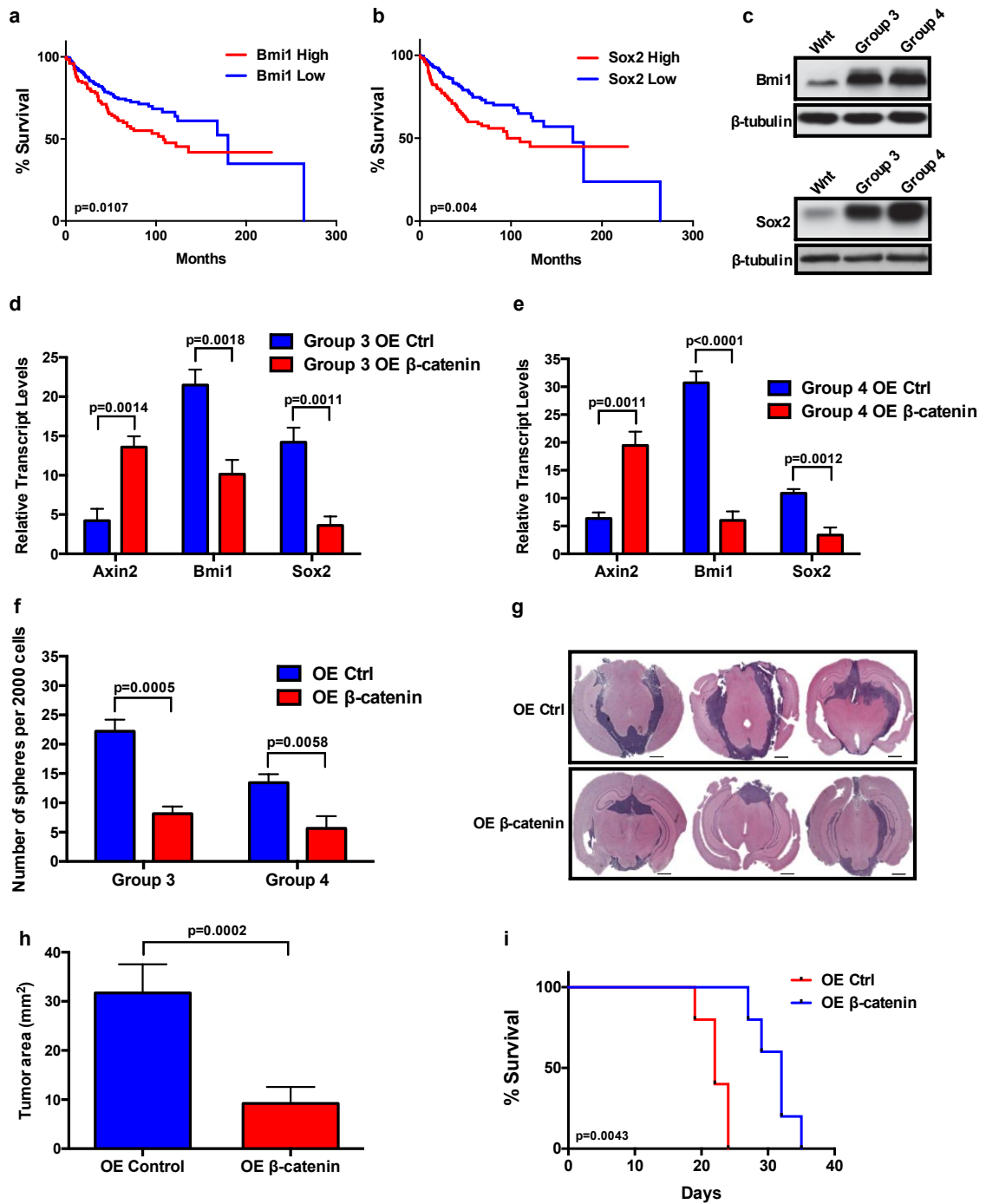


**Figure 2: Ectopic expression of  $\beta$ -catenin in treatment-refractory MBs reduces self-renewal gene expression and tumor burden while increasing overall survival. Kaplan-**

Meier survival plots show survival of combined Groups 3 and 4 patients (n=377) based on (a) the *Bmi1* signature (median survival: *Bmi1*<sup>high</sup> 103.3 months, *Bmi1*<sup>low</sup> 180.0 months; p=0.0107) and (b) *Sox2* signature (median survival: *Sox2*<sup>high</sup> 110 months, *Sox2*<sup>low</sup> 168.0 months; p=0.040). (c) *Bmi1* and *Sox2* protein levels are significantly reduced in Group 3 and 4 MB lines when compared to Wnt MB (n=1). Differential *Axin2* (Group 3: p=0.0014, Group 4: p=0.0011), *Bmi1* (Group 3: p=0.0018, Group 4: p<0.0001), and *Sox2* (Group 3: p=0.0011, Group 4: p=0.0012) transcript levels following  $\beta$ -catenin overexpression in (d) Group 3 and (e) Group 4 MB lines (n=3, independent experiments per MB line, 1 line per subgroup, all samples normalized to *GAPDH*). (f) Tumor sphere formation is impaired following  $\beta$ -catenin overexpression in Group 3 (p=0.0005) and Group 4 MBs (p=0.0058) (n=3, independent experiments per MB line, 1 line per subgroup). (g) Representative histology images showing significant reduction in tumor formation in xenografts generated from containing Group 3  $\beta$ -catenin overexpressing lines (n=5) compared to control (n=5). (h) Xenografts generated with cells ectopically expressing of  $\beta$ -catenin (n=5) contain smaller tumor volumes when compared to control xenografts (n=5) (p=0.0002). (i)  $\beta$ -catenin overexpression xenografts (n=5, median survival 32.0 days) (n=5) display a significant increase in overall survival when compared to control xenografts (n=5, median survival 22.0 days) (p=0.0043). Histology image scale bar = 5000  $\mu$ m.

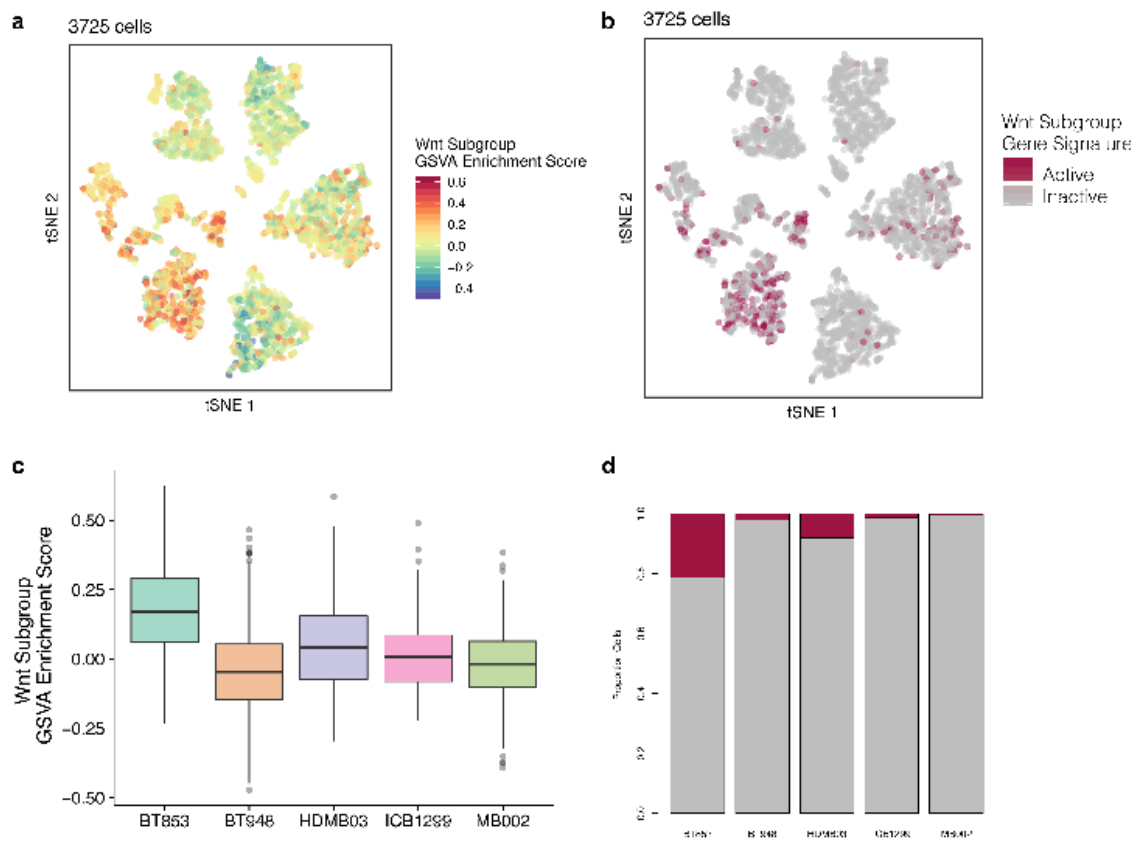


**Figure 3: Characterization of Wnt activity in Wnt and non-Wnt MBs.** Heterogeneous Wnt subgroup scored across patient-derived MB cultures. (a) tSNE of 3725 cells coloured by GSVA enrichment score for the Wnt Subgroup gene signature. (b) Cells coloured by classification for enrichment of Wnt Subgroup signature. Dark red cells surpassed the 5% cutoff and are considered significantly enriched for the gene signature. Grey cells did not pass the threshold. (c) Wnt Subgroup signature scores for each sample. Each point in the box plot represents a cell. (d) Proportion of cells enriched for the Wnt Subgroup gene signature per sample.

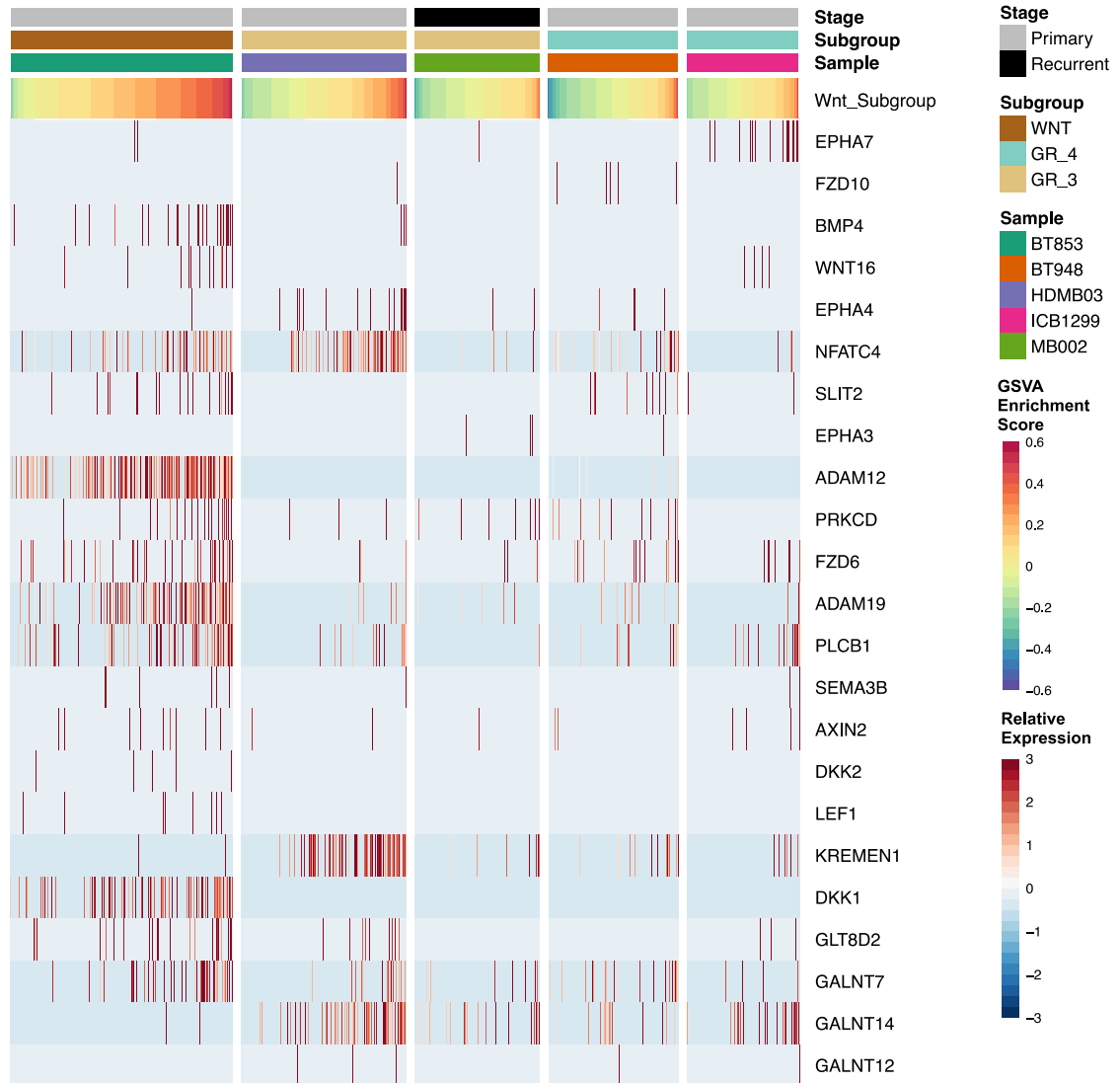


**Figure 4: Wnt signature is present in a minority of non-Wnt MB cells.** Heatmap of Wnt MB scoring for RNA seq performed on individual cells obtained from 5 patient-derived MB lines, including both Wnt and non-Wnt MBs. Gene expression (rows) represented by relative expression (Z scores). Cells (columns) are sorted by increasing Wnt subgroup GSVA enrichment score within each sample.

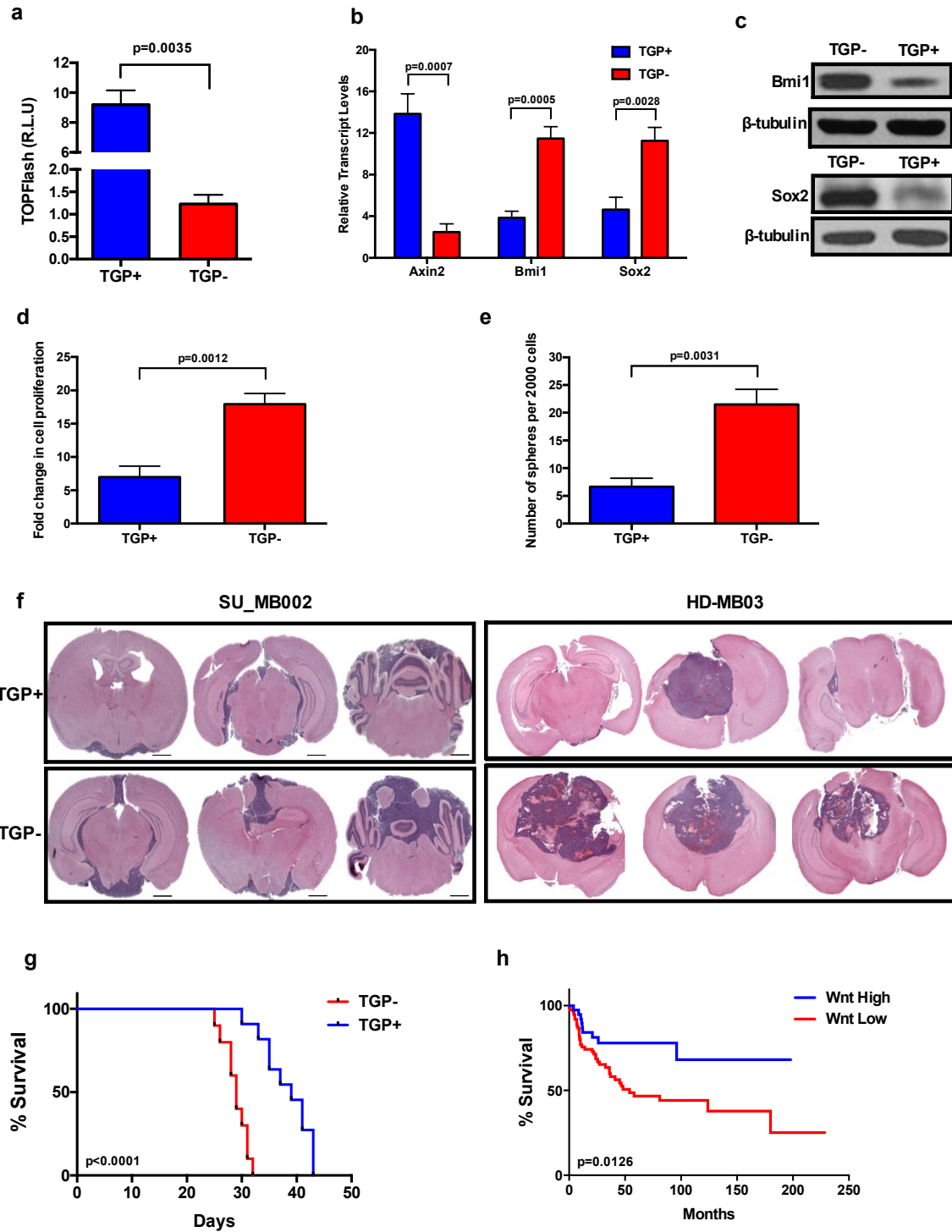


**Figure 5: Rare endogenous Wnt-active MB cells from treatment-refractory MBs have reduced tumorigenic properties.** (a) TGP+ cells contain enhanced TCF reporter activity when compared to TGP- cells ( $p=0.0035$ ) ( $n=3$ , independent experiments). (b) Differential *Axin2* ( $p=0.0007$ ), *Bmi1* ( $p=0.0005$ ), and *Sox2* ( $p=0.0028$ ) transcript levels in TGP+ and TGP- cells ( $n=3$ , independent experiments, all samples normalized to *GAPDH*). (c) *Bmi1* and *Sox2* protein levels are reduced in TGP+ when compared to TGP- cells ( $n=1$ ). (d) Proliferative ( $p=0.0012$ ) and (e) self-renewal capacity ( $p=0.0031$ ) of TGP+ cells are significantly reduced when compared to TGP- cells ( $n=3$ , independent experiments). (f) Representative histology images illustrating reduced tumor burden in SU\_MB002 TGP+ ( $n=10$ ) compared to TGP- xenografts ( $n=10$ ), and HD-MB03 TGP+ ( $n=6$ ) compared to TGP- xenografts ( $n=6$ ). (g) TGP+ xenografts ( $n=10$ , median survival 39.0 days) display a significant increase in overall survival when compared to TGP- xenografts ( $n=10$ , median survival 29.0 days) ( $p<0.0001$ ). (h) Treatment-refractory MB patients ( $n=113$ ) with high expression of the Wnt hallmark signature have an improved overall survivorship (median survival undetermined) when compared to those patients with low Wnt hallmark signature expression (median survival 54.0 months) ( $p=0.0126$ ). Histology image scale bar = 5000  $\mu\text{m}$ .

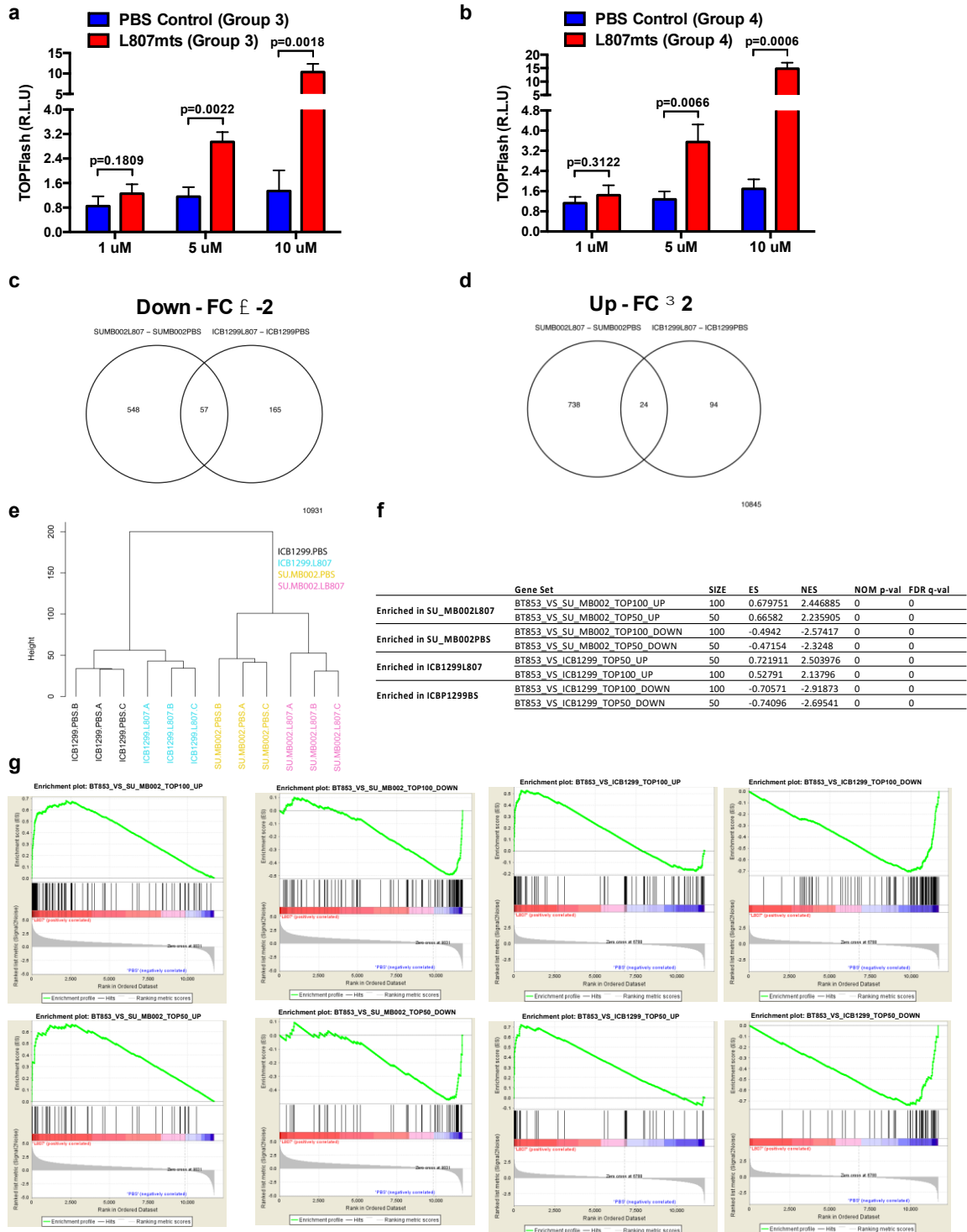


**Figure 6: Wnt activation through novel substrate-competitive peptide Wnt agonist (L807mts) alters the transcriptional profile of non-Wnt MBs and reduces their tumorigenic potential.** (a) TCF Wnt reporter assay at various concentrations of L807mts demonstrates optimal concentration for Wnt activation in Group 3 MBs (1 $\mu$ M: p=0.1809, 5 $\mu$ M: p=0.0022, 10  $\mu$ M: p=0.0018) (n=3, independent experiments, 1 line per subgroup). (b) Similarly, TCF Wnt reporter assay at various concentrations of L807mts demonstrates optimal concentration for Wnt activation in Group 4 MBs (1 $\mu$ M: p=0.3122, 5 $\mu$ M: p=0.0066, 10  $\mu$ M: p=0.0006) (n=3, independent experiments, 1 line per subgroup). Venn diagrams of differentially (c) downregulated and (d) upregulated genes between L807mts- and PBS control-treated Group 3 and 4 MB lines (n=3, independent samples per MB line, 1 line per subgroup, FC = fold change) (e) Dendrogram of L807mts- and PBS control-treated Group 3 and 4 MB samples submitted for RNA-seq (n=3, independent samples per MB line). (f, g) GSEA shows evidence for activation of Wnt in L807mts treated non-Wnt MB samples.

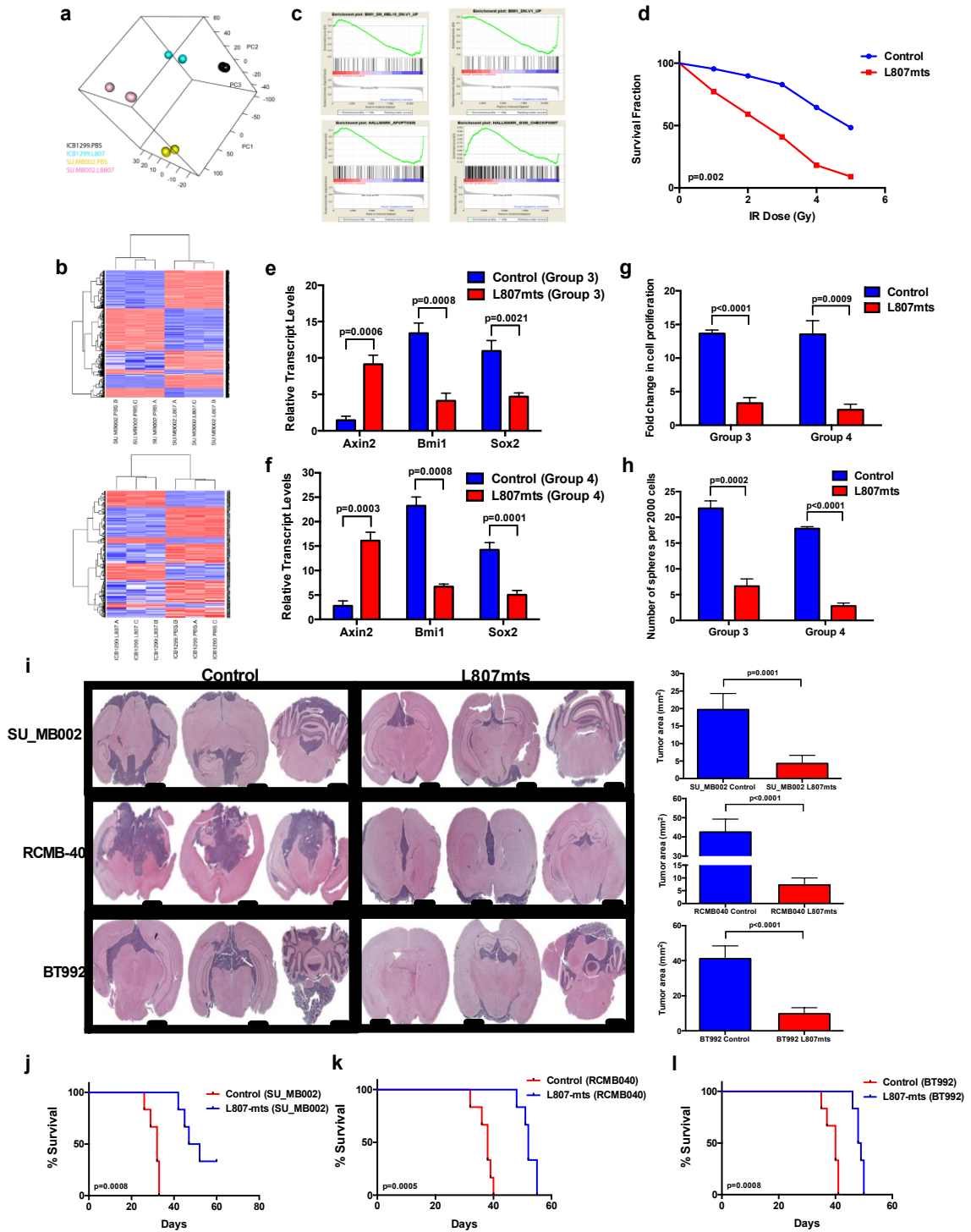
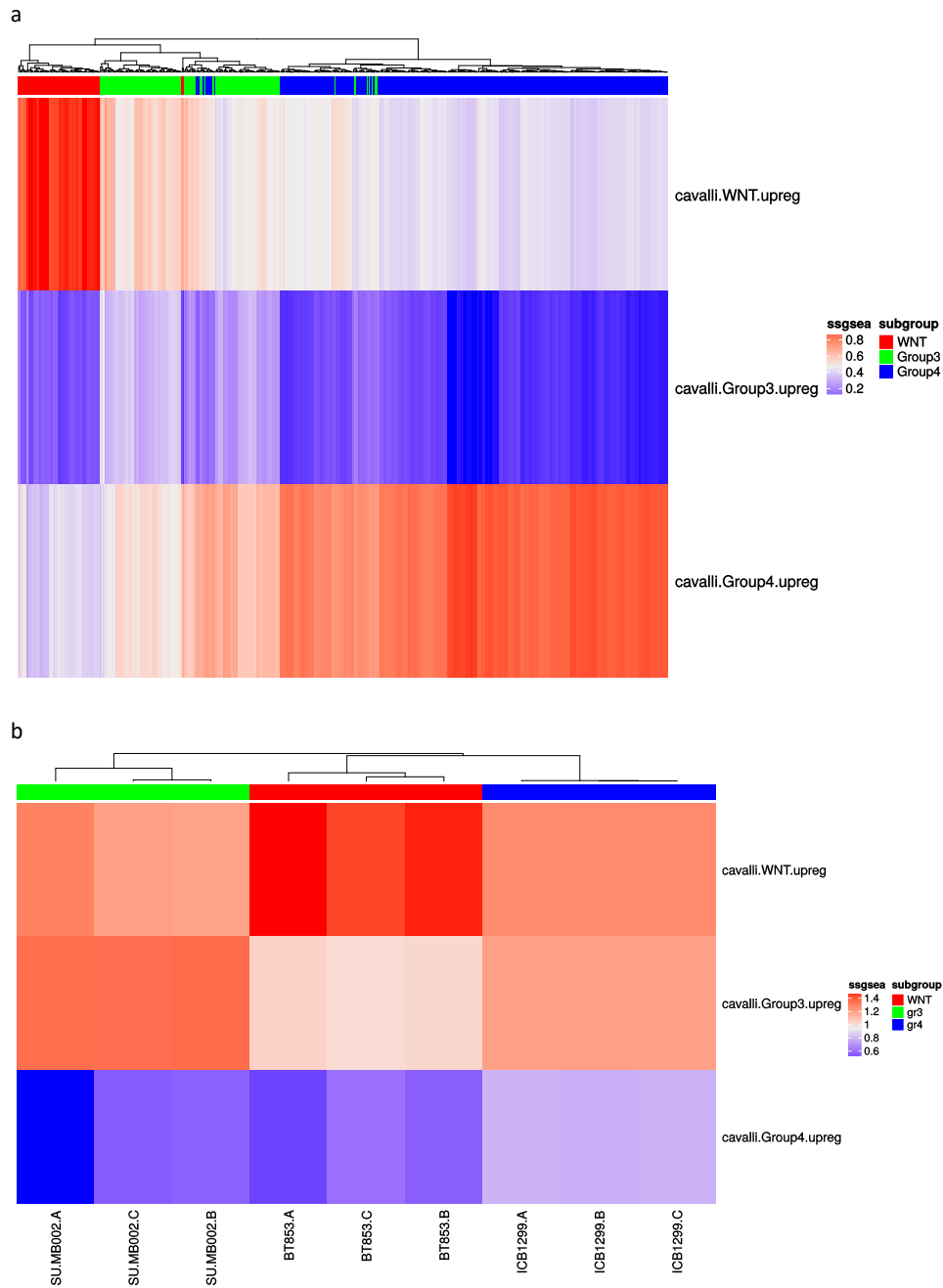


**Figure 7: Pharmacological activation of Wnt signaling in MB impairs stem cell properties and improves overall survival.** (a) Visualization of the first 3 principal components from PCA of Group 3 and 4 lines treated with small molecule Wnt activator (L807mts) or control (PBS) (n=3, independent samples per MB line, 1 line per subgroup). (b) Heatmaps of differentially-expressed genes between L807mts- and PBS-treated Group 3 (top panel) and Group 4 (bottom panel) MB lines (n=3, independent samples per MB line, 1 line per subgroup). (c) GSEA enrichment plots showing that *Bmi1* associated genes are significantly reduced while apoptosis and cell cycle inhibitors are enriched in L807mts-treated cells compared to control. (d) L807mts-treated cells are much more radiosensitive than control cells (p=0.002) (n=3, independent experiments). Differential *Axin2* (Group 3: p=0.0006, Group 4: p=0.0003), *Bmi1* (Group 3: p=0.0008, Group 4: p=0.0008), and *Sox2* (Group 3: p=0.0021, Group 4: p=0.0001) transcript levels in L807mts-treated (e) Group 3 and (f) Group 4 MB lines (n=3, independent experiments per MB line, 1 line per subgroup, all samples normalized to *GAPDH*). Both, (g) proliferation (Group 3: p<0.0001, Group 4: p=0.0009) and (h) self-renewal (Group 3: p=0.0002, Group 4: p<0.0001) are impaired following L807mts treatment in Group 3 and Group 4 MB lines (n=3, independent experiments per MB line, 1 line per subgroup). (i) Representative histology images of xenografts generated from patient-derived treatment-refractory MBs following L807mts treatment (n=6 per MB line) contain a reduction in overall tumor burden when compared to xenografts treated with PBS control (n=6 per MB line). SU\_MB002 (p=0.0001), RCMB-40 (n=12) (p<0.0001), and BT992 (p<0.0001) xenografts treated with L807mts (n=6, individual mice per MB line) contain a significant reduction in overall tumor volume when

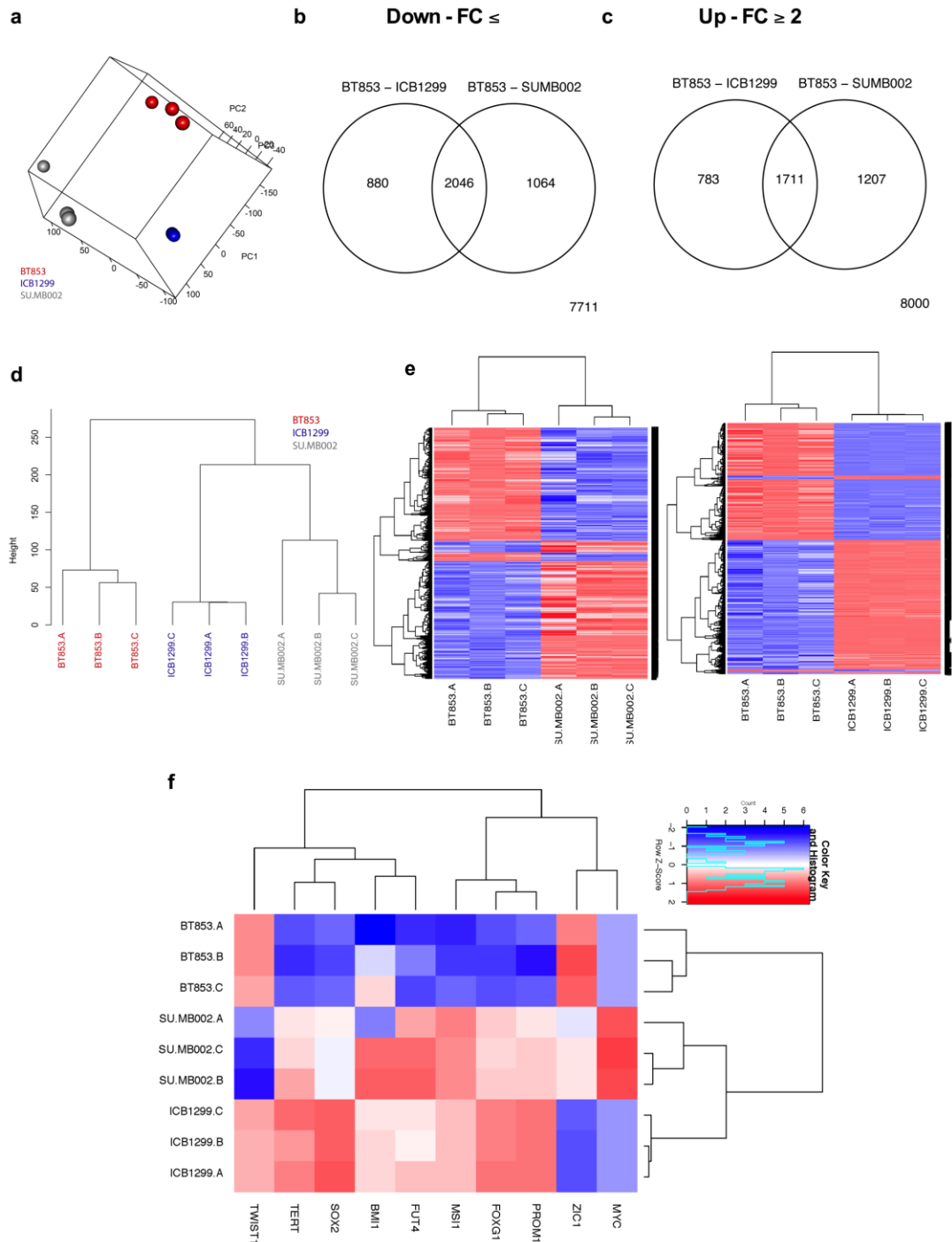
compared to PBS control-treated xenografts (n=6, individual mice per MB line). Xenografts of (j) SU\_MB002 (n=12; median survival L807mts 49.5 days, PBS 32.0 days; p=0.0008, n=12), (k) RCMB-40 (n=12; median survival L807mts 52.9 days, PBS 38.0 days; p=0.0005), and (l) BT992 (n=12; median survival L807mts 48.5 days, PBS 40.0 days; p=0.0008) treated with L807mts display a significant survival advantage when compared to control PBS-treated mice. Histology image scale bar = 5000  $\mu\text{m}$ .



**Supplementary Figure 1: MB BTIC lines maintain their subgroup affiliation. (a)**

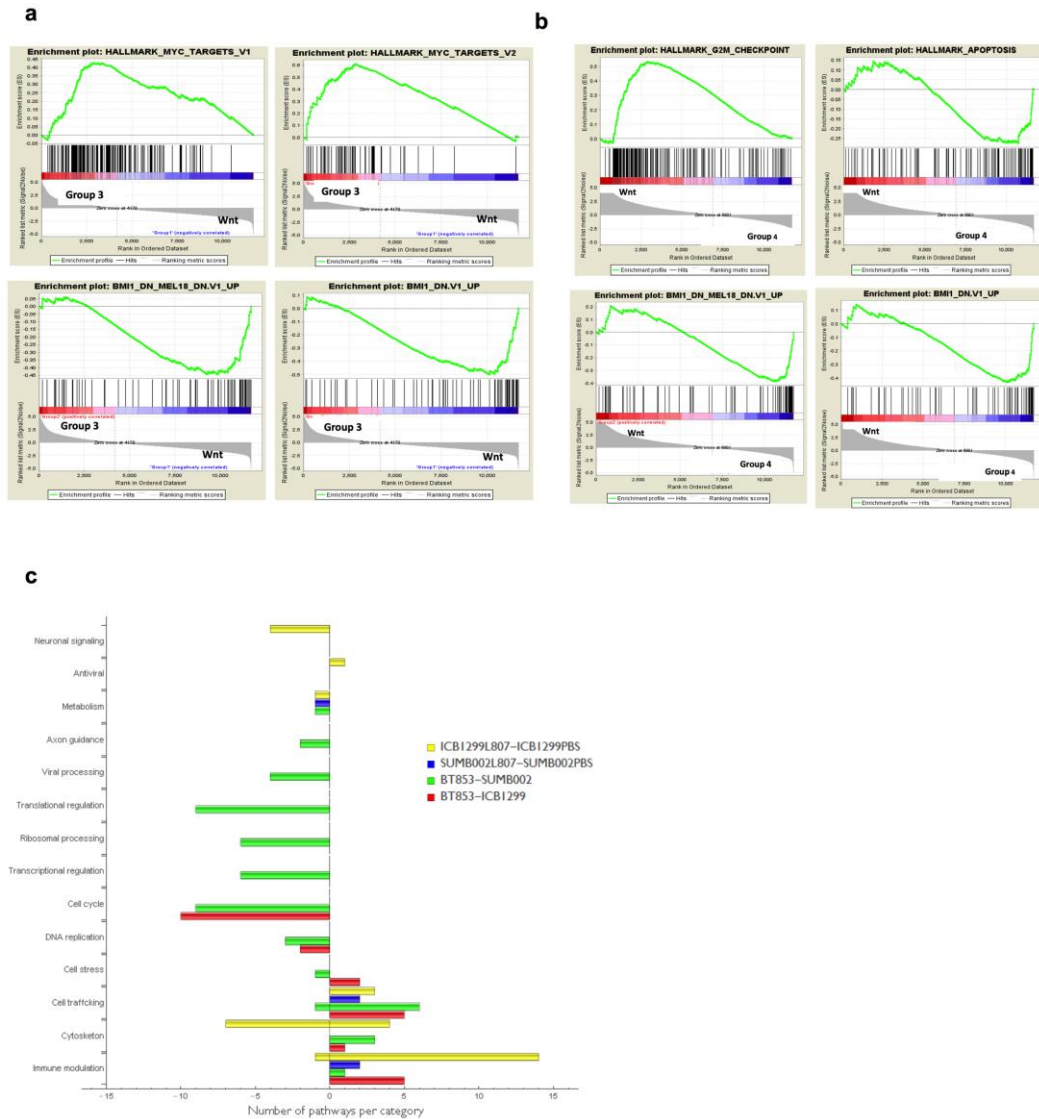
Heatmap of 540 MB samples (GSE85217) scored for relative expression of MB subgroup upregulated gene expression signatures, computed from the same data. MB subgroup gene

signatures (rows) are genes that are upregulated for a given MB subgroup relative to all other samples in this dataset. Signatures included all upregulated genes passing an FDR threshold of 0.05 in this comparison. Samples were scored for expression of these signatures using ssGSEA. ssGSEA score is plotted as color, with better matches being more red and worse matches more blue, as per legend. Sample group classification is plotted as a color bar along the top of the heatmap, as per legend. (b) Heatmap of 9 MB stem cell lines from this study, scored for relative expression of WNT, Group 3, and Group 4 MB subgroup upregulated gene signatures defined in panel A, using ssgsea. Interestingly, the WNT, Group 3, and Group 4 MB signatures showed strongest relative enrichment in our WNT (BT853), Group 3 (SU\_MB002), and Group 4 (ICB1299) BTIC lines, respectively, showing that the subgroup level differences seen in bulk tumors are preserved in our model system. Heatmap visualization is as in (a).



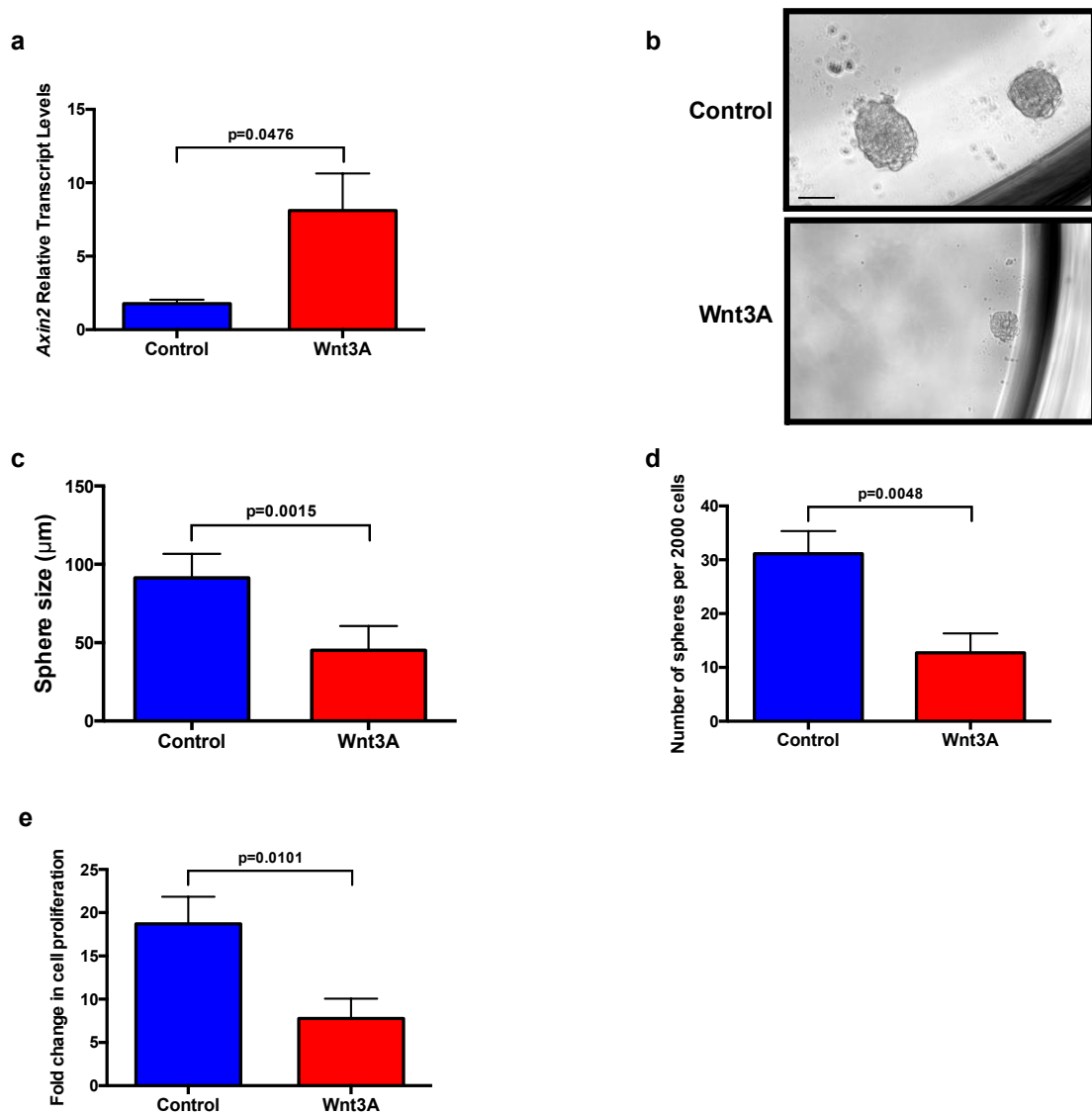
**Supplementary Figure 2: Wnt MB patient-derived lines maintain distinct transcriptional profile from Group 3 and Group 4 MB lines. (a) Visualization of the**

first 3 principal components from PCA of Wnt (BT 853), Group 3 (SU\_MB002), and Group 4 (ICB1299) primary patient-derived MB lines (n=3, independent samples per MB line; 1 line per subgroup). Venn diagrams of differentially (b) downregulated and (c) upregulated genes between Wnt/Group 3 and Wnt/Group 4 comparisons (n=3, independent samples per MB line, 1 line per subgroup, FC = fold change). (d) Dendrogram of Wnt, Group 3, and Group 4 samples submitted for RNA-seq (n=3, independent samples per MB line, 1 line per subgroup). (e) Heatmaps of differentially-expressed genes between Wnt and Group 3 (left panel) or Wnt and Group 4 (right panel) samples (n=3, independent samples per MB, 1 line per subgroup). (f) Heatmap of key genes reported to be enriched in malignant and non-cancerous stem cell populations are significantly upregulated in Group 3 and 4 MB lines when compared to Wnt MB (n=3, independent samples per MB line; 1 line per subgroup).



**Supplementary Figure 3: Non-Wnt MB lines display enriched expression in oncogenic pathways compared to Wnt MB.** (a) Myc targets and Bmi1 associated genes were significantly enriched in Group 3 when compared to Wnt MB by GSEA. (b) Similarly, Bmi1 associated genes were enriched in Group 4 when compared to Wnt MB. Further, cell cycle inhibitors and apoptotic factors were enriched in Wnt when compared to Group 4 MB. (c) Pathways found to be significantly regulated between Wnt, Group 3, Group 4,

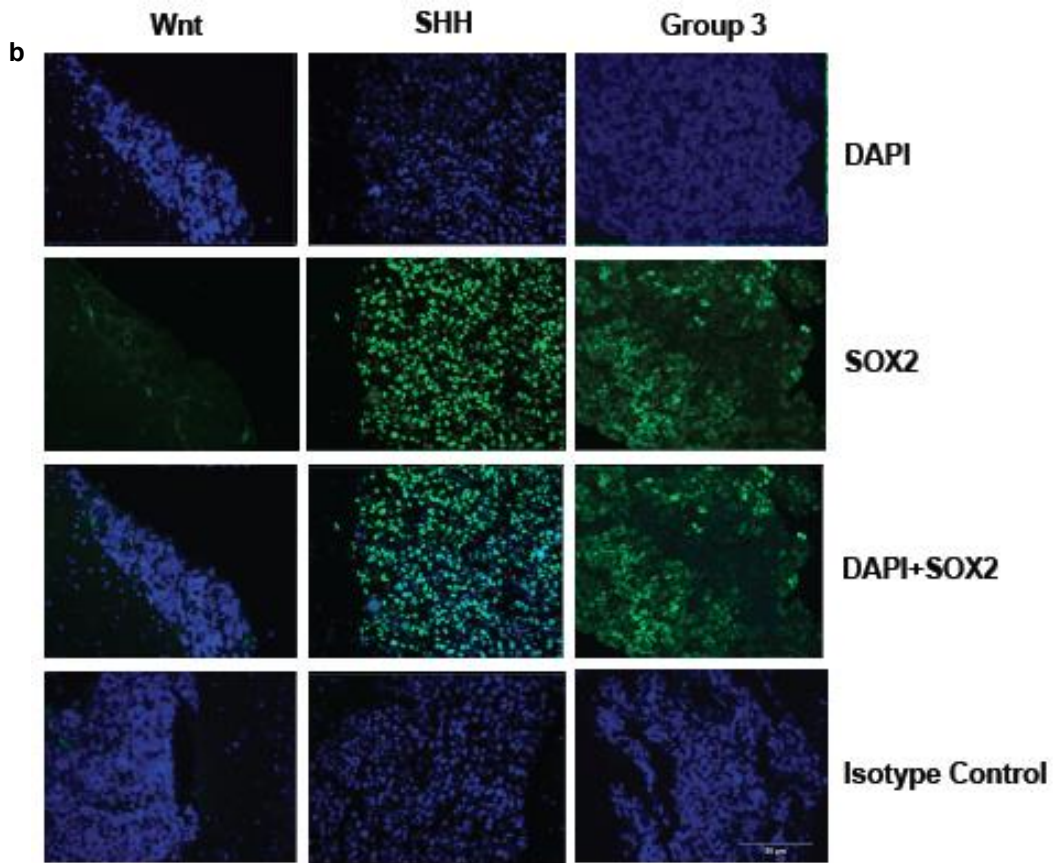
L807mts-treated and control samples (n=3, independent samples per MB line, 1 line per subgroup). Pathways were grouped based on biological categories. Each bar indicates a number of pathways found to be significantly regulated in a given comparison belonging to the category of interest.



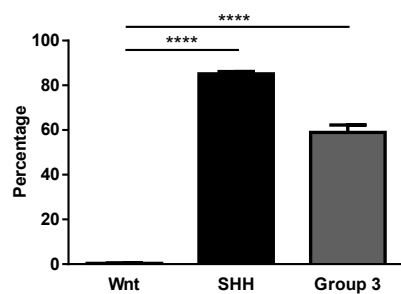
**Supplementary Figure 4: Wnt3A-conditioned medium reduces *in vitro* stemness in treatment-refractory MB lines.** (a) *Axin2* transcript levels are enriched in cells treated with Wnt3A-conditioned medium compared to control ( $p=0.0476$ ) ( $n=3$ , independent experiments, 1 line per subgroup). (b) Light microscopic images of tumor spheres treated with control and Wnt3A-conditioned medium (scale bar = 200  $\mu\text{m}$ ). (c) Wnt3A-conditioned medium-treated cells display a significant reduction in tumor sphere size ( $p=0.0015$ ) ( $n=3$ , independent experiments, 1 line per subgroup). (d) Self-renewal ( $p=0.0048$ ) and (e) proliferative ( $p=0.0101$ ) capacity of MB stem cells are significantly reduced following culture with Wnt3A-conditioned medium when compared to control ( $n=3$ , independent experiments, 1 line per subgroup).

**a**

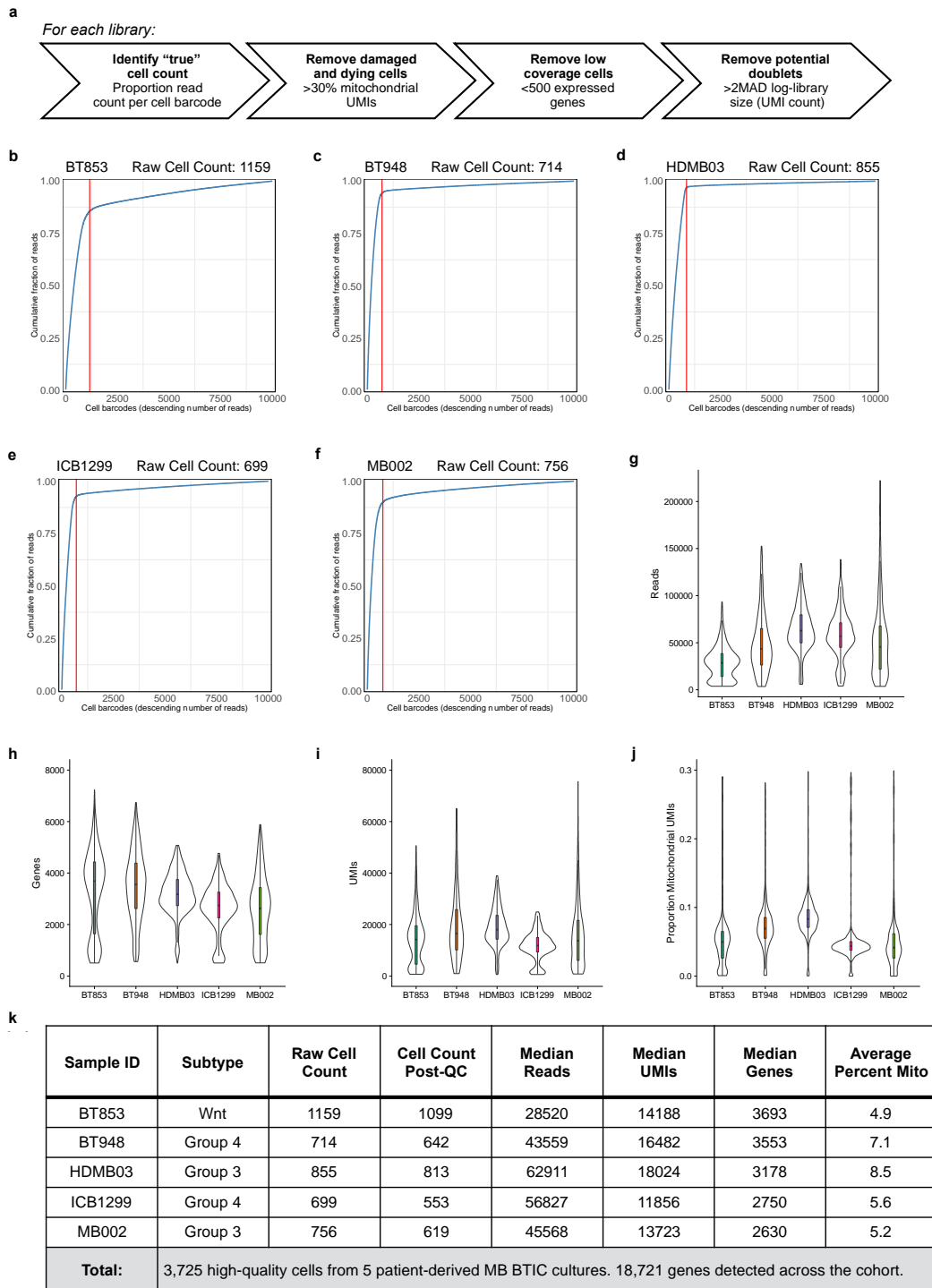
Subgroups	Samples	BMI1	Sox2
WNT	BT853	0.40%	0.11%
SHH	Daoy	66.90%	85.49%
Group 3	HD-MB03	99.90%	97.74%
	RCMB-40	100.00%	0.45%
	D425	57.10%	0.54%
	Med8A	44.32%%	89.47%
	D458	81.07%	1.61%



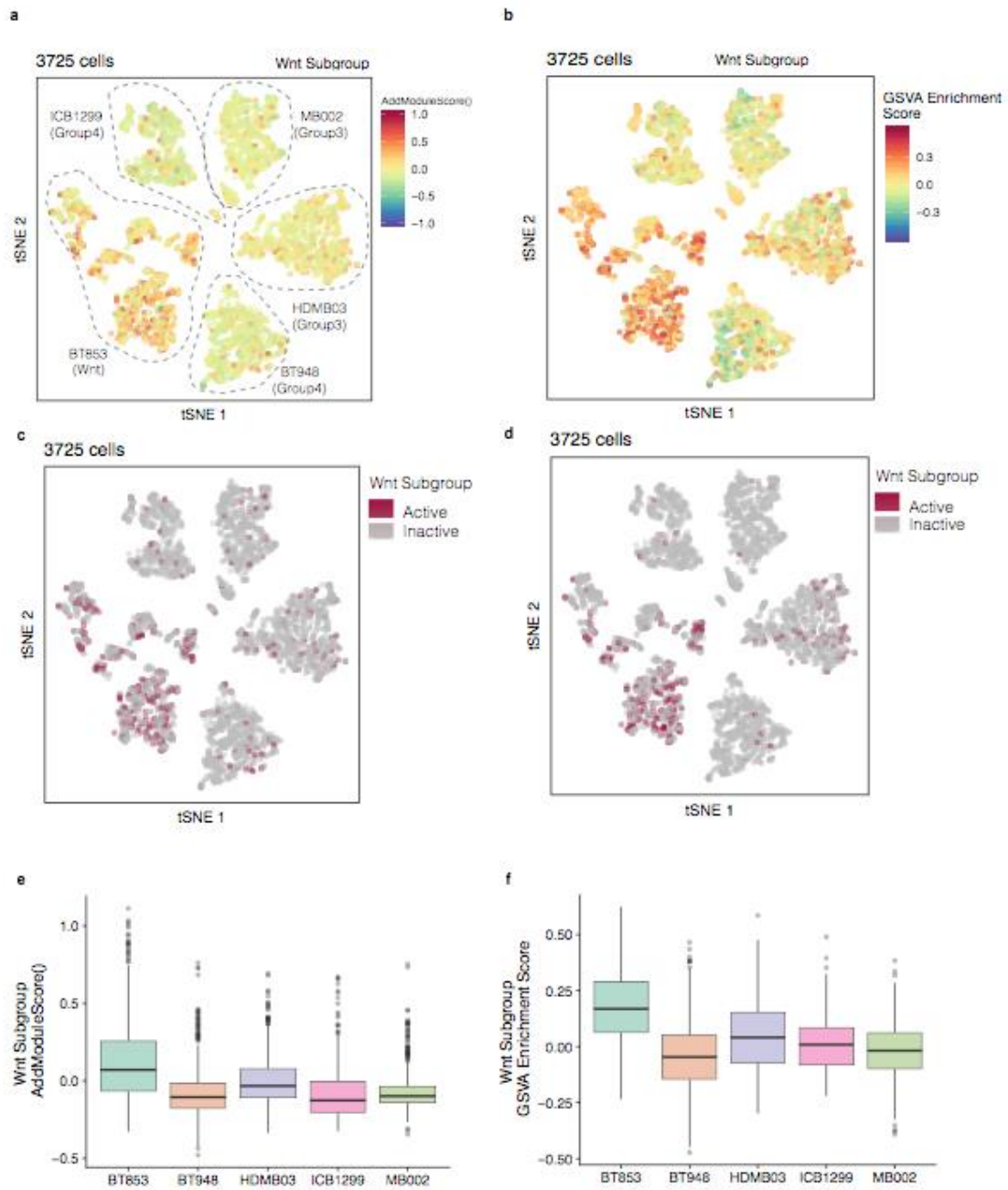
**c**



**Supplementary Figure 5: Non-Wnt MBs express higher levels of Sox2 and Bmi1 when compared to Wnt MB.** (a) Flow analysis shows higher expression of Sox2 and Bmi1 in non-Wnt MBs when compared to Wnt MBs. (b) Representative image of xenografts from Wnt MB and non-Wnt MB tumors stained for Sox2. (c) Quantification of IF staining shows non-Wnt MBs have higher Sox2 expression compared to Wnt MBs ( $p < 0.0001$ ). Scale bar = 20  $\mu\text{m}$ .

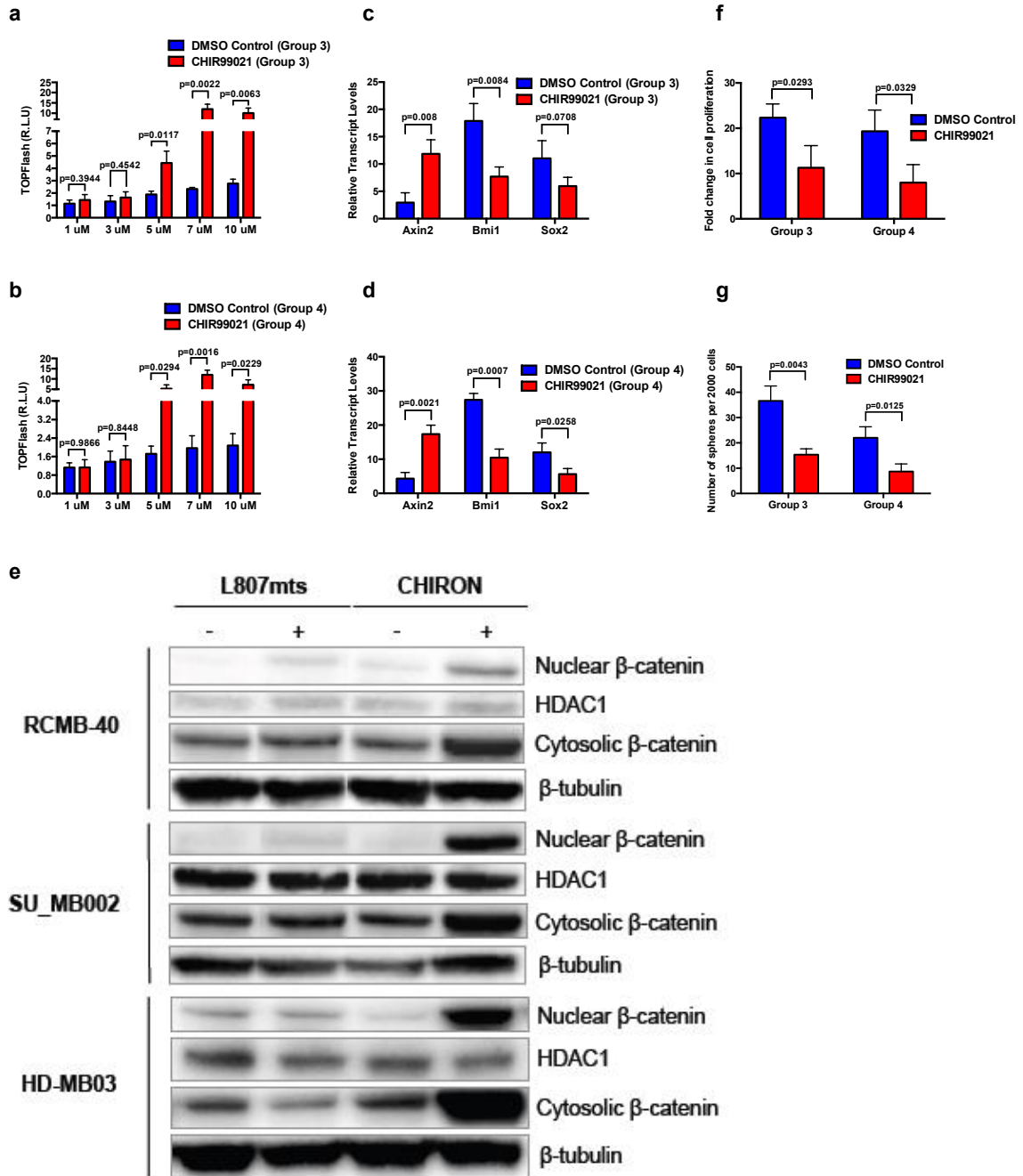


**Supplementary Figure 6: Quality control of scRNA-seq data to eliminate potential doublets, damaged and low-quality cells.** (a) Analysis pipeline to identify suspect cells. (b-f) Determining cell number from scRNA-seq libraries using droplet read counts. Cell barcodes ordered by increasing read number. Inflection point represents cell number in library. Cell barcodes to the right of the inflection point contribute minimally to total read counts and are likely empty droplets with ambient RNA. Final QC metrics of scRNA-seq data post-filtering displaying (g) number of reads per cell, (h) number of genes per cell, (i) number of transcripts / UMIs per cell and (j) proportion mitochondrial reads per cell. (k) Sequencing metrics summarized as a table for the final, high quality cohort of 3725 cells and 18721 genes across 5 samples.



**Supplementary Figure 7: Visually comparing gene signature scoring methods for scRNA-seq data.** Regardless of the scoring method used, the Wnt Subgroup sample has

the highest enrichment for Wnt Subgroup active cells and subsequent gene signature values. (a-c) AddModuleScore() (d-f) GSVA enrichment score.



**Supplementary Figure 8: Small molecule (CHIR99021) Wnt activation impairs key stem cell properties in treatment-refractory MB lines.** (a) TCF Wnt reporter assay at various concentrations of CHIR99021 demonstrates optimal concentration for Wnt activation in Group 3 MBs (1 $\mu$ M: p=0.3944, 3 $\mu$ M: p=0.4542, 5 $\mu$ M: p=0.0117, 7 $\mu$ M: p=0.0022, 10  $\mu$ M: p=0.0063) (n=3, independent experiments, 1 line per subgroup). (b) Similarly, TCF Wnt reporter assay at various concentrations of CHIR99021 demonstrates optimal concentration for Wnt activation in Group 4 MBs (1 $\mu$ M: p=0.9866, 3 $\mu$ M: p=0.8448, 5 $\mu$ M: p=0.0294, 7 $\mu$ M: p=0.0016, 10  $\mu$ M: p=0.0229) (n=3, independent experiments, 1 line per subgroup). Differential *Axin2* (Group 3: p=0.008, Group 4: p=0.0021), *Bmi1* (Group 3: p=0.0084, Group 4: p=0.0007), and *Sox2* (Group 3: p=0.0708, Group 4: p=0.0258) transcript levels in CHIR99021-treated (c) Group 3 and (d) Group 4 MB lines (n=3, independent experiments per MB line, 1 line per subgroup, all samples normalized to *GAPDH*). (e) Both cytoplasmic and nuclear extracts from cells treated with CHIR99021 or L80Smts exhibit increased  $\beta$ -catenin levels. Both, (f) proliferation (Group 3: p=0.0293, Group 4: p=0.0329) and (g) self-renewal (Group 3: p=0.0043, Group 4: p=0.0125) are impaired following CHIR99021 treatment in Group 3 and (g) Group 4 MB lines (n=3, independent experiments per MB line, 1 line per subgroup).

**Supplementary Table 1: Maximal fold changes for RNA-seq differential gene expression profile.** 2 genes (March 1 and March 2) were represented by 2 transcripts each with maximal fold changes per gene provided in the table. Only genes with a fold change of at least 2 are presented.

**Supplementary Table 2: Differential pathway networks enrichment.** Upregulated and downregulated pathways between Wnt and non-Wnt MBs or L807mts- and PBS control-treated samples.

**Supplementary Table 3: Univariate and multivariate analyses of combined Groups 3 and 4 patients based on the *Bmi1* signature**

<b>Bmi1 (Glinsky signature)</b>						
<b>Groups 3 and 4</b>						
<b>Using Index Group (High vs. Low) [Quantile 66]</b>						
<b>Characteristic</b>	<b>Description</b>	<b>N</b>	<b>Hazard Ratio</b>	<b>(95% CI)</b>	<b>p-value</b>	
<b>Univariate analyses</b>						
Index Group	High/Low	377	0.62	0.43-0.90	0.0113	*
Age	<=3years/>3years	373	2.05	1.20-3.49	0.00779	**
Metastatic status	M0/M+	343	1.32	0.90-1.94	0.153	
Subgroup	Group 3/Group4	377	0.55	0.38-0.79	0.00137	**
<b>Multivariate analysis</b>						
Index Group	High/Low	339	0.65	0.44-0.96	0.0287	*
Age	<=3years/>3years		1.45	0.82-2.58	0.20499	
Metastatic status	M0/M+		0.79	0.53-1.16	0.22704	
Subgroup	Group 3/Group4		0.55	0.37-0.83	0.00421	**

<b>Associations with Index (Log2 expression)</b>				
<b>Characteristic</b>	<b>Statistic</b>	<b>N</b>	<b>Mean (SD) Index</b>	<b>p-value</b>
Age	<=3years	35	7.69 (0.32)	0.94

	>3years	351	7.70 (0.28)	
Metastatic status	M0	214	7.67 (0.29)	0.03339
	M+	139	7.73 (0.28)	
Subgroup	Group 3	115	7.67 (0.35)	0.3761
	Group 4	275	7.71 (0.26)	

**Supplementary Table 4:** Univariate and multivariate analyses of combined Groups 3 and 4 patients based on the *Sox2* signature

Sox2 signature						
Groups 3 and 4						
Using Index Group (High vs. Low) [Quantile 66]						
Characteristic	Description	N	Hazard Ratio	(95% CI)	p-value	
<b>Univariate analyses</b>						
Index Group	High/Low	377	0.59	0.41-0.85	0.00441	**
Age	<=3years/>3years	373	2.05	1.21-3.49	0.007791	**
Metastatic status	M0/M+	343	1.32	0.90-1.94	0.153	
Subgroup	Group 3/Group4	377	0.55	0.38-0.79	0.00137	**
<b>Multivariate analysis</b>						
Index Group	High/Low	339	0.72	0.49-1.06	0.0924	.
Age	<=3years/>3years		1.46	0.82-2.59	0.1994	
Metastatic status	M0/M+		0.77	0.52-1.14	0.1897	
Subgroup	Group 3/Group4		0.59	0.39-0.89	0.0114	*

Associations with Index (Log2 expression)				
Characteristic	Statistic	N	Mean (SD) Index	p-value
Age	<=3years	35	8.18 (0.08)	0.34
	>3years	351	8.17 (0.06)	
Metastatic status	M0	214	8.16 (0.07)	0.03888
	M+	139	8.18 (0.06)	
Subgroup	Group 3	115	8.18 (0.08)	0.02943
	Group 4	275	8.16 (0.06)	

**Supplementary Table 5:** Univariate and multivariate analyses of Groups 3 patients based on the *Wnt* signature

WNT signature						
Group 3						
Using Index Group (High vs. Low) [Quantile 66]						
Characteristic	Description	N	Hazard Ratio	(95% CI)	p-value	
<b>Univariate analyses</b>						
Index Group	High/Low	113	2.45	1.18-5.07	0.0158	*
Age	<=3years/>3years	113	1.39	0.70-2.73	0.3475	
Metastatic status	M0/M+	106	1.63	0.90-2.95	0.106	
<b>Multivariate analysis</b>					0.02746	
Index Group	High/Low	105	2.73	1.27-5.88	0.0103	**
Age	<=3years/>3years		1.02	0.49-2.13	0.9491	
Metastatic status	M0/M+		0.61	0.33-1.12	0.1116	

<b>Associations with Index (Log2 expression)</b>				
<b>Characteristic</b>	<b>Statistic</b>	<b>N</b>	<b>Mean (SD) Index</b>	<b>p-value</b>
Age	<=3years	24	8.25 (0.09)	0.22
	>3years	90	8.28 (0.14)	
Metastatic status	M0	65	8.26 (0.13)	0.1736
	M+	42	8.30 (0.14)	

## **Chapter 4: A CD133-AKT-Wnt signaling axis drives glioblastoma brain tumor-initiating cells**

### **Preamble**

This chapter is an original manuscript submitted on October 15, 2018 to *Oncogene*.

Manoranjan B, Chokshi C, Venugopal C, Subapanditha M, Savage N, Tatari N, Provias JP, Murty NK, Moffat J, Doble BW, Singh SK

Experimental concept and study design were developed by myself, C. Venugopal, B.W. Doble, and S.K. Singh. GBM samples and clinical details were provided by J.P. Provias and N.K. Murty. Flow cytometric analysis and cell-sorting were performed by M. Subapanditha. I performed all Wnt/TCF reporter assays, quantitative real-time polymerase chain reactions, lentiviral studies, cell proliferation assays, self-renewal analyses, western immunoblotting, and small molecule inhibitor studies. C. Chokshi and N. Tatari performed self-renewal analyses and small molecule inhibitor studies for manuscript revision experiments. J. Moffat provided guidance for small molecule inhibitor studies. *In vivo* experiments were led and performed by myself with assistance from N. Savage.

The main objective of this body of work was to elucidate the mechanism by which the Wnt pathway is activated in GBM albeit without recurrent mutations in components of the pathway. Having identified for the first time a CD133-AKT-Wnt signaling axis in GBM where CD133 functions as a putative cell surface receptor for AKT-dependent Wnt activation, these findings have implications for targeting PI3K/AKT or Wnt as both

pathways may be activated independent of their canonical drivers, leading to treatment resistance and disease relapse.

## **A CD133-AKT-Wnt signaling axis drives glioblastoma brain tumor-initiating cells**

Branavan Manoranjan<sup>1,2,3</sup>, Chirayu Chokshi<sup>2,3</sup>, Chitra Venugopal<sup>2</sup>, Minomi Subapanditha<sup>2</sup>, Neil Savage<sup>2</sup>, Nazanin Tatari<sup>2,3</sup>, John P. Provias<sup>4</sup>, Naresh K. Murty<sup>5</sup>, Jason Moffat<sup>6</sup>, Bradley W. Doble<sup>2,3</sup>, Sheila K. Singh<sup>2,3,5</sup>

<sup>1</sup>Michael G. DeGroote School of Medicine, McMaster University, Hamilton, Ontario, L8S 4K1, Canada

<sup>2</sup>McMaster Stem Cell and Cancer Research Institute, McMaster University, Hamilton, Ontario, L8S 4K1, Canada

Departments of <sup>3</sup>Biochemistry and Biomedical Sciences, <sup>4</sup>Pathology, <sup>5</sup>Surgery, Faculty of Health Sciences, McMaster University, 1200 Main Street West, Hamilton, Ontario, L8N 3Z5, Canada

<sup>6</sup>The Donnelly Centre, University of Toronto, Toronto, Ontario, M5S 3E1, Canada

### **Running Title**

CD133 functions to regulate Wnt in glioblastoma

### **Declaration of Interests**

The authors declare that they have no conflict of interest.

### **Corresponding Author**

Sheila K. Singh, MD, PhD, FRCS(C)

Professor of Pediatric Neurosurgery,

Department of Surgery, McMaster Children's Hospital,

Scientist, McMaster Stem Cell & Cancer Research Institute

MDCL 5027, 1280 Main Street West, Hamilton, ON, L8S 4K1, Canada

T: 905-521-2100 x75237

F: 905-521-992

Email: ssingh@mcmaster.ca

### **Abstract**

Mechanistic insight into signaling pathways downstream of surface receptors has been revolutionized with integrated cancer genomics. This has fostered current treatment modalities, namely immunotherapy, to capitalize on targeting key oncogenic signaling nodes downstream of a limited number of surface markers. Unfortunately, rudimentary mechanistic understanding of most other cell surface proteins has reduced the clinical utility of these markers. CD133 has reproducibly been shown to correlate with disease progression, recurrence, and poor overall survivorship in the malignant adult brain tumor, glioblastoma (GBM). Using several patient-derived CD133<sup>high</sup> and CD133<sup>low</sup> GBMs we describe intrinsic differences in determinants of stemness, which we owe to a CD133-AKT-Wnt signaling axis in which CD133 functions as a putative cell surface receptor for AKT-dependent Wnt activation. These findings may have significant implications for personalized oncology trials targeting PI3K/AKT or Wnt as both pathways may be activated independent of their canonical drivers, leading to treatment resistance and disease relapse.

**Keywords:** glioblastoma, Wnt, beta-catenin, CD133, AKT, brain tumor-initiating cell

## Introduction

Contemporary frameworks for studying tumorigenesis consider the process as development gone awry. Cell surface markers have traditionally been used to characterize the continuum of cellular phenotypes generated in ontogeny and carried forward into oncology as tumor-initiating cells (TICs). CD133 was originally identified as a marker of self-renewing hematopoietic<sup>37</sup> and neural stem cell<sup>30</sup> populations. Subsequently, it has been used to characterize cells capable of tumor initiation and maintenance in a variety of human cancers<sup>3, 7, 19, 27</sup>, including the most malignant adult brain tumor, glioblastoma (GBM)<sup>27</sup>. With few markers of clinical utility in adult GBM, CD133 has reproducibly been shown to correlate with disease progression, recurrence, and poor overall survivorship<sup>25, 38</sup> but insight into its function remains limited. Given the activation of AKT signaling in approximately 50% of GBMs secondary to EGFR amplification and/or overexpression, activating mutations in PI3K, or inactivating mutations in PTEN<sup>32</sup>, emerging studies have suggested CD133 to function as a novel receptor for the PI3K/AKT pathway<sup>34</sup>. Although CD133 is the first identified member of the Prominin family of pentaspan membrane glycoproteins, with an implied role in cell signaling, the mechanism by which it regulates stemness to bridge developmental and oncogenic cellular programs has not yet been described.

The Wnt signaling pathway promotes the expansion of neural stem cells (NSCs) in the forebrain during fetal development<sup>2, 11</sup> and its components, namely  $\beta$ -catenin, are persistently overexpressed in GBM<sup>23, 39</sup>. Interestingly, unlike colorectal cancer or pediatric medulloblastoma in which elevated  $\beta$ -catenin expression is attributed to stabilizing

mutations in *CTNGB1*<sup>13</sup> or inactivating mutations in APC<sup>16</sup>, GBM has not been shown to contain recurrent mutations in the Wnt pathway<sup>1, 9, 10, 17, 21, 22, 32, 36, 40, 41</sup>. With recent data independently illustrating CD133-mediated<sup>13</sup> or AKT-dependent<sup>24</sup> activation of  $\beta$ -catenin, a context-dependent cross-talk pathway may be implicated in the overexpression of  $\beta$ -catenin seen in GBM.

We have used several primary patient-derived CD133<sup>high</sup> and CD133<sup>low</sup> GBM lines to describe intrinsic differences in determinants of stemness. With the aim of identifying the cellular machinery that drives self-renewal downstream of CD133, we have used small molecule inhibitors that target several components of this pathway. The use of Wnt reporters has enabled us to further illustrate a mechanism by which CD133 may contribute to the genetic and phenotypic diversity seen in GBM. Our work establishes a CD133-AKT-Wnt signaling axis in which CD133 functions as a putative cell surface receptor for AKT-dependent activation of Wnt signaling. These findings may have significant implications for personalized oncology trials targeting PI3K/AKT or Wnt as both pathways may be activated independent of their canonical drivers, leading to treatment resistance, disease relapse, and poor overall survival.

## Results

### *CD133<sup>high</sup> GBMs contain elevated levels of endogenous Wnt activity when compared to CD133<sup>low</sup> GBMs*

As recent single cell sequencing studies have highlighted the immense level of genetic and phenotypic diversity present in GBM<sup>12, 20</sup>, we initially screened our GBM

BTIC lines to assess the variability in CD133 cell surface protein expression (Supplementary Fig. 1). In keeping with the current literature on cellular diversity in GBM<sup>12, 20</sup>, our samples displayed a range in their CD133 expression from elevated levels similar to those observed in NSCs to near negligible values (Fig. 1a). As established in recent literature, CD133 expression in our samples correlated with their self-renewal potential (Supplementary Fig. 2). To determine the extent of downstream Wnt activation, we measured endogenous levels of Wnt pathway activity using the TCF reporter assay. Wnt reporter activity closely resembled the trend observed with CD133 expression, as BTIC lines either contained elevated Wnt levels mirroring those in NSCs or displayed very minimal reporter activity (Fig. 1b). These results were validated with *Axin2* transcript expression (Fig. 1c). To appreciate the marked difference in downstream Wnt activation based on CD133 cell surface expression, we compared TCF reporter activity (Fig. 1d) and *Axin2* expression (Fig. 1e) in CD133<sup>high</sup> and CD133<sup>low</sup> BTIC lines. Both comparisons yielded a significant enrichment in overall Wnt pathway activation in CD133<sup>high</sup> GBMs compared to CD133<sup>low</sup> samples. These findings support a correlative effect on stemness in a subset of GBMs where both CD133 and the Wnt pathway are enriched to maintain a BTIC state.

### ***CD133 activates Wnt/ $\beta$ -catenin signaling in an AKT-dependent manner***

In order to validate the functional significance of CD133 as a modulator of stemness, we generated stable BTIC lines by ectopically expressing CD133 in BTICs with negligible levels of CD133 on the cell surface (Supplementary Fig 3a). A significant increase in the proliferative (Fig. 2a) and self-renewal (Fig. 2b, Supplementary Fig. 3b)

potentials were observed following CD133 overexpression. To determine the effect of CD133 expression on endogenous Wnt activity, we compared TCF reporter levels in control and CD133 overexpressed samples and noted a significant increase in Wnt reporter activity with CD133 overexpression (Fig. 2c). With the surmounting evidence in support of a functional and mechanistic association between CD133 and AKT in gliomas<sup>6, 8, 31, 34</sup>, little work has been done to understand the process by which this interaction may promote a BTIC phenotype. Given that activated AKT may phosphorylate GSK-3 on Ser9<sup>29</sup>, leading to the inactivation of GSK-3, we surmised that AKT-dependent  $\beta$ -catenin stabilization may drive downstream Wnt signaling and promote self-renewal in GBM. Western blots of multiple BTIC lines comparing control and CD133 overexpression identified a marked increase in pAKT (Ser473), pGSK-3 (Ser9), and  $\beta$ -catenin following CD133 overexpression (Fig. 2d). Therefore, while CD133 may promote the proliferation and self-renewal of BTICs, this process may be through a novel context-specific AKT-dependent activation of the Wnt signaling pathway.

#### ***Inhibition of CD133 or AKT impairs downstream Wnt activity in BTICs***

To further characterize the CD133-AKT-Wnt signaling axis, we targeted both CD133 (Supplementary Fig. 4a,b) and AKT (Supplementary Fig. 4c,d) with small molecule inhibitors and assessed their downstream effects on Wnt signaling. By using RW03, a novel anti-CD133 monoclonal antibody, we have been able to further validate CD133 as a putative functional BTIC surface receptor. Treatment with RW03 resulted in down regulation of surface CD133 expression (Fig. 3a, Supplementary Fig. 5), self-renewal potential (Fig. 3b), and a significant decrease in TCF reporter activity (Fig. 3c) in multiple

independent BTIC lines when compared to controls. We then assessed the functional and mechanistic effects of AKT inhibition on GBM BTICs. Treatment with the small molecule pan-AKT inhibitor, MK-2206, significantly reduced the proliferative (Fig. 3d) and self-renewal capacity (Fig. 3e) of CD133<sup>hi</sup> BTICs. In fact, self-renewal capacity of BTICs with low surface CD133 expression was sensitized to AKT inhibition following ectopic CD133 expression (Supplementary Fig. 4e,f). TCF reporter assays confirmed the downstream inhibition of Wnt activity following AKT inhibition (Fig. 3f), which provided additional data in support of a context-specific role by which AKT may regulate Wnt/ $\beta$ -catenin signaling.

***GBM BTICs with endogenous Wnt activity promote tumorigenesis in an AKT-dependent manner***

Given the significant level of genetic intratumoral heterogeneity in GBM and having recognized the variable expression of CD133 and Wnt activity across several BTIC lines, we aimed to validate the functional importance of our novel CD133-AKT-Wnt signaling axis on perpetuating a malignant phenotype. After confirming endogenous CD133 expression (Supplementary Fig. 6a), BTICs were transduced with a lentiviral Wnt reporter construct (7XTCF-GFP)<sup>4</sup>, allowing us to isolate and compare BTICs based on their endogenous levels of Wnt activation. GFP<sup>+</sup> (referred to as TGP<sup>+</sup>) and GFP<sup>-</sup> (referred to as TGP<sup>-</sup>) cell populations were isolated using flow cytometric cell sorting (Supplementary Fig. 6b). The enhanced Wnt activity in TGP<sup>+</sup> cells compared to TGP<sup>-</sup> cells was validated with the TCF Wnt reporter assay (Fig. 4a). *In vitro* functional characterization of TGP<sup>+</sup> and TGP<sup>-</sup> cells demonstrated significant increase in the

proliferative (Fig. 4b) and self-renewal (Fig. 4c) capacity of TGP+ compared to TGP- cells. To determine if the observed differences in *in vitro* functional assays may be in part due to an AKT-dependent activation of the Wnt signaling pathway in TGP+ cells, we assessed the protein levels of pAKT (Ser473), pGSK (Ser9), and  $\beta$ -catenin in TGP+ and TGP- cells (Fig. 4d). Given that all proteins were enriched in TGP+ cells when compared to TGP- cells, our analysis confirmed the role of this novel signaling cascade in regulating Wnt activity and further illustrated how this pathway may contribute to intratumoral heterogeneity at the protein level in GBM. We then assessed the tumor-initiating capacity of TGP+ and TGP- cells and wondered if TGP+ cells formed more aggressive tumors *in vivo*. Xenografts were generated with orthotopic injections of TGP+ or TGP- cells. Overall tumor burden was significantly increased in TGP+ xenografts compared to mice with TGP- cells (Fig. 4e,f). A reduced survival advantage was also seen in TGP+ xenografts, which had a median survival of 25.0 days compared to 32.5 days in TGP- xenografts (Fig. 4g). These data highlight the functional significance of a signaling nexus in which CD133 enhances an AKT-dependent Wnt pathway and further illustrate the importance of addressing the proteomic heterogeneity that may further contribute to treatment failure and poor patient outcome in GBM.

## Discussion

The advent of molecular diagnostics and large-scale integrated genomic analyses of tumors have reconceptualized our understanding of the biology of many cancers, including GBM<sup>12, 20, 32</sup>. While these studies have uncovered several actionable therapeutic targets, their clinical utility has been inadequate with no improvements in overall

survivorship<sup>28, 35</sup>. This may in part be due to the limited efficacy of monotherapy trials and our poor understanding of cross-talk and convergence among cell signaling pathways<sup>28, 33, 35</sup>. The identification of context-specific signaling mechanisms as in the case of AKT-mediated activation of Wnt signaling may have therapeutic implications as downstream pathways may converge on common nodes of integration, which may be missed by current integrated genomics that lack corresponding proteomic data<sup>33</sup>.

Insight into the function of CD133 has been limited to the discovery of a single-nucleotide frameshift mutation in the *CD133* gene, leading to an autosomal-recessive retinal degenerative disease<sup>15</sup>. While these findings establish a role for CD133 in retinal development, they have not been carried forward into identifying the functional significance of CD133 in oncology. Through functioning as a cell surface marker for TIC populations that have been shown to interact with the PI3K/AKT pathway<sup>34</sup>, CD133 may be a novel cell surface receptor for several oncogenic pathways that converge on common signaling nodes of interaction. Although the pool of GSK-3 phosphorylated by activated AKT has historically not been associated with Wnt/ $\beta$ -catenin signaling<sup>18</sup>, emerging data have implicated an alternative pathway by which AKT may activate the Wnt/ $\beta$ -catenin pathway<sup>5</sup>. Earlier work has indicated growth factor signaling through AKT to phosphorylate GSK-3 and thereby inhibit substrate accessibility to GSK-3. The subsequent stabilization of substrates normally phosphorylated by GSK-3 remains controversial and context-dependent<sup>14</sup>. One determining factor for when AKT may not stabilize GSK-3 substrates may be in the presence of activating mutations in components of GSK-3-mediated pathways<sup>18</sup>. In contrast, since recurrent mutations of the Wnt/ $\beta$ -catenin pathway

have not been identified in GBM, AKT may stabilize and enhance  $\beta$ -catenin expression to maintain developmental signaling programs in BTIC populations.

By modulating CD133, AKT, and Wnt/ $\beta$ -catenin with a variety of targeted approaches, we have provided evidence in support of a CD133-AKT-Wnt pathway in human GBM. Specifically, this work illustrates an emerging paradigm in Wnt biology in which functions of the pathway may be elicited by non-canonical receptors and upstream activators. Using our TIC models, we have validated the clinical relevance of this pathway in its ability to drive GBM growth and lead to poor overall survivorship. The identification of GBM cells with endogenous Wnt activity having enhanced expression of our signaling axis further signifies the importance of clonal dynamics and the advantages of single cell proteomics when functionally interrogating heterogeneous cell populations for unique vulnerabilities. As molecularly-based clinical oncology trials continue to expand, novel approaches to overcome the dependence of tumors on malignant pathways are warranted such that common nodes of interaction within divergent cell signaling pathways may be targeted by multiple treatment modalities.

## **Materials & Methods**

### ***Culture of primary GBM samples***

Primary human GBMs (Supplementary Table 1) and whole 13- or 14-week fetal brain samples were obtained from consenting patients and families as approved by the Hamilton Health Sciences/McMaster Health Sciences Research Ethics Board. Samples were dissociated in PBS containing 0.2 Wünsch unit/mL of Liberase Blendzyme 3 (Roche),

and incubated at 37°C in a shaker for 15 minutes. The dissociated tissue was filtered through a 70 µm cell strainer and collected by centrifugation (1500 rpm, 3 minutes). GBM87 was a kind gift from Dr. Hiroaki Wakimoto (Massachusetts General Hospital, Boston, MA, USA). Tumor cells and human neural stem cells (hNSCs) from fetal brain were resuspended in a serum-free brain tumor-initiating cell (BTIC) enrichment media, and replated on ultra-low attachment plates (Corning). BTIC enrichment media was composed of NeuroCult complete media (StemCell Technologies), 10 ng/mL bFGF, 20 ng/mL EGF, and 2 µg/mL heparin.

#### ***Flow cytometric analysis and cell-sorting***

Tumorspheres were dissociated and single cells resuspended in PBS + 2 mmol/L EDTA. For total (internal and surface) characterization of CD133 levels, cells were fixed using Fixation/Permeabilization Solution Kit (BD). Cells were stained with APC-conjugated anti-CD133 or a matched isotype control (Miltenyi) and incubated for 30-40 minutes on ice. Samples were run on a MoFlo XDP Cell Sorter (Beckman Coulter). Dead cells were excluded using the viability dye 7AAD (1:10, Beckman Coulter) or using a near IR Live/Dead fixable staining kit (Life Technologies). Compensation was performed using mouse IgG CompBeads (BD). CD133 or GFP expression (for endogenous Wnt active cells) were defined as positive or negative based on the analysis regions set on the isotype control or untransduced cells respectively. GFP<sup>+</sup> and GFP<sup>-</sup> cells were sorted into tubes containing 1 mL BTIC enrichment media and small aliquots of each sort tube were analyzed to determine the purity of the sorted populations. Cells were allowed to equilibrate at 37°C for a few hours prior to experimentation.

### ***Wnt/TCF reporter assay***

GBM cells were cotransfected with the constructs 8XTOPFlash (1.8 mg), driving firefly luciferase, and pRL-CMV (0.2 mg), driving the expression of Renilla luciferase for normalization (Promega). After 24 hours, GBM cells were supplemented with BTIC enrichment medium. Cells were washed twice with PBS 24 hours following medium change and were lysed with passive lysis buffer (Promega). The luciferase reporter activities were measured using a luminometer as per the manufacturer's instructions (Promega Dual-Light System).

### ***Quantitative real-time polymerase chain reaction***

Total RNA was extracted using the Norgen Total RNA isolation kit and quantified using a NanoDrop Spectrophotometer ND-1000. Complementary DNA was synthesized from 0.5-1 µg RNA using the qScript cDNA Super Mix (Quanta Biosciences) and a C1000 Thermo Cycler (Bio-Rad) with the following cycle parameters: 4 minutes at 25°C, 30 minutes at 42°C, 5 minutes at 85°C, hold at 4°C. qRT-PCR was performed using the Perfecta SybrGreen (Quanta Biosciences) and CFX96 instrument (Bio-Rad). CFX Manager 3.0 software was used for quantification of gene expression and levels were normalized to GAPDH expression with secondary validation normalized to Actin expression. Primers include: *Actin* (F: 5'-TATCCCTGTACGCCTCT-3'; R: 5'-AGGTCTTTGCGGATGT-3'), *Axin2* (F: 5'-TGGAGCCGGCTGCGCTTTGAT-3'; R: 5'-CTGGGGTCCGGGAGGCAAGTC-3'), *GAPDH* (F: 5'-TGCACCACCAACTGCTTAGC-3'; R: 5'-GGCATGGACTGTGGTCATGAG-3').

### ***Lentiviral Studies***

OE-Ctrl and OE-CD133 vectors were purchased from Genecopoeia. TGP endogenous canonical Wnt reporter (8X TOPFlash TCF reporter) (#24305) was purchased from Addgene. Replication-incompetent lentiviruses were produced by cotransfection of the expression vector and packaging vectors pMD2G and psPAX2 in HEK293FT cells. Viral supernatants were harvested 72 hours after transfection, filtered through a 0.45 µm cellulose acetate filter, and precipitated with PEGit (System Biosciences). The viral pellet was resuspended in 1.0 mL of DMEM media and stored at -80°C. Stable cell lines were generated by transduction followed by maintenance of cultures with puromycin or flow cytometric cell sorting for GFP+ and GFP- cells.

#### ***Cell proliferation assay***

Single cells were plated in 96-well plates, at a density of 1,000 cells/200 µL per well in quadruplicate for each sample and incubated for four days. 20 µL of Presto Blue (Life Technologies), a fluorescent cell metabolism indicator, was added to each well approximately 4 hours prior to the readout time point. Fluorescence was measured with a FLUOstar Omega Fluorescence 556 Microplate reader (BMG LABTECH) at an excitation and emission wavelength of 540 and 570 nm, respectively. Readings were analyzed using the Omega software.

#### ***Self-renewal analysis***

GBM BTIC tumorspheres were mechanically dissociated with a 1000 µL pipette tip or enzymatically disassociated using Liberase (Roche) and DNase. To conduct a secondary sphere formation assay, cells were plated at 200 cells per well in 200 µL of BTIC enrichment media in a 96-well plate. Cultures were left undisturbed at 37°C with 5% CO<sub>2</sub>.

After 3 days, number of secondary spheres per well was counted and used to estimate the mean number of spheres/2000 cells. To conduct a limiting dilution assay, dissociated cells were plated at dilutions from 512 to 2 cells per well. After 7 days, the absence or presence of secondary spheres in each well was noted and used to determine stem cell frequency<sup>26</sup>.

### ***Western Immunoblotting***

Denatured total protein (10µg) was separated using 10% sodium dodecyl sulphate-polyacrylamide gel electrophoresis and transferred to polyvinylidene fluoride membrane. Western blots were probed with the following primary antibodies: AKT (rabbit; 1:1000; Cell Signaling #4691), pAKT (mouse; 1:1000; Cell Signaling #4051), β-catenin (mouse; 1:10,000; BD Biosciences #610154), GSK-3 (mouse; 1:2000; Sigma #44-610), pGSK-3β-Ser9 (rabbit; 1:1000; Cell Signaling #5558), and GAPDH (mouse; 1:50,000; Abcam #ab8245). The secondary antibody was horseradish peroxidase conjugated goat anti-mouse IgG (Bio-Rad). The bands were visualized using an Immobilon Western kit (Millipore) and Chemidoc.

### ***Small molecule inhibitors***

The CD133 monoclonal antibody, RW03, developed by our collaborator Dr. Jason Moffat (University of Toronto) was used to inhibit CD133 signaling at the receptor level. GBM BTICs were treated with RW03 at concentrations of 10, 25 and 50 nM. PBS or control IgG were used as control. Changes in endogenous Wnt activity were then assessed using the Wnt/TCF reporter assay. The pan-AKT inhibitor, MK-2206 was used to inhibit AKT signaling at concentrations of 1, 5, 10 µM. DMSO was used as a control. Functional assays (proliferation, self-renewal) and Wnt/TCF reporter assays were performed on pre-

treated GBM BTICs using 50 nM RW03 and 5  $\mu$ M MK-2206. Treatments were not maintained for the length of the assay.

### ***In Vivo Experiments***

All *in vivo* studies were performed according to McMaster University Animal Research Ethics Board approved protocols. Intracranial injections were performed as previously described<sup>27</sup> using human GBM BT241. Briefly, the appropriate number of live cells determined by Trypan Blue exclusion were resuspended in 10  $\mu$ L of PBS. NOD-SCID mice were anaesthetized using isoflurane gas (5% induction, 2.5% maintenance) and cells were injected into the frontal lobe using a 10  $\mu$ L Hamilton syringe. Tumor-initiating capacity, histological differences in tumor size, and survival analysis of BT241 TGP+ (endogenous Wnt active cells,  $n=10$ ) compared with BT241 TGP- (endogenous Wnt inactive cells,  $n=10$ ) were performed using 5 mice per dilution at dilutions of  $1.0 \times 10^5$  and  $5.0 \times 10^4$ . All mice were sacrificed at endpoint, brains were harvested, formalin-fixed, and paraffin-embedded for hematoxylin and eosin (H&E) staining. Sample size was determined based on prior experiments, which yielded significant differences in survival and tumor size. Mice were randomly selected for injected cell type but investigators were not blinded to treatment group. Images were taken using the Aperio Slide Scanner and analyzed using ImageScope v11.1.2.760 software (Aperio). Tumor volume was assessed using the area of tumor present on 4-6 coronal sections of the mouse brains stained with H&E. Given the heterogeneity in the location and pattern of tumor growth as some lesions tracked in the ventricular and extra-parenchymal spaces rather than invasively through the

brain, our tumor volume analysis is a gross approximation but reliably trends with *in vivo* survival analysis.

### ***Statistical analysis***

At least three biological replicates were performed for each experiment. Data represent mean  $\pm$  standard error (mean) with *n* values listed in figure legends. Student *t*-test analyses were performed using GraphPad Prism™ with significance set to  $P < 0.05$ . Kaplan-Meier survival curves were visualized using GraphPad Prism™.

### **Acknowledgements**

B.M. is supported by a Canadian Institutes of Health Research Vanier Canada Graduate Scholarship. S.K.S. is supported by the Neurosurgical Research and Education Foundation and American Association of Neurological surgeons, Pediatric Section, the Ontario Institute for Cancer Research, and McMaster University Department of Surgery.

### **Author Contributions**

BM, CV, CC, BWD, SKS conceptualized and designed the experiments. BM, CV, CC, MS, NS, NT performed experiments and acquired data. BM, CV, CC, BWD, SKS analyzed and interpreted data. BM wrote the manuscript with revisions contributed by CV, CC, BWD, and SKS. JM provided non-commercial reagents. JPP, NKK provided GBM study samples. BWD and SKS supervised the study. All authors reviewed results and commented on the manuscript.

### **Declaration of Interests**

The authors declare that they have no conflict of interest.

**References**

- 1 Brennan CW, Verhaak RG, McKenna A, Campos B, Noushmehr H, Salama SR *et al.* The somatic genomic landscape of glioblastoma. *Cell* 2013; 155: 462-477.
- 2 Chenn A, Walsh CA. Regulation of cerebral cortical size by control of cell cycle exit in neural precursors. *Science* 2002; 297: 365-369.
- 3 Cox CV, Diamanti P, Evely RS, Kearns PR, Blair A. Expression of CD133 on leukemia-initiating cells in childhood ALL. *Blood* 2009; 113: 3287-3296.
- 4 Fuerer C, Nusse R. Lentiviral vectors to probe and manipulate the Wnt signaling pathway. *PLoS One* 2010; 5: e9370.
- 5 Fukumoto S, Hsieh CM, Maemura K, Layne MD, Yet SF, Lee KH *et al.* Akt participation in the Wnt signaling pathway through Dishevelled. *J Biol Chem* 2001; 276: 17479-17483.
- 6 Hambardzumyan D, Squatrito M, Carbajal E, Holland EC. Glioma formation, cancer stem cells, and akt signaling. *Stem Cell Rev* 2008; 4: 203-210.
- 7 Hermann PC, Huber SL, Herrler T, Aicher A, Ellwart JW, Guba M *et al.* Distinct populations of cancer stem cells determine tumor growth and metastatic activity in human pancreatic cancer. *Cell stem cell* 2007; 1: 313-323.
- 8 Holland EC, Celestino J, Dai C, Schaefer L, Sawaya RE, Fuller GN. Combined activation of Ras and Akt in neural progenitors induces glioblastoma formation in mice. *Nat Genet* 2000; 25: 55-57.
- 9 Hu B, Wang Q, Wang YA, Hua S, Sauve CG, Ong D *et al.* Epigenetic Activation of WNT5A Drives Glioblastoma Stem Cell Differentiation and Invasive Growth. *Cell* 2016; 167: 1281-1295 e1218.

- 10 Ji H, Wang J, Nika H, Hawke D, Keezer S, Ge Q *et al.* EGF-induced ERK activation promotes CK2-mediated disassociation of alpha-Catenin from beta-Catenin and transactivation of beta-Catenin. *Molecular cell* 2009; 36: 547-559.
- 11 Kim WY, Wang X, Wu Y, Doble BW, Patel S, Woodgett JR *et al.* GSK-3 is a master regulator of neural progenitor homeostasis. *Nat Neurosci* 2009; 12: 1390-1397.
- 12 Lan X, Jorg DJ, Cavalli FMG, Richards LM, Nguyen LV, Vanner RJ *et al.* Fate mapping of human glioblastoma reveals an invariant stem cell hierarchy. *Nature* 2017; 549: 227-232.
- 13 Mak AB, Nixon AM, Kittanakom S, Stewart JM, Chen GI, Curak J *et al.* Regulation of CD133 by HDAC6 promotes beta-catenin signaling to suppress cancer cell differentiation. *Cell reports* 2012; 2: 951-963.
- 14 Manning BD, Toker A. AKT/PKB Signaling: Navigating the Network. *Cell* 2017; 169: 381-405.
- 15 Maw MA, Corbeil D, Koch J, Hellwig A, Wilson-Wheeler JC, Bridges RJ *et al.* A frameshift mutation in prominin (mouse)-like 1 causes human retinal degeneration. *Hum Mol Genet* 2000; 9: 27-34.
- 16 Morin PJ, Sparks AB, Korinek V, Barker N, Clevers H, Vogelstein B *et al.* Activation of beta-catenin-Tcf signaling in colon cancer by mutations in beta-catenin or APC. *Science* 1997; 275: 1787-1790.

- 17 Morris LG, Kaufman AM, Gong Y, Ramaswami D, Walsh LA, Turcan S *et al.* Recurrent somatic mutation of FAT1 in multiple human cancers leads to aberrant Wnt activation. *Nature genetics* 2013; 45: 253-261.
- 18 Ng SS, Mahmoudi T, Danenberg E, Bejaoui I, de Lau W, Korswagen HC *et al.* Phosphatidylinositol 3-kinase signaling does not activate the wnt cascade. *J Biol Chem* 2009; 284: 35308-35313.
- 19 O'Brien CA, Pollett A, Gallinger S, Dick JE. A human colon cancer cell capable of initiating tumour growth in immunodeficient mice. *Nature* 2007; 445: 106-110.
- 20 Patel AP, Tirosh I, Trombetta JJ, Shalek AK, Gillespie SM, Wakimoto H *et al.* Single-cell RNA-seq highlights intratumoral heterogeneity in primary glioblastoma. *Science* 2014; 344: 1396-1401.
- 21 Pulvirenti T, Van Der Heijden M, Droms LA, Huse JT, Tabar V, Hall A. Dishevelled 2 signaling promotes self-renewal and tumorigenicity in human gliomas. *Cancer research* 2011; 71: 7280-7290.
- 22 Rheinbay E, Suva ML, Gillespie SM, Wakimoto H, Patel AP, Shahid M *et al.* An aberrant transcription factor network essential for Wnt signaling and stem cell maintenance in glioblastoma. *Cell Rep* 2013; 3: 1567-1579.
- 23 Rossi M, Magnoni L, Miracco C, Mori E, Tosi P, Pirtoli L *et al.* beta-catenin and Gli1 are prognostic markers in glioblastoma. *Cancer Biol Ther* 2011; 11: 753-761.
- 24 Sastre-Perona A, Riesco-Eizaguirre G, Zaballos MA, Santisteban P. beta-catenin signaling is required for RAS-driven thyroid cancer through PI3K activation. *Oncotarget* 2016; 7: 49435-49449.

- 25 Shibahara I, Sonoda Y, Saito R, Kanamori M, Yamashita Y, Kumabe T *et al.* The expression status of CD133 is associated with the pattern and timing of primary glioblastoma recurrence. *Neuro-oncology* 2013; 15: 1151-1159.
- 26 Singh SK, Clarke ID, Terasaki M, Bonn VE, Hawkins C, Squire J *et al.* Identification of a cancer stem cell in human brain tumors. *Cancer research* 2003; 63: 5821-5828.
- 27 Singh SK, Hawkins C, Clarke ID, Squire JA, Bayani J, Hide T *et al.* Identification of human brain tumour initiating cells. *Nature* 2004; 432: 396-401.
- 28 Taal W, Oosterkamp HM, Walenkamp AM, Dubbink HJ, Beerepoot LV, Hanse MC *et al.* Single-agent bevacizumab or lomustine versus a combination of bevacizumab plus lomustine in patients with recurrent glioblastoma (BELOB trial): a randomised controlled phase 2 trial. *Lancet Oncol* 2014; 15: 943-953.
- 29 ter Haar E, Coll JT, Austen DA, Hsiao HM, Swenson L, Jain J. Structure of GSK-3beta reveals a primed phosphorylation mechanism. *Nat Struct Biol* 2001; 8: 593-596.
- 30 Uchida N, Buck DW, He D, Reitsma MJ, Masek M, Phan TV *et al.* Direct isolation of human central nervous system stem cells. *Proceedings of the National Academy of Sciences of the United States of America* 2000; 97: 14720-14725.
- 31 Uhrbom L, Dai C, Celestino JC, Rosenblum MK, Fuller GN, Holland EC. Ink4a-Arf loss cooperates with KRas activation in astrocytes and neural progenitors to generate glioblastomas of various morphologies depending on activated Akt. *Cancer Res* 2002; 62: 5551-5558.

- 32 Verhaak RG, Hoadley KA, Purdom E, Wang V, Qi Y, Wilkerson MD *et al.* Integrated genomic analysis identifies clinically relevant subtypes of glioblastoma characterized by abnormalities in PDGFRA, IDH1, EGFR, and NF1. *Cancer cell* 2010; 17: 98-110.
- 33 Wei W, Shin YS, Xue M, Matsutani T, Masui K, Yang H *et al.* Single-Cell Phosphoproteomics Resolves Adaptive Signaling Dynamics and Informs Targeted Combination Therapy in Glioblastoma. *Cancer Cell* 2016; 29: 563-573.
- 34 Wei Y, Jiang Y, Zou F, Liu Y, Wang S, Xu N *et al.* Activation of PI3K/Akt pathway by CD133-p85 interaction promotes tumorigenic capacity of glioma stem cells. *Proceedings of the National Academy of Sciences of the United States of America* 2013; 110: 6829-6834.
- 35 Weller M, Butowski N, Tran DD, Recht LD, Lim M, Hirte H *et al.* Rindopepimut with temozolomide for patients with newly diagnosed, EGFRvIII-expressing glioblastoma (ACT IV): a randomised, double-blind, international phase 3 trial. *Lancet Oncol* 2017; 18: 1373-1385.
- 36 Yang W, Xia Y, Ji H, Zheng Y, Liang J, Huang W *et al.* Nuclear PKM2 regulates beta-catenin transactivation upon EGFR activation. *Nature* 2011; 480: 118-122.
- 37 Yin AH, Miraglia S, Zanjani ED, Almeida-Porada G, Ogawa M, Leary AG *et al.* AC133, a novel marker for human hematopoietic stem and progenitor cells. *Blood* 1997; 90: 5002-5012.
- 38 Zeppernick F, Ahmadi R, Campos B, Dictus C, Helmke BM, Becker N *et al.* Stem cell marker CD133 affects clinical outcome in glioma patients. *Clinical cancer*

- research : an official journal of the American Association for Cancer Research  
2008; 14: 123-129.
- 39 Zhang LY, Jiang LN, Li FF, Li H, Liu F, Gu Y *et al.* Reduced beta-catenin expression is associated with good prognosis in Astrocytoma. *Pathol Oncol Res* 2010; 16: 253-257.
- 40 Zhang N, Wei P, Gong A, Chiu WT, Lee HT, Colman H *et al.* FoxM1 promotes beta-catenin nuclear localization and controls Wnt target-gene expression and glioma tumorigenesis. *Cancer cell* 2011; 20: 427-442.
- 41 Zheng H, Ying H, Wiedemeyer R, Yan H, Quayle SN, Ivanova EV *et al.* PLAGL2 regulates Wnt signaling to impede differentiation in neural stem cells and gliomas. *Cancer cell* 2010; 17: 497-509.

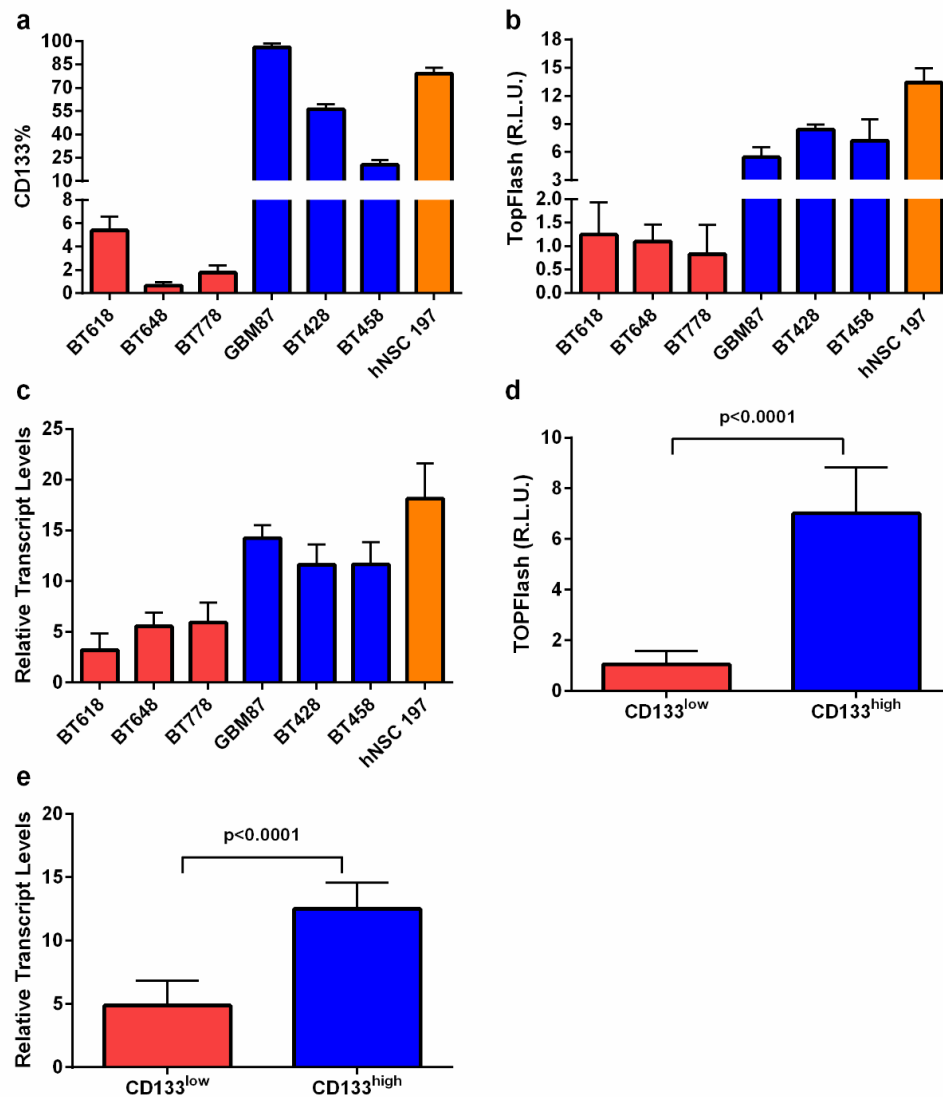


**Fig. 1: CD133 expression correlates with Wnt activity in GBM.** GBMs display differential CD133 cell surface protein expression (n=3, independent experiments per GBM line). (b) TCF reporter analysis identifies GBMs with low and high endogenous Wnt activity (n=3, independent experiments per GBM line). (c) *Axin2* is differentially expressed across several GBM samples (n=3, independent experiments per GBM line). CD133<sup>high</sup> (n=3) GBMs have higher (d) TCF reporter activity (p<0.0001) and (e) *Axin2* transcript levels (p<0.0001, all samples normalized to *GAPDH*) when compared to CD133<sup>low</sup> GBMs (n=3).

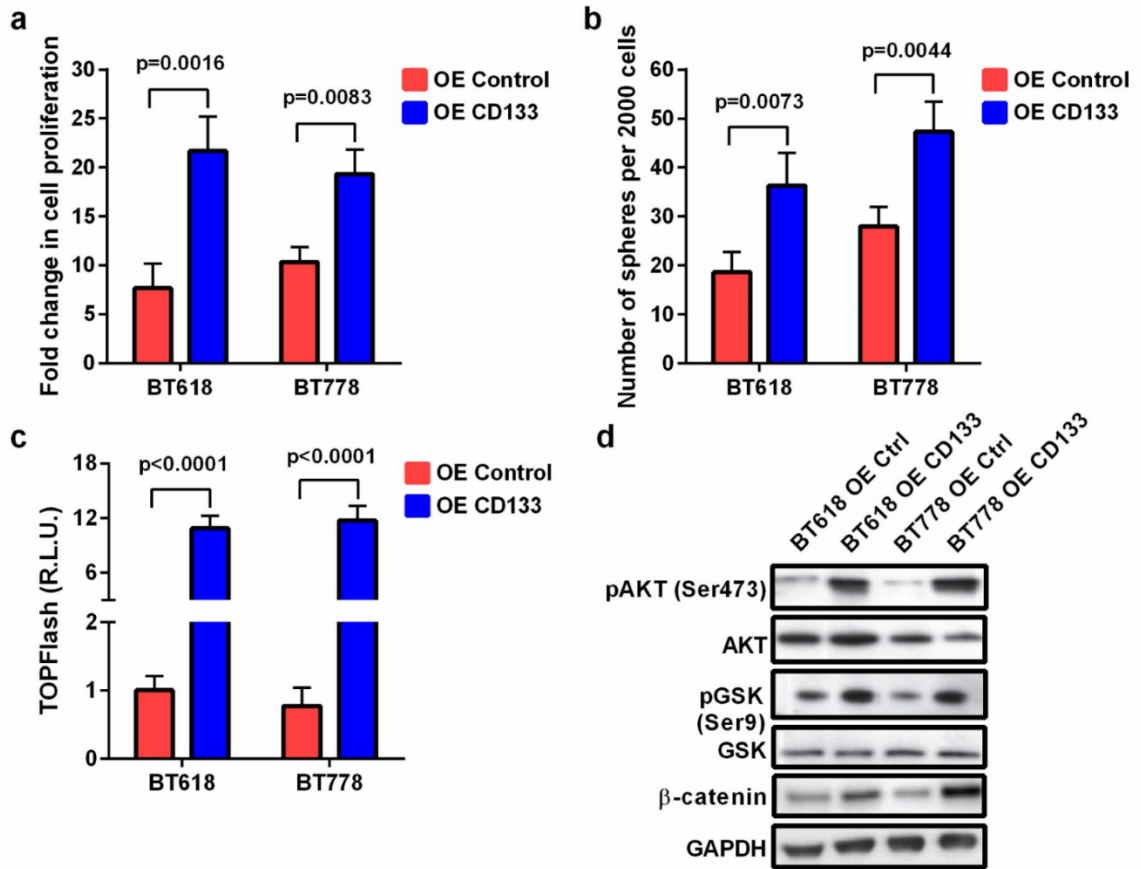


**Fig. 2: CD133 regulates Wnt in an AKT-dependent manner.** (a) Proliferation (BT618:  $p=0.0016$ , BT778:  $p=0.0083$ ) and (b) self-renewal capacity (BT618:  $p=0.0073$ , BT778:  $p=0.0044$ ) of GBM cells are significantly enhanced following CD133 overexpression ( $n=3$ , independent experiments per GBM line). (c) A marked increase in TCF reporter assay following CD133 overexpression indicates an increase in endogenous Wnt activity in response to CD133 overexpression (BT618:  $p<0.0001$ , BT778:  $p<0.0001$ ,  $n=3$ , independent experiments per GBM line). (d) Protein levels of putative CD133-AKT-Wnt signaling axis indicating an increase in pAKT, pGSK, and  $\beta$ -catenin following the ectopic expression of CD133 in two independent GBM lines ( $n=1$ ).

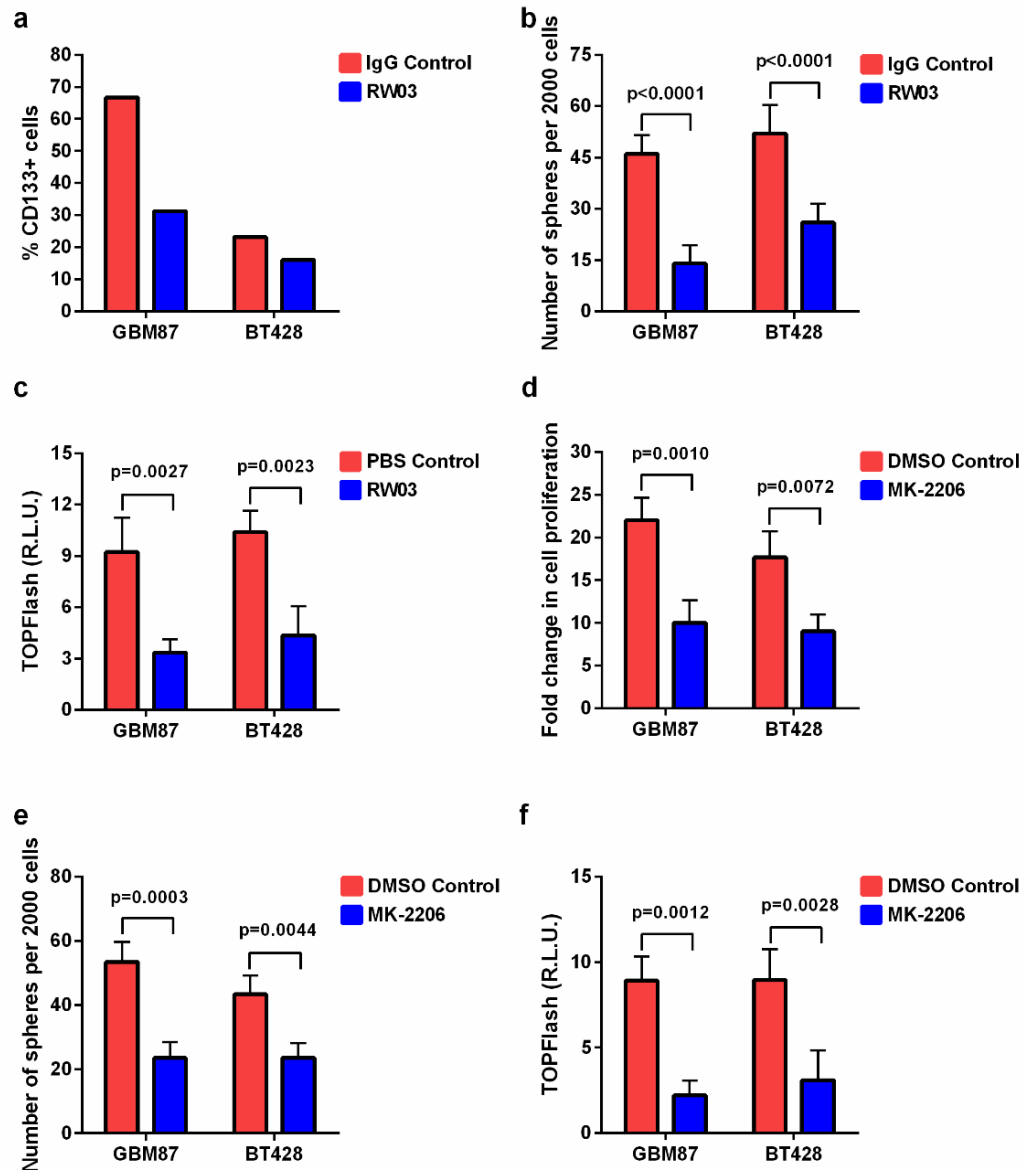


**Fig 3: Upstream inhibition of CD133 or AKT impairs downstream Wnt activity. (a)**

Treatment of CD133<sup>high</sup> GBM lines, GBM87 and BT428, with the CD133 monoclonal antibody RW03 (50nM) reduces (a) surface CD133 expression, (b) self-renewal potential (GBM87:  $p < 0.0001$ , BT428:  $p < 0.001$ ), and (c) TCF reporter activity (GBM87:  $p = 0.0027$ , BT428:  $p = 0.0023$ ) ( $n = 3$ , independent experiments per GBM line). AKT inhibition using the small molecule MK-2206 (5uM), significantly reduces (d) proliferation (GBM87:  $p = 0.0010$ , BT428:  $p = 0.0072$ ), (e) self-renewal (GBM87:  $p = 0.0003$ , BT428:  $p = 0.0044$ ), (f)

and TCF reporter activity (GBM87:  $p=0.0012$ , BT428:  $p=0.0028$ ) in CD133<sup>high</sup> GBM cells when compared to control ( $n=3$ , independent experiments per GBM line).

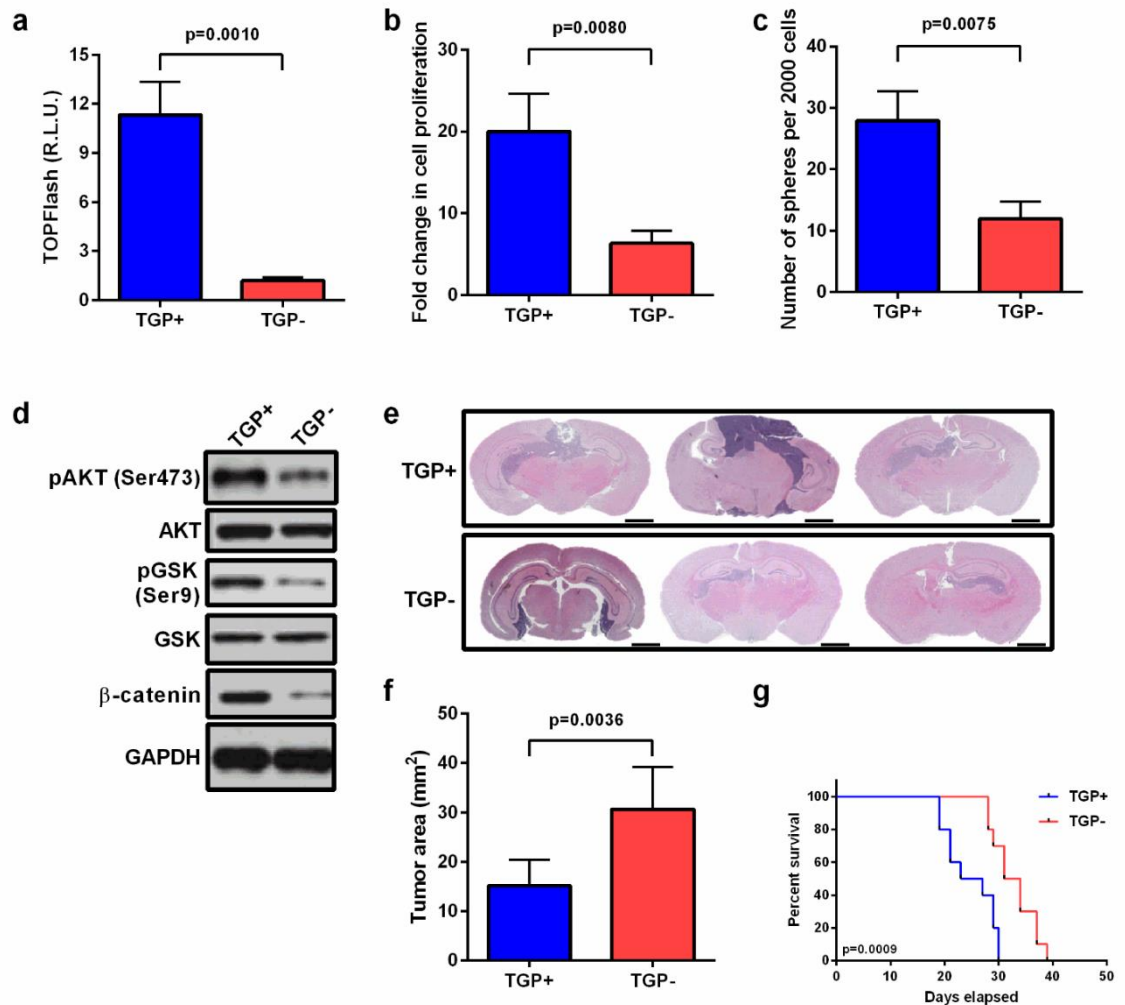
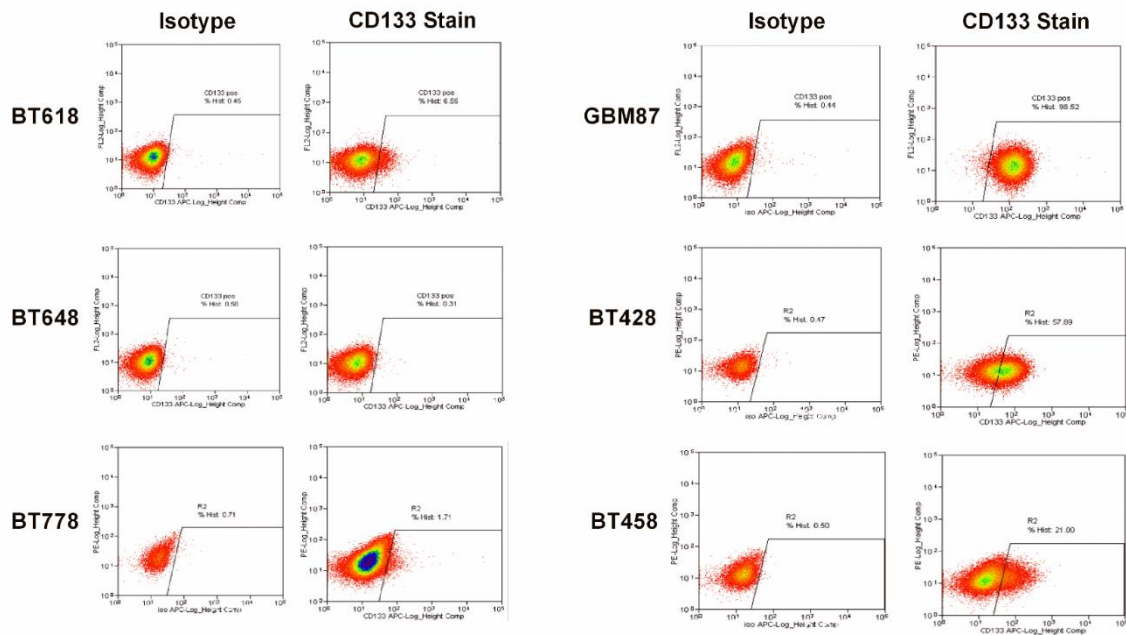
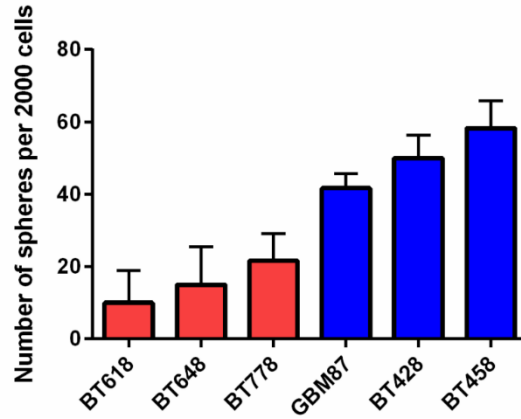


**Fig. 4: Endogenous Wnt active BT241 GBM cells display enhanced tumorigenicity in an AKT-dependent manner.** (a) TGP+ cells contain enhanced TCF reporter activity when compared to TGP- cells ( $p=0.0010$ ) ( $n=3$ , independent experiments). (b) Proliferative ( $p=0.0080$ ) and (c) self-renewal capacity ( $p=0.0075$ ) of TGP+ cells are significantly increased when compared to TGP- cells ( $n=3$ , independent experiments). (d) Protein levels of putative CD133-AKT-Wnt signaling axis indicating an increase in pAKT, pGSK, and

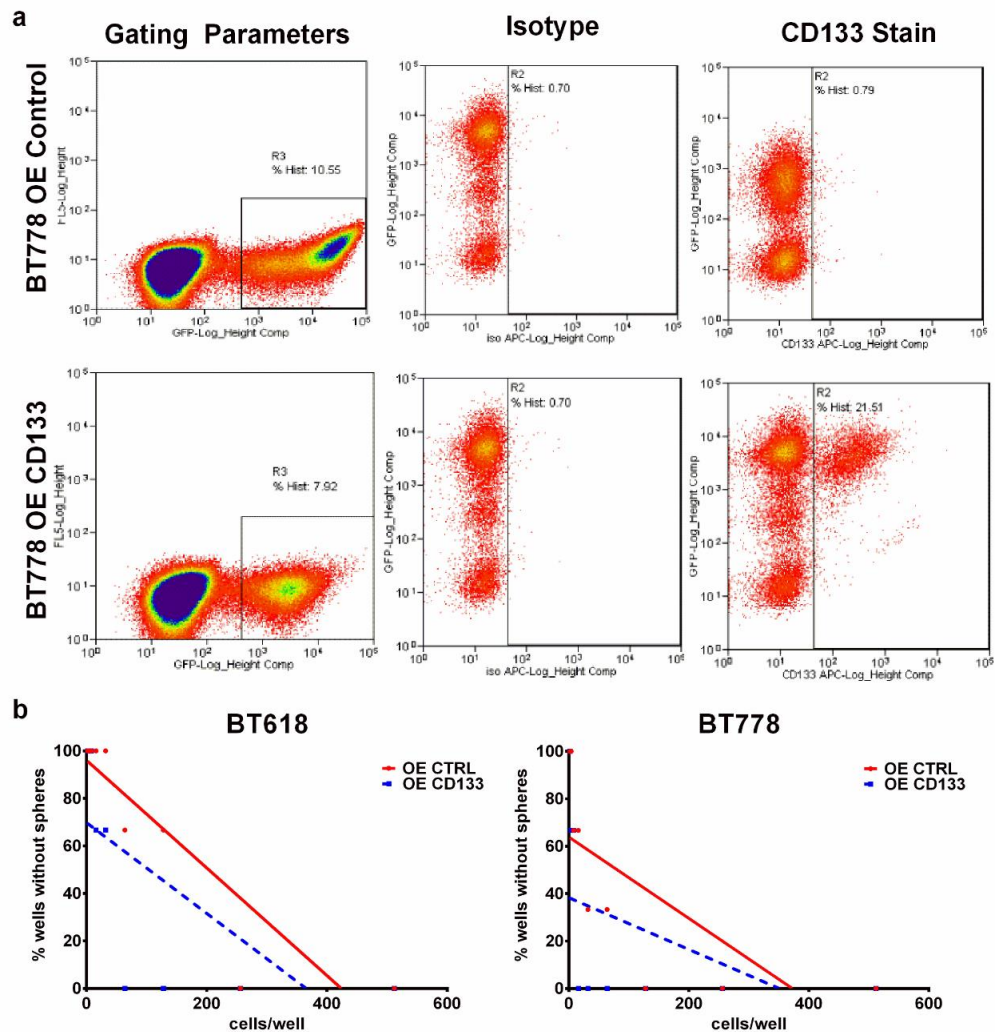
$\beta$ -catenin in TGP+ cells compared to TGP- cells (n=1). (e) Representative histology images illustrating increased tumor burden in TGP+ (n=10) compared to TGP- xenografts (n=10). (f) Xenografts generated from TGP+ cells (n=10) contain larger tumor volumes when compared to TGP- xenografts (n=10) ( $p=0.0036$ ). (g) TGP+ xenografts (n=10, median survival 25.0 days) display a significant decrease in overall survival when compared to TGP- xenografts (n=10, median survival 32.5 days) ( $p=0.0009$ ). Histology image scale bar = 5000  $\mu\text{m}$ .



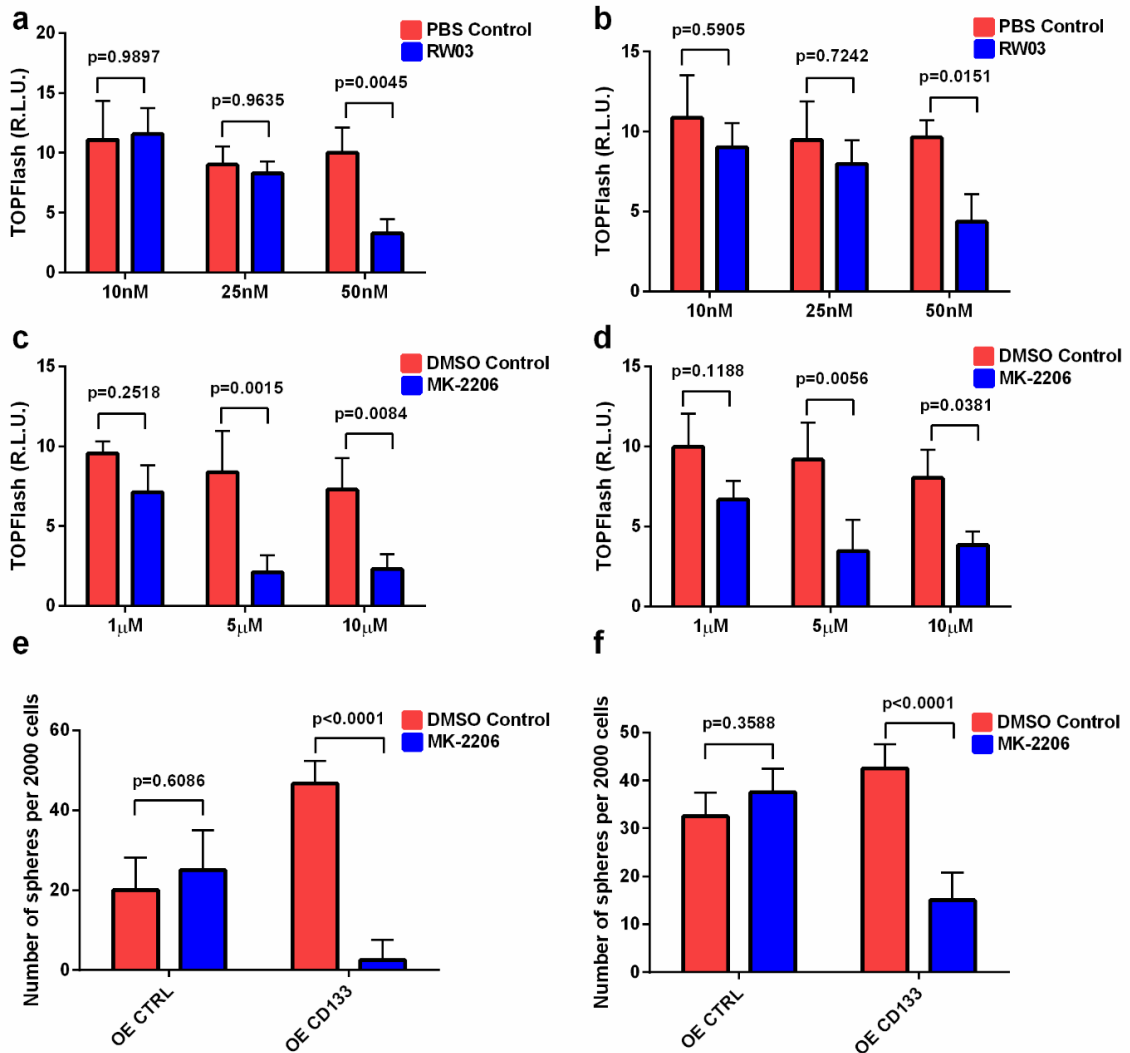
**Supp. Fig. 1: CD133 cell staining gating strategies in GBM lines.** Representative image of gating strategy for isotype control and CD133 stained GBM samples (BT618, BT648, BT778, GBM87, BT428, BT458).



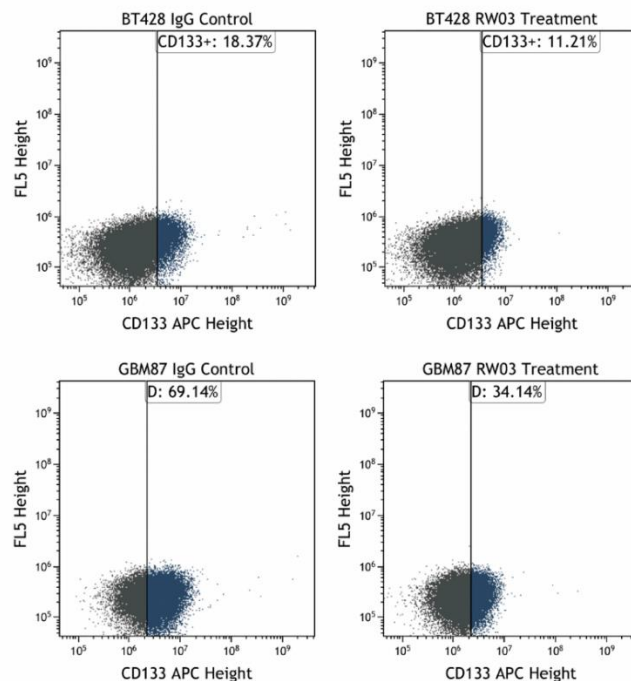
**Supp. Fig 2: Self-renewal potentials in GBM lines.** Secondary sphere formation analysis was carried out in GBM lines, displayed as the number of spheres formed per 2000 cells.



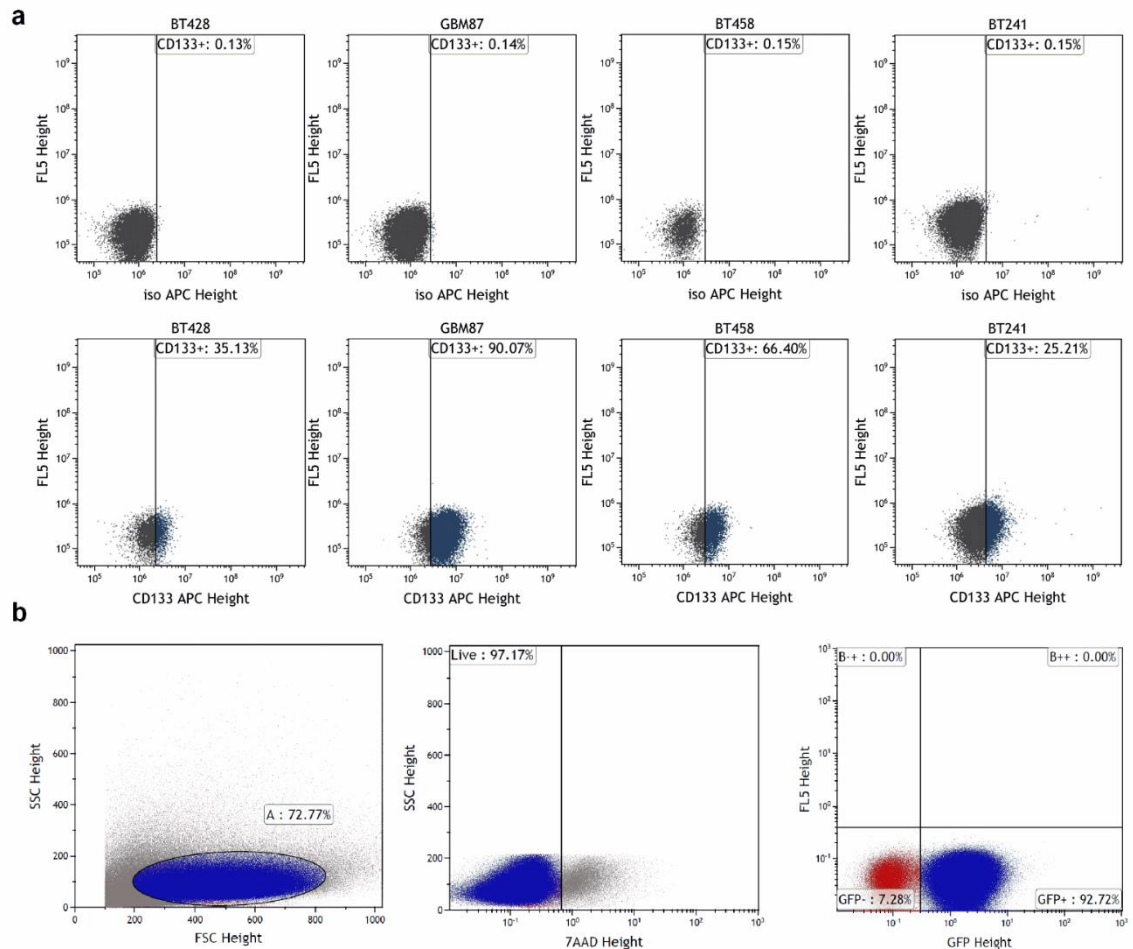
**Supp. Fig. 3: Gating strategy for GFP+ cell-sorting and limiting dilution assays of OE Control and OE CD133 GBM samples.** (a) Representative image of gating strategy for OE Control and OE CD133 GFP+ cell-sorting in BT778 displaying 20% increase in CD133 following overexpression. (b) Limiting dilution assays showcase increased stem cell frequency in OE CD133 (BT618: 1/172, BT778: 1/12) cells compared to OE Control GBM cells (BT618: 1/261, BT778: 1/157).



**Supp. Fig. 4: Small molecule targeting of CD133 or AKT impairs downstream Wnt signaling in GBM BTICs.** TCF Wnt reporter assay at various concentrations of RW03 demonstrates optimal concentration for Wnt inhibition in (a) GBM87 (10nM:  $p=0.9897$ , 25nM:  $p=0.9635$ , 50nM:  $p=0.0045$ ) ( $n=3$ , independent experiments) and (b) BT428 (10nM:  $p=0.5905$ , 25nM:  $p=0.7242$ , 50nM:  $p=0.0151$ ) ( $n=3$ , independent experiments). Similarly, TCF Wnt reporter assay at various concentrations of MK-2206 demonstrates optimal concentration for Wnt inhibition in (c) GBM87 (1 $\mu$ M:  $p=0.2518$ , 5 $\mu$ M:  $p=0.0015$ , 10 $\mu$ M:  $p=0.0084$ ) ( $n=3$ , independent experiments) and (d) BT428 (1 $\mu$ M:  $p=0.1188$ , 5 $\mu$ M:  $p=0.0056$ , 10 $\mu$ M:  $p=0.0381$ ) ( $n=3$ , independent experiments). Secondary sphere formation assay demonstrates robust reduction of self-renewal potential in OE CD133 (e) BT618 (OE CD133  $p<0.0001$ ) and (f) BT778 (OE CD133  $p<0.0001$ ) cells after treatment with 5  $\mu$ M MK-2206, compared to their respective OE Control cells (BT618 OE CTRL:  $p=0.6086$ , BT778 OE CTRL:  $p=0.3588$ ).



**Supp. Fig. 5. Flow cytometry analysis of surface CD133 expression following CD133 inhibition.** Surface expression of CD133 decreased in GBM cells after treatment with 50 nM RW03 compared to treatment with 50 nM control IgG.



**Supp. Fig. 6: Wnt activation through endogenous mechanisms increase overall tumor burden.** (a) Total CD133 expression levels in GBM lines as characterized by flow cytometry. (b) Representative image of gating strategy for untransduced cells and flow cytometric cell sorting criteria for GFP+ endogenous Wnt-active; GFP- Wnt-inactive cells.

<b>BT</b>	<b>Gender/ Age</b>	<b>Diagnosis</b>	<b>MGMT Status</b>	<b>Subgroup</b>	<b>Mutation(s)</b>
241	68/F	recurrent GBM	hypermethylated	mesenchymal	n/a
618	67/F	recurrent GBM	unmethylated	mesenchymal	n/a
648	69/M	GBM	n/a	n/a	Partial p53 positivity
778	54/F	GBM	n/a	n/a	Partial p53 positivity; Loss of heterozygosity of 19q13
GBM87	-	GBM	n/a	proneural	n/a
428	63/F	GBM	unmethylated	proneural	n/a
458	81/M	GBM	partial methylation	classical	n/a

**Supp. Table 1: Clinical demographics**

## Chapter 5: Discussion

### 5.1 Summary of Results

The advent of molecular diagnostics and large-scale integrated genomic analyses of tumors have reconceptualized our understanding of the biology of many cancers, including MB and GBM. While these studies have uncovered several actionable therapeutic targets, their clinical utility has been limited. This may in part be due to the limited efficacy of monotherapy trials and our poor understanding of the context-dependent roles of cell signaling pathways. Throughout this thesis, I have used the Wnt signaling pathway as a model to highlight conserved developmental roles that are carried forward to drive tumorigenesis and context-dependent functions that may be present in a tissue-specific manner. In Chapter 2, I ascertained a differential stem cell gene expression profile across all MB subgroups, which yielded the aberrant expression of a NSC-specific signaling axis consisting of Bmi1 and FoxG1 in MB BTICs. I further describe differential transcriptional regulatory mechanisms that exist between cell populations that are sorted and unsorted for BTIC markers in MB. Since most of the transcriptional profiling of solid tumors consist of the bulk tumor population, the pathways that regulate these rare stem cell fractions may be missed, and therefore, these findings demonstrate the value of current approaches in single cell technology, which may further uncover the clonal architecture of solid tumors. The work in Chapter 3 highlights a rational therapeutic option in which the protective effects of Wnt-driven MB may be augmented in non-Wnt MBs through targeted activation of the canonical Wnt pathway. The significance of this work will be further described in 5.2. The data presented in Chapter 4 is an extension of the principles described

in Chapter 3 where unique signaling programs may be present in a tissue-specific manner and thereby have therapeutic implications as downstream pathways may converge on common nodes of integration, which may be missed by current integrated genomics that lack corresponding proteomic data.

## **5.2 Context-specific functions of signaling pathways highlight diverse roles in oncogenesis**

One of the key findings derived from this thesis is the preservation of Wnt-mediated responses in CNS forebrain and hindbrain development in adult GBM and pediatric MB, respectively. With a confirmed role in the self-renewal of forebrain NSCs, my findings in Chapter 4 support an oncogenic role for activated Wnt signaling in maintaining the BTIC state in GBMs. By contrast, Wnt-mediated inhibition of cerebellar NSC self-renewal was highlighted in Chapter 3 by the therapeutic benefit of activated Wnt signaling in MB BTICs. Specifically, this work illustrates a paradigm in Wnt biology in which functions of the pathway may be conserved from ontogeny to oncology in a context-dependent manner.

Although Wnt signaling has historically been associated with tumor growth and the maintenance of stemness, emerging data has implicated a novel tumor suppressive function for the Wnt pathway. However, it remains to be determined whether these findings are truly indicative of tumor suppression or simply the re-emergence of developmentally conserved signaling mechanisms. Beginning with work done in melanoma (Biechele et al., 2010; Biechele et al., 2012; Chien et al., 2009), nuclear  $\beta$ -catenin expression was found to correlate with improved overall survival within primary and metastatic tumors. Similar to

the work presented in this thesis, small molecules were found to synergize with the Wnt pathway (Biechele et al., 2012) or directly activate the pathway (Biechele et al., 2010) to impair the growth of melanoma cells. Mechanistic insight into these contentious observations implicated the presence of a developmentally conserved differentiation profile following Wnt activation (Biechele et al., 2010; Chien et al., 2009). GSK-3 inhibition in neuroblastoma cells has also provided evidence to support a therapeutic role for the activation of the Wnt signaling axis (Dickey et al., 2011). Neuroblastoma cells treated with the GSK-3 inhibitor, SB415286, were found to be less viable, senescent, and show delayed tumor growth in xenografts (Dickey et al., 2011). When comparing multiple subtypes of human breast cancer, paracrine Wnt signaling inhibited the growth of triple negative breast cancers, while promoting the growth of Her2 tumors (Green et al., 2013). While such disparate outcomes in response to Wnt activation may be attributed to differences in each tumor's molecular phenotype, an alternative explanation may account for differences in gene dosage (Bakker et al., 2013). Since different tissues have been shown to have different vulnerabilities for  $\beta$ -catenin-mediated tumorigenesis, gene dosage effects may provide an additional mechanism by which activated Wnt signaling functions to promote or impede tumorigenesis. Although Wnt activation has been shown to block tumor formation in various tissues, a stemness-dependent mechanism as defined in this thesis has yet to be described.

The convergence of multiple oncogenic signaling pathways across common nodes of integration may be one of the greatest challenges in developing therapies with lasting clinical utility. While the pool of GSK-3 phosphorylated by activated AKT has historically

not been associated with Wnt/ $\beta$ -catenin signaling (Ng et al., 2009), a limited body of data has implicated an alternative pathway by which AKT may activate Wnt/ $\beta$ -catenin signaling by directly phosphorylating  $\beta$ -catenin (Fang et al., 2007; Fukumoto et al., 2001). Earlier work has indicated growth factor signaling through AKT to phosphorylate GSK-3 and thereby inhibit substrate accessibility to GSK-3. The subsequent stabilization of substrates normally phosphorylated by GSK-3 remains controversial and context-dependent (Manning & Toker, 2017). One determining factor for when AKT may not stabilize GSK-3 substrates may be in the presence of activating mutations in components of GSK-3-mediated pathways (Ng et al., 2009). By contrast, AKT may stabilize and enhance  $\beta$ -catenin expression to maintain developmental signaling programs in those tumors in which recurrent mutations of the Wnt/ $\beta$ -catenin pathway have not been identified, such as GBM. For example, AKT activated downstream of EGFR signaling has been shown to phosphorylate  $\beta$ -catenin at Ser552 resulting in the disassociation of  $\beta$ -catenin from cell-cell contacts, accumulation in the cytosol, and subsequent translocation into the nucleus where  $\beta$ -catenin promotes the activation of downstream targets leading to tumor growth (Fang et al., 2007).

Novel approaches to overcome the dependence of tumors to malignant pathways are warranted as molecularly-based clinical oncology trials continue to expand. The body of this work provides two therapeutic options – the principle of developmental re-emergence in which the non-oncogenic properties of signaling pathways are activated in a tissue-specific manner or the targeting of common nodes of interaction within divergent cell signaling pathways.

### 5.3 Future directions

As with any research endeavor, the data generated from the pursuit of scholarly activities are bound to generate more questions that will fuel another generation of scientists. Given that leptomeningeal metastasis confers a uniformly fatal prognosis in childhood MB, it is imperative to assess the effect of Wnt activation on leptomeningeal dissemination of MB. While the *in vivo* work presented in this thesis focused on the effects of monotherapy (Wnt activation alone), the combinatorial effect of Wnt agonists with our lab's standard of care chemoradiotherapy protocol (2 Gy radiation followed by 200 ng cisplatin and 2nM vincristine) may provide evidence to support Wnt activation as a radio- or chemosensitizing treatment option. To further investigate if the proposed mechanism in Chapter 3 is  $\beta$ -catenin-dependent or -independent, I propose to use an inhibitor of  $\beta$ -catenin-responsive transcription (iCRT14), which blocks the interaction between  $\beta$ -catenin and TCF7L2 (Gonsalves et al., 2011). This work may be validated with the use of TCF7L2-DN, a dominant-negative protein that lacks the  $\beta$ -catenin-binding domain while still maintaining DNA-binding capacity. Both experimental approaches should enhance the self-renewal capacity of MB BTICs if the observed effects are mediated through  $\beta$ -catenin. DNA methylation profiling Group 3 and 4 MBs following Wnt activation or of cells with and without endogenous Wnt activity would provide a deeper understanding of the epigenetic landscape corresponding to the data in Chapter 3.

Dr. Jason Moffat's lab has recently developed the Toronto KnockOut CRISPR-Cas9 library v3 for more than 18,000 genes with 4 short guide RNAs targeting each gene (Hart et al., 2017). These guides can promote gene-editing events that create indels leading

to loss-of-function mutations that can be tracked by virtue of the guide RNA sequences. Having identified L807mts as a suitable preclinical molecule that could activate the canonical Wnt pathway, it would be of particular interest to use the CRISPR library to identify synthetic lethal sensitizers of L807mts treatment in non-Wnt MBs.

With respect to the data generated in Chapter 4, the clinical utility of therapies targeting cell surface markers is encumbered by the expression of these markers in non-malignant cells. Therefore, the components of the CD133-AKT-Wnt signaling axis should be assessed in NSCs. The detection of CD133-interacting proteins using BirA-mediated biotinylation (BioID) in GBM BTICs provides an unbiased approach in identifying additional pathways activated downstream of CD133. The use of CD133 high and low GBM lines may also answer important questions regarding gene dosage effects on the activation of cell signaling pathways. With increasing data in support of immunotherapy as a plausible treatment option for GBM, comprehensive assessment of Fzd receptors using the Moffat lab's multiplex flow cytometry-based Fzd profiler (Steinhart et al., 2017) can be used to investigate the expression of all 10 human Fzd receptors. Fzd profiling among GBM BTICs with (TGP+) and without (TGP-) endogenous Wnt activity may yield monoclonal antibody-based treatments targeting key receptors. By combining this work with small molecules that may target unique transcriptional signatures generated from RNA-seq of TGP+ and TGP- GBM BTICs may provide a preclinical polytherapeutic treatment model that efficiently targets GBM BTICs at multiple points of the signaling cascade.

## Bibliography

- Abdouh, M., Facchino, S., Chato, W., Balasingam, V., Ferreira, J., & Bernier, G. (2009). BMI1 sustains human glioblastoma multiforme stem cell renewal. *J Neurosci*, 29(28), 8884-8896. doi:10.1523/JNEUROSCI.0968-09.2009
- Aberle, H., Bauer, A., Stappert, J., Kispert, A., & Kemler, R. (1997). beta-catenin is a target for the ubiquitin-proteasome pathway. *EMBO J*, 16(13), 3797-3804. doi:10.1093/emboj/16.13.3797
- Alcantara Llaguno, S., Chen, J., Kwon, C. H., Jackson, E. L., Li, Y., Burns, D. K., . . . Parada, L. F. (2009). Malignant astrocytomas originate from neural stem/progenitor cells in a somatic tumor suppressor mouse model. *Cancer Cell*, 15(1), 45-56. doi:10.1016/j.ccr.2008.12.006
- Alcantara Llaguno, S., Sun, D., Pedraza, A. M., Vera, E., Wang, Z., Burns, D. K., & Parada, L. F. (2019). Cell-of-origin susceptibility to glioblastoma formation declines with neural lineage restriction. *Nat Neurosci*. doi:10.1038/s41593-018-0333-8
- Alcantara Llaguno, S. R., Wang, Z., Sun, D., Chen, J., Xu, J., Kim, E., . . . Parada, L. F. (2015). Adult Lineage-Restricted CNS Progenitors Specify Distinct Glioblastoma Subtypes. *Cancer Cell*, 28(4), 429-440. doi:10.1016/j.ccell.2015.09.007
- Alexander, B. M., & Cloughesy, T. F. (2017). Adult Glioblastoma. *J Clin Oncol*, 35(21), 2402-2409. doi:10.1200/JCO.2017.73.0119
- Angers, S., & Moon, R. T. (2009). Proximal events in Wnt signal transduction. *Nat Rev Mol Cell Biol*, 10(7), 468-477. doi:10.1038/nrm2717
- Arozarena, I., Bischof, H., Gilby, D., Belloni, B., Dummer, R., & Wellbrock, C. (2011). In melanoma, beta-catenin is a suppressor of invasion. *Oncogene*, 30(45), 4531-4543. doi:10.1038/onc.2011.162
- Atkinson, J. M., Rank, K. B., Zeng, Y., Capen, A., Yadav, V., Manro, J. R., . . . Chedid, M. (2015). Activating the Wnt/beta-Catenin Pathway for the Treatment of Melanoma--Application of LY2090314, a Novel Selective Inhibitor of Glycogen Synthase Kinase-3. *PLoS One*, 10(4), e0125028. doi:10.1371/journal.pone.0125028
- Bachmann, I. M., Straume, O., Puntervoll, H. E., Kalvenes, M. B., & Akslen, L. A. (2005). Importance of P-cadherin, beta-catenin, and Wnt5a/frizzled for progression of melanocytic tumors and prognosis in cutaneous melanoma. *Clin Cancer Res*, 11(24 Pt 1), 8606-8614. doi:10.1158/1078-0432.CCR-05-0011
- Badodi, S., Dubuc, A., Zhang, X., Rosser, G., Da Cunha Jaeger, M., Kameda-Smith, M. M., . . . Marino, S. (2017). Convergence of BMI1 and CHD7 on ERK Signaling in Medulloblastoma. *Cell Rep*, 21(10), 2772-2784. doi:10.1016/j.celrep.2017.11.021
- BAILEY, P., & CUSHING, H. (1925). MEDULLOBLASTOMA CEREBELLI: A COMMON TYPE OF MIDCEREBELLAR GLIOMA OF CHILDHOOD. *Archives of Neurology & Psychiatry*, 14(2), 192-224. doi:10.1001/archneurpsyc.1925.02200140055002
- Bakhshinyan, D., Venugopal, C., Adile, A. A., Garg, N., Manoranjan, B., Hallett, R., . . . Singh, S. K. (2019). BMI1 is a therapeutic target in recurrent medulloblastoma. *Oncogene*, 38(10), 1702-1716. doi:10.1038/s41388-018-0549-9

- Bakker, E. R., Hoekstra, E., Franken, P. F., Helvensteijn, W., van Deurzen, C. H., van Veelen, W., . . . Smits, R. (2013). beta-Catenin signaling dosage dictates tissue-specific tumor predisposition in Apc-driven cancer. *Oncogene*, *32*(38), 4579-4585. doi:10.1038/onc.2012.449
- Bandopadhyay, P., Bergthold, G., Nguyen, B., Schubert, S., Gholamin, S., Tang, Y., . . . Cho, Y. J. (2014). BET bromodomain inhibition of MYC-amplified medulloblastoma. *Clin Cancer Res*, *20*(4), 912-925. doi:10.1158/1078-0432.CCR-13-2281
- Bao, S., Wu, Q., Li, Z., Sathornsumetee, S., Wang, H., McLendon, R. E., . . . Rich, J. N. (2008). Targeting cancer stem cells through L1CAM suppresses glioma growth. *Cancer Res*, *68*(15), 6043-6048. doi:10.1158/0008-5472.CAN-08-1079
- Bao, S., Wu, Q., McLendon, R. E., Hao, Y., Shi, Q., Hjelmeland, A. B., . . . Rich, J. N. (2006). Glioma stem cells promote radioresistance by preferential activation of the DNA damage response. *Nature*, *444*(7120), 756-760. doi:10.1038/nature05236
- Barker, N., Ridgway, R. A., van Es, J. H., van de Wetering, M., Begthel, H., van den Born, M., . . . Clevers, H. (2009). Crypt stem cells as the cells-of-origin of intestinal cancer. *Nature*, *457*(7229), 608-611. doi:10.1038/nature07602
- Biechele, T. L., Camp, N. D., Fass, D. M., Kulikauskas, R. M., Robin, N. C., White, B. D., . . . Moon, R. T. (2010). Chemical-genetic screen identifies riluzole as an enhancer of Wnt/beta-catenin signaling in melanoma. *Chem Biol*, *17*(11), 1177-1182. doi:10.1016/j.chembiol.2010.08.012
- Biechele, T. L., Kulikauskas, R. M., Toroni, R. A., Lucero, O. M., Swift, R. D., James, R. G., . . . Chien, A. J. (2012). Wnt/beta-catenin signaling and AXIN1 regulate apoptosis triggered by inhibition of the mutant kinase BRAFV600E in human melanoma. *Sci Signal*, *5*(206), ra3. doi:10.1126/scisignal.2002274
- Bienz, M., & Clevers, H. (2000). Linking colorectal cancer to Wnt signaling. *Cell*, *103*(2), 311-320.
- Brault, V., Moore, R., Kutsch, S., Ishibashi, M., Rowitch, D. H., McMahon, A. P., . . . Kemler, R. (2001). Inactivation of the beta-catenin gene by Wnt1-Cre-mediated deletion results in dramatic brain malformation and failure of craniofacial development. *Development*, *128*(8), 1253-1264.
- Brennan, C. W., Verhaak, R. G., McKenna, A., Campos, B., Noushmehr, H., Salama, S. R., . . . Network, T. R. (2013). The somatic genomic landscape of glioblastoma. *Cell*, *155*(2), 462-477. doi:10.1016/j.cell.2013.09.034
- Brodin, N. P., Vogelius, I. R., Maraldo, M. V., Munck af Rosenschold, P., Aznar, M. C., Kiil-Berthelsen, A., . . . Bentzen, S. M. (2012). Life years lost--comparing potentially fatal late complications after radiotherapy for pediatric medulloblastoma on a common scale. *Cancer*, *118*(21), 5432-5440. doi:10.1002/cncr.27536
- Bruggeman, S. W., Hulsman, D., Tanger, E., Buckle, T., Blom, M., Zevenhoven, J., . . . van Lohuizen, M. (2007). Bmi1 controls tumor development in an Ink4a/Arf-independent manner in a mouse model for glioma. *Cancer Cell*, *12*(4), 328-341. doi:10.1016/j.ccr.2007.08.032

- Bruggeman, S. W., Valk-Lingbeek, M. E., van der Stoop, P. P., Jacobs, J. J., Kieboom, K., Tanger, E., . . . van Lohuizen, M. (2005). Ink4a and Arf differentially affect cell proliferation and neural stem cell self-renewal in Bmi1-deficient mice. *Genes Dev*, *19*(12), 1438-1443. doi:10.1101/gad.1299305
- Buonamici, S., Williams, J., Morrissey, M., Wang, A., Guo, R., Vattay, A., . . . Dorsch, M. (2010). Interfering with resistance to smoothened antagonists by inhibition of the PI3K pathway in medulloblastoma. *Sci Transl Med*, *2*(51), 51ra70. doi:10.1126/scitranslmed.3001599
- Carmon, K. S., Gong, X., Lin, Q., Thomas, A., & Liu, Q. (2011). R-spondins function as ligands of the orphan receptors LGR4 and LGR5 to regulate Wnt/beta-catenin signaling. *Proc Natl Acad Sci U S A*, *108*(28), 11452-11457. doi:10.1073/pnas.1106083108
- Chemaitilly, W., & Sklar, C. A. (2010). Endocrine complications in long-term survivors of childhood cancers. *Endocr Relat Cancer*, *17*(3), R141-159. doi:10.1677/ERC-10-0002
- Chen, J., Li, Y., Yu, T. S., McKay, R. M., Burns, D. K., Kernie, S. G., & Parada, L. F. (2012). A restricted cell population propagates glioblastoma growth after chemotherapy. *Nature*, *488*(7412), 522-526. doi:10.1038/nature11287
- Chenn, A., & Walsh, C. A. (2002). Regulation of cerebral cortical size by control of cell cycle exit in neural precursors. *Science*, *297*(5580), 365-369. doi:10.1126/science.1074192
- Chenn, A., & Walsh, C. A. (2003). Increased neuronal production, enlarged forebrains and cytoarchitectural distortions in beta-catenin overexpressing transgenic mice. *Cereb Cortex*, *13*(6), 599-606.
- Chien, A. J., Moore, E. C., Lonsdorf, A. S., Kulikauskas, R. M., Rothberg, B. G., Berger, A. J., . . . Moon, R. T. (2009). Activated Wnt/beta-catenin signaling in melanoma is associated with decreased proliferation in patient tumors and a murine melanoma model. *Proc Natl Acad Sci U S A*, *106*(4), 1193-1198. doi:10.1073/pnas.0811902106
- Cho, Y. J., Tsherniak, A., Tamayo, P., Santagata, S., Ligon, A., Greulich, H., . . . Pomeroy, S. L. (2011). Integrative genomic analysis of medulloblastoma identifies a molecular subgroup that drives poor clinical outcome. *J Clin Oncol*, *29*(11), 1424-1430. doi:10.1200/JCO.2010.28.5148
- Chow, L. M., Endersby, R., Zhu, X., Rankin, S., Qu, C., Zhang, J., . . . Baker, S. J. (2011). Cooperativity within and among Pten, p53, and Rb pathways induces high-grade astrocytoma in adult brain. *Cancer Cell*, *19*(3), 305-316. doi:10.1016/j.ccr.2011.01.039
- Ciani, L., Boyle, K. A., Dickins, E., Sahores, M., Anane, D., Lopes, D. M., . . . Salinas, P. C. (2011). Wnt7a signaling promotes dendritic spine growth and synaptic strength through Ca(2+)-dependent protein kinase II. *Proc Natl Acad Sci U S A*, *108*(26), 10732-10737. doi:10.1073/pnas.1018132108
- Ciani, L., & Salinas, P. C. (2005). WNTs in the vertebrate nervous system: from patterning to neuronal connectivity. *Nat Rev Neurosci*, *6*(5), 351-362. doi:10.1038/nrn1665

- Clevers, H. (2013). The intestinal crypt, a prototype stem cell compartment. *Cell*, *154*(2), 274-284. doi:10.1016/j.cell.2013.07.004
- Clevers, H., & Nusse, R. (2012). Wnt/beta-catenin signaling and disease. *Cell*, *149*(6), 1192-1205. doi:10.1016/j.cell.2012.05.012
- Corbeil, D., Karbanova, J., Fargeas, C. A., Jaszai, J. (2013). Prominin-1 (CD133): molecular and cellular features across species. *Adv Exp Med Biol*. *777*, 3-24. doi: 10.1007/978-1-4614-5894-4\_1
- Corbeil, D., Roper, K., Fargeas, C. A., Joester, A., Huttner, W. B. (2001). Prominin: a source of cholesterol, plasma membrane protrusions and human pathology. *Traffic*, *2*(2), 82-91. doi: 10.1034/j.1600-0854.2001.020202.x
- Daniels, D. L., & Weis, W. I. (2005). Beta-catenin directly displaces Groucho/TLE repressors from Tcf/Lef in Wnt-mediated transcription activation. *Nat Struct Mol Biol*, *12*(4), 364-371. doi:10.1038/nsmb912
- de Lau, W., Barker, N., Low, T. Y., Koo, B. K., Li, V. S., Teunissen, H., . . . Clevers, H. (2011). Lgr5 homologues associate with Wnt receptors and mediate R-spondin signalling. *Nature*, *476*(7360), 293-297. doi:10.1038/nature10337
- Delmas, V., Beermann, F., Martinuzzi, S., Carreira, S., Ackermann, J., Kumasaka, M., . . . Larue, L. (2007). Beta-catenin induces immortalization of melanocytes by suppressing p16INK4a expression and cooperates with N-Ras in melanoma development. *Genes Dev*, *21*(22), 2923-2935. doi:10.1101/gad.450107
- Dickey, A., Schleicher, S., Leahy, K., Hu, R., Hallahan, D., & Thotala, D. K. (2011). GSK-3beta inhibition promotes cell death, apoptosis, and in vivo tumor growth delay in neuroblastoma Neuro-2A cell line. *J Neurooncol*, *104*(1), 145-153. doi:10.1007/s11060-010-0491-3
- Dunn, K. J., Williams, B. O., Li, Y., & Pavan, W. J. (2000). Neural crest-directed gene transfer demonstrates Wnt1 role in melanocyte expansion and differentiation during mouse development. *Proc Natl Acad Sci U S A*, *97*(18), 10050-10055.
- Fang, D., Hawke, D., Zheng, Y., Xia, Y., Meisenhelder, J., Nika, H., . . . Lu, Z. (2007). Phosphorylation of  $\beta$ -catenin by AKT promotes  $\beta$ -catenin transcriptional activity. *J Biol Chem*, *282* (15), 11221-11229.
- Fearon, E. R., & Vogelstein, B. (1990). A genetic model for colorectal tumorigenesis. *Cell*, *61*(5), 759-767.
- Forsyth, P. A., & Posner, J. B. (1993). Headaches in patients with brain tumors: a study of 111 patients. *Neurology*, *43*(9), 1678-1683.
- Friedmann-Morvinski, D., Bushong, E. A., Ke, E., Soda, Y., Marumoto, T., Singer, O., . . . Verma, I. M. (2012). Dedifferentiation of neurons and astrocytes by oncogenes can induce gliomas in mice. *Science*, *338*(6110), 1080-1084. doi:10.1126/science.1226929
- Fukumoto, S., Hsieh, C. M., Maemura, K., Layne, M. D., Yet, S. F., Lee, K. H., . . . Lee, M. E. (2001). Akt participation in the Wnt signaling pathway through Dishevelled. *J Biol Chem*, *276*(20), 17479-17483. doi:10.1074/jbc.C000880200
- Gage, F. H. (2000). Mammalian neural stem cells. *Science*, *287*(5457), 1433-1438.
- Galvao, R. P., Kasina, A., McNeill, R. S., Harbin, J. E., Foreman, O., Verhaak, R. G., . . . Zong, H. (2014). Transformation of quiescent adult oligodendrocyte precursor cells

- into malignant glioma through a multistep reactivation process. *Proc Natl Acad Sci U S A*, *111*(40), E4214-4223. doi:10.1073/pnas.1414389111
- Gargiulo, G., Cesaroni, M., Serresi, M., de Vries, N., Hulsman, D., Bruggeman, S. W., . . . van Lohuizen, M. (2013). In vivo RNAi screen for BMI1 targets identifies TGF-beta/BMP-ER stress pathways as key regulators of neural- and malignant glioma-stem cell homeostasis. *Cancer Cell*, *23*(5), 660-676. doi:10.1016/j.ccr.2013.03.030
- Gibson, P., Tong, Y., Robinson, G., Thompson, M. C., Currele, D. S., Eden, C., . . . Gilbertson, R. J. (2010). Subtypes of medulloblastoma have distinct developmental origins. *Nature*, *468*(7327), 1095-1099. doi:10.1038/nature09587
- Gilbertson, R. J. (2004). Medulloblastoma: signalling a change in treatment. *Lancet Oncol*, *5*(4), 209-218. doi:10.1016/S1470-2045(04)01424-X
- Glantz, M. J., Cole, B. F., Forsyth, P. A., Recht, L. D., Wen, P. Y., Chamberlain, M. C., . . . Cairncross, J. G. (2000). Practice parameter: anticonvulsant prophylaxis in patients with newly diagnosed brain tumors. Report of the Quality Standards Subcommittee of the American Academy of Neurology. *Neurology*, *54*(10), 1886-1893.
- Glinka, A., Dolde, C., Kirsch, N., Huang, Y. L., Kazanskaya, O., Ingelfinger, D., . . . Niehrs, C. (2011). LGR4 and LGR5 are R-spondin receptors mediating Wnt/beta-catenin and Wnt/PCP signalling. *EMBO Rep*, *12*(10), 1055-1061. doi:10.1038/embor.2011.175
- Glinsky, G. V., Berezovska, O., & Glinskii, A. B. (2005). Microarray analysis identifies a death-from-cancer signature predicting therapy failure in patients with multiple types of cancer. *J Clin Invest*, *115*(6), 1503-1521. doi:10.1172/JCI23412
- Gonsalves, F. C., Klein, K., Carson, B. B., Katz, S., Ekas, L. A., Evans, S., . . . DasGupta, R. (2011). An RNAi-based chemical genetic screen identifies three small-molecule inhibitors of the Wnt/wingless signaling pathway. *Proc Natl Acad Sci U S A*, *108*(15), 5954-5963. doi:10.1073/pnas.1017496108
- Goodrich, L. V., Milenkovic, L., Higgins, K. M., & Scott, M. P. (1997). Altered neural cell fates and medulloblastoma in mouse patched mutants. *Science*, *277*(5329), 1109-1113.
- Green, J. L., La, J., Yum, K. W., Desai, P., Rodewald, L. W., Zhang, X., . . . Wahl, G. M. (2013). Paracrine Wnt signaling both promotes and inhibits human breast tumor growth. *Proc Natl Acad Sci U S A*, *110*(17), 6991-6996. doi:10.1073/pnas.1303671110
- Grosse-Gehling, P., Fargeas, C. A., Dittfeld, C., Garbe, Y., Alison, M. R., Corbeil, D., Kunz-Schughart, L. A. (2013). CD133 as a biomarker for putative cancer stem cells in solid tumors: limitations, problems, and challenges. *J Pathol*, *229*(3), 355-378. doi: 10.1002/path.4086
- Hamilton, S. R., Liu, B., Parsons, R. E., Papadopoulos, N., Jen, J., Powell, S. M., . . . et al. (1995). The molecular basis of Turcot's syndrome. *N Engl J Med*, *332*(13), 839-847. doi:10.1056/NEJM199503303321302
- Han, T., Schatoff, E. M., Murphy, C., Zafra, M. P., Wilkinson, J. E., Elemento, O., & Dow, L. E. (2017). R-Spondin chromosome rearrangements drive Wnt-dependent tumour

- initiation and maintenance in the intestine. *Nat Commun*, 8, 15945. doi:10.1038/ncomms15945
- Hart, T., Tong, A. H. Y., Chan, K., Van Leeuwen, J., Seetharaman, A., Aregger, M., . . . Moffat, J. (2017). Evaluation and Design of Genome-Wide CRISPR/SpCas9 Knockout Screens. *G3 (Bethesda)*, 7(8), 2719-2727. doi:10.1534/g3.117.041277
- Hartsock, A., & Nelson, W. J. (2008). Adherens and tight junctions: structure, function and connections to the actin cytoskeleton. *Biochim Biophys Acta*, 1778(3), 660-669. doi:10.1016/j.bbamem.2007.07.012
- Hegi, M. E., Diserens, A. C., Gorlia, T., Hamou, M. F., de Tribolet, N., Weller, M., . . . Stupp, R. (2005). MGMT gene silencing and benefit from temozolomide in glioblastoma. *N Engl J Med*, 352(10), 997-1003. doi:10.1056/NEJMoa043331
- Hemmati, H. D., Nakano, I., Lazareff, J. A., Masterman-Smith, M., Geschwind, D. H., Bronner-Fraser, M., & Kornblum, H. I. (2003). Cancerous stem cells can arise from pediatric brain tumors. *Proc Natl Acad Sci U S A*, 100(25), 15178-15183. doi:10.1073/pnas.2036535100
- Herrlinger, U., Tzaridis, T., Mack, F., Steinbach, J. P., Schlegel, U., Sabel, M., . . . Neurooncology Working Group of the German Cancer, S. (2019). Lomustine-temozolomide combination therapy versus standard temozolomide therapy in patients with newly diagnosed glioblastoma with methylated MGMT promoter (CeTeG/NOA-09): a randomised, open-label, phase 3 trial. *Lancet*, 393(10172), 678-688. doi:10.1016/S0140-6736(18)31791-4
- Hilkens, J., Timmer, N. C., Boer, M., Ikink, G. J., Schewe, M., Sacchetti, A., . . . Bakker, E. R. M. (2017). RSPO3 expands intestinal stem cell and niche compartments and drives tumorigenesis. *Gut*, 66(6), 1095-1105. doi:10.1136/gutjnl-2016-311606
- Hirabayashi, Y., Itoh, Y., Tabata, H., Nakajima, K., Akiyama, T., Masuyama, N., & Gotoh, Y. (2004). The Wnt/beta-catenin pathway directs neuronal differentiation of cortical neural precursor cells. *Development*, 131(12), 2791-2801. doi:10.1242/dev.01165
- Hu, B., Wang, Q., Wang, Y. A., Hua, S., Sauve, C. G., Ong, D., . . . DePinho, R. A. (2016). Epigenetic Activation of WNT5A Drives Glioblastoma Stem Cell Differentiation and Invasive Growth. *Cell*, 167(5), 1281-1295 e1218. doi:10.1016/j.cell.2016.10.039
- Jacobs, J. J., Kieboom, K., Marino, S., DePinho, R. A., & van Lohuizen, M. (1999). The oncogene and Polycomb-group gene bmi-1 regulates cell proliferation and senescence through the ink4a locus. *Nature*, 397(6715), 164-168. doi:10.1038/16476
- Jakacki, R. I., Burger, P. C., Zhou, T., Holmes, E. J., Kocak, M., Onar, A., . . . Pollack, I. F. (2012). Outcome of children with metastatic medulloblastoma treated with carboplatin during craniospinal radiotherapy: a Children's Oncology Group Phase I/II study. *J Clin Oncol*, 30(21), 2648-2653. doi:10.1200/JCO.2011.40.2792
- Jaksch, M., Munera, J., Bajpai, R., Terskikh, A., Oshima, R. G. (2008). Cell cycle-dependent variation of a CD133 epitope in human embryonic stem cell, colon cancer, and melanoma cell lines. *Cancer Res*, 68(19), 7882-7886. doi:10.1158/0008-5472.CAN-08-0723

- Ji, H., Wang, J., Nika, H., Hawke, D., Keezer, S., Ge, Q., . . . Lu, Z. (2009). EGF-induced ERK activation promotes CK2-mediated disassociation of alpha-Catenin from beta-Catenin and transactivation of beta-Catenin. *Mol Cell*, *36*(4), 547-559. doi:10.1016/j.molcel.2009.09.034
- Jin, X., Kim, L. J. Y., Wu, Q., Wallace, L. C., Prager, B. C., Sanvoranart, T., . . . Rich, J. N. (2017). Targeting glioma stem cells through combined BMI1 and EZH2 inhibition. *Nat Med*, *23*(11), 1352-1361. doi:10.1038/nm.4415
- Johnson, B. E., Mazor, T., Hong, C., Barnes, M., Aihara, K., McLean, C. Y., . . . Costello, J. F. (2014). Mutational analysis reveals the origin and therapy-driven evolution of recurrent glioma. *Science*, *343*(6167), 189-193. doi:10.1126/science.1239947
- Jones, D. T., Jager, N., Kool, M., Zichner, T., Hutter, B., Sultan, M., . . . Lichter, P. (2012). Dissecting the genomic complexity underlying medulloblastoma. *Nature*, *488*(7409), 100-105. doi:10.1038/nature11284
- Kageshita, T., Hamby, C. V., Ishihara, T., Matsumoto, K., Saida, T., & Ono, T. (2001). Loss of beta-catenin expression associated with disease progression in malignant melanoma. *Br J Dermatol*, *145*(2), 210-216.
- Kahlert, U. D., Suwala, A. K., Koch, K., Natsumeda, M., Orr, B. A., Hayashi, M., . . . Eberhart, C. G. (2015). Pharmacologic Wnt Inhibition Reduces Proliferation, Survival, and Clonogenicity of Glioblastoma Cells. *J Neuropathol Exp Neurol*, *74*(9), 889-900. doi:10.1097/NEN.0000000000000227
- Kahn, S. A., Wang, X., Nitta, R. T., Gholamin, S., Theruvath, J., Hutter, G., . . . Cheshier, S. H. (2018). Notch1 regulates the initiation of metastasis and self-renewal of Group 3 medulloblastoma. *Nat Commun*, *9*(1), 4121. doi:10.1038/s41467-018-06564-9
- Kawauchi, D., Robinson, G., Uziel, T., Gibson, P., Rehg, J., Gao, C., . . . Roussel, M. F. (2012). A mouse model of the most aggressive subgroup of human medulloblastoma. *Cancer Cell*, *21*(2), 168-180. doi:10.1016/j.ccr.2011.12.023
- Kiecker, C., & Niehrs, C. (2001). A morphogen gradient of Wnt/beta-catenin signalling regulates anteroposterior neural patterning in *Xenopus*. *Development*, *128*(21), 4189-4201.
- Kim, K. A., Kakitani, M., Zhao, J., Oshima, T., Tang, T., Binnerts, M., . . . Tomizuka, K. (2005). Mitogenic influence of human R-spondin1 on the intestinal epithelium. *Science*, *309*(5738), 1256-1259. doi:10.1126/science.1112521
- Kim, W. Y., Wang, X., Wu, Y., Doble, B. W., Patel, S., Woodgett, J. R., & Snider, W. D. (2009). GSK-3 is a master regulator of neural progenitor homeostasis. *Nat Neurosci*, *12*(11), 1390-1397. doi:10.1038/nn.2408
- Kinzler, K. W., & Vogelstein, B. (1996). Lessons from hereditary colorectal cancer. *Cell*, *87*(2), 159-170.
- Kool, M., Jones, D. T., Jager, N., Northcott, P. A., Pugh, T. J., Hovestadt, V., . . . Project, I. P. T. (2014). Genome sequencing of SHH medulloblastoma predicts genotype-related response to smoothed inhibition. *Cancer Cell*, *25*(3), 393-405. doi:10.1016/j.ccr.2014.02.004
- Kool, M., Korshunov, A., Remke, M., Jones, D. T., Schlanstein, M., Northcott, P. A., . . . Pfister, S. M. (2012). Molecular subgroups of medulloblastoma: an international

- meta-analysis of transcriptome, genetic aberrations, and clinical data of WNT, SHH, Group 3, and Group 4 medulloblastomas. *Acta Neuropathol*, 123(4), 473-484. doi:10.1007/s00401-012-0958-8
- Kool, M., Koster, J., Bunt, J., Hasselt, N. E., Lakeman, A., van Sluis, P., . . . Versteeg, R. (2008). Integrated genomics identifies five medulloblastoma subtypes with distinct genetic profiles, pathway signatures and clinicopathological features. *PLoS One*, 3(8), e3088. doi:10.1371/journal.pone.0003088
- Korshunov, A., Remke, M., Kool, M., Hielscher, T., Northcott, P. A., Williamson, D., . . . Pfister, S. M. (2012). Biological and clinical heterogeneity of MYCN-amplified medulloblastoma. *Acta Neuropathol*, 123(4), 515-527. doi:10.1007/s00401-011-0918-8
- Kreso, A., & Dick, J. E. (2014). Evolution of the cancer stem cell model. *Cell Stem Cell*, 14(3), 275-291. doi:10.1016/j.stem.2014.02.006
- Laks, D. R., Masterman-Smith, M., Visnyei, K., Angenieux, B., Orozco, N. M., Foran, I., . . . Kornblum, H. I. (2009). Neurosphere formation is an independent predictor of clinical outcome in malignant glioma. *Stem Cells*, 27(4), 980-987. doi:10.1002/stem.15
- Lan, X., Jorg, D. J., Cavalli, F. M. G., Richards, L. M., Nguyen, L. V., Vanner, R. J., . . . Dirks, P. B. (2017). Fate mapping of human glioblastoma reveals an invariant stem cell hierarchy. *Nature*, 549(7671), 227-232. doi:10.1038/nature23666
- Lapidot, T., Sirard, C., Vormoor, J., Murdoch, B., Hoang, T., Caceres-Cortes, J., . . . Dick, J. E. (1994). A cell initiating human acute myeloid leukaemia after transplantation into SCID mice. *Nature*, 367(6464), 645-648. doi:10.1038/367645a0
- Lathia, J. D., Gallagher, J., Heddleston, J. M., Wang, J., Eyler, C. E., Macsworlds, J., . . . Rich, J. N. (2010). Integrin alpha 6 regulates glioblastoma stem cells. *Cell Stem Cell*, 6(5), 421-432. doi:10.1016/j.stem.2010.02.018
- Lessard, J., & Sauvageau, G. (2003). Bmi-1 determines the proliferative capacity of normal and leukaemic stem cells. *Nature*, 423(6937), 255-260. doi:10.1038/nature01572
- Leung, C., Lingbeek, M., Shakhova, O., Liu, J., Tanger, E., Saremaslani, P., . . . Marino, S. (2004). Bmi1 is essential for cerebellar development and is overexpressed in human medulloblastomas. *Nature*, 428(6980), 337-341. doi:10.1038/nature02385
- Liu, C., Li, Y., Semenov, M., Han, C., Baeg, G. H., Tan, Y., . . . He, X. (2002). Control of beta-catenin phosphorylation/degradation by a dual-kinase mechanism. *Cell*, 108(6), 837-847.
- Liu, G., Yuan, X., Zeng, Z., Tunici, P., Ng, H., Abdulkadir, I. R., . . . Yu, J. S. (2006). Analysis of gene expression and chemoresistance of CD133+ cancer stem cells in glioblastoma. *Mol Cancer*, 5, 67. doi:10.1186/1476-4598-5-67
- Lorenz, A., Deutschmann, M., Ahlfeld, J., Prix, C., Koch, A., Smits, R., . . . Schuller, U. (2011). Severe alterations of cerebellar cortical development after constitutive activation of Wnt signaling in granule neuron precursors. *Mol Cell Biol*, 31(16), 3326-3338. doi:10.1128/MCB.05718-11
- Louis, D. N., Ohgaki, H., Wiestler, O. D., Cavenee, W. K., Burger, P. C., Jouvett, A., . . . Kleihues, P. (2007). The 2007 WHO classification of tumours of the central

- nervous system. *Acta Neuropathol*, 114(2), 97-109. doi:10.1007/s00401-007-0243-4
- Maelandsmo, G. M., Holm, R., Nesland, J. M., Fodstad, O., & Florenes, V. A. (2003). Reduced beta-catenin expression in the cytoplasm of advanced-stage superficial spreading malignant melanoma. *Clin Cancer Res*, 9(9), 3383-3388.
- Magee, J. A., Piskounova, E., & Morrison, S. J. (2012). Cancer stem cells: impact, heterogeneity, and uncertainty. *Cancer Cell*, 21(3), 283-296. doi:10.1016/j.ccr.2012.03.003
- Mak, A. B., Nixon, A. M., Kittanakom, S., Stewart, J. M., Chen, G. I., Curak, J., . . . Moffat, J. (2012). Regulation of CD133 by HDAC6 promotes beta-catenin signaling to suppress cancer cell differentiation. *Cell Rep*, 2(4), 951-963. doi:10.1016/j.celrep.2012.09.016
- Manning, B. D., & Toker, A. (2017). AKT/PKB Signaling: Navigating the Network. *Cell*, 169(3), 381-405. doi:10.1016/j.cell.2017.04.001
- Manoranjan, B., Wang, X., Hallett, R. M., Venugopal, C., Mack, S. C., McFarlane, N., . . . Singh, S. K. (2013). FoxG1 interacts with Bmi1 to regulate self-renewal and tumorigenicity of medulloblastoma stem cells. *Stem Cells*, 31(7), 1266-1277. doi:10.1002/stem.1401
- McKean-Cowdin, R., Razavi, P., Barrington-Trimis, J., Baldwin, R. T., Asgharzadeh, S., Cockburn, M., . . . Preston-Martin, S. (2013). Trends in childhood brain tumor incidence, 1973-2009. *J Neurooncol*, 115(2), 153-160. doi:10.1007/s11060-013-1212-5
- Megason, S. G., & McMahon, A. P. (2002). A mitogen gradient of dorsal midline Wnts organizes growth in the CNS. *Development*, 129(9), 2087-2098.
- Molofsky, A. V., Pardal, R., Iwashita, T., Park, I. K., Clarke, M. F., & Morrison, S. J. (2003). Bmi-1 dependence distinguishes neural stem cell self-renewal from progenitor proliferation. *Nature*, 425(6961), 962-967. doi:10.1038/nature02060
- Morris, L. G., Kaufman, A. M., Gong, Y., Ramaswami, D., Walsh, L. A., Turcan, S., . . . Chan, T. A. (2013). Recurrent somatic mutation of FAT1 in multiple human cancers leads to aberrant Wnt activation. *Nat Genet*, 45(3), 253-261. doi:10.1038/ng.2538
- Morrissy, A. S., Garzia, L., Shih, D. J., Zuyderduyn, S., Huang, X., Skowron, P., . . . Taylor, M. D. (2016). Divergent clonal selection dominates medulloblastoma at recurrence. *Nature*, 529(7586), 351-357. doi:10.1038/nature16478
- Moser, A. R., Dove, W. F., Roth, K. A., & Gordon, J. I. (1992). The Min (multiple intestinal neoplasia) mutation: its effect on gut epithelial cell differentiation and interaction with a modifier system. *J Cell Biol*, 116(6), 1517-1526.
- Moser, A. R., Pitot, H. C., & Dove, W. F. (1990). A dominant mutation that predisposes to multiple intestinal neoplasia in the mouse. *Science*, 247(4940), 322-324.
- Ng, S. S., Mahmoudi, T., Danenberg, E., Bejaoui, I., de Lau, W., Korswagen, H. C., . . . Clevers, H. (2009). Phosphatidylinositol 3-kinase signaling does not activate the wnt cascade. *J Biol Chem*, 284(51), 35308-35313. doi:10.1074/jbc.M109.078261

- Nguyen, H., Rendl, M., & Fuchs, E. (2006). Tcf3 governs stem cell features and represses cell fate determination in skin. *Cell*, *127*(1), 171-183. doi:10.1016/j.cell.2006.07.036
- Northcott, P. A., Buchhalter, I., Morrissy, A. S., Hovestadt, V., Weischenfeldt, J., Ehrenberger, T., . . . Lichter, P. (2017). The whole-genome landscape of medulloblastoma subtypes. *Nature*, *547*(7663), 311-317. doi:10.1038/nature22973
- Northcott, P. A., Jones, D. T., Kool, M., Robinson, G. W., Gilbertson, R. J., Cho, Y. J., . . . Pfister, S. M. (2012). Medulloblastomics: the end of the beginning. *Nat Rev Cancer*, *12*(12), 818-834. doi:10.1038/nrc3410
- Northcott, P. A., Korshunov, A., Witt, H., Hielscher, T., Eberhart, C. G., Mack, S., . . . Taylor, M. D. (2011). Medulloblastoma comprises four distinct molecular variants. *J Clin Oncol*, *29*(11), 1408-1414. doi:10.1200/JCO.2009.27.4324
- Northcott, P. A., Lee, C., Zichner, T., Stutz, A. M., Erkek, S., Kawauchi, D., . . . Pfister, S. M. (2014). Enhancer hijacking activates GFI1 family oncogenes in medulloblastoma. *Nature*, *511*(7510), 428-434. doi:10.1038/nature13379
- Northcott, P. A., Shih, D. J., Peacock, J., Garzia, L., Morrissy, A. S., Zichner, T., . . . Taylor, M. D. (2012). Subgroup-specific structural variation across 1,000 medulloblastoma genomes. *Nature*, *488*(7409), 49-56. doi:10.1038/nature11327
- Northcott, P. A., Shih, D. J., Remke, M., Cho, Y. J., Kool, M., Hawkins, C., . . . Taylor, M. D. (2012). Rapid, reliable, and reproducible molecular sub-grouping of clinical medulloblastoma samples. *Acta Neuropathol*, *123*(4), 615-626. doi:10.1007/s00401-011-0899-7
- Nusse, R., & Varmus, H. E. (1992). Wnt genes. *Cell*, *69*(7), 1073-1087.
- Ohgaki, H., & Kleihues, P. (2013). The definition of primary and secondary glioblastoma. *Clin Cancer Res*, *19*(4), 764-772. doi:10.1158/1078-0432.CCR-12-3002
- Omholt, K., Platz, A., Ringborg, U., & Hansson, J. (2001). Cytoplasmic and nuclear accumulation of beta-catenin is rarely caused by CTNNB1 exon 3 mutations in cutaneous malignant melanoma. *Int J Cancer*, *92*(6), 839-842. doi:10.1002/ijc.1270
- Omuro, A., & DeAngelis, L. M. (2013). Glioblastoma and other malignant gliomas: a clinical review. *JAMA*, *310*(17), 1842-1850. doi:10.1001/jama.2013.280319
- Orford, K., Crockett, C., Jensen, J. P., Weissman, A. M., & Byers, S. W. (1997). Serine phosphorylation-regulated ubiquitination and degradation of beta-catenin. *J Biol Chem*, *272*(40), 24735-24738.
- Ostrom, Q. T., Gittleman, H., Truitt, G., Boscia, A., Kruchko, C., & Barnholtz-Sloan, J. S. (2018). CBTRUS Statistical Report: Primary Brain and Other Central Nervous System Tumors Diagnosed in the United States in 2011-2015. *Neuro Oncol*, *20*(suppl\_4), iv1-iv86. doi:10.1093/neuonc/now131
- Packer, R. J., Cogen, P., Vezina, G., & Rorke, L. B. (1999). Medulloblastoma: clinical and biologic aspects. *Neuro Oncol*, *1*(3), 232-250. doi:10.1093/neuonc/1.3.232
- Packer, R. J., Gajjar, A., Vezina, G., Rorke-Adams, L., Burger, P. C., Robertson, P. L., . . . Spoto, R. (2006). Phase III study of craniospinal radiation therapy followed by adjuvant chemotherapy for newly diagnosed average-risk medulloblastoma. *J Clin Oncol*, *24*(25), 4202-4208. doi:10.1200/JCO.2006.06.4980

- Pallini, R., Ricci-Vitiani, L., Montano, N., Mollinari, C., Biffoni, M., Cenci, T., . . . Larocca, L. M. (2011). Expression of the stem cell marker CD133 in recurrent glioblastoma and its value for prognosis. *Cancer*, *117*(1), 162-174. doi:10.1002/cncr.25581
- Panosyan, E. H., Laks, D. R., Masterman-Smith, M., Mottahedeh, J., Yong, W. H., Cloughesy, T. F., . . . Kornblum, H. I. (2010). Clinical outcome in pediatric glial and embryonal brain tumors correlates with in vitro multi-passageable neurosphere formation. *Pediatr Blood Cancer*, *55*(4), 644-651. doi:10.1002/pbc.22627
- Parsons, D. W., Jones, S., Zhang, X., Lin, J. C., Leary, R. J., Angenendt, P., . . . Kinzler, K. W. (2008). An integrated genomic analysis of human glioblastoma multiforme. *Science*, *321*(5897), 1807-1812. doi:10.1126/science.1164382
- Patel, A. P., Tirosch, I., Trombetta, J. J., Shalek, A. K., Gillespie, S. M., Wakimoto, H., . . . Bernstein, B. E. (2014). Single-cell RNA-seq highlights intratumoral heterogeneity in primary glioblastoma. *Science*, *344*(6190), 1396-1401. doi:10.1126/science.1254257
- Pei, Y., Brun, S. N., Markant, S. L., Lento, W., Gibson, P., Taketo, M. M., . . . Wechsler-Reya, R. J. (2012). WNT signaling increases proliferation and impairs differentiation of stem cells in the developing cerebellum. *Development*, *139*(10), 1724-1733. doi:10.1242/dev.050104
- Pei, Y., Liu, K. W., Wang, J., Garancher, A., Tao, R., Esparza, L. A., . . . Wechsler-Reya, R. J. (2016). HDAC and PI3K Antagonists Cooperate to Inhibit Growth of MYC-Driven Medulloblastoma. *Cancer Cell*, *29*(3), 311-323. doi:10.1016/j.ccell.2016.02.011
- Pei, Y., Moore, C. E., Wang, J., Tewari, A. K., Eroshkin, A., Cho, Y. J., . . . Wechsler-Reya, R. J. (2012). An animal model of MYC-driven medulloblastoma. *Cancer Cell*, *21*(2), 155-167. doi:10.1016/j.ccr.2011.12.021
- Pfaff, E., Remke, M., Sturm, D., Benner, A., Witt, H., Milde, T., . . . Pfister, S. M. (2010). TP53 mutation is frequently associated with CTNNB1 mutation or MYCN amplification and is compatible with long-term survival in medulloblastoma. *J Clin Oncol*, *28*(35), 5188-5196. doi:10.1200/JCO.2010.31.1670
- Phillips, H. S., Kharbanda, S., Chen, R., Forrest, W. F., Soriano, R. H., Wu, T. D., . . . Aldape, K. (2006). Molecular subclasses of high-grade glioma predict prognosis, delineate a pattern of disease progression, and resemble stages in neurogenesis. *Cancer Cell*, *9*(3), 157-173. doi:10.1016/j.ccr.2006.02.019
- Phoenix, T. N., Patmore, D. M., Boop, S., Boulos, N., Jacus, M. O., Patel, Y. T., . . . Gilbertson, R. J. (2016). Medulloblastoma Genotype Dictates Blood Brain Barrier Phenotype. *Cancer Cell*, *29*(4), 508-522. doi:10.1016/j.ccell.2016.03.002
- Pietila, S., Korpela, R., Lenko, H. L., Haapasalo, H., Alalantela, R., Nieminen, P., . . . Makiperna, A. (2012). Neurological outcome of childhood brain tumor survivors. *J Neurooncol*, *108*(1), 153-161. doi:10.1007/s11060-012-0816-5
- Pollock, P. M., & Hayward, N. (2002). Mutations in exon 3 of the beta-catenin gene are rare in melanoma cell lines. *Melanoma Res*, *12*(2), 183-186.
- Pomeroy, S. L., Tamayo, P., Gaasenbeek, M., Sturla, L. M., Angelo, M., McLaughlin, M. E., . . . Golub, T. R. (2002). Prediction of central nervous system embryonal tumour

- outcome based on gene expression. *Nature*, 415(6870), 436-442. doi:10.1038/415436a
- Poschl, J., Bartels, M., Ohli, J., Bianchi, E., Kuteykin-Teplyakov, K., Grammel, D., . . . Schuller, U. (2014). Wnt/beta-catenin signaling inhibits the Shh pathway and impairs tumor growth in Shh-dependent medulloblastoma. *Acta Neuropathol*, 127(4), 605-607. doi:10.1007/s00401-014-1258-2
- Poschl, J., Grammel, D., Dorostkar, M. M., Kretschmar, H. A., & Schuller, U. (2013). Constitutive activation of beta-catenin in neural progenitors results in disrupted proliferation and migration of neurons within the central nervous system. *Dev Biol*, 374(2), 319-332. doi:10.1016/j.ydbio.2012.12.001
- Pugh, T. J., Weeraratne, S. D., Archer, T. C., Pomeranz Krummel, D. A., Auclair, D., Bochicchio, J., . . . Cho, Y. J. (2012). Medulloblastoma exome sequencing uncovers subtype-specific somatic mutations. *Nature*, 488(7409), 106-110. doi:10.1038/nature11329
- Pulvirenti, T., Van Der Heijden, M., Droms, L. A., Huse, J. T., Tabar, V., & Hall, A. (2011). Dishevelled 2 signaling promotes self-renewal and tumorigenicity in human gliomas. *Cancer Res*, 71(23), 7280-7290. doi:10.1158/0008-5472.CAN-11-1531
- Rajakulendran, N., Rowland, K. J., Selvadurai, H. J., Ahmadi, M., Park, N. I., Naumenko, S., . . . Dirks, P. B. (2019). Wnt and Notch signaling govern self-renewal and differentiation in a subset of human glioblastoma stem cells. *Genes Dev*. doi:10.1101/gad.321968.118
- Ramaswamy, V., Remke, M., Bouffet, E., Bailey, S., Clifford, S. C., Doz, F., . . . Pomeroy, S. L. (2016). Risk stratification of childhood medulloblastoma in the molecular era: the current consensus. *Acta Neuropathol*, 131(6), 821-831. doi:10.1007/s00401-016-1569-6
- Read, T. A., Fogarty, M. P., Markant, S. L., McLendon, R. E., Wei, Z., Ellison, D. W., . . . Wechsler-Reya, R. J. (2009). Identification of CD15 as a marker for tumor-propagating cells in a mouse model of medulloblastoma. *Cancer Cell*, 15(2), 135-147. doi:10.1016/j.ccr.2008.12.016
- Reifenberger, J., Knobbe, C. B., Wolter, M., Blaschke, B., Schulte, K. W., Pietsch, T., . . . Reifenberger, G. (2002). Molecular genetic analysis of malignant melanomas for aberrations of the WNT signaling pathway genes CTNNB1, APC, ICAT and BTRC. *Int J Cancer*, 100(5), 549-556. doi:10.1002/ijc.10512
- Reynolds, B. A., & Weiss, S. (1996). Clonal and population analyses demonstrate that an EGF-responsive mammalian embryonic CNS precursor is a stem cell. *Dev Biol*, 175(1), 1-13. doi:10.1006/dbio.1996.0090
- Rheinbay, E., Suva, M. L., Gillespie, S. M., Wakimoto, H., Patel, A. P., Shahid, M., . . . Bernstein, B. E. (2013). An aberrant transcription factor network essential for Wnt signaling and stem cell maintenance in glioblastoma. *Cell Rep*, 3(5), 1567-1579. doi:10.1016/j.celrep.2013.04.021
- Rhinn, M., Lun, K., Luz, M., Werner, M., & Brand, M. (2005). Positioning of the midbrain-hindbrain boundary organizer through global posteriorization of the neuroectoderm

- mediated by Wnt8 signaling. *Development*, 132(6), 1261-1272. doi:10.1242/dev.01685
- Robinson, G., Parker, M., Kranenburg, T. A., Lu, C., Chen, X., Ding, L., . . . Gilbertson, R. J. (2012). Novel mutations target distinct subgroups of medulloblastoma. *Nature*, 488(7409), 43-48. doi:10.1038/nature11213
- Roper, K., Corbeil, D., Huttner, W. B. (2000). Retention of prominin in microvilli reveals distinct cholesterol-based lipid micro-domains in the apical plasma membrane. *Nat Cell Biol*, 2(9), 582-592. doi: 10.1038/35023524
- Rossi, M., Magnoni, L., Miracco, C., Mori, E., Tosi, P., Pirtoli, L., . . . Bakker, A. (2011). beta-catenin and Gli1 are prognostic markers in glioblastoma. *Cancer Biol Ther*, 11(8), 753-761.
- Rubinfeld, B., Robbins, P., El-Gamil, M., Albert, I., Porfiri, E., & Polakis, P. (1997). Stabilization of beta-catenin by genetic defects in melanoma cell lines. *Science*, 275(5307), 1790-1792.
- Ryu, B., Kim, D. S., Deluca, A. M., & Alani, R. M. (2007). Comprehensive expression profiling of tumor cell lines identifies molecular signatures of melanoma progression. *PLoS One*, 2(7), e594. doi:10.1371/journal.pone.0000594
- Samowitz, W. S., Powers, M. D., Spirio, L. N., Nollet, F., van Roy, F., & Slattery, M. L. (1999). Beta-catenin mutations are more frequent in small colorectal adenomas than in larger adenomas and invasive carcinomas. *Cancer Res*, 59(7), 1442-1444.
- Sauvageau, M., & Sauvageau, G. (2010). Polycomb group proteins: multi-faceted regulators of somatic stem cells and cancer. *Cell Stem Cell*, 7(3), 299-313. doi:10.1016/j.stem.2010.08.002
- Schepers, A. G., Snippert, H. J., Stange, D. E., van den Born, M., van Es, J. H., van de Wetering, M., & Clevers, H. (2012). Lineage tracing reveals Lgr5+ stem cell activity in mouse intestinal adenomas. *Science*, 337(6095), 730-735. doi:10.1126/science.1224676
- Schreiber, J. E., Gurney, J. G., Palmer, S. L., Bass, J. K., Wang, M., Chen, S., . . . Gajjar, A. (2014). Examination of risk factors for intellectual and academic outcomes following treatment for pediatric medulloblastoma. *Neuro Oncol*, 16(8), 1129-1136. doi:10.1093/neuonc/nou006
- Schuller, U., Heine, V. M., Mao, J., Kho, A. T., Dillon, A. K., Han, Y. G., . . . Ligon, K. L. (2008). Acquisition of granule neuron precursor identity is a critical determinant of progenitor cell competence to form Shh-induced medulloblastoma. *Cancer Cell*, 14(2), 123-134. doi:10.1016/j.ccr.2008.07.005
- Schuller, U., & Rowitch, D. H. (2007). Beta-catenin function is required for cerebellar morphogenesis. *Brain Res*, 1140, 161-169. doi:10.1016/j.brainres.2006.05.105
- Shackleton, M., Quintana, E., Fearon, E. R., & Morrison, S. J. (2009). Heterogeneity in cancer: cancer stem cells versus clonal evolution. *Cell*, 138(5), 822-829. doi:10.1016/j.cell.2009.08.017
- Shibahara, I., Sonoda, Y., Saito, R., Kanamori, M., Yamashita, Y., Kumabe, T., . . . Tominaga, T. (2013). The expression status of CD133 is associated with the pattern and timing of primary glioblastoma recurrence. *Neuro Oncol*, 15(9), 1151-1159. doi:10.1093/neuonc/not066

- Shih, D. J., Northcott, P. A., Remke, M., Korshunov, A., Ramaswamy, V., Kool, M., . . . Taylor, M. D. (2014). Cytogenetic prognostication within medulloblastoma subgroups. *J Clin Oncol*, *32*(9), 886-896. doi:10.1200/JCO.2013.50.9539
- Shmelkov, S. V., Jun, L., St. Clair, R., McGarrigle, D., Derderian C., A., Usenko, J. K., . . . Rafii, S. (2004). Alternative promoters regulate transcription of the gene that encodes stem cell surface protein AC133. *Blood*, *103*(6), 2055-2061. doi: 10.1182/blood-2003-06-1881
- Singh, S. K., Clarke, I. D., Terasaki, M., Bonn, V. E., Hawkins, C., Squire, J., & Dirks, P. B. (2003). Identification of a cancer stem cell in human brain tumors. *Cancer Res*, *63*(18), 5821-5828.
- Singh, S. K., Hawkins, C., Clarke, I. D., Squire, J. A., Bayani, J., Hide, T., . . . Dirks, P. B. (2004). Identification of human brain tumour initiating cells. *Nature*, *432*(7015), 396-401. doi:10.1038/nature03128
- Smith, M. J., Beetz, C., Williams, S. G., Bhaskar, S. S., O'Sullivan, J., Anderson, B., . . . Evans, D. G. (2014). Germline mutations in SUFU cause Gorlin syndrome-associated childhood medulloblastoma and redefine the risk associated with PTCH1 mutations. *J Clin Oncol*, *32*(36), 4155-4161. doi:10.1200/JCO.2014.58.2569
- Snippert, H. J., Schepers, A. G., van Es, J. H., Simons, B. D., & Clevers, H. (2014). Biased competition between Lgr5 intestinal stem cells driven by oncogenic mutation induces clonal expansion. *EMBO Rep*, *15*(1), 62-69. doi:10.1002/embr.201337799
- Soeda, A., Park, M., Lee D., Mintz, A., Androutsellis-Theotokis, A., McKay, R. D., . . . Park, D. M. (2009). Hypoxia promotes expansion of the CD133-positive glioma stem cells through activation of HIF-1alpha. *Oncogene*, *28*(45), 3949-3959. doi: 10.1038/onc.2009.252
- Son, M. J., Woolard, K., Nam, D. H., Lee, J., & Fine, H. A. (2009). SSEA-1 is an enrichment marker for tumor-initiating cells in human glioblastoma. *Cell Stem Cell*, *4*(5), 440-452. doi:10.1016/j.stem.2009.03.003
- Sottoriva, A., Spiteri, I., Piccirillo, S. G., Touloumis, A., Collins, V. P., Marioni, J. C., . . . Tavaré, S. (2013). Intratumor heterogeneity in human glioblastoma reflects cancer evolutionary dynamics. *Proc Natl Acad Sci U S A*, *110*(10), 4009-4014. doi:10.1073/pnas.1219747110
- Sparks, A. B., Morin, P. J., Vogelstein, B., & Kinzler, K. W. (1998). Mutational analysis of the APC/beta-catenin/Tcf pathway in colorectal cancer. *Cancer Res*, *58*(6), 1130-1134.
- Stamos, J. L., & Weis, W. I. (2013). The beta-catenin destruction complex. *Cold Spring Harb Perspect Biol*, *5*(1), a007898. doi:10.1101/cshperspect.a007898
- Steinhart, Z., Pavlovic, Z., Chandrashekar, M., Hart, T., Wang, X., Zhang, X., . . . Angers, S. (2017). Genome-wide CRISPR screens reveal a Wnt-FZD5 signaling circuit as a druggable vulnerability of RNF43-mutant pancreatic tumors. *Nat Med*, *23*(1), 60-68. doi:10.1038/nm.4219
- Stupp, R., Mason, W. P., van den Bent, M. J., Weller, M., Fisher, B., Taphoorn, M. J., . . . National Cancer Institute of Canada Clinical Trials, G. (2005). Radiotherapy plus

- concomitant and adjuvant temozolomide for glioblastoma. *N Engl J Med*, 352(10), 987-996. doi:10.1056/NEJMoa043330
- Swartling, F. J., Savov, V., Persson, A. I., Chen, J., Hackett, C. S., Northcott, P. A., . . . Weiss, W. A. (2012). Distinct neural stem cell populations give rise to disparate brain tumors in response to N-MYC. *Cancer Cell*, 21(5), 601-613. doi:10.1016/j.ccr.2012.04.012
- Tamai, K., Zeng, X., Liu, C., Zhang, X., Harada, Y., Chang, Z., & He, X. (2004). A mechanism for Wnt coreceptor activation. *Mol Cell*, 13(1), 149-156.
- Tang, Y., Gholamin, S., Schubert, S., Willardson, M. I., Lee, A., Bandopadhyay, P., . . . Cho, Y. J. (2014). Epigenetic targeting of Hedgehog pathway transcriptional output through BET bromodomain inhibition. *Nat Med*, 20(7), 732-740. doi:10.1038/nm.3613
- Taylor, M. D., Northcott, P. A., Korshunov, A., Remke, M., Cho, Y. J., Clifford, S. C., . . . Pfister, S. M. (2012). Molecular subgroups of medulloblastoma: the current consensus. *Acta Neuropathol*, 123(4), 465-472. doi:10.1007/s00401-011-0922-z
- Thomas, A. J., & Erickson, C. A. (2008). The making of a melanocyte: the specification of melanoblasts from the neural crest. *Pigment Cell Melanoma Res*, 21(6), 598-610. doi:10.1111/j.1755-148X.2008.00506.x
- Thomas, K. R., & Capecchi, M. R. (1990). Targeted disruption of the murine int-1 proto-oncogene resulting in severe abnormalities in midbrain and cerebellar development. *Nature*, 346(6287), 847-850. doi:10.1038/346847a0
- Thompson, M. C., Fuller, C., Hogg, T. L., Dalton, J., Finkelstein, D., Lau, C. C., . . . Gilbertson, R. J. (2006). Genomics identifies medulloblastoma subgroups that are enriched for specific genetic alterations. *J Clin Oncol*, 24(12), 1924-1931. doi:10.1200/JCO.2005.04.4974
- Tortori-Donati, P., Fondelli, M. P., Rossi, A., Cama, A., Caputo, L., Andreussi, L., & Garre, M. L. (1996). Medulloblastoma in children: CT and MRI findings. *Neuroradiology*, 38(4), 352-359.
- Tsui, K., Gajjar, A., Li, C., Srivastava, D., Broniscer, A., Wetmore, C., . . . Armstrong, G. T. (2015). Subsequent neoplasms in survivors of childhood central nervous system tumors: risk after modern multimodal therapy. *Neuro Oncol*, 17(3), 448-456. doi:10.1093/neuonc/nou279
- Uchida, N., Buck, D. W., He, D., Reitsma, M. J., Masek, M., Phan, T. V., . . . Weissman, I. L. (2000). Direct isolation of human central nervous system stem cells. *Proc Natl Acad Sci USA*, 97(26), 14720-14725. doi: 10.1073/pnas.97.26.14720.
- Valenta, T., Hausmann, G., & Basler, K. (2012). The many faces and functions of beta-catenin. *EMBO J*, 31(12), 2714-2736. doi:10.1038/emboj.2012.150
- van de Wetering, M., Francies, H. E., Francis, J. M., Bounova, G., Iorio, F., Pronk, A., . . . Clevers, H. (2015). Prospective derivation of a living organoid biobank of colorectal cancer patients. *Cell*, 161(4), 933-945. doi:10.1016/j.cell.2015.03.053
- van Linde, M. E., Brahm, C. G., de Witt Hamer, P. C., Reijneveld, J. C., Bruynzeel, A. M. E., Vandertop, W. P., . . . Verheul, H. M. W. (2017). Treatment outcome of patients with recurrent glioblastoma multiforme: a retrospective multicenter analysis. *J Neurooncol*, 135(1), 183-192. doi:10.1007/s11060-017-2564-z

- Vanner, R. J., Remke, M., Gallo, M., Selvadurai, H. J., Coutinho, F., Lee, L., . . . Dirks, P. B. (2014). Quiescent sox2(+) cells drive hierarchical growth and relapse in sonic hedgehog subgroup medulloblastoma. *Cancer Cell*, 26(1), 33-47. doi:10.1016/j.ccr.2014.05.005
- Venugopal, C., Li, N., Wang, X., Manoranjan, B., Hawkins, C., Gunnarsson, T., . . . Singh, S. K. (2012). Bmi1 marks intermediate precursors during differentiation of human brain tumor initiating cells. *Stem Cell Res*, 8(2), 141-153. doi:10.1016/j.scr.2011.09.008
- Venugopal, C., Hallett, R., Vora, P., Manoranjan, B., Mahendram, S., Qazi, M. A., . . . Singh, S. K. (2015). Pyrvinium targets CD133 in human glioblastoma brain tumor-initiating cells. *Clin Cancer Res*, 21(23), 5324-5337. doi:10.1158/1078-0432.CCR-14-3147
- Verhaak, R. G., Hoadley, K. A., Purdom, E., Wang, V., Qi, Y., Wilkerson, M. D., . . . Cancer Genome Atlas Research, N. (2010). Integrated genomic analysis identifies clinically relevant subtypes of glioblastoma characterized by abnormalities in PDGFRA, IDH1, EGFR, and NF1. *Cancer Cell*, 17(1), 98-110. doi:10.1016/j.ccr.2009.12.020
- Vermeulen, L., Morrissey, E., van der Heijden, M., Nicholson, A. M., Sottoriva, A., Buczaccki, S., . . . Winton, D. J. (2013). Defining stem cell dynamics in models of intestinal tumor initiation. *Science*, 342(6161), 995-998. doi:10.1126/science.1243148
- Villanueva, J., Vultur, A., Lee, J. T., Somasundaram, R., Fukunaga-Kalabis, M., Cipolla, A. K., . . . Herlyn, M. (2010). Acquired resistance to BRAF inhibitors mediated by a RAF kinase switch in melanoma can be overcome by cotargeting MEK and IGF-1R/PI3K. *Cancer Cell*, 18(6), 683-695. doi:10.1016/j.ccr.2010.11.023
- Vivancos, V., Chen, P., Spassky, N., Qian, D., Dabdoub, A., Kelley, M., . . . Guthrie, S. (2009). Wnt activity guides facial branchiomotor neuron migration, and involves the PCP pathway and JNK and ROCK kinases. *Neural Dev*, 4, 7. doi:10.1186/1749-8104-4-7
- von Bueren, A. O., Kortmann, R. D., von Hoff, K., Friedrich, C., Mynarek, M., Muller, K., . . . Rutkowski, S. (2016). Treatment of Children and Adolescents With Metastatic Medulloblastoma and Prognostic Relevance of Clinical and Biologic Parameters. *J Clin Oncol*, 34(34), 4151-4160. doi:10.1200/JCO.2016.67.2428
- Wang, X., Venugopal, C., Manoranjan, B., McFarlane, N., O'Farrell, E., Nolte, S., . . . Singh, S. K. (2012). Sonic hedgehog regulates Bmi1 in human medulloblastoma brain tumor-initiating cells. *Oncogene*, 31(2), 187-199. doi:10.1038/onc.2011.232
- Ward, R. J., Lee, L., Graham, K., Satkunendran, T., Yoshikawa, K., Ling, E., . . . Dirks, P. B. (2009). Multipotent CD15+ cancer stem cells in patched-1-deficient mouse medulloblastoma. *Cancer Res*, 69(11), 4682-4690. doi:10.1158/0008-5472.CAN-09-0342
- Wei, Y., Jiang, Y., Zou, F., Liu, Y., Wang, S., Xu, N., . . . Jiang, J. (2013). Activation of PI3K/Akt pathway by CD133-p85 interaction promotes tumorigenic capacity of glioma stem cells. *Proc Natl Acad Sci U S A*, 110(17), 6829-6834. doi:10.1073/pnas.1217002110

- Woodhead, G. J., Mutch, C. A., Olson, E. C., & Chenn, A. (2006). Cell-autonomous beta-catenin signaling regulates cortical precursor proliferation. *J Neurosci*, *26*(48), 12620-12630. doi:10.1523/JNEUROSCI.3180-06.2006
- Wright, J. H. (1910). Neurocytoma or Neuroblastoma, a Kind of Tumor Not Generally Recognized. *J Exp Med*, *12*(4), 556-561.
- Wu, X., Northcott, P. A., Dubuc, A., Dupuy, A. J., Shih, D. J., Witt, H., . . . Taylor, M. D. (2012). Clonal selection drives genetic divergence of metastatic medulloblastoma. *Nature*, *482*(7386), 529-533. doi:10.1038/nature10825
- Yang, W., Xia, Y., Ji, H., Zheng, Y., Liang, J., Huang, W., . . . Lu, Z. (2011). Nuclear PKM2 regulates beta-catenin transactivation upon EGFR activation. *Nature*, *480*(7375), 118-122. doi:10.1038/nature10598
- Yang, Z. J., Ellis, T., Markant, S. L., Read, T. A., Kessler, J. D., Bourbonlous, M., . . . Wechsler-Reya, R. J. (2008). Medulloblastoma can be initiated by deletion of Patched in lineage-restricted progenitors or stem cells. *Cancer Cell*, *14*(2), 135-145. doi:10.1016/j.ccr.2008.07.003
- Yin, A. H., Miraglia, S., Zanjani, E. D., Almeida-Porada, G., Ogawa, M., Leary, A. G., . . . Buck, D. W. (1997). AC133, a novel marker for human hematopoietic stem and progenitor cells. *Blood*, *90*(12), 5002-5012.
- Zacchigna, S., Oh, H., Wilsch-Brauninger, M., Missol-Kolka, E., Jaszai, J., Jansen, S., . . . Carmeliet, P. (2009). Loss of the cholesterol-binding protein prominin-1/CD133 causes disk dysmorphogenesis and photoreceptor degeneration. *J Neurosci*, *29*(7), 2297-2308. doi: 10.1523/JNEUROSCI.2034-08.2009
- Zechner, D., Fujita, Y., Hulsken, J., Muller, T., Walther, I., Taketo, M. M., . . . Birchmeier, C. (2003). beta-Catenin signals regulate cell growth and the balance between progenitor cell expansion and differentiation in the nervous system. *Dev Biol*, *258*(2), 406-418.
- Zeltzer, P. M., Boyett, J. M., Finlay, J. L., Albright, A. L., Rorke, L. B., Milstein, J. M., . . . Packer, R. J. (1999). Metastasis stage, adjuvant treatment, and residual tumor are prognostic factors for medulloblastoma in children: conclusions from the Children's Cancer Group 921 randomized phase III study. *J Clin Oncol*, *17*(3), 832-845. doi:10.1200/JCO.1999.17.3.832
- Zeppernick, F., Ahmadi, R., Campos, B., Dictus, C., Helmke, B. M., Becker, N., . . . Herold-Mende, C. C. (2008). Stem cell marker CD133 affects clinical outcome in glioma patients. *Clin Cancer Res*, *14*(1), 123-129. doi:10.1158/1078-0432.CCR-07-0932
- Zhang, L. Y., Jiang, L. N., Li, F. F., Li, H., Liu, F., Gu, Y., . . . Li, Q. (2010). Reduced beta-catenin expression is associated with good prognosis in Astrocytoma. *Pathol Oncol Res*, *16*(2), 253-257. doi:10.1007/s12253-009-9219-0
- Zhang, N., Wei, P., Gong, A., Chiu, W. T., Lee, H. T., Colman, H., . . . Huang, S. (2011). FoxM1 promotes beta-catenin nuclear localization and controls Wnt target-gene expression and glioma tumorigenesis. *Cancer Cell*, *20*(4), 427-442. doi:10.1016/j.ccr.2011.08.016
- Zheng, H., Ying, H., Wiedemeyer, R., Yan, H., Quayle, S. N., Ivanova, E. V., . . . DePinho, R. A. (2010). PLAGL2 regulates Wnt signaling to impede differentiation in neural

stem cells and gliomas. *Cancer Cell*, 17(5), 497-509.  
doi:10.1016/j.ccr.2010.03.020

Zhukova, N., Ramaswamy, V., Remke, M., Martin, D. C., Castelo-Branco, P., Zhang, C. H., . . . Tabori, U. (2014). WNT activation by lithium abrogates TP53 mutation associated radiation resistance in medulloblastoma. *Acta Neuropathol Commun*, 2, 174. doi:10.1186/s40478-014-0174-y

Zhukova, N., Ramaswamy, V., Remke, M., Pfaff, E., Shih, D. J., Martin, D. C., . . . Tabori, U. (2013). Subgroup-specific prognostic implications of TP53 mutation in medulloblastoma. *J Clin Oncol*, 31(23), 2927-2935.  
doi:10.1200/JCO.2012.48.5052

### **Appendix I: Copyright Statement**

On Thu, Feb 28, 2019 at 3:46 PM Wiley Global Permissions <permissions@wiley.com> wrote:

Dear Branavan:

Thank you for your request.

Permission is hereby granted for the use requested subject to the usual acknowledgements (author, title of material, title of book/journal, ourselves as publisher). You should also duplicate the copyright notice that appears in the Wiley publication; this can be found on the copyright page if the material is a book or within the article if it is a journal.

Any third party material is expressly excluded from this permission. If any of the material you wish to use appears within our work with credit to another source, authorization from that source must be obtained.

This permission does not include the right to grant others permission to photocopy or otherwise reproduce this material except for accessible versions made by non-profit organizations serving the blind, visually impaired and other persons with print disabilities (VIPs).

Sincerely,

Paulette Goldweber

Permissions Manager

Global Sales Partnerships

[pgoldweb@wiley.com](mailto:pgoldweb@wiley.com)

+1 201-748-8765

111 River Street

Hoboken, NJ 07030-5774

U.S.

[permissions@wiley.com](mailto:permissions@wiley.com)

**From:** Branavan Manoranjan [<mailto:branavan.manoranjan@medportal.ca>]  
**Sent:** Wednesday, February 27, 2019 7:55 PM  
**To:** StemCells AMP <[stemcells@alphamedpress.com](mailto:stemcells@alphamedpress.com)>  
**Subject:** Permission to Reprint for PhD Thesis

Dear Editorial Office,

I am completing a PhD thesis at McMaster University titled, "Bi-directional vulnerability of brain tumors to Wnt signaling." I would like your permission to reprint in full the following journal article in my thesis:

Manoranjan B, Wang X, Hallet RM, Venugopal C, Mack SC, McFarlane N, Nolte SM, Scheinemann K, Gunnarsson T, Hassell JA, Taylor MD, Lee C, Triscott J, Dunham C, Hawkins C, Dunn SE, Singh SK. FoxG1 interacts with Bmi1 to regulate self-renewal and tumorigenicity of medulloblastoma stem cells. *Stem Cells*. 2013;31:1266-1277. <https://doi.org/10.1002/stem.1401>

Please note that I, Branavan Manoranjan, am the first author of this work, which was performed under the supervision of Dr. Sheila Singh.

I am also requesting that you grant irrevocable, nonexclusive license to McMaster University (and to the National Library of Canada) to reproduce this material as part of the thesis. Proper acknowledgement of your copyright of the reprinted material will be given in the thesis. Thank you for considering my request.

Best Wishes,

Branavan

## Appendix II: Accomplishments

**The following are a list of the publications generated with my involvement over the course of my doctoral thesis.**

### **PUBLISHED REFEREED PAPERS (\*EQUAL CONTRIBUTIONS BY AUTHORS)**

- 1 Bakhshinyan D, Venugopal C, Adile A, Garg N, **Manoranjan B**, Hallett R, Wang X, Mahendram S, Vora P, Vijayakumar T, Subapanditha M, Singh M, Kameda-Smith MM, Qazi M, McFarlane N, Mann A, Ajani OA, Yarascavitch B, Ramaswamy V, Farooq H, Morrissy S, Cao L, Sydorenko N, Baiazitov R, Du W, Sheedy J, Weetall M, Moon YC, Lee CS, Doble B, Kwiecien JM, Delaney K, Cho YJ, Mitra SS, Kaplan D, Taylor M, Davis T, Singh SK. Bmi1 as a therapeutic target in recurrent medulloblastoma. *Oncogene*. 2019;38:1702-1716. PMID: 30348991.
- 2 Yang K, Nath S, Koziarz A, Badhiwala JH, Ghayur H, Sourour M, Catana D, Nassiri F, Alotaibi MB, Kameda-Smith M, **Manoranjan B**, Aref MH, Mansouri A, Singh S, Almenawer SA. Biopsy versus subtotal versus gross total resection in patients with low-grade glioma: A systematic review and meta-analysis. *World Neurosurgery*. 2018;120:e762-e775. PMID: 30172972.
- 3 **Manoranjan B**, Provias JP. Central neurocytoma represents a tumor consisting of diverse neuronal phenotypes. *Journal of Clinical Neuroscience*. 2018;53:209-213. PMID: 29747899.
- 4 El Malik B, **Manoranjan B**, Ajani O, Zidan A. Hypophysitis due to paranasal sinusitis: A neurosurgical perspective from the developing world. *World Neurosurgery*. 2018;115:162-165. PMID: 29678705.
- 5 Singh M, Venugopal C, Tokar T, Brown K, McFarlane N, Bakhshinyan D, Vijayakumar T, **Manoranjan B**, Mahendram S, Vora P, Qazi M, Dhillon M, Tong A, Durrer K, Murty N, Hallett R, Hassell JA, Kaplan DR, Cutz JC, Jurisica I, Moffat J, Singh SK. RNAi screen identifies essential regulators of human brain metastasis-initiating cells. *Acta Neuropathologica*. 2017;134:923-940. PMID: 28766011.
- 6 **Manoranjan B**, Koziarz A, Kameda-Smith M, Provias JP. Multiple recurrences require long-term follow-up in patients diagnosed with spindle cell oncocyoma of the sella turcica. *Journal of Clinical Neuroscience*. 2017;43:134-146. PMID: 28668473.
- 7 Sergeant A, Kameda-Smith MM, **Manoranjan B**, Karmur B, Duckworth J, Petrelli T, Savage K, Ajani O, Yarascavitch B, Samaan MC, Scheinemann K, Alyman C, Almenawer S, Farrokhyar F, Fleming AJ, Singh SK, Stein N. Analysis of surgical and

- MRI factors associated with cerebellar mutism. *Journal of Neuro-Oncology*. 2017;133:539-552. PMID: 28527006.
- 8 **Manoranjan B**, Dey A, Wang X, Kuzyk A, Petticrew K, Charruthers C, Arnold I. Role of non-government organizations in engaging medical students in research. *Journal of Investigative Medicine*. 2017;65:709-716. PMID: 28151398.
  - 9 Rusiecki D, Lach B, **Manoranjan B**, Fleming A, Ajani O, Singh SK. Progression of atypical extraventricular neurocytoma to anaplastic ganglioglioma. *Human Pathology*. 2017;59:125-130. PMID: 27597523.
  - 10 Garg N, Bakhshinyan D, Venugopal C, Mahendram S, Rosa DA, Vijayakumar T, **Manoranjan B**, Hallett R, McFarlane N, Delaney KH, Kwiecien JM, Arpin CC, Lai PS, Gomez-Biagi RF, Ali AM, de Araujo ED, Ajani OA, Hassell JA, Gunning PT, Singh SK. CD133+ brain tumor-initiating cells are dependent on STAT3 signaling to drive medulloblastoma recurrence. *Oncogene*. 2017;36:606-617. PMID: 27775079.
  - 11 **Manoranjan B**, Mahendram S, Almenawer SA, Venugopal C, McFarlane N, Hallett R, Vijayakumar T, Algird A, Murty NK, Sommer DD, Provias JP, Reddy K, Singh SK. The identification of human pituitary adenoma-initiating cells. *Acta Neuropathologica Communications*. 2016;4:125. PMID: 27894339.
  - 12 Badhiwala JH, **Manoranjan B**, Almenawer SA. Letter to the Editor: Mechanical thrombectomy for acute ischemic stroke. *Journal of the American College of Cardiology*. 2016;67:2449-2450. PMID: 27199072.
  - 13 Lucke-Wold B, Logsdon AF, **Manoranjan B**, Turner RC, McConnell E, Vates GE, Huber JD, Rosen CL, Simard JM. Aneurysmal subarachnoid hemorrhage and neuroinflammation: A comprehensive review. *International Journal of Molecular Sciences*. 2016;17:E497. PMID: 27049383.
  - 14 Venugopal C, Hallett R, Vora P, **Manoranjan B**, Qazi M, McFarlane N, Mahendram S, Nolte SM, Singh M, Garg N, Bakhshinyan D, Lach B, Provias JP, Reddy K, Mury NK, Dunn SE, Doble BW, Bhatia M, Hassell J, Singh SK. Pyrvinium targets CD133 in human glioblastoma brain tumor-initiating cells. *Clinical Cancer Research*. 2015;21:5324-5337. PMID: 26152745.
  - 15 Singh M, Garg N, Venugopal C, Hallett R, Tokar T, McFarlane N, Mahendram S, Bakhshinyan D, **Manoranjan B**, Vora P, Qazi M, Arpin CC, Page B, Haftchenary S, Rosa DA, Lai PS, Gomez-Biagi RF, Ali AM, Lewis A, Geletu M, Murty NK, Hassell JA, Jurisica I, Gunning PT, Singh SK. STAT3 pathway regulates lung-derived brain metastasis initiating cell capacity through miR-21 activation. *Oncotarget*. 2015;6:27461-27477. PMID: 26314961.

- 16 **Manoranjan B**, Singh SK. Letter to the Editor: Temporal evolution of medulloblastoma subgroups. *Journal of Neurosurgery: Pediatrics*. 2015;16:349-350. PMID: 26023848.
- 17 Singh M, **Manoranjan B**, Mahendram S, McFarlane N, Venugopal C, Singh SK. Brain metastasis-initiating cells: Survival of the fittest. *International Journal of Molecular Sciences*. 2014;15:9117-9133. PMID: 24857921.
- 18 Almenawer SA, Farrokhyar F, Hong C, Alhazzani W, **Manoranjan B**, Yarascavitch B, Armjand P, Baronia B, Murty N, Singh SK. Chronic subdural haematoma management: Systematic review and meta-analysis. *Annals of Surgery*. 2014;259:449-457. PMID: 24096761.
- 19 Triscott J, Lee C, Foster C, **Manoranjan B**, Pambid MR, Berns R, Fotovati A, Fotovati A, Venugopal C, O'Halloran K, Narendran A, Hawkins C, Ramaswamy V, Taylor MD, Singhal A, Hukin J, Rassekh R, Northcott P, Singh SK, Dunn SE. Personalizing the treatment for medulloblastoma: Polo-Like Kinase 1 as a molecular target for high-risk children. *Cancer Research*. 2013;73:6734-6744. PMID: 24019381.
- 20 **Manoranjan B**, Wang X, Hallet RM, Venugopal C, Mack SC, McFarlane N, Nolte SM, Scheinemann K, Gunnarsson T, Hassell JA, Taylor MD, Lee C, Triscott J, Dunn SE, Hawkins C, Dunn SE, Singh SK. FoxG1 interacts with Bmi1 to regulate self-renewal and tumorigenicity of medulloblastoma stem cells. *Stem Cells*. 2013;31:1266-1277. PMID: 23592496. *\*Identified by Stem Cells editors as one of top five papers published in 2014*
- 21 Nolte SM, Venugopal C, McFarlane N, Morozova O, Hallett RM, O'Farrell E, **Manoranjan B**, Murty NK, Klurfan P, Kachur K, Provias JP, Hassell JA, Marro M, Singh SK. A cancer stem cell model for studying brain metastases from primary lung cancer. *Journal of the National Cancer Institute*. 2013;105:551-562. PMID: 23418195.
- 22 **Manoranjan B**, Venugopal C, McFarlane N, Doble BW, Dunn SE, Scheinemann K, Singh SK. Medulloblastoma stem cells: Modeling tumor heterogeneity. *Cancer Letters*. 2013;338:23-31. PMID: 22796365.
- 23 Venugopal C, McFarlane NM, Nolte SM, **Manoranjan B**, Singh SK. Processing of primary brain tumor tissue for stem cell assays and flow sorting. *Journal of Visualized Experiments*. 2012;67:4111. PMID: 23051935.
- 24 Venugopal C, Wang SX, **Manoranjan B**, McFarlane N, Nolte S, Li M, Murty N, Siu MKW, Singh SK. GBM secretome induces transient transformation of human neural precursor cells. *Journal of Neuro-Oncology*. 2012;109:457-466. PMID: 22752853.

- 25 **Manoranjan B**, Venugopal C, McFarlane N, Doble BW, Dunn SE, Scheinemann K, Singh SK. Medulloblastoma stem cells: Where development and cancer cross pathways. *Pediatric Research*. 2012;71:516-522. PMID: 22430388.
- 26 Venugopal C\*, Li N\*, Wang X, **Manoranjan B**, Hawkins C, Gunnarsson T, Hollenberg R, Klurfan P, Murty N, Kwiecien J, Wynder C, Singh SK. Bmi1 marks intermediate precursors during differentiation of human brain tumor initiating cells. *Stem Cell Research*. 2012;8:141-153. PMID: 22265735.

#### **PUBLISHED NON-REFEREED PAPERS**

- 1 Kameda-Smith MM, **Manoranjan B**, Venugopal C, Bakhshinyan D, Singh SK. Brain tumor-initiating cells: With great technology comes great understanding. *Future Neurology*. 2017;12:223-236.
- 2 Ali M, **Manoranjan B**. On vaccines and irrationality: Leveraging emotion for the greater good. *Meducator: McMaster Undergraduate Health Sciences Journal*. 2013;23:15-16.
- 3 Singh SK, **Manoranjan B**, Venugopal C. Evolution of brain tumor-initiating cell research: In pursuit of a moving target. *Future Neurology*. 2013;8:1-3.
- 4 **Manoranjan B**, Ali M. Tumour heterogeneity and treatment: One step forward or two steps back? *Meducator: McMaster Undergraduate Health Sciences Journal*. 2012;22:7-9.

#### **PUBLISHED REFEREED BOOK CHAPTERS (\*EQUAL CONTRIBUTIONS BY AUTHORS)**

- 1 **Manoranjan B**, Vora P, Venugopal C, Singh SK. (2014). Brain tumor genomics: Sequencing to clinical utility. In G Dellaire, JN Berman, RJ Arceci (Eds.), *Cancer Genomics: From Bench to Personalized Medicine*. (pp. 321-338). San Diego, CA: Academics Press.
- 2 Mann A\*, van Omeren R\*, **Manoranjan B**, McFarlane N, Vora P, Venugopal C, Singh SK. (2014). Glioblastoma stem cells drive tumor recurrence and patient relapse: What's the evidence? In VK Rajasekhar (Ed.), *Cancer Stem Cells*. (pp. 193-208). Hoboken, NJ: Wiley Press.
- 3 **Manoranjan B**, Garg N, Bakhshinyan D, Singh SK. (2015). The role of stem cells in pediatric central nervous system malignancies. In M Ehtesham (Ed.), *Stem Cell Biology in Neoplasms of the Central Nervous System*, Advances in Experimental Medicine and Biology. (pp. 49-68). Switzerland: Springer Press.

**The following is a list of oral presentations at national and international conferences given throughout the course of my doctoral thesis.**

**SCIENTIFIC MEETINGS: INVITED PODIUM ORAL PRESENTATIONS  
(\*PRESENTER)**

1. **Manoranjan B\***, Venugopal C, Kameda-Smith M, Bakshinyan D, Subapanditha M, Doble BW, Singh SK. Context-specific tumor suppressive function of the canonical Wnt pathway in pediatric medulloblastoma highlights a therapeutic strategy for treatment-refractory subgroups. 22<sup>nd</sup> Annual Scientific Meeting of the Society for Neuro-Oncology (SNO), San Francisco, California, November 16-19, 2017.
2. **Manoranjan B\***, Venugopal C, Mahendram S, Subapanditha M, Savage N, Qazi M, Vora P, Moffat J, Doble BW, Singh SK. A CD133-Akt-Wnt signaling axis provides functional insight into the role of CD133 in glioblastoma brain tumor-initiating cells. 22<sup>nd</sup> Annual Scientific Meeting of the Society for Neuro-Oncology (SNO), San Francisco, California, November 16-19, 2017.
3. **Manoranjan B\***, Mahendram S, Bakshinyan D, Kameda-Smith M, Venugopal C, Doble BW, Singh SK. Activated Wnt signaling for the therapeutic targeting of treatment-refractory medulloblastoma stem cells. *Canadian Journal of Neurological Sciences*. 2016;43(Suppl4):S2-S3. 17<sup>th</sup> Biennial Canadian Neuro-Oncology Meeting, Toronto, Ontario, June 9-11, 2016.
4. **Manoranjan B\***, Mahendram S, Bakshinyan D, Kameda-Smith M, Venugopal C, Doble BW, Singh SK. Activated Wnt signaling for the therapeutic targeting of treatment-refractory medulloblastoma stem cells. 84<sup>th</sup> American Association of Neurological Surgeons (AANS) Annual Scientific Meeting, Chicago, Illinois, April 30–May 4, 2016.
5. Singh SK\*, **Manoranjan B**, Venugopal C, Vora P, McFarlane N, Garg N, Singh M, Mann A, Bakshinyan D, Mahendram S, Dunn S. Sox2 identifies the treatment-refractory stem cell population in Group 2 medulloblastoma. *Neuro-Oncology*. 2014;16(Suppl3):iii5. 20<sup>th</sup> International Brain Tumor Research and Therapy Conference (IBTRTC), Lake Tahoe, California, July 20–23, 2014.
6. **Manoranjan B\***, Venugopal C, McFarlane N, Dunn SE, Singh SK. Sox2 represents the treatment-refractory cell population in Shh-dependent medulloblastoma stem cells. 2013 Clinician Investigator Trainee Association of Canada (CITAC) Annual General Meeting, Canadian Society for Clinician Investigators (CSCI/CIHR) Young Investigators Forum, Ottawa, Ontario, September 16–18, 2013.
7. **Manoranjan B\***. Cancer stem cells: The evil twin. 2013 Federation of Tamil Sangams of North America (FeTNA), Toronto, Ontario, July 5–7, 2013.

8. **Manoranjan B\***, Venugopal C, McFarlane N, Dunn SE, Singh SK. Sox2 represents the treatment-refractory cell population in Shh-dependent medulloblastoma stem cells. 17<sup>th</sup> Annual Conference & Workshop on Technological Advances in Science, Medicine, and Engineering (TASME), Toronto, Ontario, July 6–7, 2013.
9. **Manoranjan B\***, Hallett RM, Venugopal C, McFarlane N, Hassell JA, Singh SK. The developmentally conserved Bmi1-FoxG1-p21 axis regulates tumour heterogeneity and self-renewal in medulloblastoma brain tumour-initiating cells. 5<sup>th</sup> Annual Canadian National Medical Student Research Symposium, Winnipeg, Manitoba, June 4–6, 2013.
10. **Manoranjan B**, Wang X, Hallett R, Venugopal C, Mack S, McFarlane N, Nolte S, Scheinemann K, Gunnarsson T, Hassell J, Taylor M, Lee C, Triscott J, Foster C, Dunham C, Hawkins C, Dunn S, Singh S\*. Regulation of medulloblastoma stem cell self-renewal through the developmentally conserved FoxG1-Bmi1-p21 axis. 2<sup>nd</sup> Biennial Pediatric Neuro-Oncology Basic & Translational Research Conference, Fort Lauderdale, Florida, May 16–17, 2013.
11. **Manoranjan B\***, Provias JP. Glioblastoma in young adults: The McMaster experience. 6<sup>th</sup> Annual Neuropathology Day at McMaster: Progress in head injury research and neuro-oncology, Hamilton, Ontario, April 19, 2013.
12. **Manoranjan B\***, Hallett RM, Venugopal C, McFarlane N, Hassell JA, Singh SK. The developmentally conserved Bmi1-FoxG1-p21 axis regulates tumour heterogeneity and self-renewal in medulloblastoma brain tumour-initiating cells. 4<sup>th</sup> Annual McMaster Medical Student Research Day, Hamilton, Ontario, April 17, 2013.
13. **Manoranjan B\***, Hallett RM, Venugopal C, Hassell JA, Singh SK. Bmi1 and FoxG1 interact to regulate medulloblastoma stem cells. 16<sup>th</sup> Annual Conference & Workshop on Technological Advances in Science, Medicine, and Engineering (TASME), Toronto, Ontario, July 7, 2012.
14. **Manoranjan B**, Hallett RM, Wang X, Venugopal C, McFarlane N, Hassell JA, Singh SK\*. Bmi1 and FoxG1 interact to regulate self-renewal in CD15+ medulloblastoma stem cells. 19<sup>th</sup> International Brain Tumor Research and Therapy Conference (IBTRTC), Niagara Falls, Ontario, June 22–24, 2012.

**The following are a list of research-based awards and grants that supported my training and doctoral thesis.**

Department of Biochemistry & Biomedical Sciences Cancer Research Bursary (Value: \$650) 12/2017

McMaster University Faculty of Health Sciences Research Plenary 05/2017

## Outstanding Oral Presentation Award.

McMaster University Faculty of Health Sciences Graduate Program Outstanding Achievement Award.	05/2017
American Association of Neurological Surgeons (AANS) Young Neurosurgeons Abstract Award (Value: \$1000).	05/2016
Nomination for 2014 Stem Cells Young Investigator Award – Top 5 Papers published in Stem Cells (Manoranjan, <i>et al.</i> Stem Cells, 2013, PMID: 23592496).	01/2015
Best Oral Presentation, McMaster Medical Student Research Day.	04/2013,2014
Lee Nielson Roth Award for Cancer Research (Value: \$1,000).	04/2014
Cancer Research Society Operating Grant, Co-Author with Dr. Sheila Singh (Value: \$120,000).	08/2013
American Brain Tumor Association Medical Student Summer Fellowship (Value: \$3,000).	05/2013
Alex's Lemonade Stand Foundation for Childhood Cancer Pediatric Oncology Student Training Program (POST) (Value: \$2,000).	04/2013
Mach-Gaensslen Foundation of Canada Medical Student Research Grant (Value: \$5,000).	03/2013
Brain Tumour Foundation of Canada Medical Student Research Scholarship (Value: \$10,000).	02/2013
McMaster Doctoral Graduate Student Entrance Scholarship (Value: \$6,500).	09/2012
Best Oral Presentation, Technological Advances in Science, Medicine and Engineering Conference (TASME)	07/2012,2013
Ontario Graduate Scholarship (Value: \$15,000). (Declined).	06/2011,2012
Vanier Canada Graduate Scholarship (Value \$150,000).	04/2012